PEOPLE'S DEMOCRATIC REPUBLIC OF ALGERIA
MINISTRY OF HIGHER EDUCATION AND SCIENTIFIC RESEARCH
MOHAMED BOUDIAF UNIVERSITY OF M'SILA
FACULTY OF TECHNOLOGY
DEPARTMENT OF HYDRAULIC

Serial number: ……
Registration number: **D.HYD/3C/01/19**

Watershed scale flood hazard modeling at the Hodna large basin in central Algeria

A Ph. D. thesis submitted to the Department of Hydraulic in fulfilment of the requirements for the degree of Ph.D. in Hydraulic Sciences (Doctorat of 3rd cycle LMD)

Submitted by: Mrs. **Nour El Houda BELAZREG**

Presented and publicly defended on 22/06/2023

Board of Examiners:

Mr. Mostefa Dougha	**Associate Professor**	**University of M'sila**	**Chairman**
Mr. Mahmoud Hasbaia	**Full Professor**	**University of M'sila**	**Supervisor**
Mr. Zekâi Şen	**Full Professor**	**Medipol University, Beykoz, Istanbul,Turkey**	**Co-Supervisor**
Mr. Salim Djerbouai	**Associate professor**	**University of M'sila**	**Examiner**
Mr. Tayeb Boulmaiz	**Associate professor**	**University of Ghardaia**	**Examiner**

2022/2023

Acknowledgments

First of all, I would like to thank Allah for his blessing and giving me the strength to accomplish this thesis and achieving my goal.

This work would not have been possible without the help, suggestions, encouragements and collaboration of my promotors Prof. Mahmoud HASBAIA and Prof. Zekai ŞEN throughout these years.

I would like to express my gratitude to Dr. Ahmed FERHATI who offered me a full formation in GIS software, geomorphology, hydrogeology and modeling fields. To Prof. Abdelkader BENKHALED who encouraged and supported me to continue with this thesis.

My great gratitude also goes to the Department of Hydraulics in the University of M'sila, and CEHST laboratory for providing the necessary material resources as well as helping and assisting Ph. D students during their study.

I would like to thank those that are close to me and have been with me through the ups and downs since the start of my Ph. D studies in 2019. To the pillar of my life, my mother, who has stayed by my side and encouraged through all these years. To my great husband, who has supported me to continue this work. To my wonderful son, Seif Elislam, who has been in my life during the accomplishment of this thesis. My deep gratitude also goes to my sister and my brother.

I dedicate this work to those that have passed away; to my grandmother Ourida and my uncle Rafik.

I thank the support of all people whose help made this thesis possible.

ملخص

تعتبر الفيضانات احدى أكبر المشاكل في جميع أنحاء العالم، خاصة في دول شمال إفريقيا. اعتبرت الهيئة الحكومية الدولية المعنية بتغير المناخ (IPCC) شمال إفريقيا كواحدة من أكثر المناطق التي تواجه التأثيرات الناتجة عن تغير المناخ. تتكون مخاطر الفيضانات من ثلاثة عناصر رئيسية، بما في ذلك احتمالية الفيضانات، التعرض للفيضانات و خسائر الفياضات. بالإضافة الى ذلك، تتزايد أضرار الفيضانات نتيجة تغير المناخ و تغير استغلال الأراضي الى جانب زيادة عدد المناطق السكنية على طول المناطق المعرضة للفيضانات. لذلك، فإن التقييم و التجهيز الجيد لتفادي أو تخفيف أضرار الفيضانات أمر ضروري. في هذه الأطروحة، حوض الحضنة، بمساحة تقدر 26 000 كم^2 ، و باعتباره خامس أكبر الأحواض الصبابة في الجزائر، قد تم اختياره في هذا البحث. يتكون حوض الحضنة الكبير من ثمانية أحواض صغيرة، من بينها حوض البحيرة المالحة المسمى شط الحضنة.

للرد على المشكلات المطروحة، تهدف هذه الأطروحة إلى: 1) تقييم تدفقات الذروة للفيضانات لفترات مختلفة (10 سنوات، 50 سنة، 100 سنة و 1000 سنة) بناء على صيغ تجريبية و إحصائية و ذلك باستخدام بيانات هطول الأمطار اليومي الأقصى، 2) استخدام النموذج الهيدروليكي أحادي البعد للتدفق المستمر بهدف محاكاة امتداد الفيضانات والحصول على بيانات عن ارتفاع منسوب المياه في مناطق مختلفة من حوض الحضنة خلال فترات مختلفة بالاعتماد على التدفقات القصوى المتحصل عليها سابقا و ذلك باستخدام برنامج HEC-RAS، 3) استخدام نظام المعلومات الجغرافية (GIS) لإنشاء خرائط تمركز الفيضانات باستعمال عملية التسلسل الهرمي التحليلي (AHP)، 4) توقع متوسط هطول الأمطار الشهري و درجة الحرارة القصوى خلال الفترة الممتدة من 2021 الى غاية 2100، بالاعتماد على الجيل الأخير لسيناريوهات المناخ (SSPs) و ستة من النماذج المناخية.

تشير خريطة الفيضانات الى أن مدن سيدي عيسى، بوسعادة، بريكة، برج بوعريريج و المسيلة هي أكثر المناطق تعرضا لخطر الفيضانات, كما توضح نتائج المحاكاة ارتفاعات مناسيب المياه بالنسبة لفيضان الخمسين عاما، لتصل الى 3.43 متر كحد أقصى في المسيلة، 3.27 متر في برج بوعريريج، 2.77 متر في بريكة، 4.16 متر في بوسعادة و 6.46 متر في سيدي عيسى. و قد سمحت النماذج الستة المختارة لتوقع الأمطار و درجة الحرارة القصوى الى التوصل الى النموذجين IPSL-CM6A-LR و GFDL-ESM4 هما الأفضل لتقدير التغييرات المتوقع حدوثها في حوض الحضنة في الفترة 2021-2100.

الكلمات المفتاحية: مخاطر الفيضانات؛ التدفق الأقصى ؛ فترة العودة ؛ تغير المناخ ؛ التساقطات؛ GIS؛ HEC-RAS ؛ SSP؛ حوض الحضنة ؛ الجزائر

Abstract

Flooding is a huge problem worldwide, especially in North african countries. The Intergovernmental Panel on climate change (IPCC) has considered North Africa as one of the major regions facing climate change impact in the world. Flood risk is composed of three main elements, including hazard, exposure and vulnerability. In addition, flood damages have been increasing as a result of climate change, land use change as well as the increased number of residential areas along flood-prone areas. Therefore, assessment of flood discharge rates and flood risk is essential for a good management and mitigation measures. The Hodna basin has been considered for this research. With its large area equals to 26 000 km², the Hodna basin is the fifth largest basin in Algeria. It is an endorheic basin constitutes of eight sub-basins, among them the saline lake Chott-El-Hodna.

To respond to the previous mentioned issues, this thesis aims at: i) assess peak flows for different return periods (10-year, 50-year, 100-year and 1000-year) based on empirical and statistical formulas and extreme daily precipitation; ii) use the one dimensional steady flow hydraulic model of HEC-RAS software to assess the impact of these peak flows on provinces may be facing flooding risk in Hodna basin; iii) use the Geographic Information System (GIS) to generate flood hazard and risk maps on the basis of Analytical Hierarchy Process (AHP) technique ; iv) project average monthly precipitation and maximum temperature changes over the period 2021-2100 using the last generation of climate scenarios Shared Socio-economic Pathways (SSPs) and six climate models.

The flood risk map indicates that the cities of Sidi Aïssa, Boussaada, Barika, Bordj Bou Arreridj and M'sila are the most cities exposed to flooding risk. The application of 1D steady flow model shows the water heights at different parts in these cities. It reaches a maximum of 3.43 m in M'sila, 3.27 m in Bordj Bou Arreridj, 2.77 m in Barika, 4.16 m in Boussaada and 6.46 m in Sidi Aïssa for a 50-year flood. Besides, historical evaluation of the six climate models allows the validation of the best ranking model for both average monthly precipitation and maximum temperature variables. The models IPSL-CM6A-LR and GFDL-ESM4 have been used to project future changes over the period 2021-2100.

Keywords: flood risk; peak flow; return period; climate change; precipitation; GIS; HEC-RAS; SSP; Hodna basin; Algeria.

Résumé

Les inondations sont un problème major, en particulier dans les pays d'Afrique du Nord. Le groupe d'expert intergouvernemental sur l'évolution du climat (IPCC) a considéré l'Afrique du Nord comme l'une des principales régions confrontées à l'impact du changement climatique dans le monde. Le risque d'inondation est composé de trois éléments principaux, à savoir l'aléa, l'exposition et la vulnérabilité. En outre, les dommages causés par les inondations ont augmenté en raison du changement climatique, du changement de l'occupation du sol ainsi que le grand nombre des habitations le long des plaines d'inondation. Par conséquent, l'évaluation des débits de crue et des risques d'inondation est essentielle pour le bon management et les mesures de protection. Le bassin versant de Hodna est considéré pour cette recherche. Avec sa grande superficie égale à 26 000 km², le bassin versant de Hodna est le cinquième grand bassin en Algérie. C'est un bassin endoréique constitué de huit sous-bassins, dont le lac salé Chott-El-Hodna.

Pour répondre aux problématiques évoquées précédemment, cette thèse vise à : i) évaluer les débits de pointe pour différentes périodes de retour (10 ans, 50 ans, 100 ans et 1000 ans) sur la base de formules empiriques et statistiques et des précipitations journalières, ii) utiliser le modèle hydraulique unidimensionnel à débit constant du logiciel HEC-RAS pour évaluer l'impact de ces débits de pointe sur les villes susceptibles d'être confrontées à un risque d'inondation dans le bassin du Hodna, iii) utiliser le système d'Information Géographique (SIG) pour générer des cartes des aléas et des risques d'inondation sur la base de la technique du Processus de Hiérarchie Analytique (AHP) ; iv) projeter l'impact du changement climatique sur les précipitations mensuelles moyennes et les températures maximales sur la période 2021-2100 en utilisant la dernière génération de scénarios climatiques Pathways socio-économiques Partagés (SSPs) et six modèles climatiques.

Les cartes de risque d'inondation indiquent que les villes de Sidi Aïssa, Boussaada, Barika, Bordj Bou Arreridj et M'sila sont les villes les plus exposées au risque d'inondation. L'application du modèle d'écoulement constant montre les hauteurs d'eau à différentes parties de ces villes. Elle atteint au maximum 3.43 m à M'sila, 3.27 m à Bordj Bou Arreridj, 2.77 m à Barika, 4.16 m à Boussaada et 6.46 m à Sidi Aïssa pour une crue de 50 ans. En outre, l'évaluation historique de six modèles climatiques a permet de choisir le plus adéquat modèle aux précipitations et température. Les modèles IPSL-CM6A-LR et GFDL-ESM4 ont été donc utilisés pour projeter les changements futurs durant la période 2021-2100.

Mots-clés: risque d'inondation ; débit de crue ; période de retour ; changement climatique ; précipitation ; SIG ; HEC-RAS ; SSP ; bassin de Hodna, Algérie.

Table of contents

Chapter 2: Study area: the large Hodna basin

Chapter 3: Data and methodologies

Chapter 4: Peak flow assessment and flood mapping: interpretation of results

List of figures

List of tables

List of acronyms

AHP	Analytical Hierarchy Process
ANRH	National Agency of Hydraulic Resources
AR	Assessment Report
BCC-CSM2-MR	Beijing Climate Center Climate System Model
CanESM5	Canadian Centre for Climate Modelling and Analysis, Environment and Climate Change
CI	Consistency Index
CMIP	Coupled Model Intercomparison Project
CP	Compromise Programming
CR	Consistency Ratio
CRU	Climatic Research Unit of the university of East Anglia
DD	Drainage density
ESGF	Earth System Grid Federation
FAO	Food and Agriculture Organization of the United Nations
FAR	First Assessment Report
FHI	Flood Hazard Index
FRI	Flood Risk Index
GCMs	General Circulation/Climate Models
GFDL-ESM4	Geophysical Fluid Dynamics Laboratory Earth System Model
GHGs	Greenhouse Gases
GIS	Geographic Information Systems
GPCC	Global Precipitation Climatology Center
GWR	Geographically Weighted Regression
HEC-RAS	Hydrologic Engineering Center's River Analysis System
HUC	Hydrologic Unit Codes
IDW	Inverse Distance Weighted
IPCC	Intergovernmental Panel on Climate Change
IPSL-CM6A-LR	Institut Pierre-Simon Laplace Climate Modeling Center, Low Resolution
LULC	Land Use / Land Cover
MB	Mean Absolute Bias
MCA	Multi Criteria Analysis

MIROC6	Model for Interdisciplinary Research On Climate
NASA	National Aeronautics and Space Administration
NetCDF	Network Common Data Form
OSM	Open Street Map
PD	Population density
Pmax (d)	Annual Maximum Daily Precipitation
R^2	Coefficient of determination
RCM	Regional Climate model
RCP	Representative Concentration Pathways
RI	Random Index
RMSE	Root Mean Square Error
S	Slope
SAR	Second Assessment Report
SRES	Special Report on Emission Scenarios
SSP	Shared Socio-economic Pathways
ST	Soil Type
UN	United Nations
UNEP	United Nations Environment Program
WMO	World Meteorological Organization

GENERAL INTRODUCTION

General introduction

1. General background

Floods are the main natural disaster risk in the world in terms of human and economic losses. Likewise, they can cause serious damages to the environment. Globally, almost one billion people live in floodplains (Alfieri et al., 2017). With the increase in anthropogenic activities and urbanization, floods have become more harmful, especially in areas that are at risk of flooding. Flood risk is defined as the probability of flood multiplied by the possible consequences (Kron, 2005; Samuels & Gouldby, 2005; Ward et al., 2011). Rather, flood hazard is represented by hazard maps that show one or more characteristics. The most commonly used one is the depth of inundation (Goodell and Warren, 2006; Ward et al., 2011).

The hydrological cycle describes the continuous movement of water through the climate system (Stocker et al., 2013). Observations of hydrological cycle change are clear evidence of global warming. A warmer atmosphere can carry more water vapour, lead to more heat and humidity and cause intensification of sea level rise, strong rainfall events and long drought spells (Willner et al., 2018). More than half of the observed increase in global average surface temperature from 1951 to 2010 is extremely likely to be caused by human activities, especially industrialization, burning of fossil fuels and land use/land cover changes (Stocker et al., 2013). In fact, past and present anthropogenic greenhouse gas (GHG) emissions may lead to an increase in surface air temperature and increase the occurrence and magnitude of extreme flood events (Fewtrell and Kay, 2008).

Climate change is primarily a scientific topic and is probably one of the most contentious because of its inherent scientific uncertainty (Shameem, 2016). Intergovernmental Panel on Climate Change (IPCC) assessment reports include simulations of different climate models to project future changes. Indeed, climate models have continued to be improved since the third AR, particularly in simulating different climate variables such as surface temperature and precipitation. These models simulate changes based on a range of anthropogenic forcing scenarios. The Shared Socio-economic Pathways (SSPs) are the latest generation of scenarios run under the Coupled Model Intercomparison Project Phase 6 (CMIP6). Downscaling techniques serve as an efficient tool in providing climate information on the smaller scales needed for many climate impact studies.

According to IPCC (2014), water resources in Africa are the most vulnerable to climate change, particularly changes in frequency of droughts, floods, and extreme temperature causing heat waves. IPCC (2014; 2017) scenarios show increased aridity in currently dry areas. In effect, in addition to flood and drought preparedness and mitigation measures, a reliable prediction of precipitation and temperature is important for water resources management and flood, risk management. Thus, climate models are used to evaluate past events, and also to predict future changes in climate.

2. Statement of the problem and objectives

In the global debate on climate change, North Africa is considered one of the most vulnerable regions. Algeria is frequently exposed to flash and violent flooding processes, especially in semi-arid and arid regions. Sudden flash flood occurrences are difficult to forecast and manage. The random nature of the phenomenon is associated with intensive rainfall and an unfavorable land use as well adverse anthropic factors complicating the phenomenon extremely with very serious hazard consequences.

Many provinces witnessed numerous inundation disasters. The flooding of Chlef in 1966, 63 casualties, the Tizi-Ouzou (Azzazga) flood of 1971, 40 deaths and hundreds of residential destroyed areas, the Algiers-Tizi Ouzou flood of 1974, 52 deaths and 4570 destroyed houses and in the flood of 1980, 44 deaths, 50 injured and 365 homeless families in the flooding of El-Eulma (Setif). Furthermore, the flooding of Annaba in 1982 has caused 47 deads, the flooding of Ain Temouchent in 1984, which has caused 33 casualties and floods of Laghouat in 1995 with more than 40 casualties. Moreover, the flooding of Algiers (Bad El Oued) in 2001, which had caused 752 deaths and important economic losses, in addition to the M'zab wadi flooding in Ghardaïa in 2008, which killed more than 40 people and destroyed 600 places and caused a significant property damages (Abdeddaim, 2018; Boutaghane et al., 2022). In the province of M'sila, the inundations of May 2021 have caused the death of six persons and locked 60 other persons in their houses, in addition to the inundation of September 2021, which have caused important damages near the rivers of Ain El Melh wadi, Maiter wadi and in the commune of Khatouti Sed Al Djir.

Nowadays, the effects of climate change on human and environmental life in Algeria are influencing the frequency and intensity of floods and increase their damages (Guellouh et al., 2016). This trend can be more dangerous according to climate variability. Therefore, deep knowledge of the hydrological processes and their spatio-temporal features, allows local

communities and decision-makers to conduct a detailed analysis of flood risk extensions and then implement flood risk management strategies related to rivers overflowing. For this purpose, hydrometeorological data, particularly rainfall and runoff data are essential for successful flood prediction and mitigation.

The Hodna basin is no exception as it has witnessed significant catastrophic flooding. Flood modeling has become essential since the changing climate affects the frequency and increasing severity of floods. In this context, this research examines the relative importance of future climate change in identifying flood risk areas in the Hodna basin. It is based on:

- Flood discharge rates have been assessed using statistical and empirical formulas (Gradex, Giandotti, Possenti, Turazza and Temez) for the case of El-Ham sub-basin. Different return periods (10-year, 50-year, 100-year and 1000-year),
- Flood hazard and areas that might face flooding risk, have been mapped and identified over the whole Hodna basin. For this, two techniques are used, which are the Analytical Hierarchy Process (AHP) technique, and one dimensional hydraulic steady flow model.
- Possible future effect of climate change on precipitation and temperature especially on highly populated areas in Hodna basin. Six (06) GCMs from the Coupled Model Intercomparison Project phase 6 (CMIP6) are chosen for this purpose. These are: ACCESS-ESM4, BCC-CSM2-MR, CanESM5, GFDL-ESM1-5, IPSL-EM6A-LR and MIROC6. Evaluation of these six climate models is implemented under two different scenarios; SSP 1-2.6 and SSP3-7.0.

This study will be carried out using many tools, especially the combination of Geographical Information System (GIS), Hydrologic Engineering Center's River Analysis System (HEC-RAS), Open Street Map (OSM) as well as Google Earth Imagery. A particular attention is given to the spatial and temporal variability of the phenomenon.

Annual maximum daily precipitation datasets are obtained from the National Agency of Hydraulics Resources (ANRH) for two periods. In the case of peak flow assessment in El-Ham wadi, the rainfall data available are considered for the period 1966-2011. While, the case of the flood propagation assessment and mapping for the whole Hodna basin, rainfall datasets for the period starting from 1980 to 2020 have been used. In contrast, monthly precipitation and maximum air temperature gridded datasets are retrieved from The Climatic Research Unit (CRU) for the period 1901-2014.

3. Significance of the study

This research may make a new contribution to the understanding of the relationship between flooding and climate change (climate variables: precipitation, temperature) in the Hodna basin. The usefulness of the combined use of geospatial modeling, hydraulic modeling and climatic modeling is emphasized in this research. Hence, the findings from this research suggest that flooding and climate change are two related issues, unlike many previous studies that have largely treated and publically treated them as two separate issues.

4. Thesis outline

After a general introduction to the subject of this research, the Ph. D thesis is organized in five chapters, as follows:

Chapter 1 provides an overview of watersheds characteristics such as morphology, climate, geology, hydrogeology and land use, flood hazard definition and risk modeling as well as an overview of the climate system, greenhouse gas (GHG) effect and climate change modeling.

Chapter 2 provides detailed literature review on the Hodna basin and its general behavior. In addition to the physic-morphometric features of the study area, are geological, hydrological, stream outlet and land use/ land cover settings are mentioned.

Chapter 3 provides the data and key methodologies used to achieve the objectives of this study. Peak discharge rates assessment for different return periods, flood hazard and risk modeling, and also historical evaluation and future projections of precipitation and temperature using CMIP6 GCMs in the Hodna basin are included.

Chapters 4 and 5 discuss and focus on the outcomes of this research. Evaluation of flood discharge rates and flood water heights for different provinces in the Hodna basin is evaluated and discussed in Chapter 4. The final chapter examines future precipitation and maximum temperature projections for the period 2021 -2100.

The last section presents the general conclusions and limitations of this research and provides recommendations and overview for further studies.

CHAPTER 1

Flooding risk in river basins, and climate change impact: literature review

Chapter 1 Flooding risk in river basins, and climate change impact: literature review

1.1. Introduction

In this chapter, hydrology, flooding assessment, and climate change impacts studies are discussed. Nowadays, these three domains (affecting each other) are presenting a serious political and social issue. Concepts of hydrology in natural system, in particular in river basins and their response to flooding as a result of climate change implications are discussed.

1.2. River basin, hydrological cycle and its constituents

1.2.1. Hydrology

Hydrology plays a major role in environmental engineering domain. According to Roche (1963), Brooks et al. (2013) and Şen (2018), it is the science of water concerned with the origin, circulation, distribution, and properties of waters in the Earth. It is the science of water occurrence, movement, and transport that deals with rainfall, runoff, drought, flood, and groundwater occurrences. As it is concerned with natural systems, it is also important for anthropogenic systems management concerning urban areas and industry (Musy and Higy, 1998).

1.2.2. Drainage basin

Many definitions are found in the literature and thus drainage basin scientific studies include many uncertainties. In the following various definitions are presented according to different researchers:

- ✓ Praskievicz (2009): Drainage basins are natural hydrological units, each with its own water balance.
- ✓ Brooks et al. (2013): Watersheds are biophysical systems that define the land surface draining water, sediments and chemical constituents to a point (especially outlet) in a stream channel or a river channel defined by topographic boundaries. They are the systems used to study the hydrological cycle and its components.
- ✓ Edwards et al. (2015): In hydrology, the land unit is the watershed, which may also be referred to as drainage basin or catchment. It is defined as an area of land in which all of the precipitation drains to topographically low locations. The watershed boundaries as water divide lines are topographic highest points, and their identification becomes

hard task in flatland watersheds contrary to mountainous areas. The lowest point of a watershed is its outlet, where the principal river can meet another water channel.

Drainage basins or watersheds are identified numerically by hydrologic unit codes (HUC) with different levels, and are organized by size of watershed in descending order. These HUCs are defined by the Federal Interagency Geographic Agency Committee to identify basins' locations, and their hierarchical nature. The HUC levels are defined as region, sub-region, basin, sub-basin, watershed and sub-watershed (Figure 1.1).

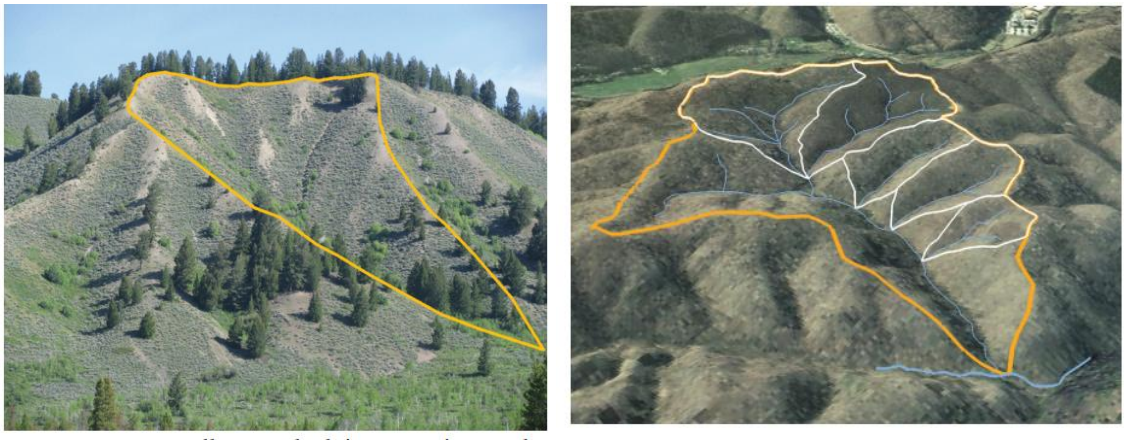

Fig. 1.1 Small watersheds representing the high topographic points and delineation (to the left), and smaller sub-watersheds representation where streams are the blue lines (to the right) after Edwards et al. (2015)

1.2.3. Hydrological cycle

Hydrological cycle is thus important element in both hydrology and climatology (Figure 1.2). The hydrological cycle refers to the movement of water among the ocean, land, and atmosphere by evaporation, precipitation and flow in rivers (Mathez and Smerdon, 2018). According to Brooks et al. (2013), the hydrological cycle represents the circulation of water in the troposphere, land surface and subsurface. It involves the processes and pathways by which the water evaporates from the Earth's surface and surface water bodies to the atmosphere and returns to the surface as precipitation. Some parts of this precipitation is then evaporated once again, flows on the surface as streamflow or even as groundwater recharge and flow through infiltration and percolation. It is also the combination of all possible pathways between the atmosphere, lithosphere, biosphere, hydrosphere, and cryosphere (Şen, 2018):

- ✓ Atmosphere constitutes important gases which are essential for living organisms to breath,
- ✓ Hydrosphere constitutes of oceans, lakes and rivers,

- ✓ Lithosphere forms the continental crust,
- ✓ Biosphere forms the plants including forests and green plants on continents.

A part of the rainwater sinks into the ground to form groundwater (percolation), and part of it forms streams and rivers that flow ultimately into the sea (runoff). Some of the water in the soil is taken up by the plants and is evapotranspirated in turn by the leaves (transpiration), and the rest is lost to the atmosphere from the land and water surface due to the heat of the sun (evaporation) (Banjoko, 2014).

However, because of anthropogenic practices (fossil fuels burning and carbon release, deforestation and agricultural activities), the exchanges take place between the various components of the hydrological cycle and reaches a disequilibrium state (Goosse et al., 2010).

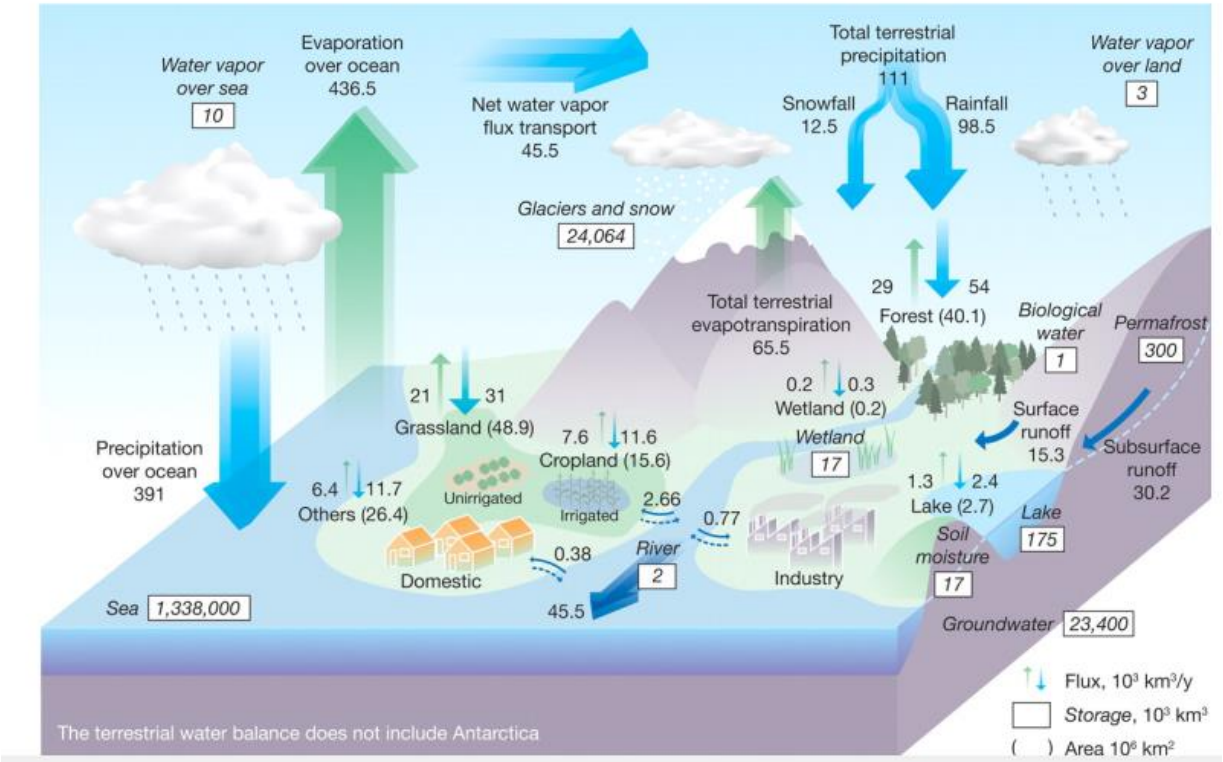

Fig. 1.2 The hydrological cycle adapted from Oki and Kanae (2006)

1.2.3.1. Hydrological cycle components

Understanding how water is moving and circulated through a basin/watershed provides the foundation for water-landscape interactions. For this reason, the hydrological cycle term is applied here to describe the water movement within a basin through multiple components which are described here to understand the hydrological cycle (Musy and Higy, 1998).

Precipitation

In the hydrological cycle, rainfall is the prime source of all water. It is one of the dynamic parameters and has diverse range of impact on livelihood namely, agricultural operations, hydropower, and sustainability of different ecosystems (Brooks et al., 2013; Şen, 2018). The major factors that cause precipitation (Figure 1.3), according to Morell et al. (1999), are the followings:

- ✓ Convergence lifts: they appear when two air masses of different temperatures come into contact. Particularly, it is when these two layers become hotter by solar radiation. Therefore, they become lighter and rise until they become cooler to the level of condensation where the clouds are formed,
- ✓ Frontal lifts: they result from lifting of hot air upward over a cold air mass,
- ✓ Orographic lifts: the presence of relief of higher altitude when a mass of air is passing by, provoke its rise to higher levels. The mass of air becomes cooler and leads to clouds formations and rainfall.

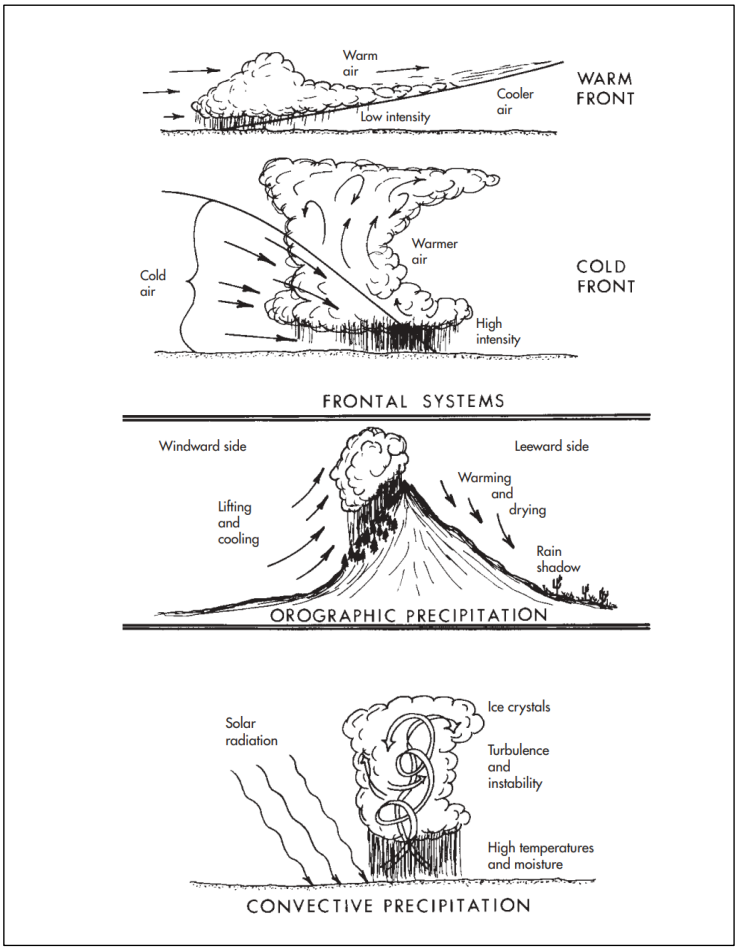

Fig. 1.3 Precipitation mechanisms (Brooks et al., 2013)

Evaporation / evapotranspiration

Evapotranspiration has two components: Evaporation which is the water loss from the soil surface and water bodies, in addition to transpiration as the consumed water by plants (Jutla, 2006). It defines the ensemble of phenomenon related to plants transpiration, in addition to the evaporation which can be generated from the soil surface or from vegetation (Musy and Higy, 1998). Thus, it has relationship with temperature, pressure, air moisture, solar radiation.

Infiltration

Infiltration can be defined as the downward movement of water into the subsoil (Jutla, 2006). It constitutes the major sources of water for sustaining the growth of vegetation, the groundwater supply to wells, springs and streams. The infiltration rate is controlled by the soil physical characteristics, soil cover, water content of soil, soil temperature (viscosity rises with heat), and rainfall intensity.

Surface water (streamflow)

Surface water consists of all sources in which the water flows over the Earth's surface, including rivers, lakes, seas, man-made reservoirs, and wadis (Banjoko, 2014). Runoff is generated when the soil exceeds its infiltration capacity. Figure 1.4 shows the change of runoff with time after an individual precipitation.

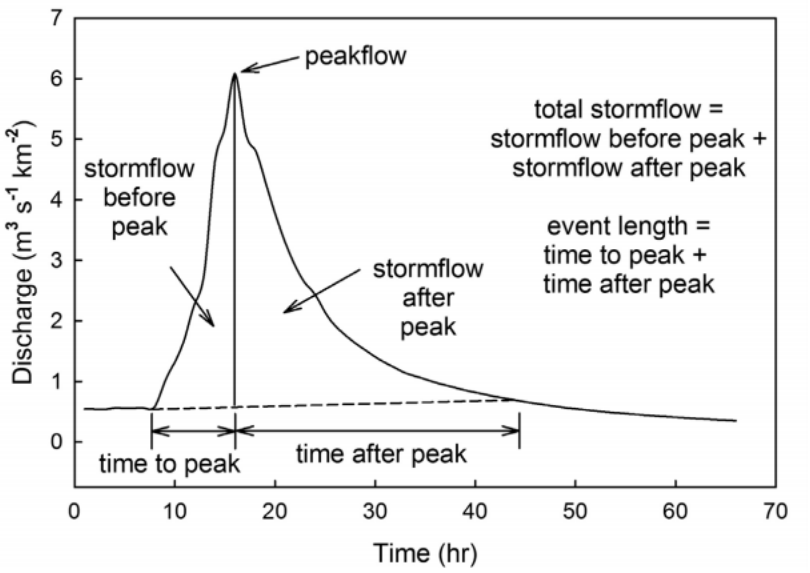

Fig. 1.4 The storm hydrograph drawn by Edwards et al. (2015): the hydrograph variables, streamflow volume before peak, and after peak.

Groundwater

Underground water results from rainwater percolating into the ground and constitutes as the easiest source of fresh water. The usual groundwater sources are wells and springs. It is referred to as an aquifer, which is a saturated geologic layer that sits atop of a confining bed, and water movement is controlled by its permeability. Infiltration coming from the surface runoff is the responsible for the groundwater recharge.

1.3. Flood assessment, modeling and mitigation

At the beginning of this section, the definition of terms ‘risk’ and ‘hazard’ is necessary for a clear view. Thus, this section sheds light on the different flood characteristics with a focus on prediction and mitigation measures, in addition to flood prone regions assessment and modeling.

1.3.1. Floods

Recent events in 2021 indicate that flood and flash flood events affect many countries and societies. Scientists state that natural disasters such as droughts and floods are becoming more frequent and severe due to climate change impact. Intensive rainfalls triggered severe flooding and landslides in Turkey, Iran, Oman, Saudi Arabia, Japan, China, Germany, Belgium and France. In Africa, numerous flooding events are also recorded in 2021, following heavy rains in Niger, Cameroon, Sudan, Ethiopia, Chad and Ghana (the period from 26 July to 14 August). In Algeria from the same year, severe flooding of Oued Meknassa, Boussaada, Laghouat, Chlef, Batna and Médéa caused dozens of deaths and thousands of injuries (Figure 1.5).

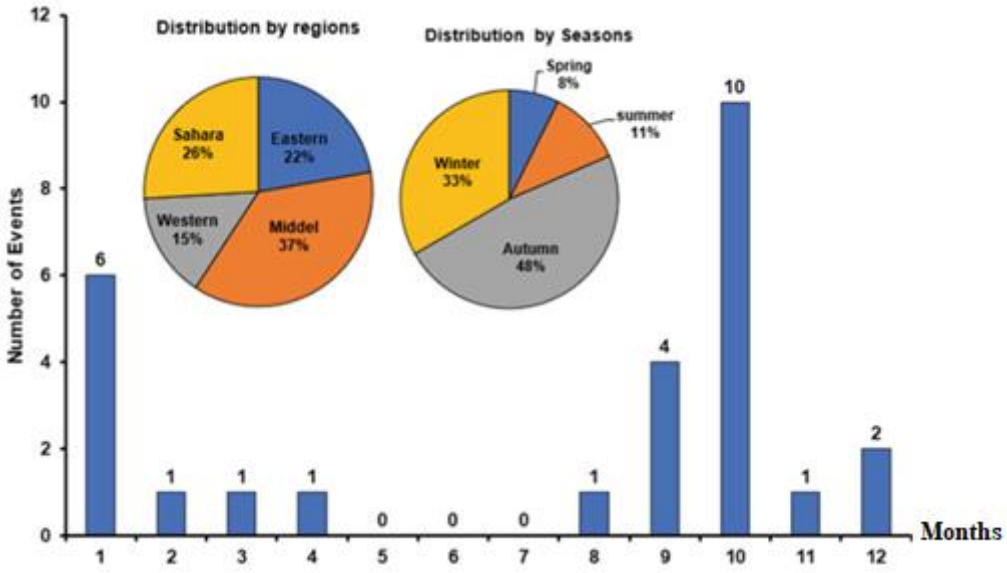

Fig. 1.5 Distribution of flood events in Algeria (1965-2013) after Boutaghane et al. (2022)

Many definitions of floods are found in the scientific literature, which are summarized in the following points:

- ✓ According to EU Floods Directive (2007) floods are a natural part of the hydrological cycle. However, they have the potential to cause fatalities, displacement of people, and damage to the environment, which may also severely endanger the economic development.
- ✓ According to Şen (2018) floods are among the extreme natural events that occur after intensive storm rainfall events as excessive water volumes over the Earth surface more than the capacity of surface natural or artificial conveyance systems (stream and river basins, wadis, canals, dams, cities).
- ✓ According to Phongsapan et al. (2019) floods are one of the most recurrent natural hazards which rapidly become significant disasters, following the land cover changes, urbanization and changing climate.

1.3.2. Flood hazard

Predicting and reporting extreme events, especially the risk of floods and droughts, is what every country should care for at the top of strategic planning hazard studies. Flooding in arid regions is an extremely beneficial event as it is the main source of groundwater recharge along drainage basins where there is no human habitation or flood-prone urban areas (Şen, 2018). But floods are the most dangerous natural disasters. They are governed by various

factors such as precipitation characteristics, drainage geomorphological features, land use, and water management in river basins (Chang et al., 2013).

Floods occur when the water of streams or storm water drainage systems overflows drainage channel cross-sections and consequently invades floodplain or urban areas (Konrad, 2003). Impacts associated with such events depend on the geographical and climatic characteristics of the watersheds, as well as on anthropogenic factors.

1.3.2.1. Definition of a flood hazard

Flood hazard is a damaging event that may be due to natural events and/or human activities (UNISDR, 2011). It is also defined as the probability exceedance of potentially damaging flood situations in a given area and within a specified period of time (Adjinacou, 2016). It can also be defined by the spatial extent and temporal frequency of floods events (Winsemius et al., 2013).

Hazard management is defined as the multiple processes including the identification of hazards, assessment and analysis of associated risks and understanding public perceptions (Wisner et al., 2012).

For any flood occurrence, rainfall intensity, drainage basin features, land use or vegetation cover and geological compositions are indispensable. Flood hazards may be the result of some natural causes (river banks, flood plains, erosion, sedimentation), while others are due to human activities (dams, highways, agriculture, land use, towns) (Figure 1.6).

1.3.2.2. Different types of floods

Floods can be subcritical or supercritical according to the nature of their flows. Subcritical floods are often seasonal, and occur in large river basins, where flow is typically slow. On the contrary, supercritical flood is often rapid and violent, and characterized by high flow discharge. In general, urban floods can be generally categorized in diverse types (Adjinacou, 2016; Vargas, 2016), as follows:

- Pluvial floods: they are due to very high intensity and long duration of rainfall. In addition, impervious areas increase the surface runoff,
- Riverine floods: they are due to heavy rainfalls where urban areas are situated in lower reaches of rivers. Moreover, urbanization has aggravated their intensity by decreasing some of the natural flood plains (Figure 1.8),

- Flash floods: they are due to rapid accumulation of surface runoff and intensive and short term rainfalls. In this type, flow discharge reaches its peak values rapidly (Figure 1.7).

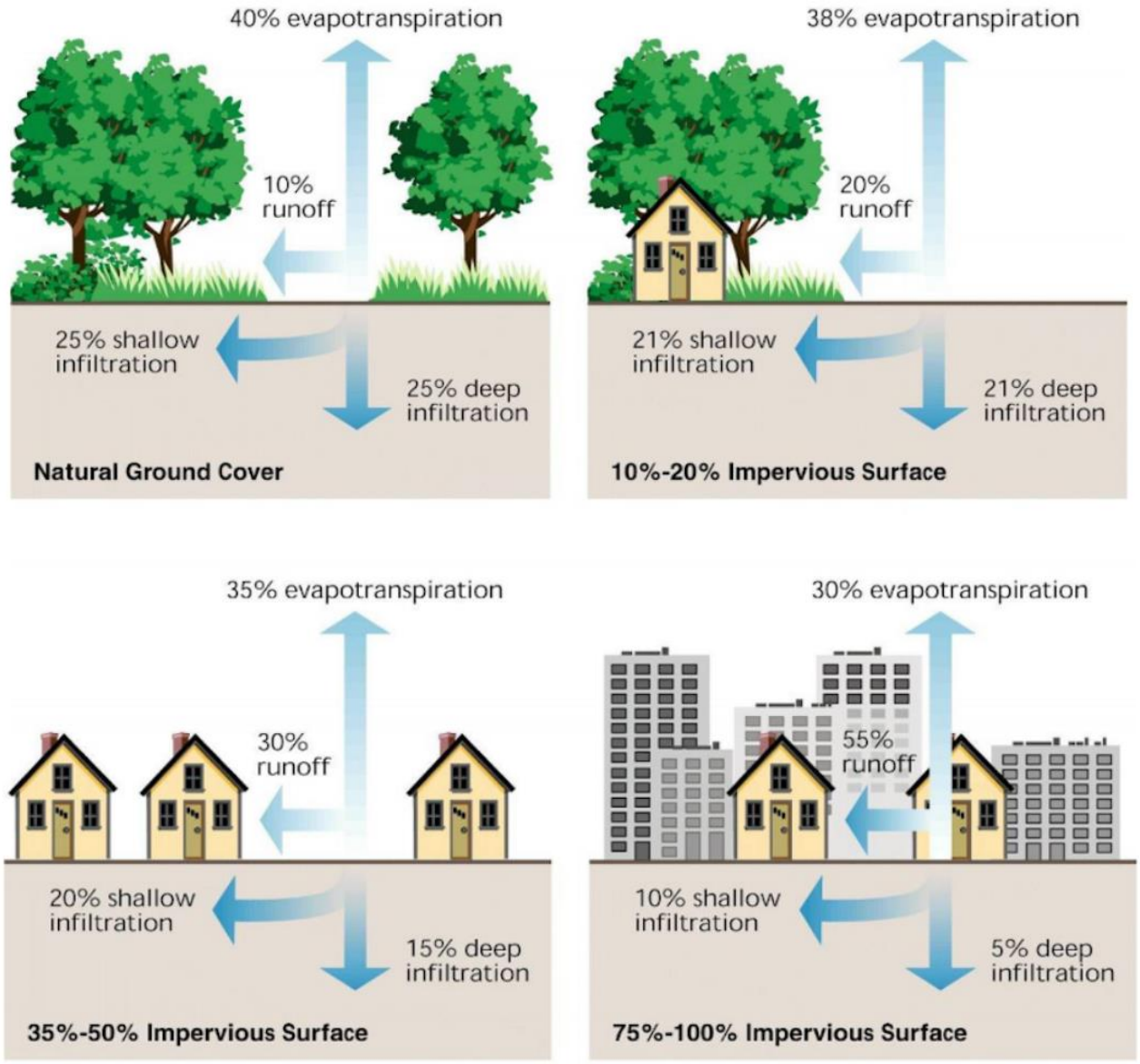

Fig. 1.6 Urbanization impact on infiltration and surface runoff (Vargas, 2016)

Fig. 1.7 Urban flash flood of: (A) Bad El Oued (Algiers, 2001), (B) M'zab wadi (Ghardaia, 2008) (After Boutaghane et al., 2022)

Fig. 1.8 Riverine flood of Boussaada wadi (Bendine, 2019)

1.3.2.3. Flood-causing factors

Flood generation is a non-linear system (Maidement and Tate, 1999). It depends on natural, spatial and temporal variability of meteorological and hydrological parameters, climate variables and land use conditions (Figure 1.9). Therefore, the following points present the main causes of flooding (UNISDR, 2011; Kundzewicz et al., 2014; Adjinacou, 2016; Şen, 2018):

- ✓ Increased urbanization, especially in flood prone regions,
- ✓ Increased paved areas which result in increased runoff rates and prevent infiltration,
- ✓ Climate change impacts due to anthropogenic activities may alter precipitation, evapotranspiration and temperature values (increased flood events and longer dry periods),

- ✓ Reduction of forests (deforestation) and land use changes which decreases the amount of rainfall that is captured by vegetation,
- ✓ Inadequate river regulation,
- ✓ Development of sewer system slower than the development of the city,
- ✓ Human modifications of watersheds have led to change their runoff characteristics.

Fig. 1.9 Damages caused by floods (M'sila city, National roads 40 and 60) (Redjem et al., 2020)

1.3.3. Flood risk

1.3.3.1. Definition of a flood risk

Flood risk is a function of spatio-temporal hazards of floods, exposure to floods, and vulnerability to floods depending on their magnitude and frequency. The intersection of hazard with population and assets represents the exposure, whereas vulnerability refers to the susceptibility of these people and assets to potential loss (EU Flood Directive, 2007; UNISDR, 2011; Phongsapan et al., 2019).

Moreover, flood risk comprises many other domains including flood risk management which is basically divided into two categories as flood risk analysis and assessment, in addition to risk mitigation (Vojtek and Vojtekova, 2016). For example, flood risk assessment is a key component in risk management and reduction. Disaster management aims to avoid or reduce potential risks from floods and assure rapid and appropriate response to flood events (Phongsapan et al., 2019).

1.3.3.2. Flood risk analysis and assessment

Flood risk analysis and assessment are the establishment of highly exposed areas to flooding risk, where mitigation measures should be taken. The most known approach for assessing

flood risk is the product of hazard and vulnerability (EU Flood Directive, 2007). To analyze the flood risk, multiple disciplines are concerned, namely meteorology, hydrology and hydraulics. Thus, flood intensity, hazard categories, vulnerability of the model area, and flood risk can be determined once performing analysis and assessment procedures.

Therefore, some basic steps are indispensable to perform flood hazard and risk assessment along the following points:

- ✓ Estimation of maximum flood discharges out of the gauging stations using rainfall-runoff methods,
- ✓ Preparation (acquisition or generation) of necessary input data (Digital Elevation Model (DEM), slope map, hydrological data, etc),
- ✓ Flood modeling using 1D (for steady and unsteady flow analysis) or 2D (for unsteady flow analysis) hydraulic models, and Geographic Information System (GIS) tools

1.3.3.3. Flood risk mitigation

Group of measures are proposed to evaluate and select to decrease risks in the areas exposed to flooding. With regard to the increasing flood damages, flood prevention and flood risk management are highly important in order to minimize the different flooding consequences and prevent its negative impacts (EU Flood Directive). The following points are key-factors to prevent and mitigate negative flooding consequences:

- ✓ Public awareness
- ✓ Flood risk maps help people as risk from flooding,
- ✓ Geographic Information System (GIS) are useful in analyzing and preparing necessary data in order to better understand the spatio-temporal dynamics of flood risk,
- ✓ Usefulness of short-term preparedness system, where a flooding warning contains specific timely information, based on a reliable forecast (expectation of high water level at a specific timing),
- ✓ Prediction of a change in flood frequency compared to a reference period (100-year flood may occur with a 50-year flood in a defined future time.

1.4. Climate system modeling and climate change impacts on the environment

Understanding potential climate-related impacts on hydrology is important because of its interactions at the basin scale, which are likely to affect water resources management

(Praskievicz, 2009). Climate change is rising as a threat, in particular to poor populations' properties and general health. The following sections introduce the climate change background, concepts, in addition to climate system components and development of climatic modeling and scenarios.

1.4.1. Climate system

1.4.1.1. Definition and components of a climate system

Climate is a synthesis or an average state of weather where atmospheric variables such as temperature, precipitation, air moisture, evaporation and wind speed. It is also considered as a dynamic system resulting from the combined interactions of all these variables (Trenberth, 1992; Robinson, 2001; Goosse et al., 2010, Neelin, 2011, Hong et al., 2014; Mathez and Smerdon, 2018).

According to the World Meteorological Organization (WMO), 30 years is the standard period for performing the statistics used to define climate. This is adapted for studying climate change in recent decades. However, a longer period is necessary when studying the most distant past. Contrary to weather, where only average quantities are considered, climate would include, for example, the probability of an extreme rainfall event, or the range of temperature variations that occur during a specific month or year (Neelin, 2011).

Thus, a climate system includes the analysis of its components behaviour (Figure 1.10). Climate systems are subdivided into two principle categories; namely natural and human systems, i.e., anthropogenic (Hansen, 2015). The natural climate system comprises the atmosphere, hydrosphere, biosphere, cryosphere and lithosphere:

- ✓ Atmosphere : The gaseous envelope surrounding the earth,
- ✓ Lithosphere: Any natural or human-made land surfaces,
- ✓ Hydrosphere : Any liquid water source,
- ✓ Cryosphere : Any solid water source,
- ✓ Land surface and the biosphere: Any living organisms.

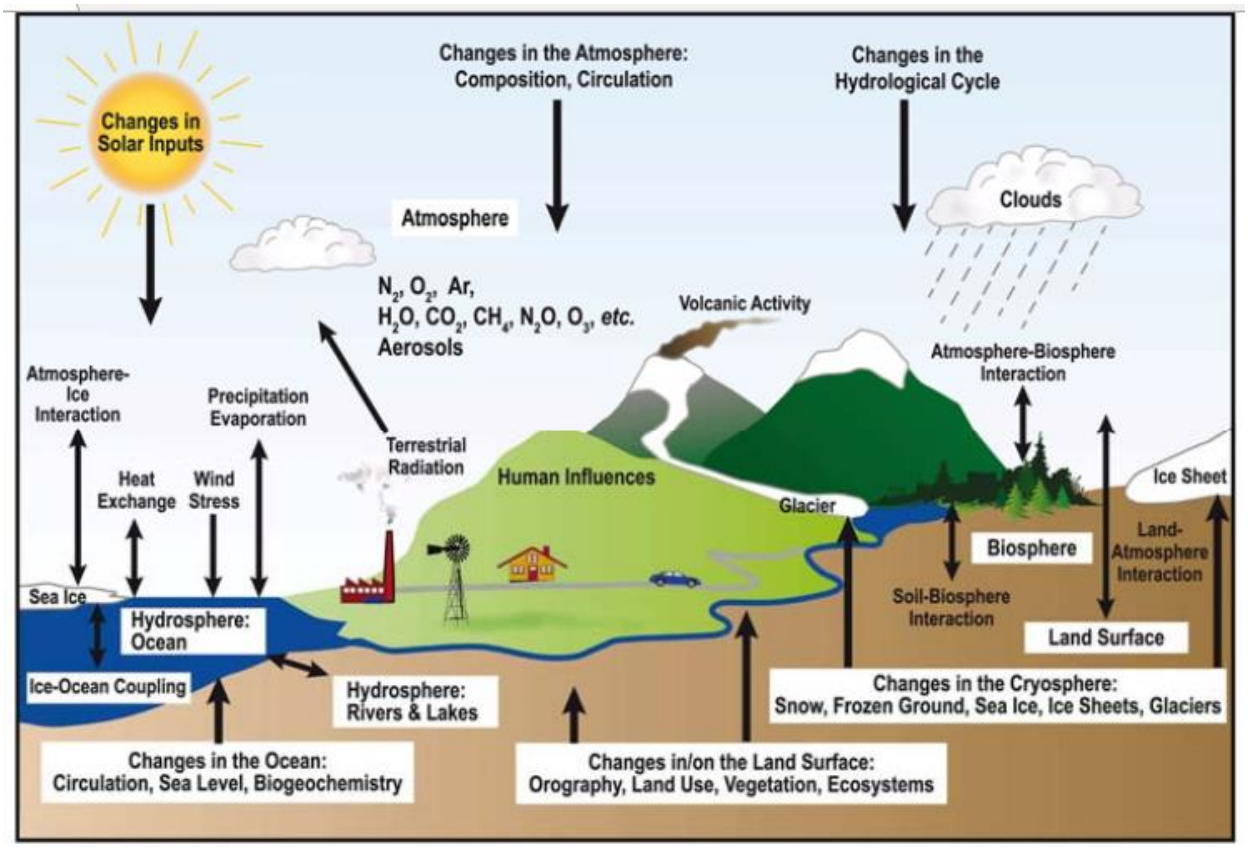

Fig. 1.10 Climate system and its components as represented by IPCC (2007)

1.4.1.2. General circulation of the atmosphere

Atmospheric circulation is the large-scale movement of air, where hot air rises in the tropics, moves towards north and south poles, descends and returns to the equatorial. It is the pattern of wind movement that changes as a result of differences in air temperatures (Goosse et al., 2010). In addition to temperature, precipitation is also influenced by atmospheric circulation which represents the most important variables defining the climate of any region.

1.4.2. Greenhouse effect

The atmosphere is the protective blanket that makes life possible on Earth (Mathez and Smerdon, 2018). Without it, Earth's surface would be frozen. The Sun serves as the primary energy source for our climate on Earth. About 30% of the sunlight is reflected directly back to space, while the rest is absorbed by the surface and the atmosphere, and then re-emitted as heat for the surface. This is called the greenhouse gas (GHG) effect, and it is what serves life on our planet (Schneider, 1992).

Human activities have also started to participate in emitting more GHGs (carbon dioxide, methane, and nitrous oxide) to the atmosphere, since the Industrial Revolution. However,

more greenhouse gases alter the Earth's climate in negative ways, by affecting the number of particles in the atmosphere (Glantz and Krenz, 1992; Goosse et al., 2010). Anthropogenic changes include the ozone hole, acid rain and global warming. These most effective GHGs are given along the following points:

- ✓ Carbon dioxide (CO_2) has both natural and human sources. Its levels are riven principally because of fossil fuels, cement production, deforestation (reduction of CO_2 absorbed by trees), land use changes,
- ✓ Methane (CH_4) : has also both natural and human sources (raising livestock, and growing paddy rice),
- ✓ Nitrous oxide (N_2O): risen levels are primarily because of agricultural activities (fertilizers) and land use changes,
- ✓ Water vapor (H_2O).

A general picture of GHGs existence in the atmosphere is given in Figure 1.11.

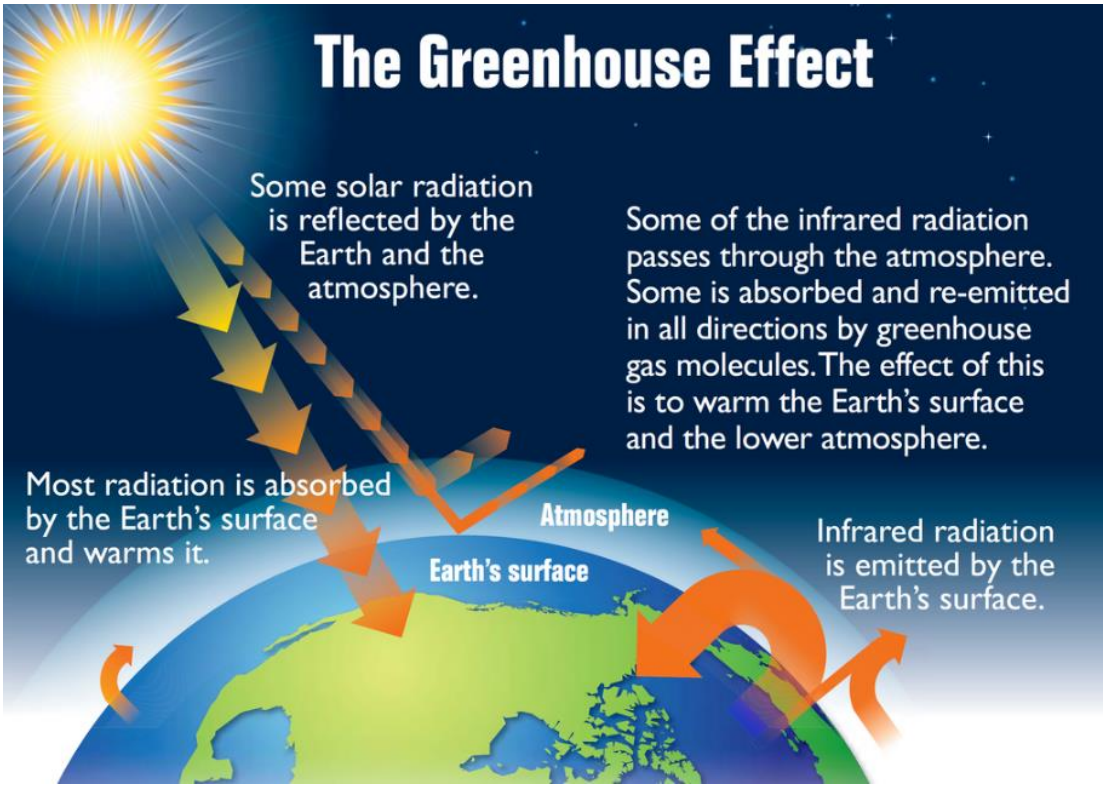

Fig. 1.11 Greenhouse gases in the atmosphere from the US Environmental protection Agency (US EPA, 2012)

The burning of fossil fuels represents a transfer of carbon from the rock reservoir to the surface reservoirs (Mathez and Smerdon, 2018). However, the natural system cannot return the excess carbon to the rock reservoir, and the lifetime of CO_2 in the atmosphere is thousands of years.

Many researchers have found that climate change is likely to accelerate the global hydrological cycle (Oki and Kanae, 2006; Huntington, 2006). This acceleration has evolved the flooding rates in some regions, while other regions have been experiencing water stress. The snowpack reduction during the winter and earlier peak runoff and higher temperatures during spring are some real examples of climate change impacts. Therefore, water quality is highly impacted by increases in temperatures which favorites the growth of algal blooms and decrease in dissolved oxygen and pollutant concentrations (Praskievicz, 2009).

1.4.3. Climate change

1.4.3.1. Definition of a climate change

Global warming is widely known as the rising of Earth temperature. It is the main reason of the change in the global climate that has been witnessed throughout the world. It is the predicted warming, and other associated changes in the climate system, which has begun to occur in response to the increased numbers of GHGs emitted to the atmosphere (Neelin, 2011; Mathez and Smerdon, 2018).

Climate change is the negative effects on the regional landscape system, water cycles, and particularly catchment hydrology, due to the increased concentrations of greenhouse gases (Chowdhury and Eslamian, 2014). It also refers to a statistically significant variation in either the mean state of the climate or its variability, due to natural and anthropogenic changes in the atmosphere and land use (Mujere and Eslamian, 2014).

The basic physics proves that GHGs absorb radiant heat or infrared energy (from measurement and observations), which cause a warming climate. Since 1970s, climate change has caused the death of over 150,000 persons annually, as a result to the higher temperatures and changing in rainfall patterns resulting from global climate change (Marolla, 2013). In general, climate change is believed to pose risks, not only at the global scale, but also regional variability of climate is included (Shameem, 2016).

1.4.3.2. Development of global warming and climate change concepts

Earth's climate has changes throughout history. Many evidences of climate change at regional and global scales have appeared since the late 20th century. In response to the previous-mentioned climate issues, the Intergovernmental Panel on Climate Change (IPCC) has been established.

The World Meteorological Organization (WMO) and the United Nations Environmental Program (UNEP) have established the IPCC initially in 1988. In effect, the main purpose for the IPCC was to provide an international and global recent scientific view (provide policy-makers with regular assessments of the scientific basis) on the current information in climate change, its impacts and future risks on the environmental and socio-economic scale (Neelin, 2011; Mathez and Smerdon, 2018). In addition, adaptation and mitigation options are also included. The IPCC assessment reports were principally a direct pathway to communicate these scientific findings to decision-maker. These studies, from around the world, have been synthesized in the form of Assessment Reports (AR). Table 1.1 below presents history of global warming and proves of climate change existence through different periods.

Table 1.1 History of global warming and scientific development on the climate change issue

Name of scientist/event	Year of research	Domain of study	Reference
Joseph B. Fourier	1822	The atmosphere has trapped part of the radiation from heated surfaces and prevented it from escaping into space. Beginning of using concepts of the warming effect of the atmosphere and the analogy to a greenhouse.	Neelin (2011)
Beginning of the industrial revolution	1850	Building up of the greenhouse gases	Mathez and Smerdon (2018)
John Tyndall	1857	The heat rinsing from the surface of the Earth was blocked by carbon dioxide in the atmosphere	Treut et al. (2007)
John Tyndall	1861	H2O and CO2 are especially important for infrared absorption and thus potentially for climate.	
Jozef Stefan	1868	Development of blackbody radiation law. The greenhouse effect has caused the surface temperature to be much more than the temperature radiated to space.	Neelin (2011)
Svante A. Arrhenius	1896-1908	The impact of increased concentration of carbon dioxide in the atmosphere. The global warming	Arrhenius (1896), Treut et al. (2007), Mathez and

		may be the result of coal burning.	Smerdon (2018)
Guy Stewart Callendar	1938	Development of human-induced global warming theory, and results of fossil fuel burning in emission of millions of tons of carbon dioxide in the atmosphere.	Weart (2010)
Roger Revelle	Late 1950s	Popularization of a global warming as a problem.	Neelin (2011)
Scipps Institute of Oceanography in California	1957	Scientists have declared for the first time, the dangers that might the changing in climate present in next decades	Whitmarsh (2005)
Charles David Keeling	1958	Beginning of CO2 monitoring at Mauna Loa volcano in Hawaii.	Mathez and Smerdon (2018)
Manabe and Wetherald	1967	First 3D global climate model of CO2-induced climate change, known today as GCMs	Neelin (2011)
NASA	1969	Earth's temperature measured with NASA's Nimbus III for the first time	Moser (2010)
US National Academy of Sciences	1979	The Charney report is a study group on CO2 and climate. It is one of the earliest scientific assessments about global warming.	Neelin (2011)
Policy recognition by UN	Late 1980s	Remarkable increase in global annual mean temperature: seven of eight warmest years of the century to that point.	Moser (2010)
British Antarctic Survey Scientists	1985	Ozone hole discovery above Antarctica	Chowdhury and Eslamian (2014)
James Hansen (NASA)	1988	Long-term trend probability towards human-induced global warming, caused by the greenhouse effect	Wilson (2000), Hamblyn (2009)
UNEP and WMO	1988	Initiation of the IPCC to collect and assess evidence of anthropogenic climate change	Moser (2010)
IPCC (FAR)	1990	First assessment report of the IPCC	Whitmarsh (2005)
United Nations	1992	Rio de Janeiro Conference on the environment development; Framework Convention on climate change.	Neelin (2011)
IPCC (SAR)	1995-1996	Second assessment report of the IPCC	Whitmarsh (2005)
Kyoto protocol	1997	Protocol that sets targets on greenhouse gas emissions at 5% by 2008-2125.	Neelin (2011)
IPCC (TAR)	2001	Third assessment report of the IPCC	Whitmarsh (2005)
United Nations	2004	Nine of ten warmest years since 1856 occurred in past ten years	Neelin (2011)

		(1995-2004)	
IPCC (AR4)	2007	Fourth assessment report of the IPCC	Chowdhury and Eslamian (2014)
IPCC (AR5)	2013	Fifth assessment report of the IPCC	Hong et al. (2014)
IPCC (AR6)	2014	Sixth assessment report of the IPCC	Eyring et al. (2016); Tokarska et al. (2020)

1.4.4. Causes and consequences of a changing climate

Knowledge on the climate change causes has been shown to be a key factor of mitigation actions and prediction strategies. As a result of lack of advanced technology and capable manpower, causes leading to changing in climate are increasing, as well as their consequences on the environment. Thus, Table1.2 presents some of the major causes of carbon GHGs emissions and impacts of changing in climate (Trenberth, 1992; Praskievicz, 2009; Chaudhary and Aryal, 2009; Fagan, 2009, Maslin, 2009; Portier et al., 2010c; Marolla, 2013; Mujere and Eslamian, 2014; Hansen, 2015; Olson, 2022):

Table 1.2 Causes, consequences and affected sectors by the changing climate

Causes	Consequences
✓ Increasing urbanization of the world's population and infrastructure development	✓ Increased runoff during winter and decreased summer flows ✓ Decrease in groundwater recharge ✓ Increased disturbances like noise, light, pollution ✓ Shoreline changes ✓ Degradation of coastal ecosystem ✓ Increased wastewater input
✓ Increasing global warming (Heat waves)	✓ More destructive floods (flash floods) ✓ Long drought periods (evapotranspiration, desertification) ✓ Large and destructive wildfires ✓ Snow melting (salination of freshwater supplies as a result of sea level rise) ✓ Warming soil ✓ Change in water supply ✓ Change in air quality (higher temperatures affect the range and concentration of air pollutants)
✓ Land use and land cover change (conversion of meadows to croplands, construction of dams)	✓ Biodiversity loss ✓ Changes in soil carbon and nutrient balance ✓ Desertification

	✓ Erosion ✓ Morphology change
✓ Pollution (pesticide and nutrient runoff into rivers and lakes, increased NOx input)	✓ Change in ecosystem composition ✓ Fertilization effect on forests ✓ Change in soil dynamics
✓ Technological change	✓ Increase in water use ✓ Change in the composition of micro-organisms in soil and soil water balance ✓ Human health decline
✓ Anthropogenic activities (emission of greenhouse gases, fossil fuel utilization, industrial and agricultural practices)	✓ Change in the atmospheric composition and global warming (carbon dioxide CO2, nitrous oxide N2O, methane CH4, ozone O3, sulfur hexafluoride SF6, primary aerosols (black carbon, organic carbon), and secondary aerosols (sulfate, nitrate, ammonium)) ✓ Deforestation (reduction of rainforests which can absorb some of carbon dioxide)

1.4.5. Assessment and modeling of climate change

Climate change has emerged over the past decades, as a global issue. Enhanced greenhouse gases or human-induced greenhouse gases are suggested to be the main cause for this increase in carbon dioxide concentrations in the atmosphere. Many climate research centers around the world have developed measurement tools for global temperatures, carbon dioxide concentrations and other climatic variables to track any changes. Moreover, climate modeling using super developed computers has increasingly been utilized, since 1959, to validate observations and predict climate changes (Whitmarsh, 2005). By 2100, greenhouse gas emissions are suggested to be five times higher.

1.4.5.1. Climate modeling

A model is a simplification of reality. Climate modeling is a very important area of climate science where mathematical models are used (Neelin, 2011). They can be as defined as mathematical representations of the climate system which typically consist of equations for many climate variables (Figure 1.12). Therefore, the climate system is based on physical, biological, and chemical principals (Goosse et al., 2010). They have been developed to perform climate projections, as well as identification of the role of a particular process in the climate system.

As the equations governing the climate system laws are so complex, climate models serve a numerical solution for these equations. In addition, climate models require some observations or other models studies. Therefore, climate models are developed ultimately along many lines of computer code that represent equations for calculating how energy, mass and momentum move through the climate system. These calculations are performed on supercomputers. These equations are partial differential equations (PDFs). The finite difference method is one of the easiest methods of numerically solving partial differential equations (Goosse et al., 2010).

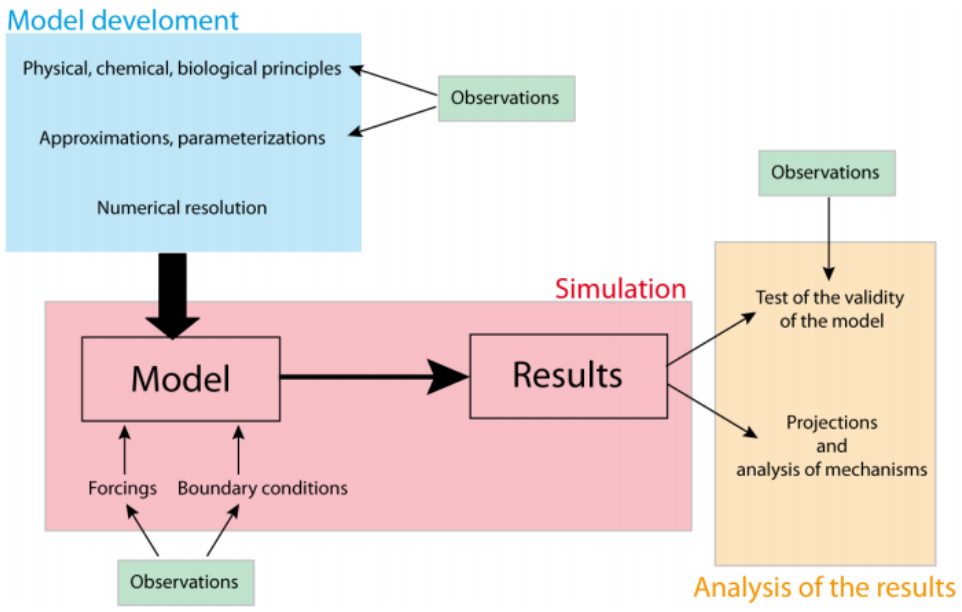

Fig. 1.12 Representation of climate models development (adapted from Goosse et al., 2010)

Effectively, the community of climate modeling, including multiple climatic research centers, has synchronized the climate system models development with the IPCC assessment cycles (Hansen, 2015). This has been achieved using several portals known as the Earth System Grid Federation (ESGF) portals, such as *https://esgf-node.llnl.gov/*. They provide access to the output of the climate models contributing to all Assessment Reports of the IPCC through the Coupled Model Intercomparison Project (CMIP).

The Coupled Model Intercomparison Project (CMIP) has started twenty years ago in response to a growing need to systematically analyze models outputs from multiple climate modeling centers (Carlson et al., 2017). Well-defined model experiment protocols, and distribution mechanisms were introduced in CMIP principally to ensure model output availability to the whole scientific public community (Figure 1.13).

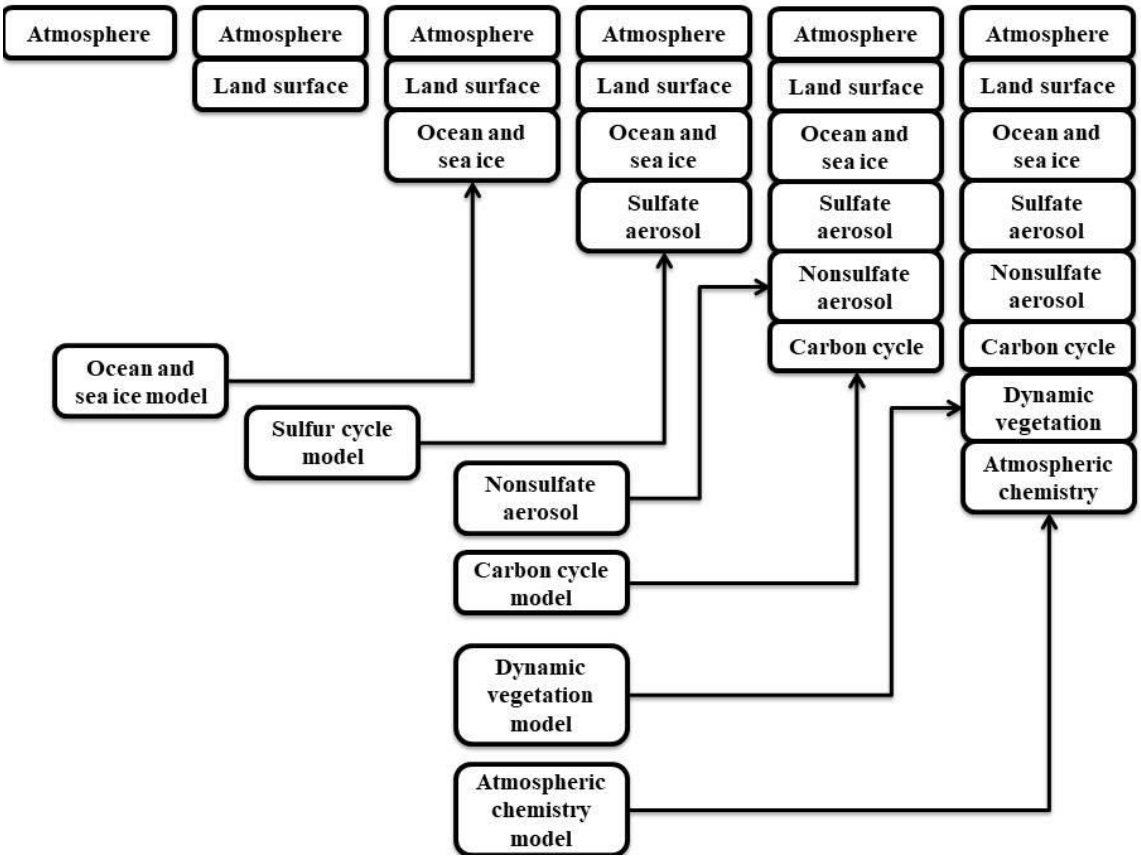

Fig. 1.13 Development of climate models (IPCC, 2001)

1.4.5.2. Global Climate (Circulation) Models (GCMs)

The examination of climate change impacts on water resources began with series of models usually from the IPCC's emission scenarios, which are, then, used in General Circulation Models (GCMs). Hence, to understand the meaning and usefulness of GCMs and Emission Scenarios in climate change studies, detailed definitions are given as follows:

GCMs are big physical accounting machines that calculate the flow of mass, energy and momentum through gridded volumes of space in the atmosphere, ocean and land surfaces (Mathez and Smerdon, 2018). The closer the grid points, the better the model's spatial resolution.

As one of the first goals of climate models was to simulate the three dimensional structure of wind, hence the GCMs were introduced (Goosse et al., 2010). These models were then divided into two separate parts, as Atmospheric General Circulation Models (AGCMs), and Ocean General Circulation Models (OGCMs) (Neelin, 2011; Mathez and Smerdon, 2018).

For about last three decades, GCMs are applied to simulate climatic sensitivity to increased concentration of GHGs to predict future climatic change (Chowdhury and Eslamian, 2014). They have been developed over decades to study the global climate impact. GCMs nowadays are capable of capturing global climate characteristics temporally and spatially.

However, GCM outputs usually have coarse resolutions and perform poorly at smaller scales, therefore inappropriate for regional impact assessment (Hong et al., 2014). For this reason, downscaling techniques are applicable for regional and local studies. These techniques are given in detail in the next sections. A performance comparison study among many GCMs in the projection of any climate variable is required. Therefore, a unique climate model can then be selected following its good performance. Figure 1.14 shows observed and simulated precipitation patterns.

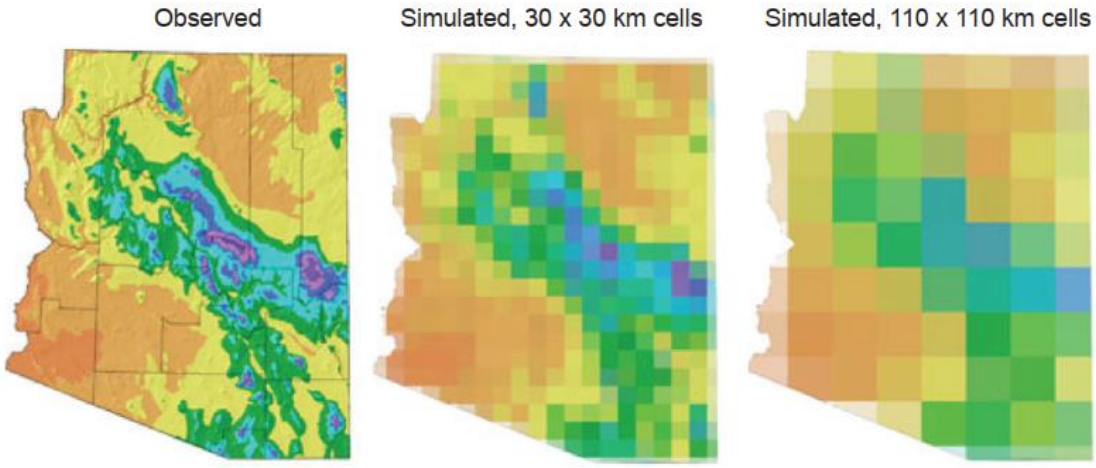

Fig. 1.14 Representation of precipitation patterns over Arizona (USA) (Mathez and Smerdon, 2018)

Seven equations formulate the atmosphere, where are: three components of the velocity V, the pressure p, the temperature T, the specific humidity q, and the density ρ (Goosse et al., 2010), which are:

- The first three belongs to Newton's second law (momentum balance, force equals mass times acceleration $\vec{F} = m.\vec{a}$),

$$\frac{d\vec{V}}{dt} = -\frac{1}{\rho}\vec{\nabla}p - \vec{g} + \vec{F}_{fric} - 2\overrightarrow{\Omega}\, x\, \vec{v} \qquad (Eq.\ 1.1)$$

  Where d/dt is the total derivative,

$$\frac{d}{dt} = \frac{\partial}{\partial t} + \vec{v}\,.\overrightarrow{\nabla} \qquad (Eq.\ 1.2)$$

And $\vec{g}$ is the apparent gravity vector, $\vec{F}_{fric}$ is the force due to friction, and $\overrightarrow{\Omega}$ is the angular velocity vector of the Earth.

- The continuity equation

$$\frac{\partial \rho}{\partial t} = -\overrightarrow{\nabla} . (\rho\, \vec{v}) \qquad (Eq. 1.3)$$

- The conservation of mass of water vapour equation

$$\frac{\partial \rho q}{\partial t} = -\overrightarrow{\nabla} . (\rho\, \vec{v} q) + \rho\,(E - C) \qquad (Eq. 1.4)$$

Where E and C are evaporation and condensation respectively

- The first law of thermodynamics (the conservation of energy)

$$Q = C_p \frac{dT}{dt} - \frac{1}{\rho} . \frac{dp}{dt} \qquad (Eq. 1.5)$$

Where Q is heating rate per unit mass and Cp the specific heat

- The equation of state

$$p = \rho\, R_0\, T \qquad (Eq. 1.6)$$

1.4.5.3. Emission scenarios

Various types of scenarios have been developed by the IPCC (Table 1.4) during the recent years and past decades (Hong et al., 2014; Chowdhury and Eslamian, 2014; Eyring et al., 2016; Tokarska et al., 2020). Generally, emission scenarios are used in GCMs on the basis of large-scale simulations to predict the response of climate to the projected increase in GHG concentrations (Praskievicz, 2009).

Global warming is associated with a global increase in precipitation, as a result of the huge evaporation over the oceans and increase in water-holding capacity of the atmosphere in warm regions. Different models and scenarios are used for the prediction of temperature and precipitation changes. Increased warming would increase evaporation rates, and as a result, increase the capacity of the atmosphere to hold water in-between precipitation events (Brooks et al., 2013).

The climate scenario or emission scenario is the use of an indication of what future may look like over the decades or centuries, given a set of assumptions, including land use change and future emissions of greenhouse gases (Trzaska & Schnarr, 2014; Ayalew, 2019). The first and second sets of SA90 and IS92 scenarios were utilized in 1990 and 1992, respectively. Moreover, the Special Report on Emission Scenarios (SRES) had been used since 2000 after the Third and Fourth Assessment Reports (TAR & AR4). The Sixth and Fifth Assessment Reports (AR5 and AR6) confirmed the usefulness of Representative Concentration Pathways (RCPs) and Shared Social Pathways (SSPs) compared to previous SRES scenarios (Gidden et al., 2019; Van Vuuden et al., 2011), which correspond to CMIP5 and CMIP6 respectively.

In the first assessment report (FAR) of IPCC, the most important factor in the radiative forcing was the increase carbon dioxide at 1.5-4.5°C with approximately 60% compared climate (IPCC, 1990). The second assessment report (SAR) has estimated the well-mixed greenhouse gases to be 1.56 Wm^{-2} from carbon dioxide as the highest surface air temperature value, and a range of 1.0-3.5°C surface air temperature (IPCC, 1996). In the third (TAR), fourth (AR4) and fifth assessment report (AR5), the carbon dioxide radiative forcing was 1.46, 1.66 and 1.68 Wm^{-2} and equilibrium climate sensitivity range was 1.5-4.5°C, 2.0-4.5°C and 1.5-4.5°C respectively (IPCC, 2001; 2007; 2013). The SSP2-4.5 (5-8.5) considers radiative forcing of 4.5 (8.5) Wm^{-2} and predicts an increase of 1.8±0.7 (3.7±1.1) °C globally before the twenty-second century (IPCC, 2014; Ajjur and Al-Ghamdi, 2021). All these emissions scenarios are given in Table 1.3.

According to the World Meteorological Organization's (WMO) 2020 State of the Global Climate Report, the average global temperature reached 1.2 °C, during 2020, and is classified as one of the hottest years in all records measured globally. Currently, changes in precipitations, temperature, evaporation, wind, and sea levels prove the outcomes of previous future projections studies (Bustos Usta and Torres Parra, 2021; Gehrels, 2010). The temperature of the Earth's surface depends on the incoming and reflected solar radiation (Ayalew, 2019). It increased by about 0.74°C ± 0.18°C between 1906 and 2005 (IPCC, 2007,2013; Mahmood et al., 2019). The concentration of CO_2 in the atmosphere will double in 2100 and the average temperature will also increase between 1.4 and 5.8°C in 2100. These changes will lead to sea level among other negative consequences (IPCC, 2007).

Table 1.3 Emission scenarios developed by the IPCC and their details

Assessment Report (AR) of IPCC	Developed scenarios	Purpose of the AR emission scenarios	Scenario families of possible future change
4th AR (IPCC AR4)	Special Report on Emission Scenarios (SRES)	The main driving forces influencing the emission scenarios from demographic, social and economic development are identified. The results are future emissions of greenhouse gases and land use changes until the year 2100.	Four families: -A1 corresponds to a very rapid economic growth, low population increase, and the rapid technology (where A1F means fossil intensive, A1F is nonfossil fuels, and A1B is the balance across all sources). -A2 corresponds to a high population growth, and slow technological change. -B1 corresponds to a low population growth and facter technological change than in A1. -B2 corresponds to intermediate population and economic growth, and less rapid technological change than in B1 and A1.
5th AR (IPCC AR5)	Representative concentration pathways (RCPs)	Socio-economic changes are included. The advantage of these new scenarios is that they include future changes to short-term (2035) and long-term (2300)	Four families: -RCP8.5 (the most extreme one) corresponds to a continuous increase of radiative forcing (8.5 W.m-²). -RCP6.0 and RCP 4.5 correspond to a steady rise of radiative forcing (6 and 4.5 W.m-² respectively). -RCP3-PD (peak and decline) corresponds to a peak of 3 W.m-² and then declines
6th AR (IPCC AR6)	Shared Socio-economic Pathways (SSPs)	Socio-economic scenarios are used to derive emissions scenarios without (baseline period) and with climate policies (mitigation scenarios). They are also used to derive climate change projections. In addition to their ability to better integration of mitigation, adaptation and climate impact research in future assessments.	Four families: -SSP1-2.6 (low challenges for mitigation (resource efficiency) and adaptation (rapid development)) -SSP2-4.5 (high challenges for mitigation (regionalized energy) and adaptation (slow development) -SSP3-7.0 (low challenges for mitigation (global high tech economy), high for adaptation (regional low technology economies)

	-SSP5-8.5 (high challenges for mitigation (fossil fuel intensive) and low for adaptation (rapid development))

The most important question about climate models is whether they can be trusted? Although there are numerous methods, but none is sufficient alone, and so they should be all verified (Goosse et al., 2010). Therefore, large numbers of observations are needed to test the validity of the models in order to gain confidence in the conclusions derived from their results.

1.4.5.4. Downscaling techniques

As these large-scale simulation outputs are not useful for hydrological applications, a downscaling procedure must be performed. In light of the downscaling outcomes, hydrological models can be applied to basin-scale studies. Furthermore, these outcomes can be used as inputs to water resources management models for the socioeconomic aspects.

The dynamical and statistical downscaling are the most known techniques (Hong et al., 2014; Chowdhury and Eslamian, 2014; Mujere and Eslamian, 2014), where:

The two downscaling techniques commonly used in regional and local studies are as follows:

- ✓ Dynamic downscaling methods require the application of Regional Climate Models (RCMs) to the GCM outputs. However, they are too expensive and hard to use.

- ✓ Statistical downscaling methods find the statistical relationship between large-scale climate features and local climate, and then simply perform the downscaling to the GCM outputs. They are more popular than the dynamic ones. However, they are less relevant compared to RCMs. Weather classification, weather generator, and regression models are the three branches of this downscaling technique.

1.4.6. Strategies for tackling climate change

As climate change has started to be considered as a serious threat to the public security and health, multiple countries and organizations (IPCC) around the world have been working together to mitigate the impacts of climate change and reduce carbon emissions. To combat global warming and climate change and search for the way out of unwanted future conditions that are likely to happen, three are indispensable: adaptation, legislation, and also mitigation (see Table 1.4).

Table 1.4 The three major strategies for combating climate change (Stakhiv, 1996; Burton et al., 1998; Pittok and Jones, 2000; Neelin, 2011; Farzaneh et al., 2014; Olson, 2022).

Strategy	Details
Adaptation	✓ Reduce our vulnerability to the harmful effects of climate change (new food systems, new crops, new ways of coping with a changing climate), ✓ Different actions that attempt to minimize the impacts of climate change as it occurs. ✓ It makes the system prepared to overcome the present situation in order to lessen the burden in the future, ✓ It is the process or action that stakeholder groups try to maximize benefits and minimize damages
Legislation	✓ Laws and and international conventions that encourage protection of environment and reduce its degradation. Laws that restrain carbon production
Mitigation	✓ Reduce human interference with the climatic system and stabilize GHG levels can allow the natural adaptation of ecosystems to changing in climate, ✓ Strong policies are required for any carbon emission decrease, ✓ They are multiple actions aimed at limiting the size of the climate change

The useful technologies that are expected to come into play in reducing global emissions include the following points (Mathews, 2007; Farzaneh et al., 2014)

- ✓ Reducing deforestation (reforestation, compensating countries for preserving rainforest),
- ✓ Banning aerosols,
- ✓ Implementing air pollution controls,
- ✓ Energy conservation (generation and furtherance of markets for renewable electricity energy generation like wind power, solar power, and hydroelectric power),
- ✓ Green driving (Use of electric motors for transport),

- ✓ Carbon can be captured from the atmosphere to being used so that it cannot return to the atmosphere,
- ✓ Isolate carbon dioxide from the atmosphere (decarbonization) (Capture of carbon from fossil fuels, it is compressed, and then injected back into geological formations),
- ✓ A global carbon pricing regime (an effective and market-driven system to reduce carbon emissions by introducing taxes),
- ✓ Global satellite monitoring of GHG emission (to control the product the GHG emissions to ensure that countries are adopting emission rules regulated for them).

1.5. Conclusion

Climate change is a global and long-term phenomenon. What we do know from the available records, both geological and observational, is that the climate is changing. Our planet's climate is warming, CO_2 and other GHGs concentrations are increasing in the atmosphere because of fossil fuels burning. From these previous definitions, we have concluded that hazards are natural phenomena which occur in inhabited and uninhabited areas, while risk and disaster can only occur where people and infrastructures are located. Flooding is understood to be an impact of climate change. For example, future water stress, particularly in the Mediterranean and semi-arid regions, will be influenced by climate changes and more water demand as a result to population growth.

Moreover, in this chapter, climate change impacts on the environment have been also included. Although numerous studies on climate change impact have been performed, most of these studies acted as just initials step, using previous climate models, towards developed new climate models and global simulations. This day-to-day development ensures better understanding of current climate and update of any previous projections that were effectively based on old climate scenarios.

CHAPTER 2

Study area: the large Hodna basin

Chapter 2 Study area: the large Hodna basin

2.1. Introduction

The purpose of this chapter is to highlight the main features of the Hodna basin as a study basin, and the hydrological and physical behavior of its constituted rivers.

2.2. Geographical location of Hodna basin

In the center of the vast Sahara Desert from the coastal region of the Mediterranean is one of Algeria's largest river basins. The Hodna basin is located between latitudes 36°10' in the North and 34°29' in the South and longitudes 3°02' West and 6°11' East (Adoui, 2013; Boudjemline and Semar, 2018; Zeroual, 2022). The Hodna basin (Figure 2.1) is a plain surrounded by mountains and characterized by a 26,000 km² landlocked bowl (Savornin, 1908; Hasbaia et al., 2012; Hasbaia and Adoui, 2015).

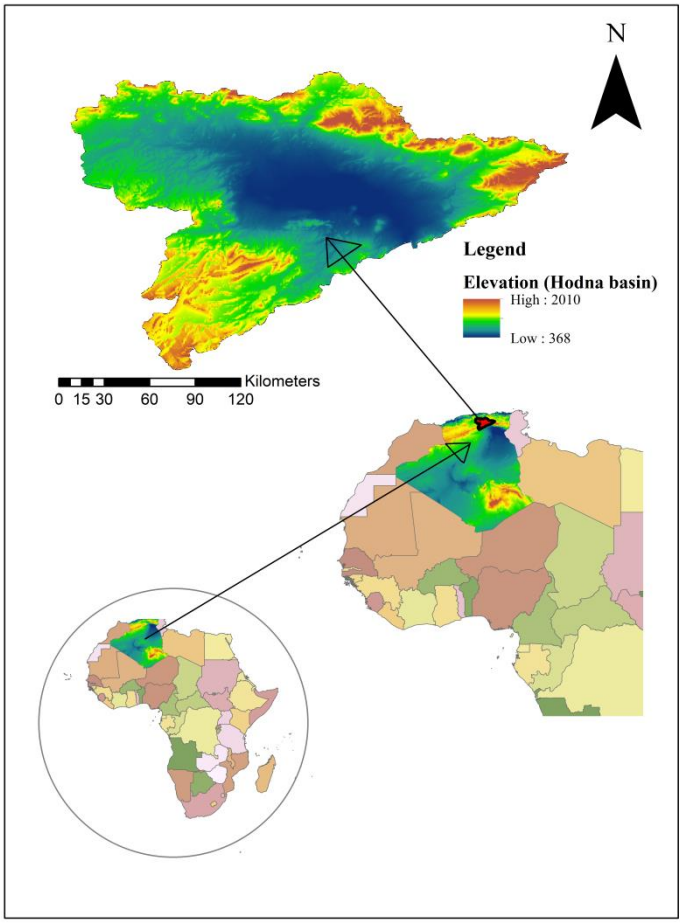

Fig. 2.1 Geographical location of Hodna basin (Belazreg et al., 2023)

The lowest and middle part of the Hodna basin consists of a salty lake called Chott-El-Hodna. It covers an area of approximately 1,150 km² and reaches an altitude of 400 m (Kebiche, 1994; Abdesselam et al., 2013; Messad and Moussai, 2015; Amroune et al., 2020; Khoudour et al., 2021). It is also the outlet of many rivers and is covered only by water in winter (Figure 2.2), dry and covered with salt crust in summer (Figure 2.3) (Ladgham-Chicouche and Zerguine, 2001).

Fig. 2.2 Saline lake "Chott-El-Hodna" during rainy season (after Barech et al., 2016)

Fig. 2.3 Saline lake "Chott-El-Hodna" during dry season (after Messad and Moussai, 2015)

The Hodna basin extends into numerous subdivisions (communes) of the states of M'sila, Batna, Bordj Bou Arriredj (BBA), Setif, Medea, Djelfa and Bouira; Including Maadhid,

M'tarfa, M'sila, Souamaa, Ouled Madhi, M'cif, Mâarif, Khoubana, Houamed, Boussaada (see Figure 2.4 and 2.5).

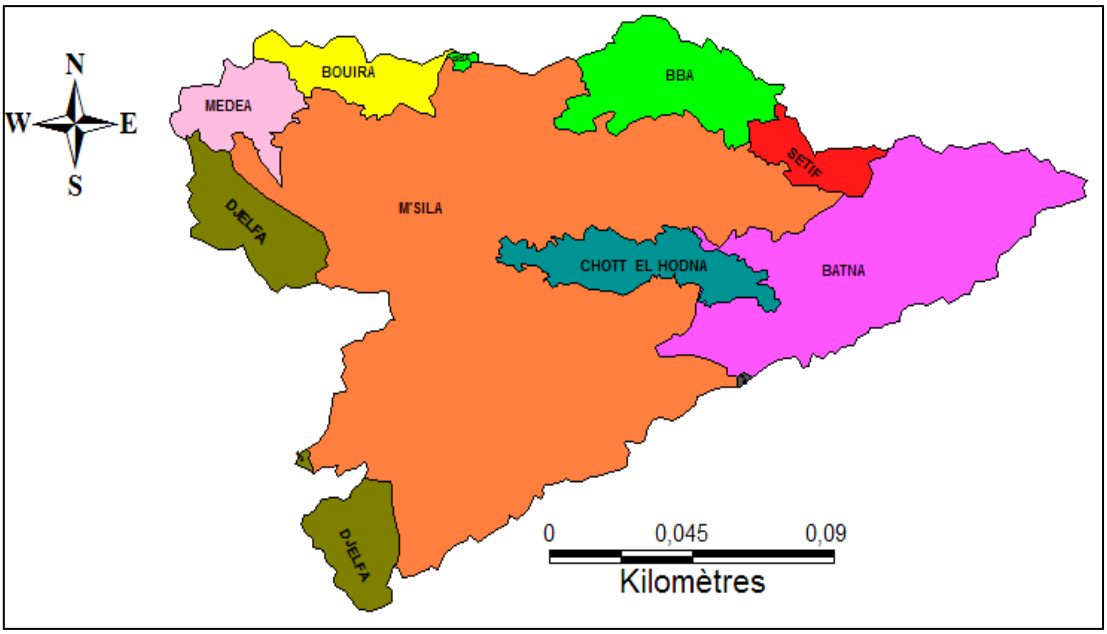

Fig. 2.4 Administrative location of Hodna basin (Adoui, 2013)

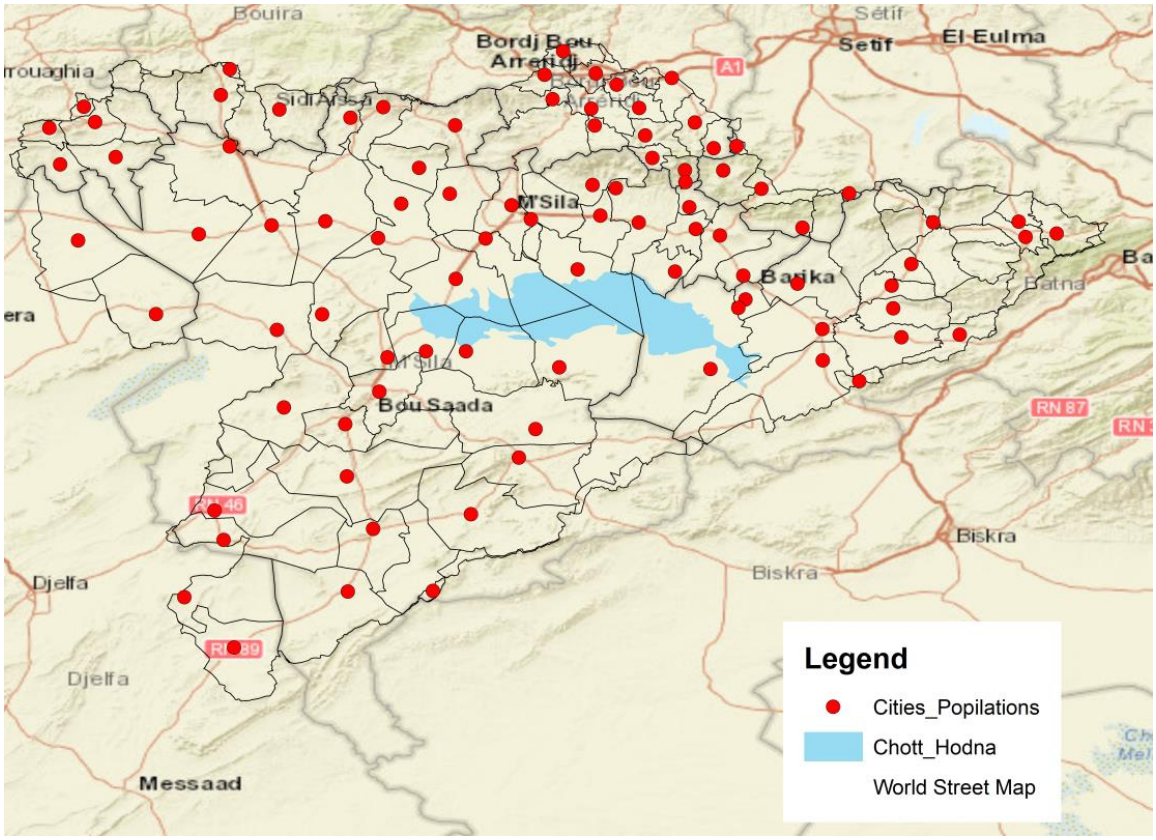

Fig. 2.5 Communes of Hodna basin cities

2.3. Morphometric characteristics of Hodna basin and corresponding sub-basins

The majority of Hodna wadis are characterized by long dry spells including short wet spells. Several wadis constitute the Hodna basin, namely El-Ham, Leham, Lougmane, Barika, Boussaada, M'cif, K'sob, and Soubella wadis, as presented in Figures 2.6, 2.7 and 2.8.

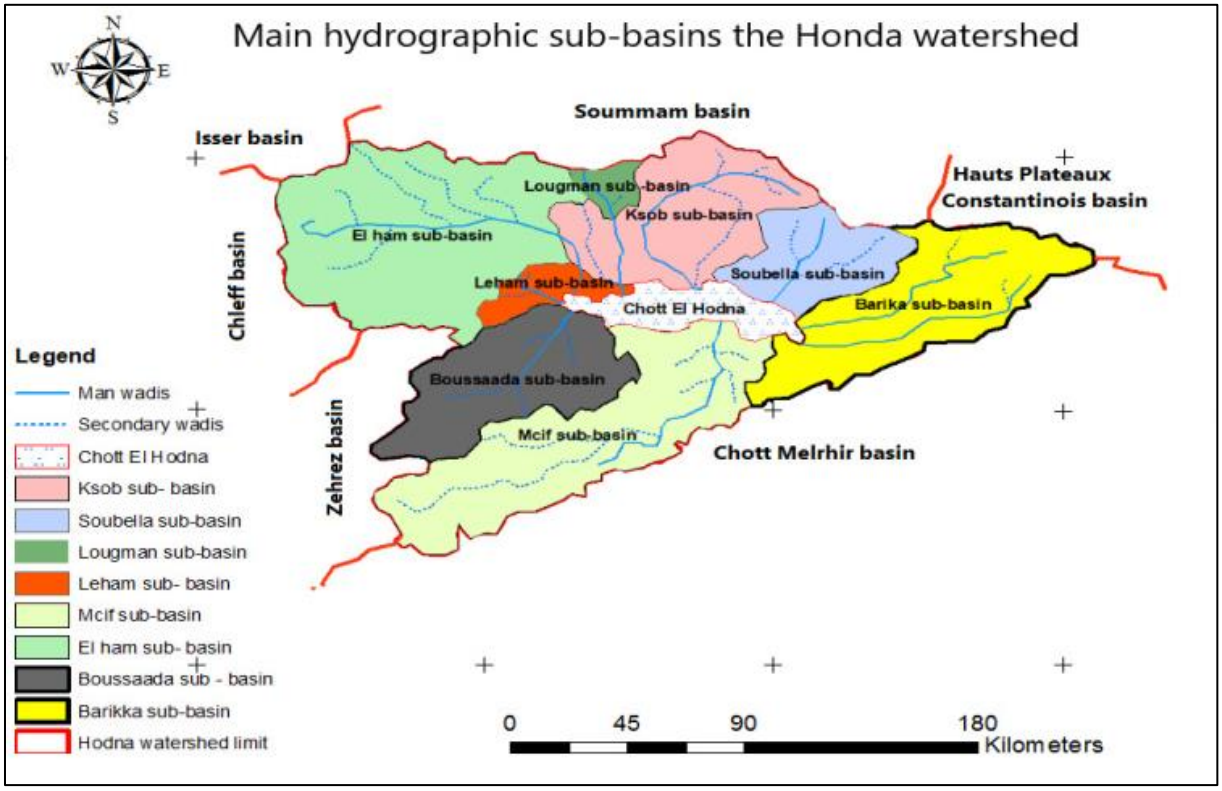

Fig. 2.6 Delimitation of Hodna's sub-basins (adapted from Khoudour et al., 2021)

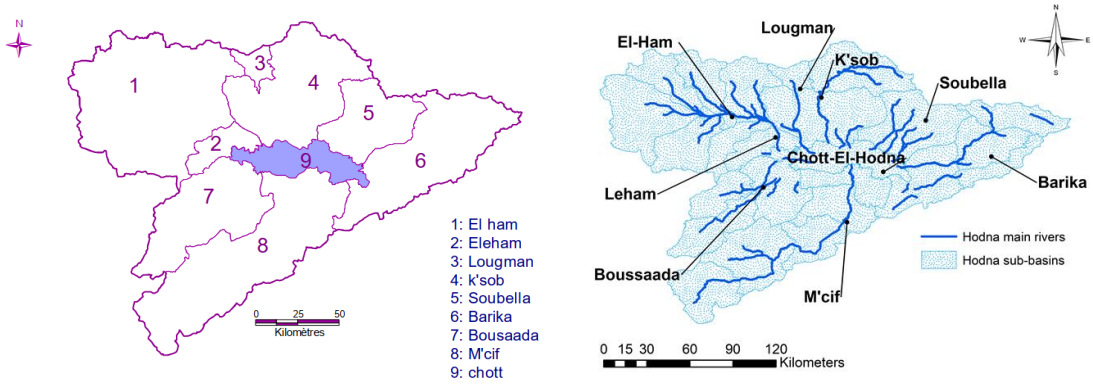

Fig. 2.7 Main wadis of Hodna basin (modified from Hasbaia and Adoui, 2015)

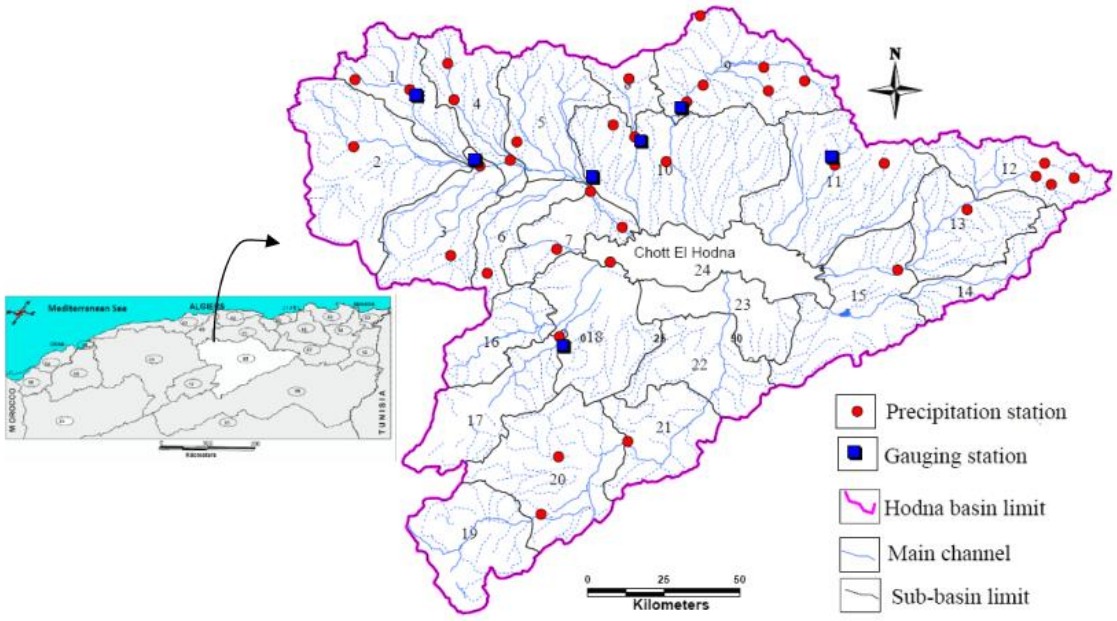

Fig. 2.8 Watersheds of each sub-basin in the large Hodna basin (after Kebiche, 1994; Hasbaia et al., 2012)

Where: 1) El-Ham, 2)Sbissebe, 3)Guernini, 4)Djenene, 5)Torga, 6)El-Karse, 7)El-Leham, 8)Lougman, 9)K'sob, 10)M'sila, 11)Soubella, 12)Barika Amont, 13)Barika Aval, 14)Barriche, 15)Bithem-Barika, 16)Maiter Amont, 17)Boussaada, 18)Maiter Aval; 19)Ain Rich, 20)Chair Amont; 21)Chair Aval; 22)M'cif Amont, 23)M'cif Aval; 24)Chott El-Hodna

Morphometric characteristics of each watershed are explained in details in the following points:

2.3.1. Drainage area (A)

The drainage area (A) is a space where all streams and rivers in a basin flow towards a unique outlet. Therefore, it can be calculated using any GIS tool and then classified as large, average or small basin (Table 2.1). The term drainage basin is usually used in American whereas watershed in England and catchment.

Table 2.1 Basin classification according to Chow (1964)

Basin area (km²)	Classification
<25	Very small
25-250	Small
250-500	Intermediate-small
500-2500	Intermediate-large
2500-5000	Large
>5000	Very large

2.3.2. Perimeter (P)

The perimeter is the outer boundary of a drainage basin that limits its drainage surface area. The Hodna basin has a circumference of approximately 1,053 km. GIS tools are useful in determining these features.

2.3.3. Gravelius Compactness index (K_G)

The surface shape of a drainage basin gives the runoff hydrograph shape physically. The compactness coefficient proposed by Gravelius (1914) is one of the most widely accepted shape indexes. For example, a circular basin is defined by a short concentration period before peak flow is recorded at the outlet. The higher the K_G, the more is the elongation (Figure 2.9). The Compactness Index (K_G) is expressed by the following law:

$$K_G = \frac{P}{2\sqrt{\pi A}} = 0.28 * \frac{P}{\sqrt{A}} \qquad (Eq.\ 2.1)$$

Where: P is the circumference of the basin (km); A is the drainage area (km²); K_G is the compactness index (KG = 1 compact pool and KG > 1.3 long pool).The compactness index of the Hodna basin is equal to 1.85.

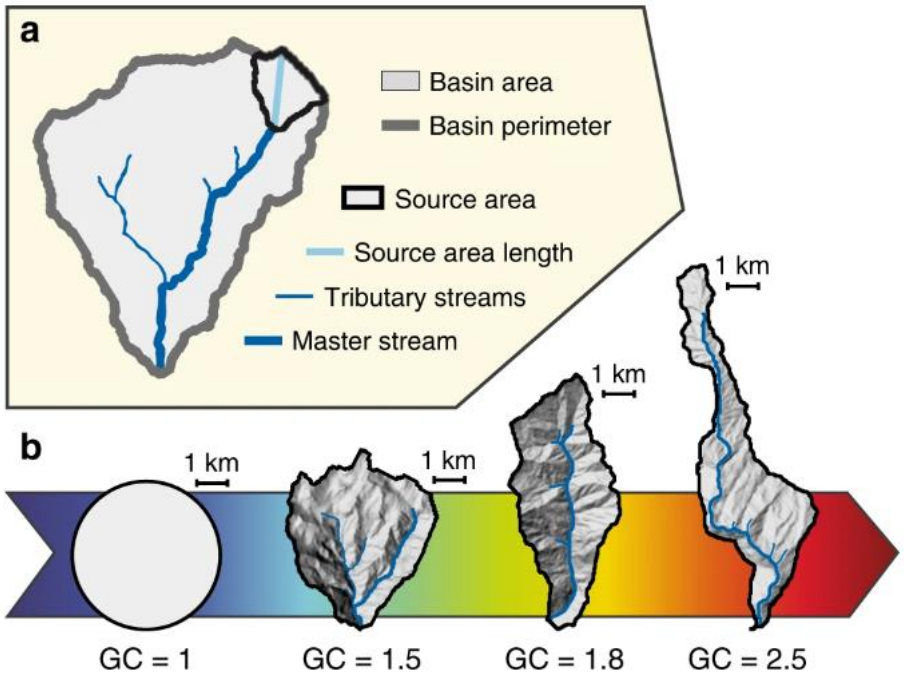

Fig. 2.9 Different basin shapes associated with Gravelius coefficients (K_G is referred here as GC) for a constant basin area (17.5 km²) adapted from Sassolas-Serrayet et al. (2018)

2.3.4. Equivalent rectangle

The term equivalent rectangle is used to compare the hydrological behavior of two different drainage basins. Thus, the length L and width l, for a drainage area, are given by the following expressions (Roche, 1963):

$$L = \frac{K_G \sqrt{A}}{1.12}\left[1 + \sqrt{1 - \left(\frac{1.12}{K_G}\right)^2}\right] \qquad (Eq.2.2)$$

$$l = \frac{K_G \sqrt{A}}{1.12}\left[1 - \sqrt{1 - \left(\frac{1.12}{K_G}\right)^2}\right] \qquad (Eq.2.3)$$

Where: L and l are the length and width of a rectangle, respectively; A is drainage (km²); K_G is the compactness index. The length L and width of the study drainage area are 476.76 km and 54.18 km, respectively.

2.3.5. Relief, hypsometry, and corresponding altitudes (H_{max}, H_{min}, H_{mean} and $H_{50\%}$, $H_{5\%}$, $H_{95\%}$)

Relief is primarily the result of geological evolution and erosion over the past time. It is usually expressed by topography (Figure 2.10). The minimum altitude represents the lowest level in a drainage river basin, usually at the outlet. On the contrary, the maximum height represents the highest altitude. For example, the Hodna basin has low altitude equal to 351 m and high altitude equal to 2157 m.

Analysis of the hypsometry of a drainage basin mainly deals with the drainage area and elevations of the basin in order to understand the influence of topographic, climatic and geological factors. Therefore, GIS tools are often used to obtain basic split areas.

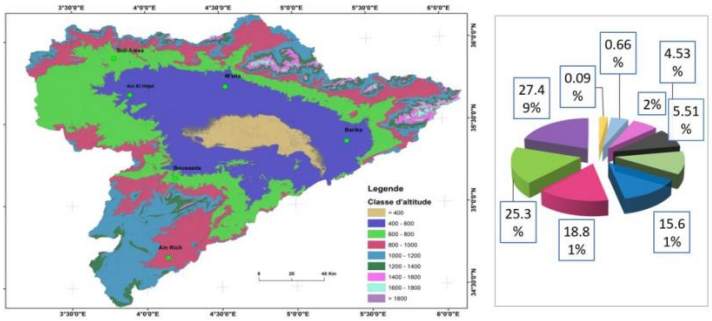

Fig. 2.10 Hypsometric map of the Hodna basin to the left, and the basic split areas to the right side (after Zeroual, 2022)

Average height represents the ratio between the sum of the foundation split areas per average, A_i, foundation height, H_i, and the total drainage area, A_{tot}.

$$H_{mean} = \sum \frac{A_i \; x \; H_i}{A_{tot}} \qquad (Eq. 2.4)$$

The average height of the studied basin is equal to 682 m and is calculated by the previous expression (Table 2.2).

Also, $H_{50\%}$, $H_{5\%}$ and $H_{95\%}$ are projections of points corresponding to 50%, 5% and 95% of the cumulative areas of the hypsometry curve. These altitudes define the spatial distribution of elevations in the drainage basin. For the Hodna basin, their amounts are 735, 1,300 and 396 m, respectively.

Table 2.2 Distribution of the drainage area along with the different altitudes (after Zeroual, 2022)

Altitude (m)	Minimal Altitude (m)	Split areas		Cumulated areas		Sum
$H_i - H_{i+1}$	H_{min}	A_i (km²)	A_i (%)	$\sum A_i$ (km²)	$\sum A_i$ (%)	$A_i * H_i$ (m.km²)
351 - 400	351	1424.3	5.51	1424.3	5.51	499929.3
400 - 600	400	7095.9	27.47	8520.2	32.99	2838360
600 – 800	600	6527	25.27	15047.2	58.26	3916200
800 - 1000	800	4857.8	18.82	19905	77.07	3886240
1000 - 1200	1000	4043.1	15.65	23948.1	92.72	4043100
1200 - 1400	1200	1170.9	4.53	25119	97.26	1405080
1400 - 1600	1400	516.01	2	25635.01	99.26	722414
1600 - 1800	1600	169.4	0.66	25804.41	99.91	271040
1800 - 2157	1800	22.919	0.09	25827.329	100	41254.2
		$H_{mean} = \sum A_i * H_i / A_{tot}$			H_{mean} =	682.36

2.3.6. Drainage network, drainage density and stream layout

A drainage network is a collection of many temporary and permanent rivers and streams through which waters flow to reach a unique outlet of the river basin (Roche, 1963). The Hodna basin is characterized by an irregular precipitation regime. In fact, all the valleys associated with the Hodna basin flow into the salty Chott-El-Hodna lake (Figure 2.11).

One of the most important features of a drainage basin is its network. Streams are ordered according to their importance. Streamline terminology is established by Horton (1945) and Strahler (1964) (see Figure 2.12). All non-branching flow channels are classified as first order

flows for all classification methods. The drainage basin feeding the network system takes the same order as an upper river order (Brooks et al., 2013).

Therefore, a drainage density D_d is defined as the total length of flows per unit of surface and expresses the dynamics of a basin's drainage network (Figure 2.13). Hence, it is expressed by the following formula:

$$D_d = \frac{\sum_{i=1}^{n} Li}{A} \qquad (Eq.\,2.5)$$

Where D_d is the drainage density (km/km²); L_i is the total length of all streams in the basin; A is the total drainage area (km²)

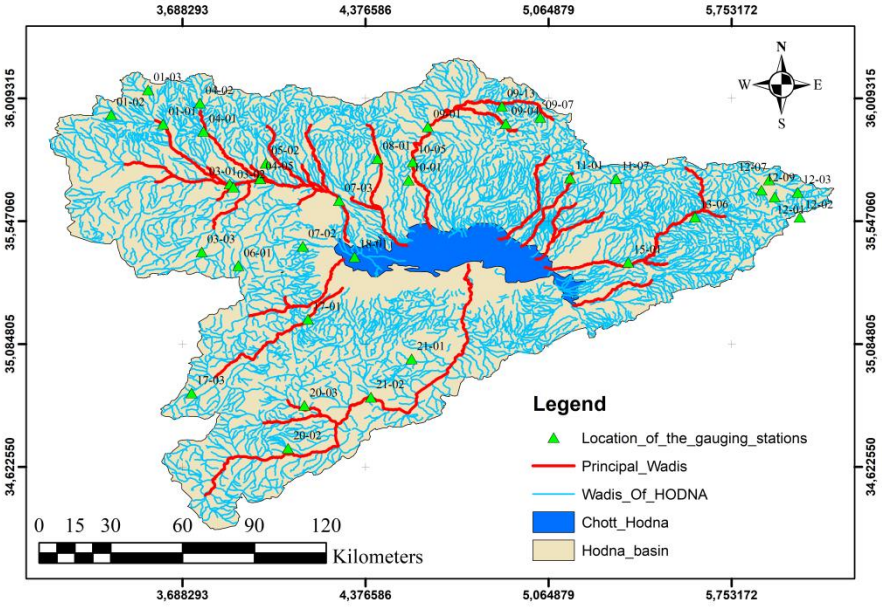

Fig. 2.11 Drainage network with main wadis of Hodna basin

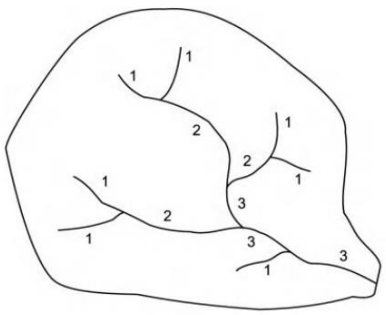

Fig. 2.12 Stream order numbering (Horton, 1945; Strahler, 1964)

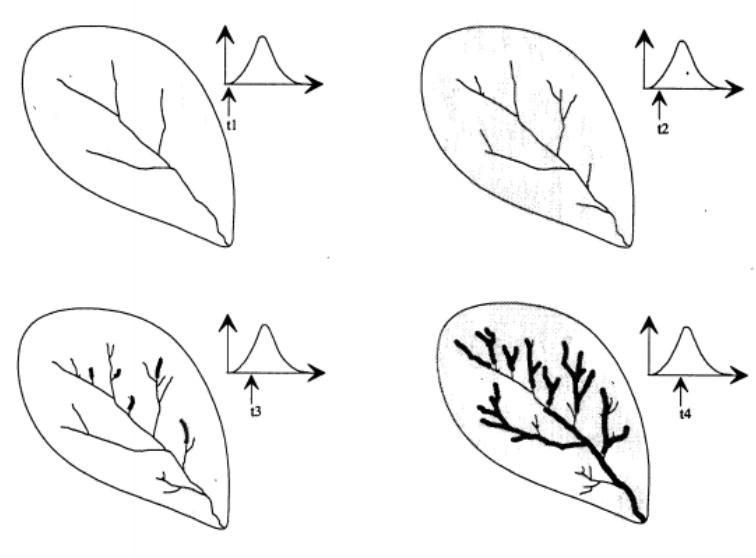

Fig. 2.13 Drainage network extension during an intensive storm (Musy and Higy, 1998)

2.3.7. Average slope

Slope classification is obtained using GIS tools. In addition, the average slope helps determine the water velocity, flow rate, and infiltration rate into the soil towards the outlet of a river basin. The average slope of a river is calculated as:

$$I_{mean} = \sum \frac{H_{max} - H_{min}}{l_p} \qquad (Eq.2.6)$$

Where: I_{mean} is the mean slope; H_{max} is the highest altitude (m); H_{min} is the lowest altitude (m); l_p is the length of main stream (km).

Moreover, slope global index, Ig, is the difference between $H_{5\%}$ and $H_{95\%}$, which is calculated using the following formula:

$$I_g = \frac{H_{5\%} - H_{95\%}}{L} \qquad (Eq.2.7)$$

Where Ig is the global index of slope (m/km); $H_{5\%}$ is the height corresponding to 5% of the total drainage surface; $H_{95\%}$ is the altitude corresponding to 95% of the total drainage surface; L is the length of the equivalent rectangle (km).

At the end of this section, Table 2.3 and Table 2.4 summarize all morphometric features of Hodna basin and its sub-basins respectively, according to numerous researchers, namely Hasbaia et al. (2012); Adoui (2013); Hasbaia and Adoui (2015); Hasbaia et al. (2017); Hasbaia et al. (2018); ANRH (2020); Khoudour et al. (2021); Belazreg et al. (2022); Zeroual

(2022); Djoukbala et al. (2022). In addition to Table 2.4 which summarizes the morphometric features of each sub-basin within Hodna basin.

Table 2.3 Summary of morphometric features of Hodna basin

Basin name	Sub-basin name	Characteristics of Hodna basin
Hodna	✓ El-Ham ✓ K'sob ✓ Barika ✓ Lougman ✓ Leham ✓ Boussaada ✓ Soubella ✓ M'cif	✓ A: 26 000 km² ✓ P: 1053 km ✓ L and l: 476.76 km and 54.18 km ✓ K_G: 1.85 ✓ H_{max}: 2157 m ✓ H_{min}: 351 m ✓ Ig: 1.9 % ✓ I_{mean}: 24.67 %

Table 2.4 Summary of morphometric features of Hodna's sub-basins

Watershed name	Sub-watershed name	Characteristics
El-Ham	✓ El-Ham ✓ Sbissebe ✓ Guernini ✓ Djenene ✓ Torga ✓ El-Karse	✓ A: 6165 km² ✓ P: 417.76 km ✓ L and l: 173.15 and 40.30 km ✓ K_G: 1.498 ✓ H_{max}: 1818 m ✓ H_{min}: 422 m ✓ Ig: 6.53 % ✓ I_{mean}: 7.19 % ✓ The longest river in the Hodna basin, starting from Dira mountain (Medea province) ✓ River length: 110 km ✓ Time of concentration: 31.01 h ✓ Dd: 0.44 km/km² ✓ Runoff velocity: 3.97 km/h
K'sob	✓ K'sob ✓ M'sila	✓ Area: 3628.72 km² ✓ P: 344.27 km ✓ L and l: 147.44 and 27.85 km ✓ K_G: 1.609 ✓ Hmax: 1882 m ✓ Hmin: 366 m ✓ Ig: 7 % ✓ I_{mean}: 11.19 % ✓ It flows starting from Medjana plain in Bordj Bou Arriredj province, and the northern limits of Maadhid commune ✓ River length: 89.70 km ✓ Time of concentration: 15.54 h ✓ Dd: 3.55 km/km² ✓ Runoff velocity: 1.52 km/h

Barika	✓ ✓ ✓ ✓	Barika amont Barika aval Barriche Bithem Barika	✓ Area: 3823.4 km² ✓ Perimeter: 405.11 km ✓ L and l: 181.48 and 23.76 km ✓ K_G: 1.848 ✓ Hmax: 2200 m ✓ Hmin: 200 m ✓ Ig: 11 % ✓ I_{mean}: 11.67 % ✓ begins from Hadjret El Bida mountain ✓ river length: 102 km ✓ Time of concentration: 14.82 h ✓ Dd: 0.3 km/km² ✓ Runoff velocity: 5.38 km/h
Lougman	✓	Lougman	✓ Area: 337.3 km² ✓ Perimeter: 105.18 km ✓ L and l: 45.11 and 8.43 km ✓ K_G: 1.615 ✓ Hmax: 1713 m ✓ Hmin: 533 m ✓ Ig: 14 % ✓ I_{mean}: 12.16 % ✓ It begins from Kteuf mountain and receives in particular flows of forests ✓ River length: 60 km ✓ Time of concentration: 07.88 h ✓ Dd: 0.3 km/km² ✓ Runoff velocity: 8.88 km/h
Boussaada	✓ ✓ ✓	Maiter amont Boussaada Maiter aval	✓ Area: 3823.4 km² ✓ Perimeter: 405.11 km ✓ L and l: 128.63 and 25.9 km ✓ K_G: 1.573 ✓ Hmax: 1600 m ✓ Hmin: 400 m ✓ Ig: 8 % ✓ I_{mean}: 14.49 % ✓ It is situated in the southwestern part of the Hodna ✓ River length: 59 km ✓ Time of concentration: 11.35 h ✓ Dd: 0.208 km/km² ✓ Runoff velocity: 4.44 km/h
Soubella	✓	Soubella	✓ Area: 1838.7 km² ✓ Perimeter: 217.67 km ✓ L and l: 87.92 and 23.58 km ✓ K_G: 1.432 ✓ Hmax: 1886 m ✓ Hmin: 720 m ✓ Ig: 12 % ✓ I_{mean}: 10.68 % ✓ River length: 34.45 km

			✓ Time of concentration: 06.30 h ✓ Dd: 0.865 km/km² ✓ Runoff velocity: 4.63 km/h
Leham	✓	Leham	✓ Area: 638.60 km² ✓ Perimeter: 152.95 km ✓ L and l: 66.93 and 10.76 km ✓ K_G: 1.707 ✓ Hmax: 1239 m ✓ Hmin: 377 m ✓ Ig: 7.9 % ✓ I_{mean}: 5.45 % ✓ River length : 30 km ✓ Time of concentration: 04.56 h ✓ Dd: 0.248 km/km² ✓ Runoff velocity: 3.76 km/h
M'cif	✓ ✓ ✓ ✓ ✓	Ain Rich Chair Amont Chair Aval M'cif Amont M'cif Aval	✓ Area: 5321 km² ✓ Perimeter: 481.81 km ✓ L and l: 215.91 and 27.8 km ✓ K_G: 1.860 ✓ Hmax: 1600 m ✓ Hmin: 400 m ✓ Ig: 6 % ✓ I_{mean}: 23.29 % ✓ River length: 104 km ✓ Time of concentration: 28.83 h ✓ Dd: 0.22 km/km² ✓ Runoff velocity: 4.46 km/h

2.4. Climate

2.4.1. Climate classes

In general, the Hodna region belongs to arid to semi-arid climate (Ladgham –Chicouche and Zerguine, 2001). According to Köppen-Geiger's climate classification (Köppen, 1923; Kottek et al., 2006), the northeastern Hodna region has a temperate climate with dry and hot summers (Csa) and a steppe arid climate with cold winters in the central part (BSk). (Lohmann et al., 1993; Beck et al., 2005; Boultif and Benmessaoud, 2017). The following Figure 2.14 shows these classifications for the Algerian region.

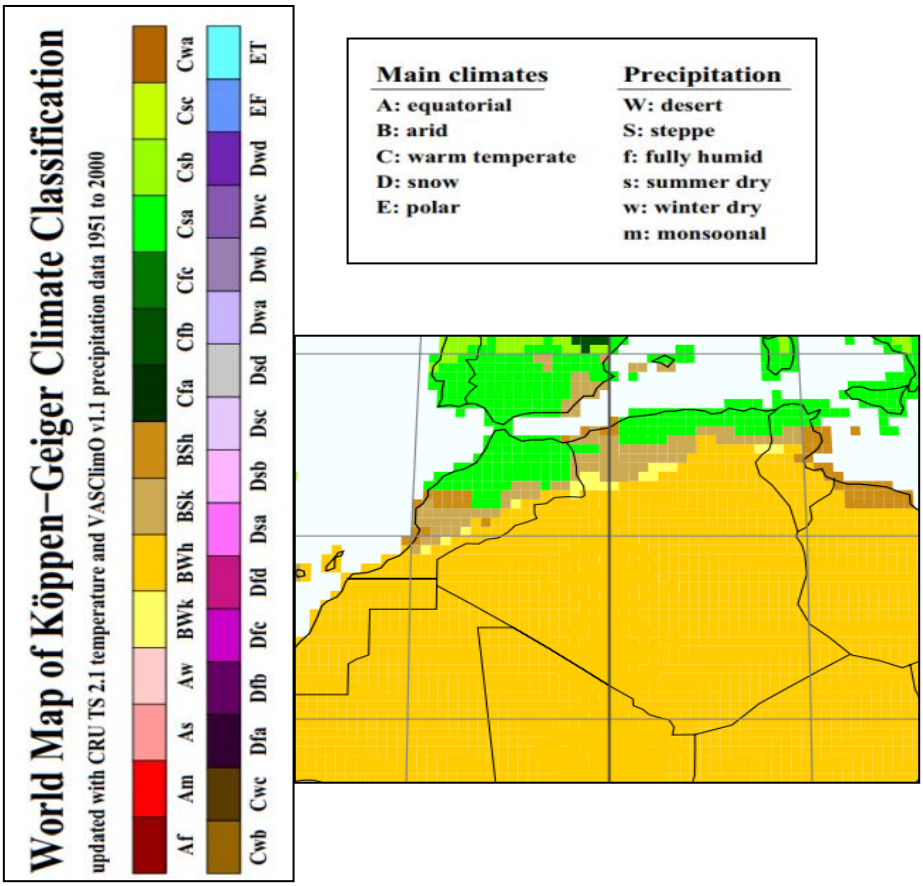

Fig. 2.14 Köppen-Geiger climate classification adapted and modified from Kottek et al. (2006)

2.4.2. Precipitation

Precipitation is heavily influenced by topography, where steep slopes are characterized by rapid flow and consequently short concentration time. While the average precipitation in the north varies between 400 and 800 mm per year, the precipitation in the south varies between 200 and 350 mm per year (Abdesselam et al., 2013; Boudjemline and Semar, 2018). However, the average annual precipitation of the Chott-El-Hodna Salt Lake is about 172 - 200 mm (Abdesselam et al., 2013; Adoui, 2013; Messad and Moussai, 2015).

The precipitation map was prepared based on the Climate Research Unit's (CRU) high resolution grid datasets (CRU TS v.4.04, 2019, 0.5° resolution). For example, Figure 2.15 below shows the spatial distribution of mean inter-year (1971-2000) precipitation for the Hodna region. Near the Hodna mountains, precipitation reaches 500 to 600 mm and below 200 mm in Chott-El-Hodna, while in the southern regions it reaches 300 to 390 mm (Hasbaia et al., 2017; Zeroual, 2022). The Hodna region is also characterized by short periods of

precipitation interspersed with long periods of drought (see Table 2.5). Locations of available rainfall gauging stations in the Hodna basin are highlighted in Figure 2.16.

Table 2.5 Average annual rainfall values (Hasbaia et al., 2017; Khoudour et al., 2021)

Sub-basin	El-Ham	Leham	Lougman	K'sob	Soubella	Barika	Boussaada	M'cif
Average annual rainfall (mm)	250	292	300	300	250	345	290	251

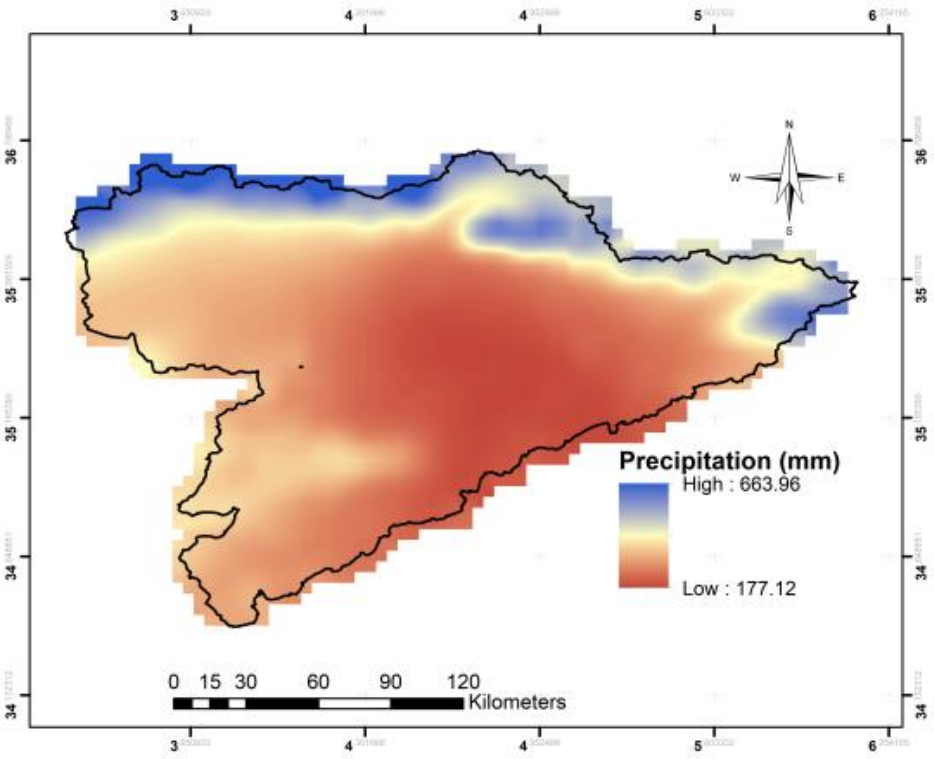

Fig. 2.15 Mean monthly precipitations of Hodna basin during the period 1971-2000 (Kebiche, 1994; Belazreg et al., 2023)

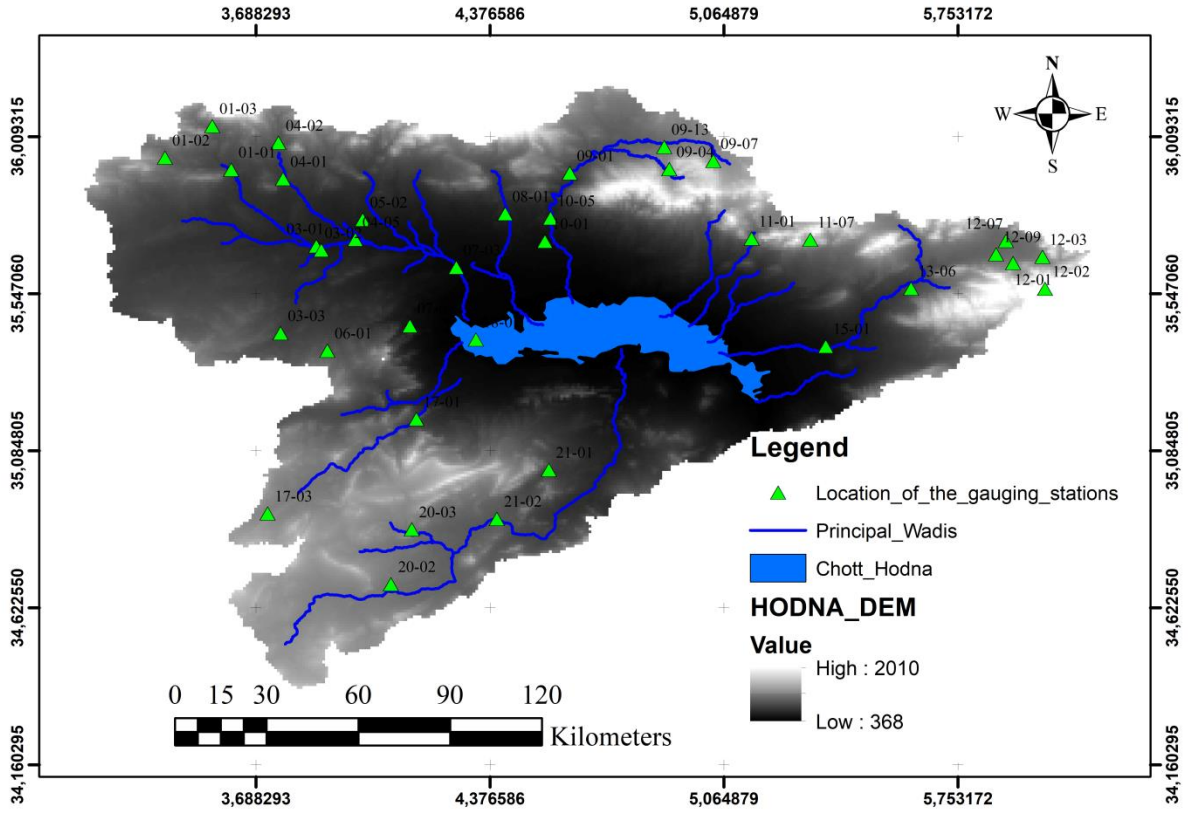

Fig. 2.16 Location of gauging stations in the Hodna basin

2.4.3. Temperature

Surface air temperature is one of the factors that define the climate of any region, in particular when studying evaporation and evapotranspiration of the drainage basin. Air temperature is affected mainly by four parameters, namely, latitude, altitude, sea or water surfaces, and wind (Roche, 1963). A region near the equator is characterized by a warm climate, while when the altitude of a region is higher, the climate is colder. In addition, in regions close to the sea or water surfaces, winters are cold, and summers are cool, while north winds, especially those coming from the sea direction, are cold but south winds are warmer.

The lowest temperature is between 3.6°C – 4.02°C (January), and the highest temperature varies between 38.8°C – 39.22°C (July) (Abdesselam et al., 2013; Boudjemline and Semar, 2018). The average annual temperature is about 22°C (-3°C to 40°C) (Messad and Moussai, 2015) (see Table 2.6). Mean monthly maximum temperature, in Hodna basin, is shown in Figure 2.17.

Table 2.6 Average annual temperature values (Hasbaia et al., 2017; Khoudour et al., 2021)

Sub-basin	El-Ham	Leham	Lougman	K'sob	Soubella	Barika	Boussaada	M'cif
Average annual temperature (°C)	15.44	16.20	16.27	15.80	15.70	15.00	16.50	14.70

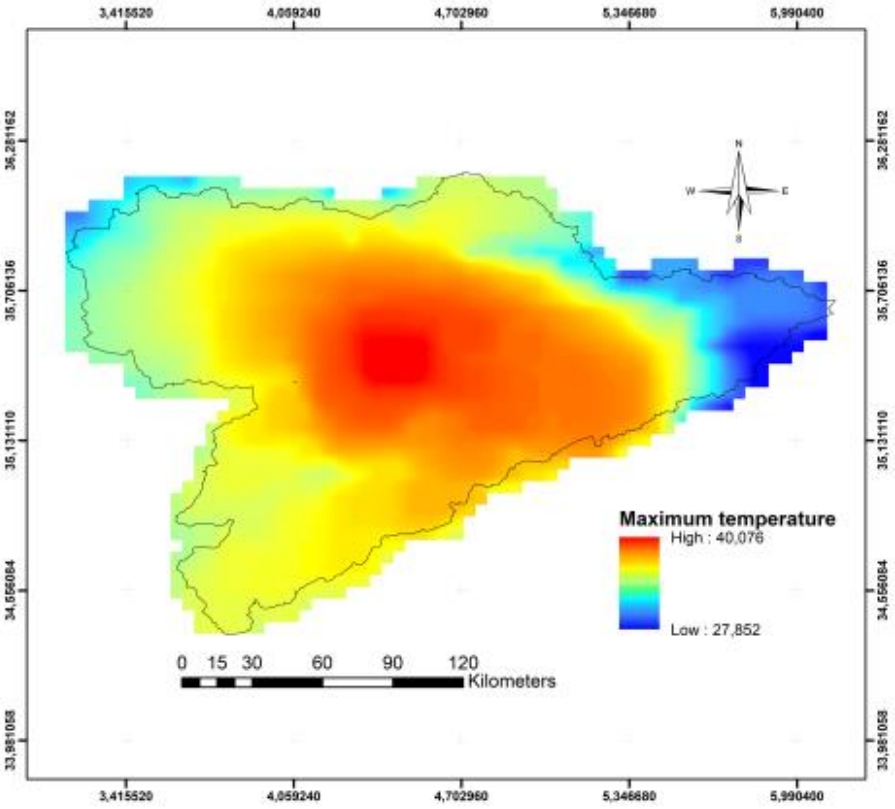

Fig. 2.17 Mean monthly maximum air temperature of Hodna basin during the period 1971-2000 (Belazreg et al., 2023)

2.4.4. Evaporation/evapotranspiration

Evaporation is mostly affected by the temperature of the area. The annual evaporation in the study area is measured at Bordj Bou Arriredj station as 2548 mm. Monthly values range from 73.2 mm to 89 mm in December, reaching 446 and 399 mm in July.

In addition, there is excessive evaporation of both ground and surface waters in the Hodna basin. Evapotranspiration reaches 1,330 mm/year in the salty lake of the Hodna basin (Messad and Moussai, 2015). This often leads to salt precipitation on the land surface of Chott-El-Hodna.

2.5. Land cover and land use

Significant changes in land and water resource usage have occurred in Algeria as a result of successive agricultural policies, the agricultural revolution, access to private land ownership, and the national agricultural development program (Abdesselam) and others, 2013).

Land cover flow rate depends on evaporation ratio and catchment storage capacity. It also prefers infiltration and plays an important role in soil conservation (Belagoune, 2012). Vegetation plays an important role in soil conservation and favors infiltration of sub-critical flows. Agricultural practices are especially flourishing where water resources are available (sandy lands south of chott-El-Hodna). For example, forested areas dominate in Mount Messaad, Medjedel, Slim, Maadhid, Hammam-El-Dalaa and Boussaada,. In addition, agricultural areas dominate the Hodna plain, where there are cereals and fruit trees.

In Figure 2.18, the Hodna river basin consists of different soil types. According to FAO-UNESCO (1974) and Sime and Abebe (2022), each region is characterized by the following points:

- Bk (Calcic Cambisols): These are well-drained soils developed on calcareous structures in semi-arid climatic conditions known as brown soil and are not affected by degradation processes due to clay with depth increase,

- I (Lithosols): Fine soils composed of weathered rocks,

- Lc (Chromic luvisols): Clay is washed from the surface towards an accumulation horizon at a certain depth. They are most common in warm temperate regions with dry and rainy seasons. They are sandy-loamy textured and reddish colored soils and greatly affected by water erosion and have low levels of organic matter,

- Xh and Xk (Haplic and calcic Xerosols): These are found in the lowland of the drainage basin covered with grassland and bushes and they are rich in loam. Desert soils with low organic matter levels, depending on wind erosion and the concentration of soluble salts,

- Yh, Yk and Yy (Haplic, Calcic and Gypsic Yermosols): Even drier and more problematic than xerosols,

- Zg, Zo and Zt (Gleyic, Orthic and Takyric Solonchaks): They have high salinity concentration. They are gray soils, which are found under arid to semi-arid and poorly drained conditions. They occur when evaporation is greater than their sedimentation volumes.

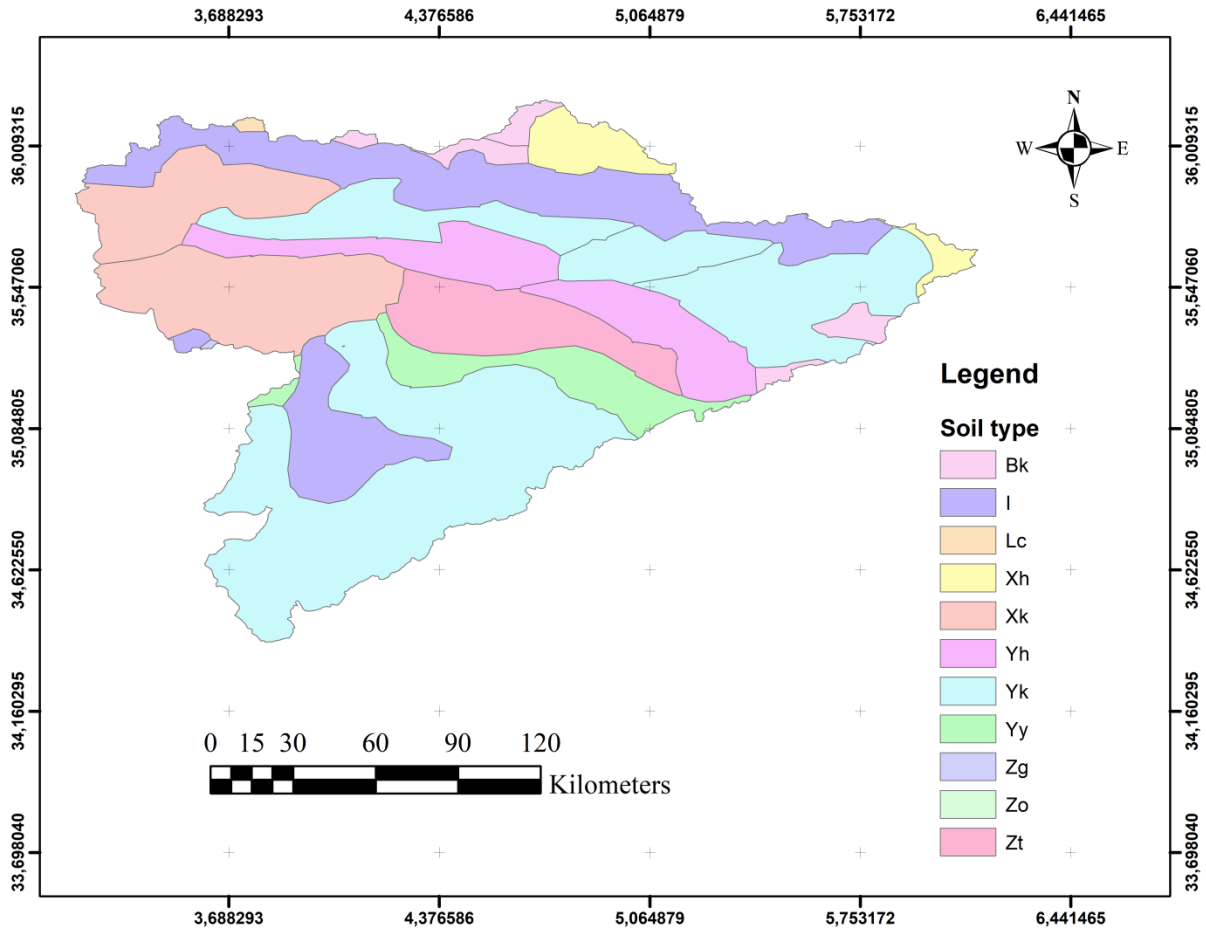

Fig. 2.18 Different soil types in the Hodna basin

Where: Bk: calcic cambisols; l: lithosols; Lc: Chromic luvisols, Xh: Haplic Xerosols, Xk: Calcic Xerosols; Yh: Haplic Yermosols; Yk: Calcic Yermosols; Yy: Gypsic Yermosols; Zg: Gleyic Solonchaks; Zo: Orthic Solochaks; Zt: Takyric Solonchaks (according to FAO-UNESCO, 1974)

2.6. Geological, geomorphological and hydrogeological settings

2.6.1. Geology

Geology has a significant impact on groundwater and surface flows (discharge, seepage rate, permeability, erosion as well as flood events). There are four main geological units related to

the study area (Savornin, 1908; Belagoune, 2012; Amroune et al., 2020). From the oldest to the most recent ages, these geological structures are as follows (see Figure 2.19):

Primary

This structure is characterized by Paleozoic formations with sedimentary, eruptive and metamorphic rocks in the northern parts of the basin.

Secondary

Triassic formations (Boussaada area) are mainly based on gray gypsum clay, in addition to dolomite rocks. It is characterized by the Cretaceous formation with secondary, carbonate and sandstone formations. Significant marl, dolomite and limestone formations are also found. In addition, the Jurassic formations (central and east of Hodna) are also secondary. Numerous folds exist near dolomite limestone structures, as well as marly limestones (Mount Soubella).

Tertiary

The Tertiary is located on Cretaceous formations (Boutaleb mountain) resulting from the erosional phenomenon of the Sahara Atlas. It is characterized by the presence of sand, sandstone, marl and conglomerates. This formation is presented by dolomite-limestone rocks covered with sandstone near Boutaleb Mountain, sandstone-clay-dolomite facies near Maadid Mountain, marl facies in the east of the basin and marl-limestone formations at K'sob wadi level.

As a matter of fact, it covers Paleocene, Eocene and Miocene. The first consists of grayish limestone and black marly gypsum. The latter consists of gray colored limestone with some gray, white and yellow marl formations. The latter is represented by red marl, conglomerates, light yellow or beige fine sandstone and massive gypsum.

Quaternary

There are three main ages or quaternaries: old, average and new quaternaries. The oldest contains red orange gypsum limestone facies in addition to some large conglomerates 20 m to 40 m below valley level. The latter is presented with large blocks of limestone, sandstone limestone shells, conglomerates and clay. The new structures of the Quaternary (the large area of northern Hodna) are characterized by the presence of gray alluvium containing some

gypsum. On the contrary, alluvial deposits with fine sand, clay and gypsum are found near the dunes.

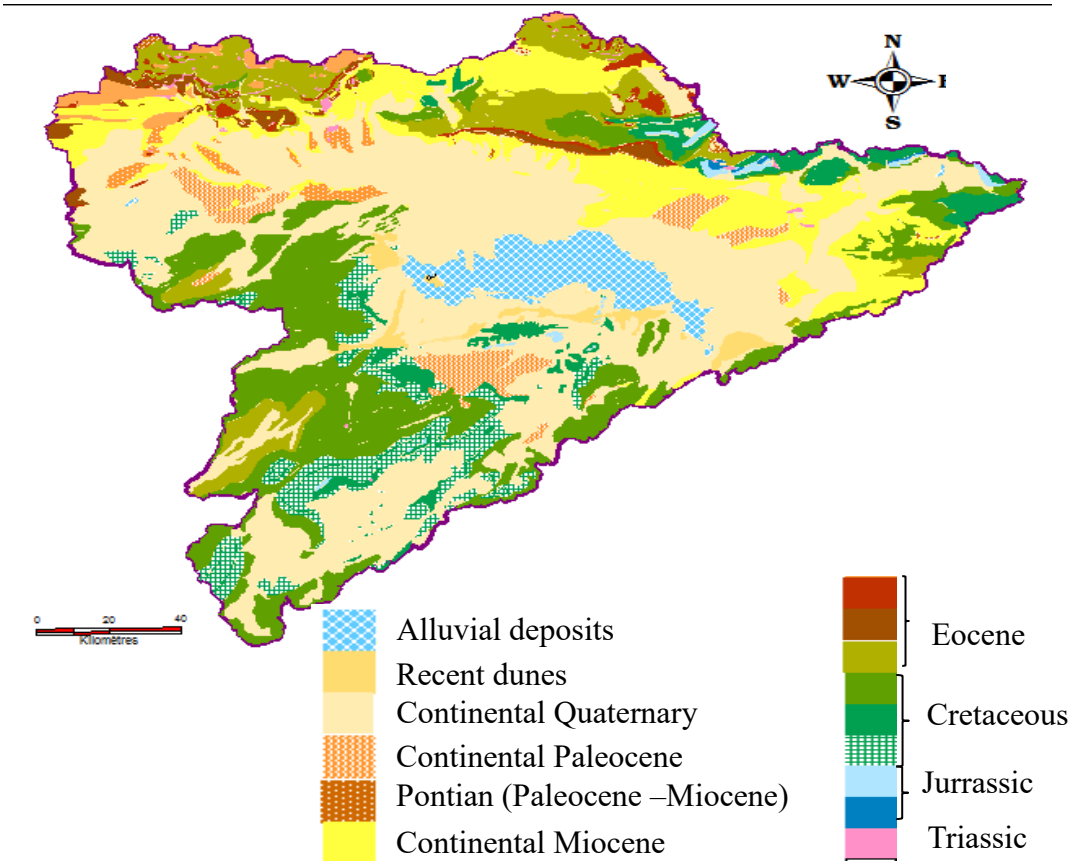

Fig. 2.19 Geological map of the Hodna basin (ANRH, 2020)

2.6.2. Geomorphology

The basin is located between two different geological and geomorphological areas. There is the Tellian Atlas in the north and northeast and the Saharan Atlas in the south (Boudjemline and Semar, 2018). It is divided into four geomorphological units, namely, the mountains, the Hodna plain, the salty Chott-El-Hodna lake, and the R'mel region.

For example, it is bounded by the Bibans mountains and Setifian plateau in the northeast, the high plains of Algeria in the northwest, the Boussaada mountains in the southwest, and the Ouled Nail mountains in the southeast of the basin (Sahari Atlas (Khoudour) et al., 2021). The elevation of the Hodna Mountains decreases from east to west (between 1900 m and 1000 m). However, only a few hills can be seen towards the south (1200 m). The Hodna plain has an area of approximately 8,500 km² (Adoui, 2013). The sediments deposited in this plain are usually made up of sand, gravel and alluvium from the solid load of the valleys before they

reach the salty lake. In particular, this land is used for agricultural activities (Belagoune, 2012). The Chott-El-Hodna lake is composed of natural clay with no vegetation. It is divided between M'sila and Batna provinces. Finally, the R'mel region is the southern part of Chott-El-Hodna and includes the alluvial plain of Hodna. It takes its name from the sandy structure of this region.

In addition, sand, limestone, clay, carbonates (calcite), gypsum and salts dominate the soil components of Hodna (Abdesselam et al., 2013). The northern and southern parts of Chott-El-Hodna are characterized by clay-silty and sandy soils, respectively. The middle part of the salty lake is in the form of a mineral layer as a result of the presence of salts. Quartz-sandy soil is dominant in the R'mel region north of Boussaada. The northern hills of the Hodna basin are characterized by alluvial deposits, gypsum, limestone-gypsum and sandy-silty soils.

2.6.3. Hydrogeology

Groundwater in Hodna is located between the Jurassic and quaternary structures. From the point of hydrogeology, two main aquifers are recognized as phreatic (shallow) and deep aquifer (confined). The first can be operated at 40 m, while the second can reached from 150 m to 250 m in Mio-Pliocene structures. The water salinity study showed that the first aquifer had very high salt concentrations, while the other had lower salinity values. The main reason for this is the increase in groundwater usage for agricultural purposes (Adoui, 2013; Amroune et al., 2020).

For this reason, impermeable soil layers occur near marly, marly limestone and clay soils. Under these conditions, seepage of water is very low from the soil. Semi-permeable soil layers consist of limestone, dolomite formations and marl. Dolomite formation is based on some pores that increase permeability but rarely found. Finally, the highly permeable soil layers consist of conglomerates, sandstone limestone and marly limestone formations and sand silty layers.

2.7. Conclusion

In this second chapter, Hodna drainage basin is presented as the study area. In the previous sections, various features of this drainage basin were discussed concerning morphometric features, land use and cover characteristics, climate classification, precipitation, temperature and evaporation. The chapter ends with the geological, geomorphological and hydrogeological features of the Hodna basin.

CHAPTER 3

Data and methodologies

Chapter 3 Data and methodologies

3.1. Introduction

Considering the aim of this thesis, the methods used require the application of different data and specialized software. Therefore, ArcGIS, HEC-RAS and Origin Pro have been applied.

3.2. Data processing tools

3.2.1. ArcGIS version 10.4

The Geographic Information Systems (GIS) platform is the open-source program Map Window (Praskievicz, 2009). Indeed, data processing can be carried in different forms, such as:

- Transfer of collected data to ArcGIS 10.4,
- Generation of a GeoDataBase in the software to record all data concerning Hodna basin,
- Identify and extract the Hodna basin and their sub-basins (Digital Elevation Model (DEM), shapefile, attribute table),
- Import, store, manage and export diverse hydrological data (rainfall, temperature),
- Extract and generate different maps (location of the basin, average maximum daily precipitation, flow direction and accumulation, slope, flood hazard and risk, land use, presentation of different climate models outputs,..),
- Perform the statistical calculation on a spatio-temporal scale.

3.2.2. HEC-RAS version 6.3.1

HEC-RAS (Hydrologic Engineering Center's River Analysis System) software is based on Saint-Venant equations, and is developed by the U.S. Army Corps of Engineers, Hydraulic Engineering Center. These equations are used to determine the water levels and flow discharge, which are deduced from Navier-Stokes equations.

The current work with 1D model was preceded prior to preparing geometric input data directly into HEC-RAS vs 6.3.1. The HEC-RAS model version 6.3.1 allows hydraulics calculations of one dimensional steady and unsteady river flow to run. It can calculate water surface profiles and energy gradient lines. On the contrary to older versions where geometric input data had to be prepared under any GIS and then the conversion between the two

softwares had to be performed, newer versions of HEC-RAS have the advantage of directly introducing the geometric data into the HEC-RAS using RAS Mapper tool (Bekhira et al., 2019).

Geometry data consists of Manning's roughness coefficients and stream centerlines, banks lines, flow paths, cross-sections, and land use. To compute water surface elevation at any location of interest, for either steady or unsteady flow simulations; data needed are geometric data, peak discharge data, cross-sections, flow paths, manning's coefficient, boundary conditions, flow regime (subcritical, supercritical).

Using energy conservation equation, HEC-RAS calculates the water level in one section based on the water level of the previous one. In addition, Saint-Venant equations express both continuity equation and mouvement quantity conservation equation, also called 1D Navier-Stokes equation (Hasbaia et al., 2015; Demir and Kisi, 2016; Papaioannou et al., 2017). Thus, the solution of these equations is based on the finite difference method for 1D steady flow simulation. These equations are expressed as follows:

$$Z_2 + Y_2 + \frac{a_2 * {V^2}_2}{2\,g} = Z_1 + Y_1 + \frac{a_1 * {V^2}_1}{2\,g} + h_e \qquad (Eq.\,3.1)$$

Where Z1 and Z2 are the elevations of the main river; Y1 and Y2 are the water levels near to cross-sections; V1 and V2 are the average velocities (total flow discharge/ total flow surface); a_1 and a_2 are the weighting velocity equal to 1; g is the gravity acceleration; h_e is the total energy loss.

$$\frac{\partial A}{\partial t} + \frac{\partial Q}{\partial x} = q_l \qquad (Eq.\,3.2)$$

$$\frac{\partial Q}{\partial t} + \frac{\partial}{\partial x}\left(\frac{Q^2}{A}\right) + gA\frac{\partial h}{\partial x} - gA * I_x + gA * J = 0 \qquad (Eq.\,3.3)$$

Where Q is the flow discharge rate; h is the water depth; A is the wet area, Ix is the river slope; J is the slope of the energy line; q_l is the lateral flow discharge; g is gravitational acceleration; x and t are the space and time variables.

3.3. Peak discharge assessment for different return periods (El-Ham sub-basin)

Hill floods have devastating effects on the physical environment and infrastructure. In most of the southern Mediterranean basins, the identification of these floods is complicated by

the lack of reliable and sufficient data (Salhi et al., 2019). Therefore, the initial flood discharge analyzes rely on different techniques prior to hydraulic modeling to identify flood zones. Algeria is one of the many Mediterranean countries facing the flooding phenomenon in arid and semi-arid regions. The Algerian valleys are characterized by a very irregular hydrological regime. More recently, various parts of Algeria are marked by some degree of human and property damage including Adrar (October 2004, January 2009, August 2013), Ghardaïa (October 2008, January 2009), Biskra (September 2009), Bechar (October 2008), El Bayadh (October 2011), Tamanrasset (March 2005) , Tindouf (October 2015), M'sila (September 2007, June 2015, May & September 2021) (Hachemi & Benkhaled, 2016; ANRH, 2020).

3.3.1. Objective of the study

The aim of this study is to evaluate the peak flood discharge through the application of empirical and statistical analysis of the flood for different return periods (10-year, 20-year, 50-year, 100-year and 1000-year) in El-Ham wadi of the Hodna basin in central Algeria. This study was conducted primarily to obtain the discharge data of the Hodna basin, previously estimated previously by several scientific researches, but also to gather more data of this basin needed for further researches, due to the paucity and insufficiency data of this basin. Hodna basin flow discharges data, particularly in flash flood study, which implies the knowldge of peak flow over several return periods.

3.3.2. Methodology

The methodology used to determine the hydrological distribution that best represents the maximum precipitation data and maximum peak flow rates associated with different return periods are presented below after Belazreg et al. (2022).

a) Selection of precipitation data

The sample consists of 46 years (1966 - 2011) precipitation data for each gauge station from the National Agency for Hydraulic Resources (ANRH, 2020). Annual Maximum Daily Precipitation data (Pmax, d) records were collected from 8 precipitation measuring stations 050101, 050301 and 050703 distributed throughout the El-Ham wadi sub-basin (Figure 3.1 and 3.2).

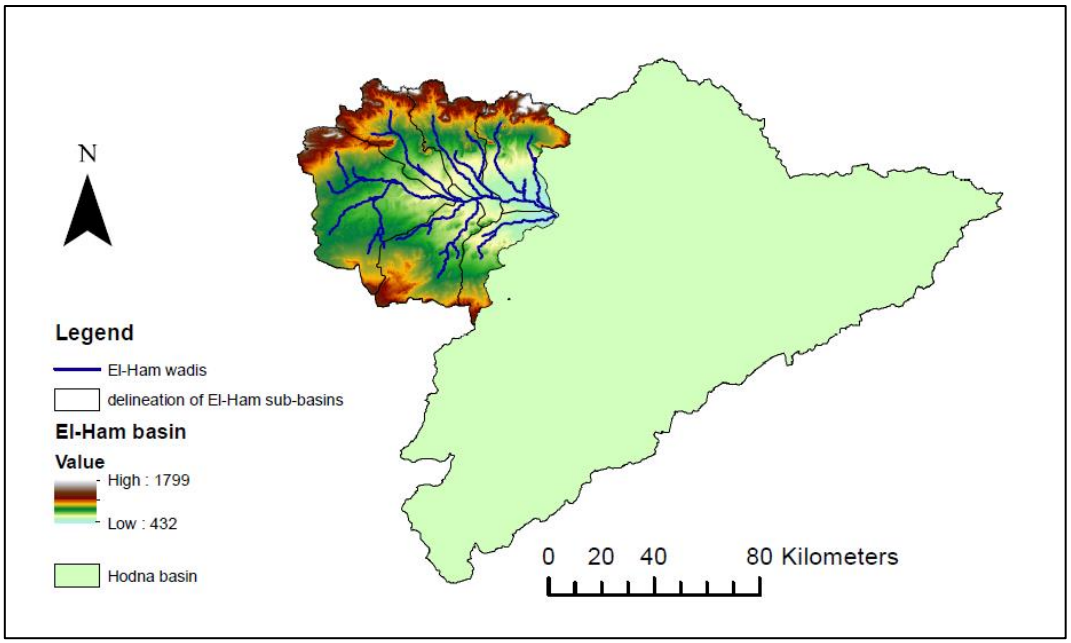

Fig. 3.1 Location of El-Ham watershed within the Hodna basin and altitudes distributions

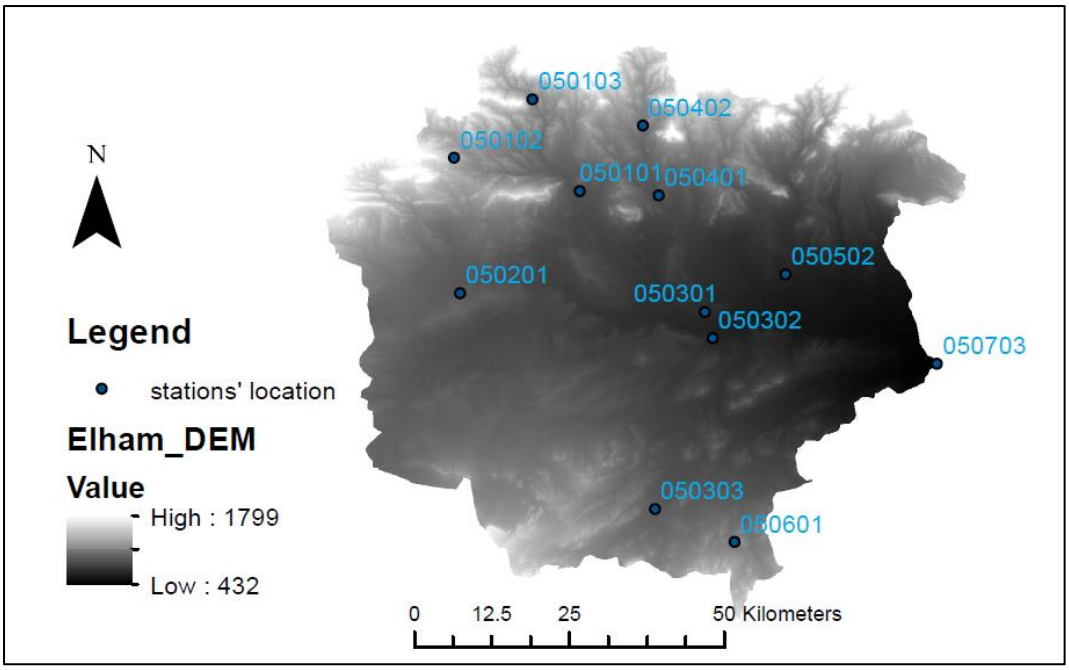

Fig. 3.2 Location of rainfall gauged stations (050101, 050301, 050703) at El-Ham watershed (Hodna basin)

b) Frequency analysis

The series of annual maximum precipitation values adjusted by the Gumbel probability distribution function (PDF), which gives rise to precipitations for the return periods 2-year,

10-year, 20-year, 50-year, 100-year and 1000-year. Short-term precipitations Ptc (T) is used for the flood estimation. The Ptc (T) calculation can be achieved by using the Body formula as,

$$Ptc(T) = Pmax,d(T).(\frac{t}{24})^b \qquad (Eq.3.4)$$

Where: Ptc (T) is the short-term rainfall for a given return period T (mm); Pmax,d (T) is the maximum daily precipitation for a given return period T (mm); t is duration of precipitation (hours); b is coefficient calculated using the following equation :

$$b = 1 + \frac{Ln\left(\frac{Pmax,d(m)}{24}\right) - Ln(25)}{Ln(24) - Ln(0.5)} \qquad \text{(Eq. 3.5)}$$

Where: Pmax,d (m) is the average maximum daily precipitation (mm).

In this study we have determined the rainfall intensity corresponding to different return periods for the concentration time using the following formula:

$$Itc(T) = \frac{Ptc(T)}{t} \qquad \text{(Eq. 3.6)}$$

Where Itc (T) is the rainfall intensity for duration equals to the time of concentration of a given return period T, and t is the duration of precipitation (hours).

Pmax(d) is very variable during time period. Gumbel law is often used for the frequency to estimate Pmax(d)s for any return period.

$$F(x_i) = e^{-e^{-\alpha\,(x-x_0)}} \qquad (Eq.3.7)$$

$$X_{max} = \frac{1}{\alpha}\,Y_G + X_0 \qquad (Eq.3.8)$$

$$X_0 = \overline{X} - \frac{0.577}{\alpha} \qquad (Eq.3.9)$$

$$\frac{1}{\alpha} = 0.78\,\sigma \qquad (Eq.3.10)$$

Where α, X_0 : Adjustment coefficients of Gumbel ; Y_G : Gumbel variable ; X_{max} : Pmax(d) (mm).

Once the data has been fitted with a Gumbel PDF (as it is the most adequate PDF), it is possible to generate the corresponding intensity duration frequency (IDF) curves, which are the basis for every rainfall runoff model in flood studies. Their elaboration presents the first requirement in the planning, management and prediction of rainfall risk. This leads, firstly, the estimation of the concentration time T_c using ANRH-Sogreah, Basso and Giandotti formulas. To build the IDF curves, it is first necessary to determine the time series for each event, the rainfall maximum intensity corresponding to the different cumulative durations at 1, 5, 7, 10, 13, 15, 17, 20, 22 and 24 hours. This intensity is determined according to short-term rainfalls Ptc. Starting from the previous sample of maximum daily precipitation values one can assign to each of these values an empirical frequency of non-exceedence.

c) Estimation of the time of concentration (Tc)

The time of concentration Tc in a watershed is defined as the maximum time required for water to flow from the farthest point to the watershed outlet. Several empirical formulas have been proposed over the previous decades and centuries. Here, ANRH-Sogreah, Basso and Giandotti formulas are used, and their expressions are as follows (Table 3.1):

Table 3.1 Empirical formulas for calculating time of concentration

Methods	Formulas	Details
Giandotti	$Tc = \frac{4\sqrt{A}+1.5*Lp}{0.8\sqrt{H_{mean}-H_{min}}}$ (Eq. 3.11)	Tc: concentration time (h), A: basin area (km²), Hmean: mean altitude of the basin (m), Hmin: minimal altitude of the basi (m).
Basso	$Tc = 0.067 * \frac{Lr^{1.115}}{(H_{max}-H_{min})\text{^}0.385}$ (Eq. 3.12)	Tc: concentration time (h), Hmin: minimal altitude of the basin (m), Hmax: maximal altitude of the basin, Lr: length of the basin (km).
ANRH-Sogreah	$Tc = 3\,(\frac{A*Lr}{10*I^{3/2}})\text{^}¾$ (Eq. 3.13)	Tc: concentration time (h), Lr: length of the basin (km), A: basin area (km²), I: slope of the basin (%).

d) Design flood estimation formulas

Following the goal of estimating peak flow rates (design flood) using maximum daily precipitation data for different return periods, the formulas in Table 3.2 are useful.

Table 3.2 Peak flow assessment formulations

Methods	Formulas or mode of application	Details
Giandotti	$Q_p = \frac{C.A.(Hm-Hmin)^{0.5}}{4.(A)^{0.5}+1,5.L}.Ptc$ % (Eq. 3.14)	C : coefficient ranges between 66 and 166, A: basin area (km²), Hm: Average elevation (m); Hmin: minimal elevation (m); L: length of the main water course (km); Ptc: short-term rainfall (mm).
Possenti	$Q_{p\%} = \frac{\mu.Pmax,d.A}{L}$ (Eq. 3.15)	µ: coefficient ranges between 700 and 800; Pmax,d: maximum daily precipitation of a given return period; A: basin area (km²); L: length of the main water course (km).
Turazza	$Q_p = \frac{Cr.H.A}{3,6.Tc}$ (Eq. 3.16)	Cr: runoff coefficient ranges between 0.4 and 0.65 (for the study area); H: maximum precipitation of duration equals to the concentration time (mm); A: basin area (km²); Tc: concentration time (h).
Temez	$Q_p = C.I.\frac{A_b}{3}$ (Eq. 3.17)	C: runoff coefficient ranges between 0.4 and 0.65 (for the study area); I: rainfall intensity for a duration equals to the concentration time of a given return period (mm/h); A: basin area (km²).
Gradex	$F(x) = \frac{r-0,5}{N}$ (Eq. 3.18) $U = -Ln(-Ln(F(x))$ (Eq. 3.19) $Pmax,d(T) = U.Gp(T) + Pmax,d(i)$ (Eq. 3.20)	F(x): Hazen non-exceedance probability equation r: range number; N: total sample; U: reduced variable of Gumbel; Pmax,d: maximum daily precipitation (mm); Gp(T): precipitation Gradex (mm).

3.4. Flood hazard and risk assessment in Hodna basin

Proper flood risk assessment is an essential component of flood mitigation especially in urban areas. It considers the consequences of floods on population, economy and environment.

Flood risk estimation can be produced by three main methods: analysis of flood frequency, analysis of storm progression, and flood hazard maps (Rincón et al., 2018). Flood risk assessment is a combination of hazard and multiple vulnerability dimensions.

Much research has been done in the area of flood hazard and risk assessment and increasing damage severity. They provide valuable information that complements flood analysis and quantification to integrate Multi-Criteria Analysis (MCA) approaches with GIS and performs risk analysis to analyze flood-prone areas and evaluate effective causal factors. MCA is a decision-making tool developed for solving complex multi-criteria problems involving qualitative and/or quantitative aspects of the problem (Mendoza et al., 1999). It mainly focuses on flood risk mitigation assessment rather than flood risk mapping (Sharma et al., 2017).

3.4.1. Flood assessment using Analytical Hierarchy Process (AHP) technique

Numerous factors causing flooding can be used to derive flood risk maps, namely monthly and annual rainfall, main drainage channel slope, drainage density, topographical factors, flood frequency, land use/cover, elevation, soil type, flood depth, flood duration, flood velocity, economic and social vulnerability (Yalcin et al., 2004; Raaijimaket et al., 2008; Deng et al., 2010; Scheuer et al., 2011; Abdalla, 2012; Musungu et al., 2012; Sharma et al., 2012; Elsheikh et al., 2015; Rincón et al., 2018; Mokadem et al., 2018; Saidi et al., 2019; Ogato et al., 2020) through Analytical Hierarchy Process (AHP) method. Some studies were applied flood modeling approaches to demonstrate the feasibility of flood modeling in data-scarce environments and limited resources. However, others have generated flood hazard and risk maps for different scenarios each with different criteria taking into account the floodplain, the distance to the streams, the height above the nearest drainage, the number of flow curves, the total precipitation and the effective precipitation maps.

3.4.1.1. Objective of the study

The main objective, of the first part of this study, is to apply the MCA concept, GIS and AHP weighting methods for flood hazard and risk mapping generations in the Hodna basin in Central Algeria. This objective is achieved by preparing flooding causal factors maps such as slopes, drainage density, rainfall, population density, soil type and land use/cover parameters.

3.4.1.2. Methodology

The data covered in this study are Digital Elevation Model (DEM) of Hodna basin, 40 years (1980-2020) Annual Maximum Daily Precipitation (Pmax, d) data from the National Hydraulic Resources Agency (ANRH), Algerian population density (2008 census), soil type, land cover/land use, slope, and drainage density maps. Integration of remote sensing data with GIS and AHP is a very effective tool for flood vulnerability data generation (Elsheikh et al., 2015; Rimba et al., 2017). The criteria used in this study are chosen because of their relevance and importance in the study area.

Ranking and Rating methodologies have been used (Yehaneh et al., 2014; Sharma et al., 2017; Mokadem et al., 2018; Saidi et al., 2019; Ogato et al., 2020). Ranking is assigned to each decision item reflecting the degree of importance it affects the decision; Ranking is somewhat similar to Rating with numerical scores assigned to indicate its level of importance.

a) AHP methodology and weighting procedures

The AHP method was presented by Saaty (1980) to develop multi-criteria decision (MCD) problems that take pairwise comparisons as input and produces relative weights as output for each criterion on a scale of 1 to 9 (Saaty, 1977; Malczewski, 1996; Yalçın et al., 2004; Rincon et al., 2018). The parameters need to be weighted to determine the degree of impact of each on the flood risk in the study area (Saidi et al., 2019). In the overall evaluation, the most important criterion has more weight (Yalçın et al., 2004; Dall'Osso et al., 2006). The next step consists of a linear normalization of the matrix: the parameter of each matrix column is divided by its total sum and then the normalized values of each row are averaged to obtain the final weights (Yeganeh et al., 2014; Elsheikh et al., 2015; Ogato et al., 2020).

The Consistency Index should be calculated to verify the level of inconsistency, which should be less than 0.1 (Rimba et al., 2017; Ogato et al., 2020). The calculations are as follows:

i) Weighted sum vector calculation by multiplying the weights of the criteria with the matrix values,
ii) Consistency vector calculation, which is the ratio between the weighted sum vector and the weights,
iii) Lambda calculation, which is the mean of the consistency vector.

$$CI = \frac{\lambda - n}{n - 1} \qquad \text{(Eq. 3.21)}$$

Where CI is the consistency index, λ is the average of the consistency vector and n is the size of the matrix. The final calculation is the consistency ratio (CR), which is the ratio of CI and Random Index (RI). The CR value should be less than 10% (Yeganeh et al., 2014; Sharma et al., 2017; Saidi et al., 2019).

$$CR = \frac{CI}{RI} \qquad (Eq.\ 3.22)$$

Where CR is the consistency ratio, CI is the consistency index and RI is the random index representing the consistency of the randomly generated pairwise comparison matrix. The RI values can be obtained from Table 3.3 (Saaty, 1980).

Table 3.3 Random Index (RI) values for the CR calculation

N	1	2	3	4	5	6	7	8	9	10	11	12	13	14
RI	0	0	0.58	0.90	1.12	1.24	1.32	1.41	1.45	1.49	1.51	1.48	1.56	1.57

b) Flood Hazard mapping

- *Rainfall spatial distribution map (R)*

Heavier rains are more likely to cause flooding and especially flash floods (Few et al., 2004). The 40-year Pmax,(d) data are collected from measurement stations in the Hodna basin (Figure 3.3). Rainfall station data is then calculated and arranged in the Attribute table in ArcGIS. The Inverse Distance Weighted (IDW) technique allowed the precipitation distribution map to be drawn using the IDW Tool in ArcToolBox. The final result is reclassified into five classes using the Natural Breaks classification. For this, the highest precipitation value is 5, and the lowest value is 1 due to its low contribution to the flood hazard.

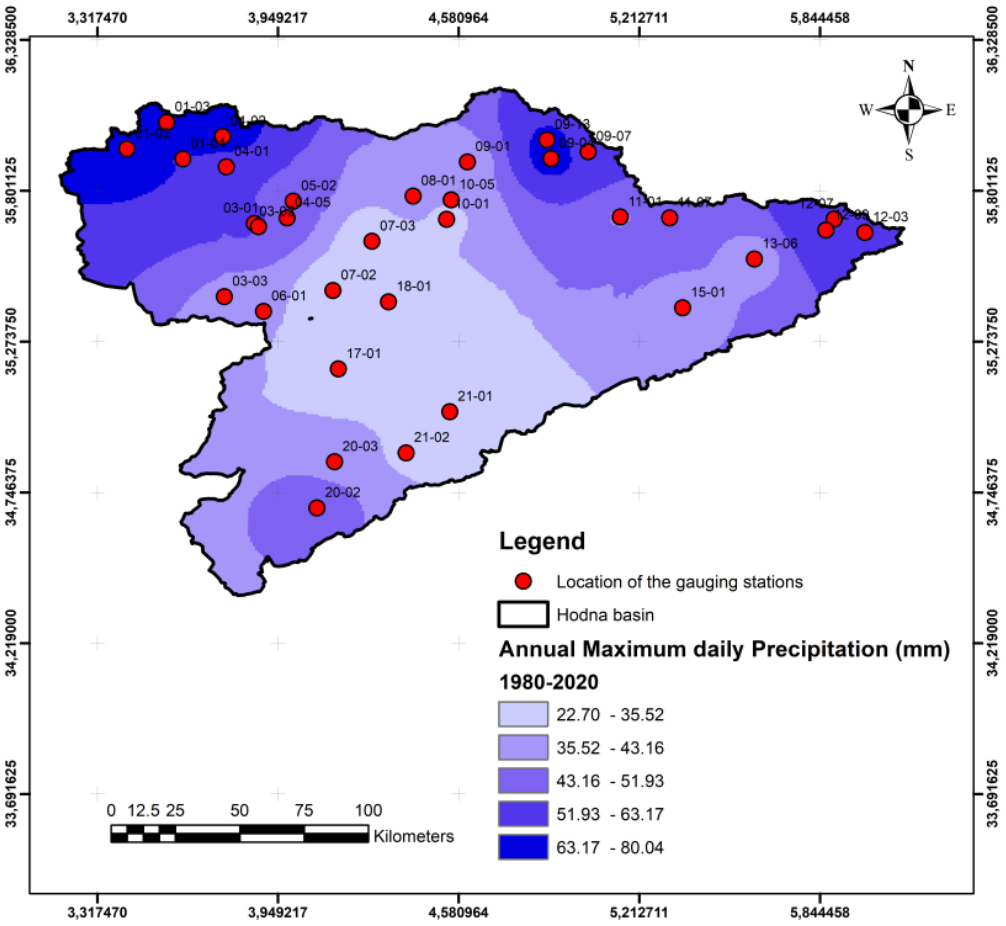

Fig. 3.3 Annual maximum daily precipitation for the Hodna basin during the period 1980-2020

- *Slope map (S)*

Precipitation movement depends on the drainage basin slope, which is an important factor in determining the discharge rate. Low slope values increase the risk of water accumulation on flat surfaces (Ogato et al., 2020) in contrast to the high slope which reduced the risk of water accumulation as a result of the high water velocity. The slope raster map was generated using DEM and the *Slope* tool is ArcGIS software (Figure 3.4). It is then reclassified into five classes, from “very low” to “very high” susceptibility to flood risk.

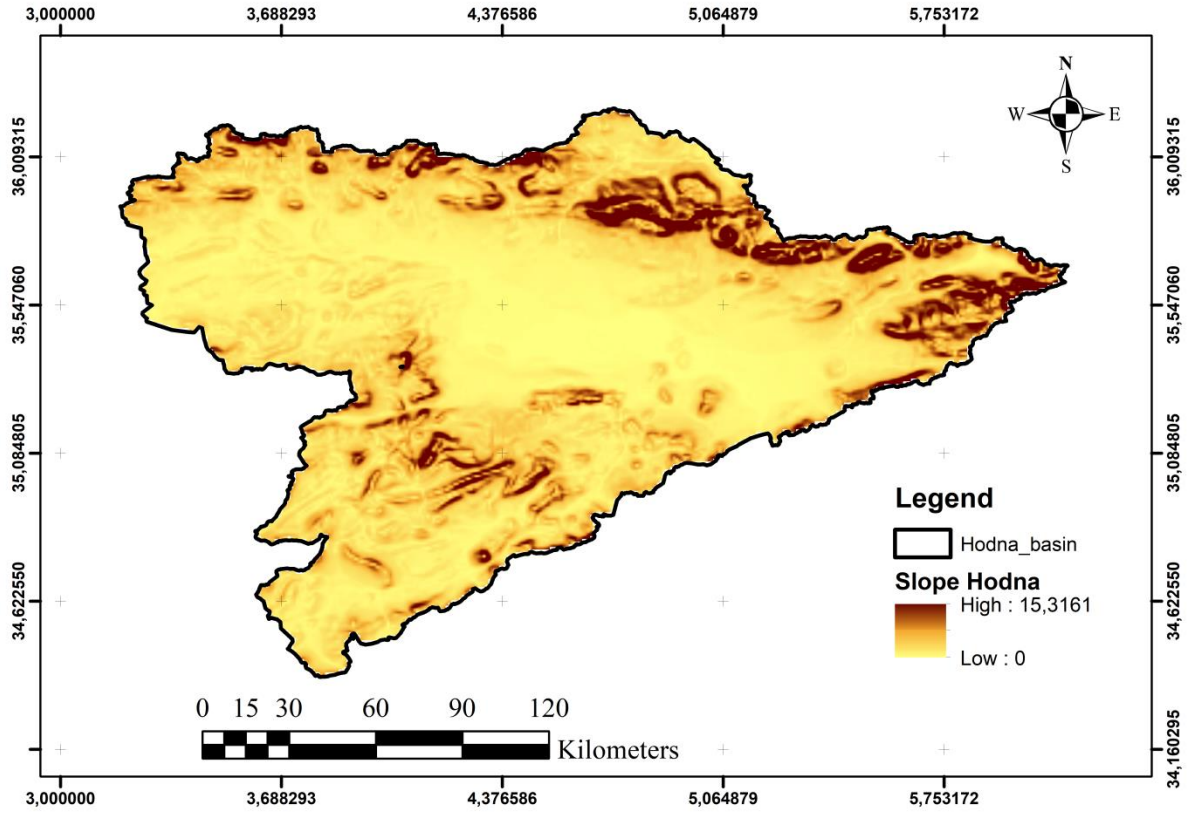

Fig. 3.4 Slope map of the Hodna basin

- *Drainage Density map (DD)*

Drainage Density is a fundamental concept in hydrology as it is the ratio of total drainage lengths per catchment area. Permeability is controlled by the whetherability of surface materials, vegetation, slope and duration. It is an inverse function of infiltration (Abdalla, 2012; Mokadem et al., 2018; Ogato et al., 2020).

DEM is employed to obtain the drainage network using several tools such as *Fill*, *Flow Direction*, *Flow Accumulation*, *Raster Calculator* and also the *Density* tools to extract the drainage density (Figure 3.5). Rank 5 is for the lowest drainage density, while rank 1 is for the highest value. This classification was generated using the Natural Breaks (Jenks) classification.

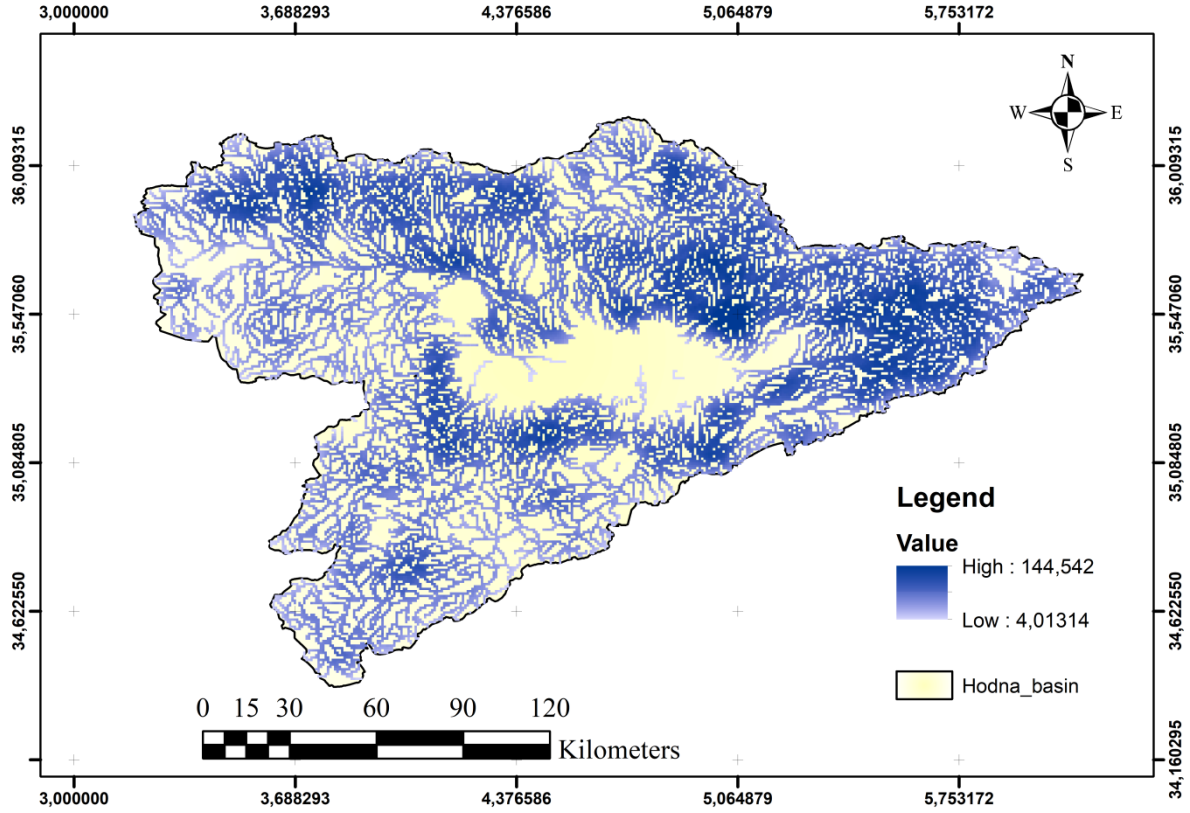

Fig. 3.5 Drainage density map of the Hodna basin

- *Land use/land cover map (LULC)*

Seepage and runoff are dependent on land use/cover type. As defined in the literature, forest, glaciers, rivers, and bare soil or rocks are among significant factors (Cihlar and Jansen, 2001). Land use/land cover features are generated by municipalities, such as buildings and roads in an urban area.

For the Hodna basin, the *clip* tool in ArcGIS is used to clip the study area from the global land use/cover map (Figure 3.6). The existing land cover classes of the area are then reclassified into five groups according to their susceptibility to flood risk and ranked from 1 to 5 according to their impact on flooding.

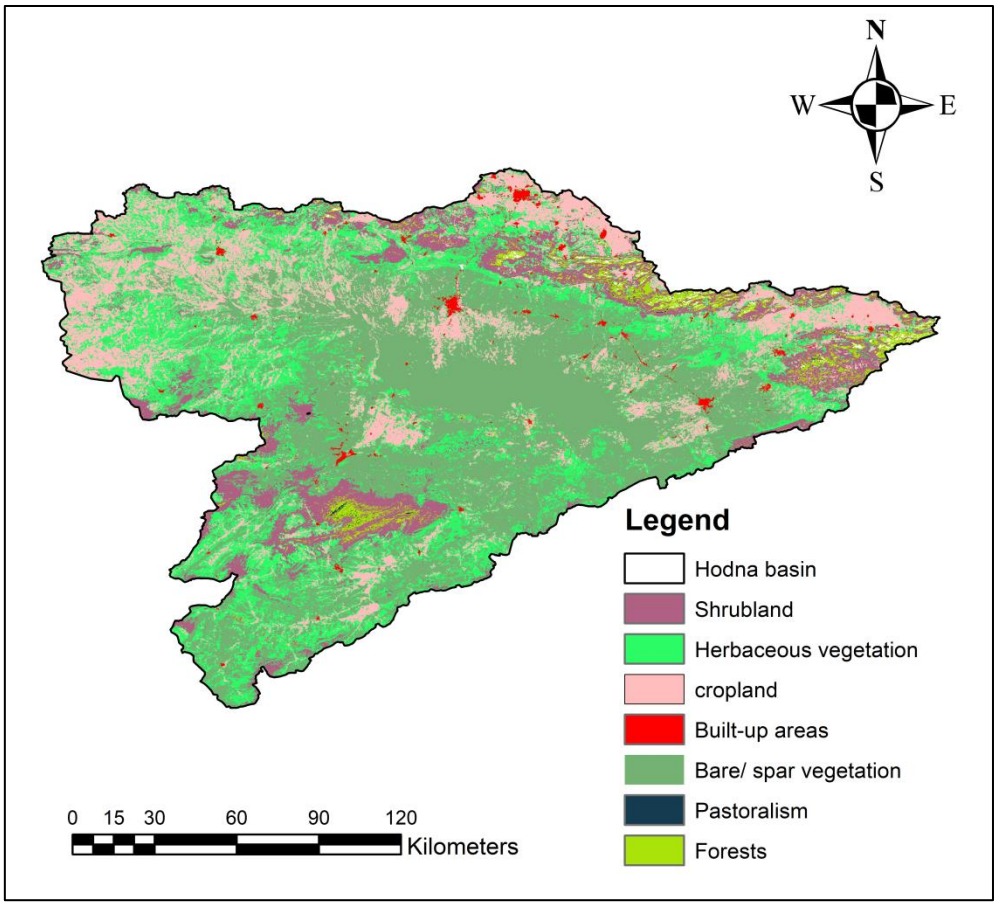

Fig. 3.6 Land use/ land cover map of Hodna basin (ANRH, 2020)

- *Soil type*

The soil type map for the Hodna basin was drawn using FAO (1974) global soil map (see Figure 2.18 in Chapter 2). The final map is then converted to a raster and reclassified into five classes ranging from very low (value 1) to very high (value 5) depending on overflow sensitivity.

- *Population Density*

Population density data correspond to Algeria's 2008 census as the number of people per square kilometer. A population density map is prepared using the Clip tool based on the Algerian districts map, and then the density data is introduced in the attribute table in ArcGIS software (Figure 3.7). The final map is then converted into a raster and reclassified into five classes ranging from very low (value 1) to very high (value 5) depending on overflow sensitivity.

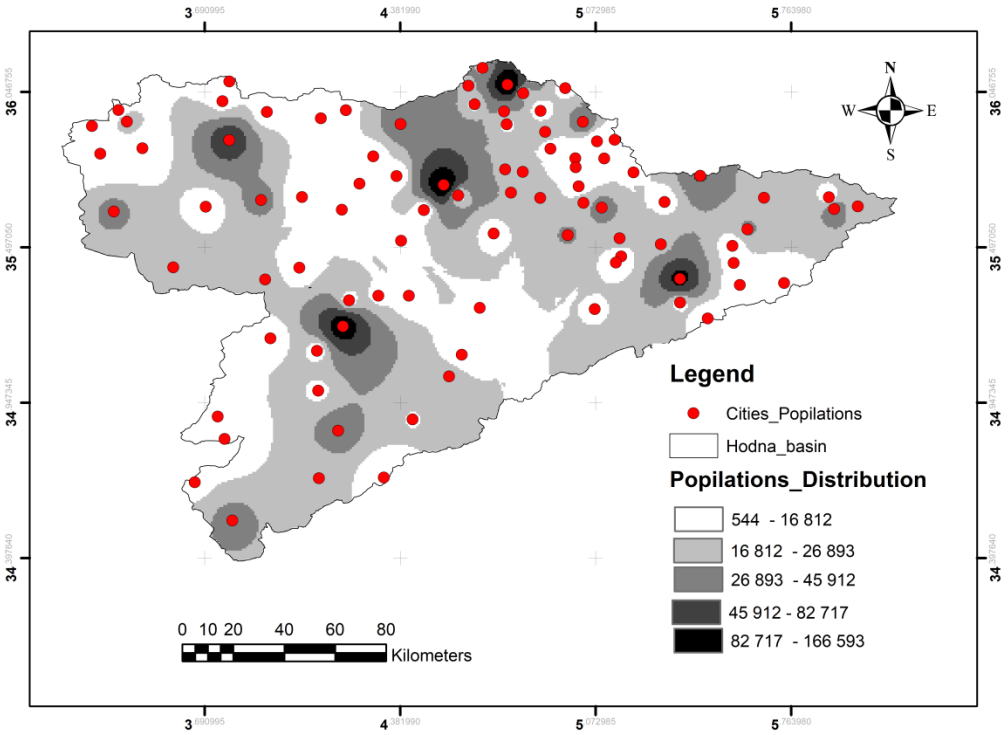

Fig. 3.7 Population distribution of 2008 in the Hodna basin (habitant/km²)

c) Flood risk mapping

- *Flood hazard map*

Hazard refers to the possibility of future occurrence natural or man-made physical events that may have adverse effects on sensitive and exposed elements (UNDHA, 1992). Flood hazard factors are selected through literature review and expert views. Among the factors are precipitation distribution, slope, soil type, drainage density and land use/cover maps (see flowchart in Figure 3.8). The same classification of the previous layers applies to the flood hazard layer, as follows:

$$FHI = (R*W1) + (S*W2) + (DD*W3) + (LULC*W4) + (ST+W5) \quad \text{(Eq. 3.23)}$$

Where FHI is flood hazard index, R is rainfall distribution parameter, S is slope, DD is drainage density, LULC is land-use/land-Cover parameter, ST is soil type parameter, and finally, W1, W2, W3, W4 and W5 are suitable weight parameters.

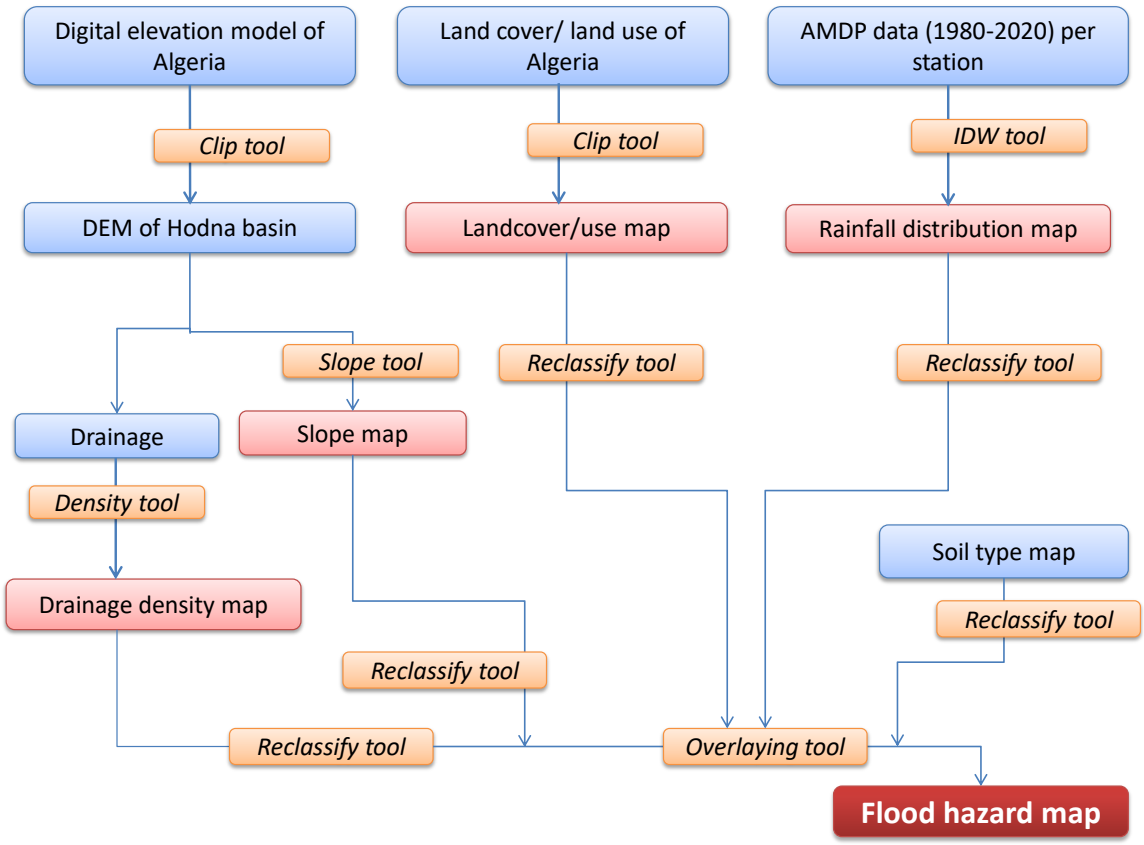

Fig. 3.8 Procedures of flood hazard map extraction using ArcGIS software

- *Flood risk map*

Risk for a natural disaster event is defined as the mathematical product between vulnerability and danger, which expresses the expected loss from a particular element at risk (Dall'Osso et al., 2006). Flood risk assessment is performed by flood hazard zoning and the summation of vulnerabilities derived from various vulnerability indicators (Shivaprasad et al., 2017). Flood risk factors are taken into consideration while preparing flood hazard and population density maps. The flood risk map is obtained by a spatial overlay tool with ArcGIS software (see Figure 3.9). Five risk classes have been defined to classify the sub-basin according to various risk severity zones ranging from high to low (Musungu et al., 2012; Elsheikh et al., 2015).

$$FRI = (FHI * \mathrm{W6}) + (PD * W7) \qquad (Eq.\ 3.24)$$

Where FRI is flood risk index, FHI is flood hazard index, PD is population density parameter and W6 and W7 are the appropriate weight parameters.

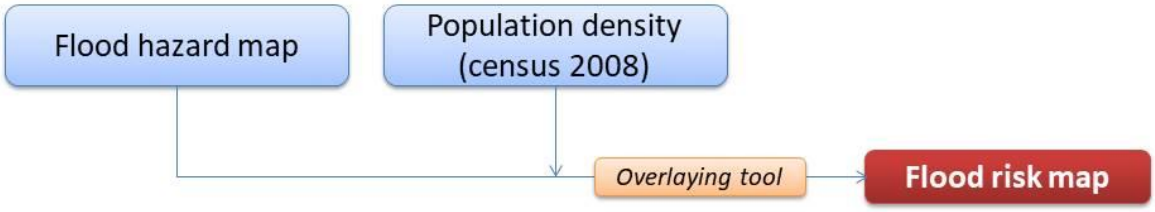

Fig. 3.9 Procedures of flood risk map extraction using ArcGIS software

3.4.2. Flood assessment using HEC-RAS 1D model

3.4.2.1. Objective of the study

The objective of the second part of the thesis, is to analyze flood hazard and inundation area mapping of high density cities forming the Hodna basin. The selected cities are Sidi Aïssa, Boussaada, Barika, M'sila and Bordj Bou Arreridj, which correspond to El-Ham, Boussaada, Barika and K'sob wadis respectively. Therefore, the HEC-RAS model is used for the purpose of this study. Hence, the 1D model is used to simulate the steady flow response during the flood for different return periods of 10-year, 50-year, 100-year and 1000-year.

3.4.2.2. Methodology

The HEC-RAS vs. 6.3.1 floodplain mapping hydraulics model has been used based on the assessed peak flows data (Table 3.4) found in the scientific literature (e.g. Hasbaia et al., 2012; Adoui, 2013; Zeroual, 2016; Redjem et al., 2020). One dimensional (1D) models are simplified models, utilized to characterize the study terrain through calculation of water depth and flow velocity (Vargas, 2016). Figure 3.10 shows the geometry input within the RAS mapper in HEC-RAS.

Table 3.4 Peak discharge values used to perform the hydraulic simulation in selected cities

City	Sub-basin/ Watershed	Station code	Surface area (km^2)	Return period	Peak discharge (m^3/s)	References
Sidi Aïssa	Sub-basin: El-Ham Watershed: Djenene	050104	848.929	10-year 50-year 100-year 1000-year	1731.669 3157.493 3608.198 4945.023	Hasbaia and Adoui (2015); Bendjeddou (2013)
M'sila	Sub-basin: K'sob Watershed: M'sila	050410	2187.02	10-year 50-year 100-year 1000-year	1680.06 2789.62 3210.34 3629.18	Hasbaia et al. (2015); Hasbaia et al. (2018); Redjem et al. (2020)
Boussaada	Sub-basin:	050718	1253	10-year	929.83	Hasbaia et al.

	Boussaada Watershed: Boussaada			50-year 100-year 1000-year	1535.8 1760.3 2412.9	(2012); Hasbaia and Benayada (2010)
Barika	Sub-basin: Barika Watershed: Bithem – Barika	050615	1400.93	10-year 50-year 100-year 1000-year	993.78 1836.28 2061.11 2747.18	Bendjeddou (2013); Hasbaia et al. (2015)
Bordj Bou Arreridj	Sub-basin: K'sob Watershed: K'sob	050409	1453.58	10-year 50-year 100-year 1000-year	1520 2200.3 2840.7 3350.8	Hasbaia et al. (2018); Zeroual (2016)

a) Required dataset

Numerous steps are required to obtain the water heights corresponding to the previously predicted flows, namely:

- 30 x 30 meters Digital Elevation Model (DEM) of the Hodna basin,
- Google Earth imagery (available in RAS mapper),
- Open Street Map (available in RAS mapper),
- Manning's roughness coefficient table,
- Geometry data of each wadi (stream lines, bank lines, flow paths, cross sections),
- Downstream boundary conditions,
- Peak flow of rivers passing through selected cities corresponding to 10-year, 50-year, 100-year and 1000-year return periods.

DEM was used as satellite images and overlaid maps in RAS mapper to define streams lines of each wadi of the OSM, El-Ham, Boussaada, K'sob and Barika sub-basins. Because HEC-RAS requires the bank stations of each cross section, bank lines are drawn along the stream. These are used finally to determine the shape of the riverbed at each point. In addition, flow paths are also drawn to determine floodplains.

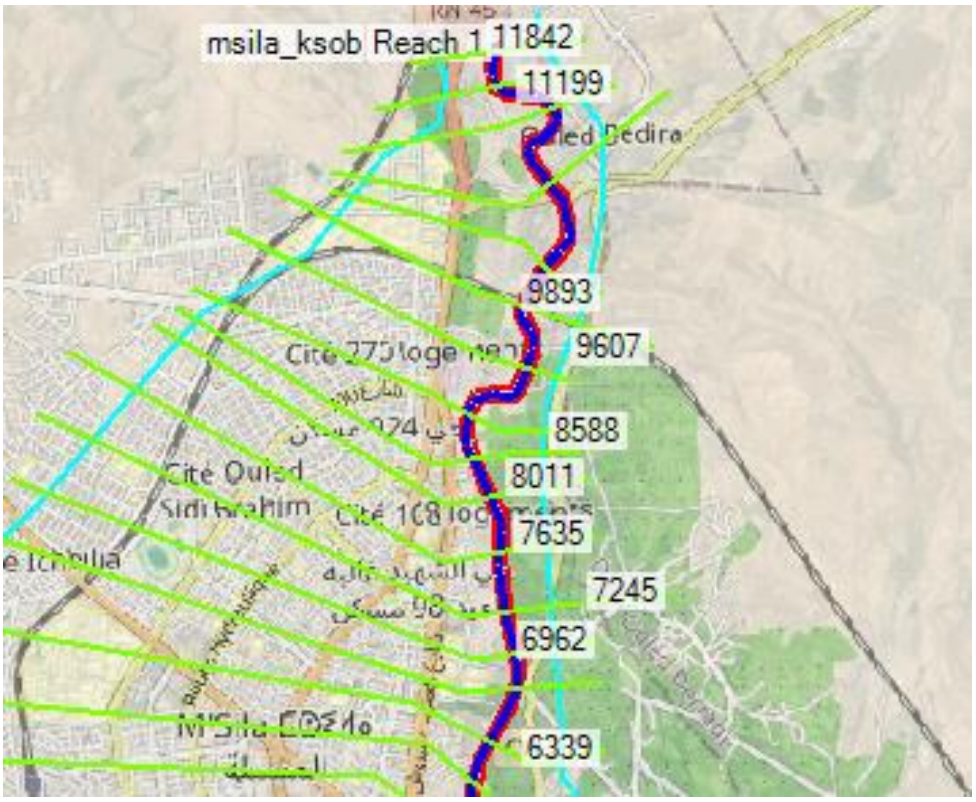

Fig. 3.10 Stream lines (blue), banks lines (red), flow paths (light blue), and cross-sections (green) in K'sob wadi

The next step is to assign Manning's roughness coefficient values to the geometry data. Table 3.5 presents the land use and Manning values utilized in the presented case study. They are used to define roughness in each cross-section (Goodell and Warren, 2006).

Table 3.5 Roughness values for different land cover types used in the model simulation (Albertson and Simons, 1964; Barnes, 1967)

Land use	Manning's roughness coefficient
Stream (natural channel)	0.02-0.04
Stream (natural channel with vegetation)	0.04-0.1
Built-up area	0.100
Forest	0.150
Residential areas (high density)	0.2-0.5
Residential areas (low density)	0.1-0.2
Grassland	0.045
Default	0.035

b) Hydraulic simulation

Hydraulic simulation has been performed for five different wadis in the cities of Sidi Aïssa, Boussaada, M'sila, Bordj Bou Arreridj and Barika. For instance, the studied reach of Sidi Aïssa is a part of El-Ham sub-basin in the large Hodna basin particularly in the Djenene wadi

watershed (Figure 3.11). First of all, Djenene wadi has been drawn on the basis of a google earth image in RAS mapper as presented in Figure 3.12.

The boundary condition used in this study, is the normal depth slope assumption. Therefore, only downstream boundary conditions are introduced as the flow analysis type is steady. Peak flow discharges have been also added to the same window according to Table 3.4. After entering flow and boundary conditions data, HEC-RAS can simulate a steady flow for a sub-critical flow. Floodplain mapping is then performed for four profiles PF1, PF2, PF3 and PF4 correspond to 10-year, 50-year, 100-year and 1000-year return periods respectively.

Geographical location, satellite imagery and geometry data of Sidi Aïssa city are presented in Figures 3.11 and 3.12, of Boussaada city in Figures 3.13 and 3.14 and of Barika city in Figures 3.15 and 3.16. In addition, the same data are shown in Figures 3.17 and 3.18 for Bordj Bou Arreridj city and M'sila city in Figures 3.19 and 3.20.

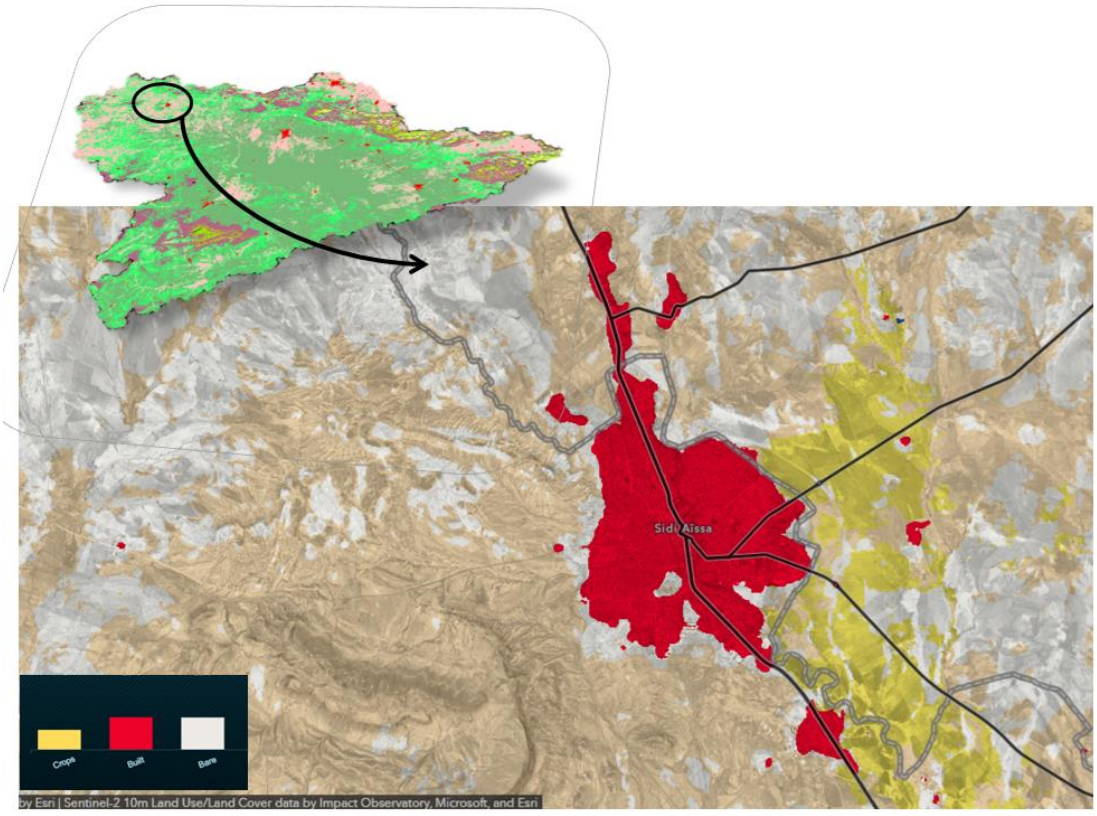

Fig. 3.11 Location of Sidi Aïssa city within Hodna basin and land use map (obtained from Esri Sentinel2- 10m Land cover Explorer 2020)

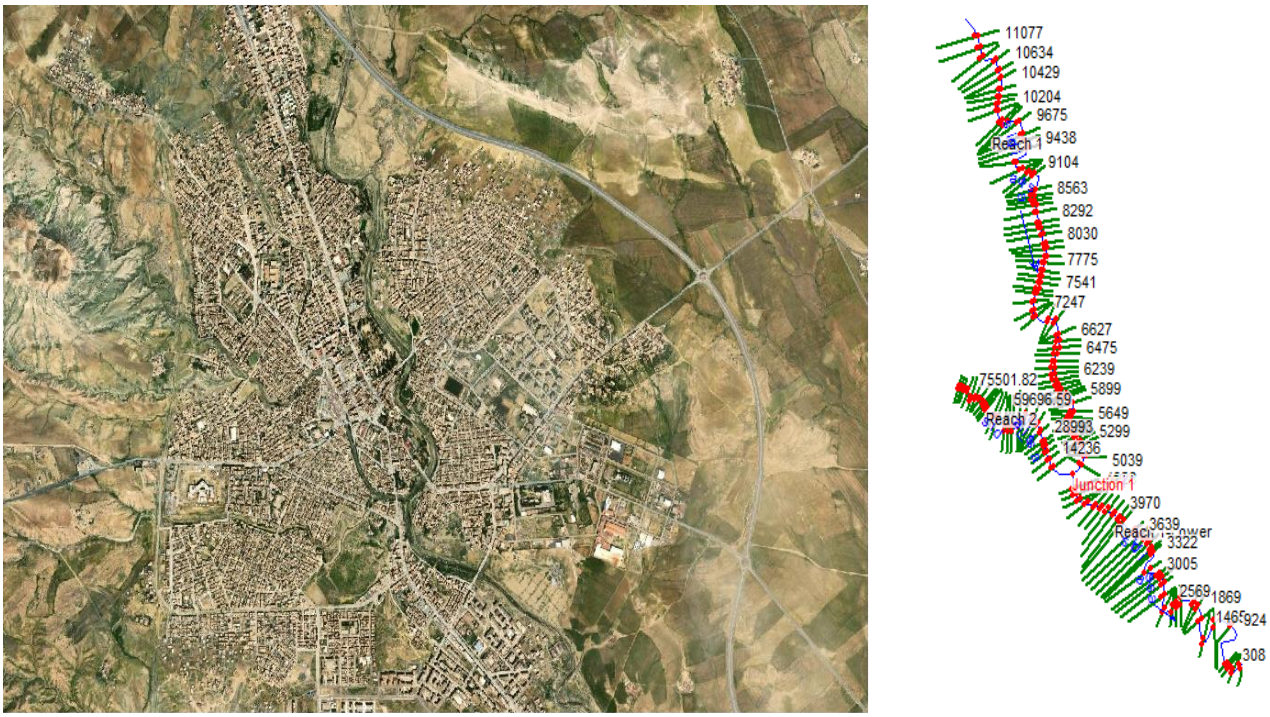

Fig. 3.12 Satellite imagery of Sidi Aissa city (to the left) and Djenene reach geometry in HEC-RAS (to the right)

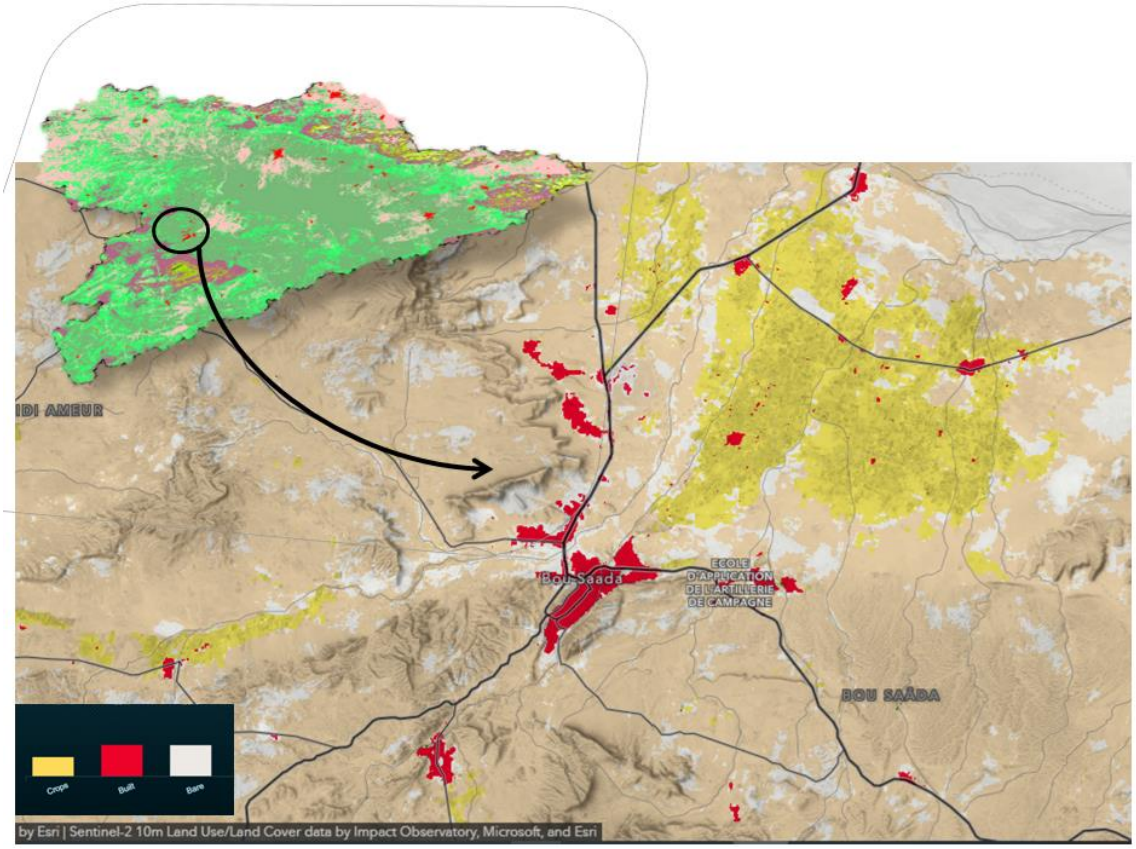

Fig. 3.13 Location of Boussaada city within Hodna basin and land use map (obtained from Esri Sentinel2- 10m Land cover Explorer 2020)

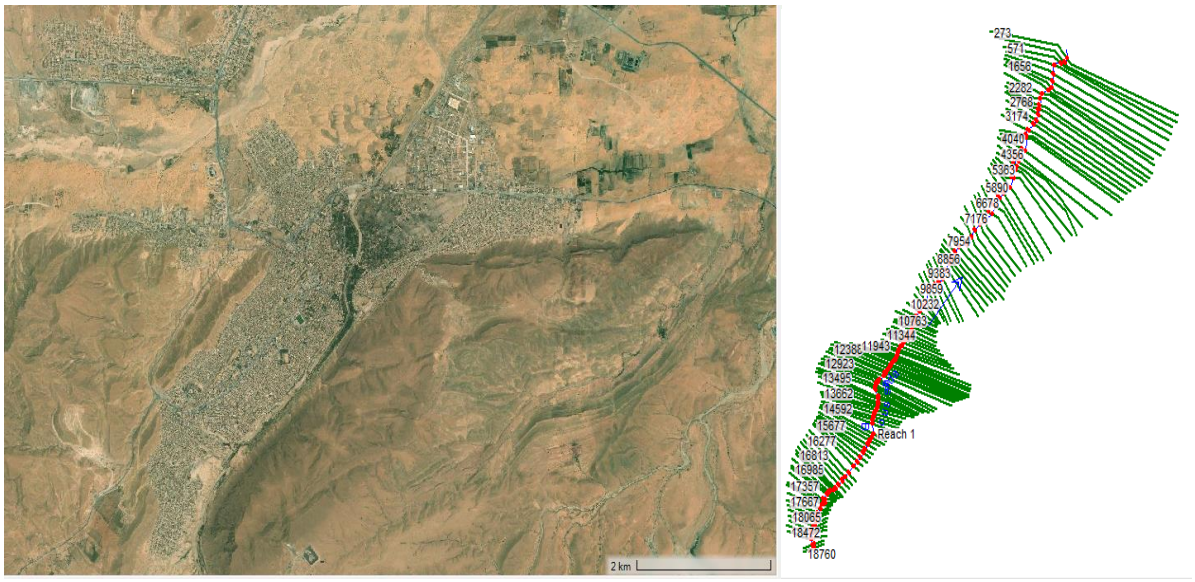

Fig. 3.14 Satellite imagery of Boussaada city (to the left) and Boussaada reach geometry in HEC-RAS (to the right)

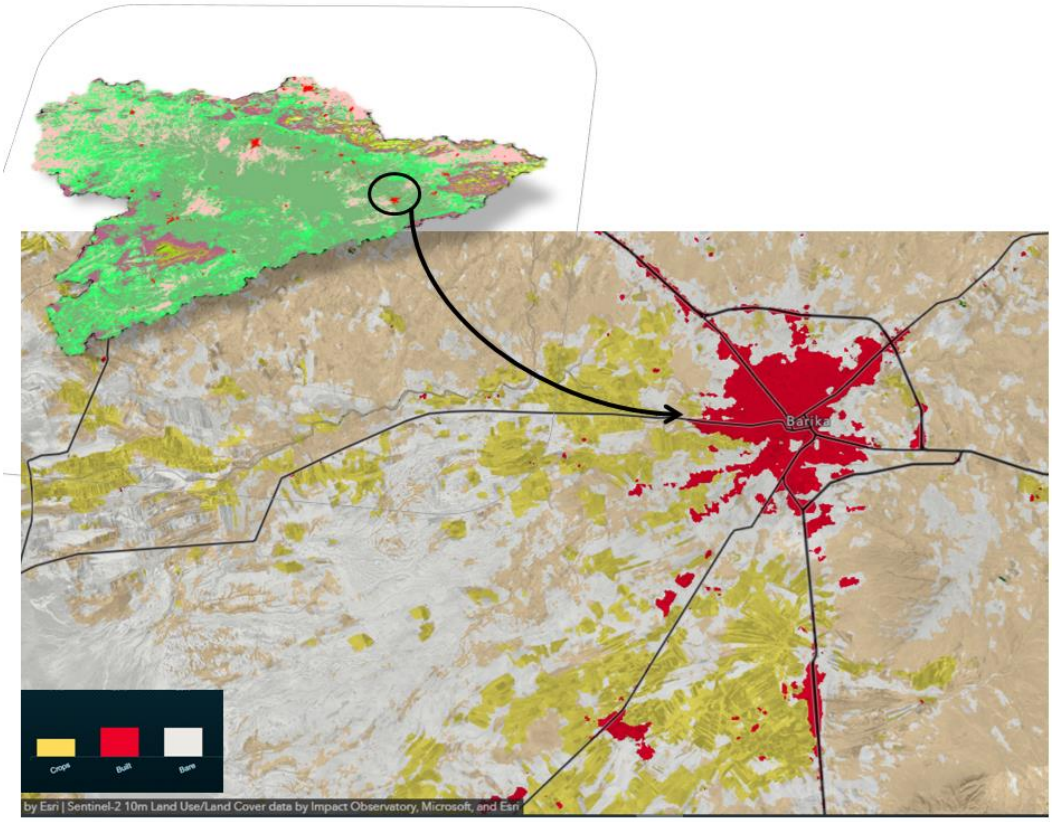

Fig. 3.15 Location of Barika city within Hodna basin and land use map (obtained from Esri Sentinel2- 10m Land cover Explorer 2020)

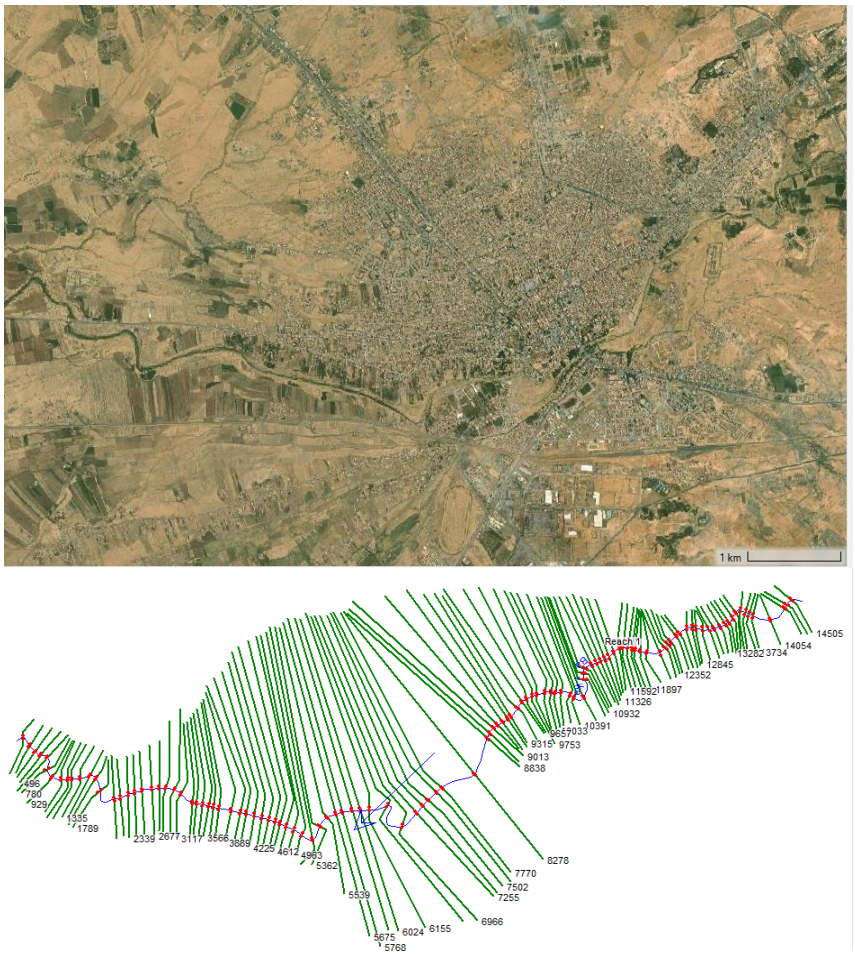

Fig. 3.16 Satellite imagery of Barika city (at the top) and Barika reach geometry in HEC-RAS (at the bottom)

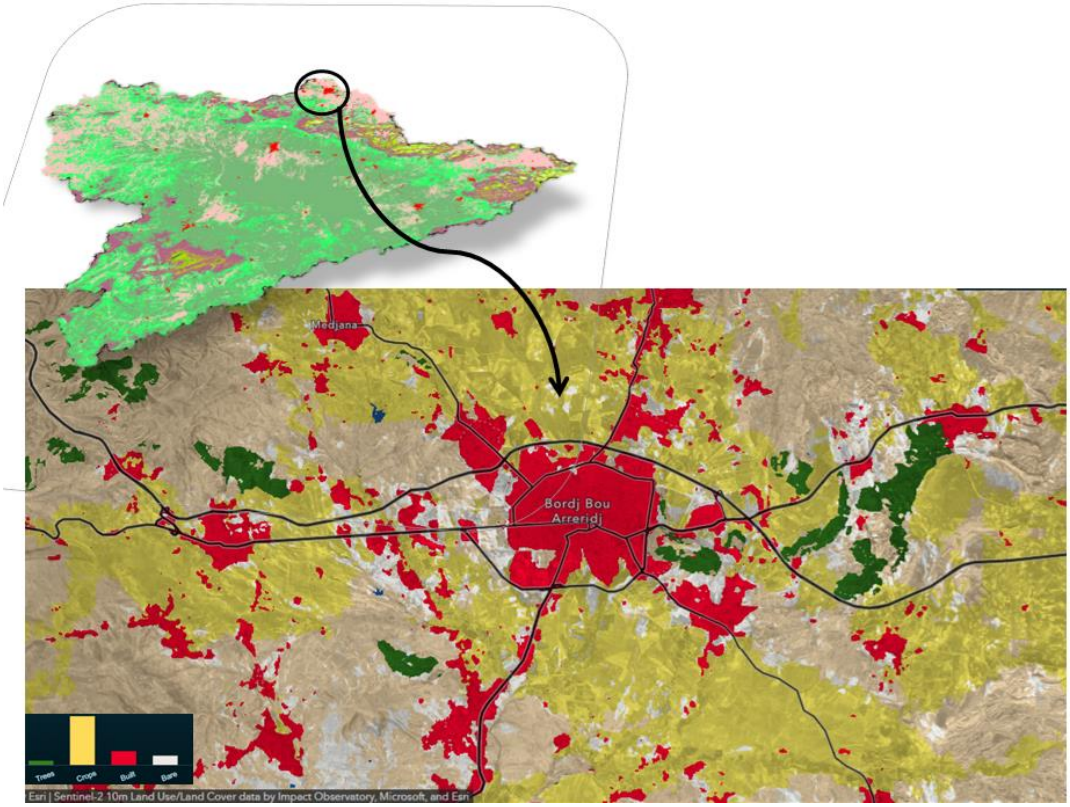

Fig. 3.17 Location of Bordj Bou Arreridj city within Hodna basin and land use map (obtained from Esri Sentinel2- 10m Land cover Explorer 2020)

Fig. 3.18 Satellite imagery of Bordj Bou Arreridj city (to the left) and upstream K'sob reach geometry in HEC-RAS (to the right)

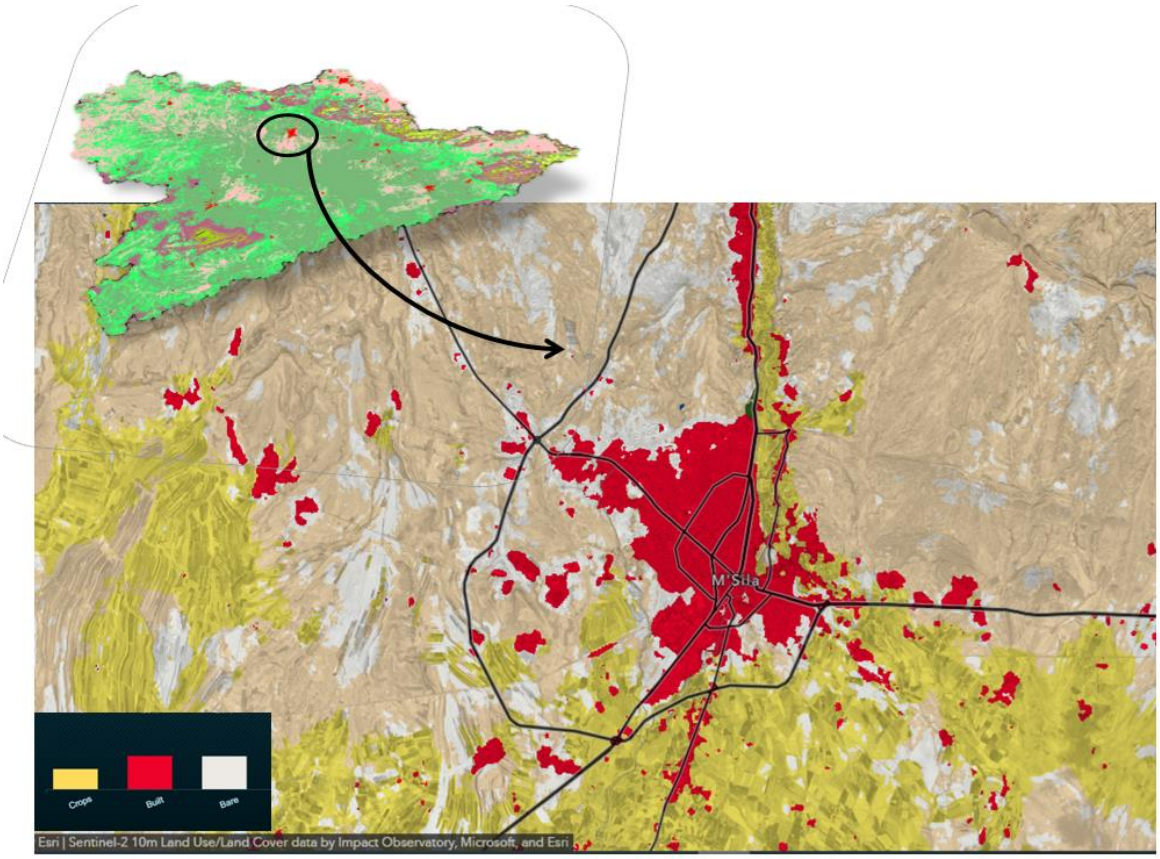

Fig. 3.19 Location of M'sila city within Hodna basin and land use map (obtained from Esri Sentinel2- 10m Land cover Explorer 2020)

Fig. 3.20 Satellite imagery of M'sila city (to the left) and downstream K'sob reach geometry in HEC-RAS (to the right)

3.5. Historical evaluation of future projections of monthly precipitation and maximum temperature

The impacts of climate change are becoming a very serious problem in our continent, Africa on environment, society and economy. According to IPCC reports (IPCC 2007, 2012, 2013) an increase in temperature and a decrease in rainfall can be clearly observed in most parts of Africa. In fact, North Africa has been identified as the most vulnerable region to climate change, particularly water resources (UNFCCC, 2010; IPCC, 2014). For many years, this region has been subject to extreme temperatures and severe droughts leading to water scarcity (IPCC, 2018). Mahmoud et al. (2019) is a recent example that highlights the sensitivity of land cover to change, especially changes in temperature and precipitation, which are considered to be the most relevant drives of climate change. Ajibola et al. (2020) focused on evaluating High-Resolution Model Inter-comparison Project (HighResMIP) simulations and used three different precipitation dataset sources (CRU, GPCC and UDEL). Ayugi et al. (2021) reported the main outcomes of the assessment and projection of mean surface temperature based on statistical metrics and ranking using CP method. Additionally, Lim Kam Sian et al. (2021) investigated spatio-temporal precipitation variability and trends with the Theil-Sen slope estimator. Rivera and Arnould (2020) confirmed the decline in precipitation for different GCMs and presented its temporal and spatial changes over the studied region.

Similar to southern countries of the Mediterranean, Algeria faces the challenge of management and sustainable development of its limited water resources due to high demand for irrigation and human utilization, at a time, when the risks of desertification and global warming are very high (Meddi et al., 2010; Zeroual et al., 2013). The increase in temperature (droughts events since 1970s) (Meddi & Humbert, 2000) and precipitation (decrease of approximately 25%) in Algeria since 1960s is one noticeable example of climate change. However, only a few studies have been conducted on Algeria, most of which are in regional context (Zeroual et al., 2019, Babaousmail et al., 2021; Ajjur and Al-Ghamdi, 2021).

3.5.1. Objective of the study

The main purpose of the last part of the study is to evaluate and rank CMIP6 GCMs for the 1901-2014 baseline period over the Hodna basin region in central Algeria. Total monthly precipitation and maximum surface temperature are the variables chosen for the past simulations of GCMs. Best-ranking climate models are projected for future simulations (2021-2040, 2041-2060, 2061-2080 and 2081-2100) under two different SSPs scenarios (SSP1-2.6 and SSP3-7.0). Six GCMs are selected for the purpose of this study, which are ACCESS-ESM1-5, BCC-CSM2-MR, CanESM5, GFDL-ESM4, IPSL-EM6A-LR and MIROC6.

As there is no previously reported research on the Hodna basin, this study can be considered as an excellent contribution towards more detailed findings and accurate outcomes in the Hodna basin as it is for the whole Algeria. Under the light of present and future global warming effects, climate change impacts on water resources availability, droughts and floods cause to inflicting damages.

3.5.2. Methodology

The World Meteorological Organization (WHO, 2019) recommends the most-recent 30-year period in a year whose climatological standard normal ends with zero. 30-years period for climate study is considered the basic for characterizing the statistics of weather at a specific location and thus determining the climate in that location. At some point, climate can be considered more or less stationary (Görgen et al., 2010). For this reason, the period between 1901 and 2014 was chosen as the reference period. Finally, monthly total precipitation and maximum surface air temperature future projections are calculated over Hodna basin region in Algeria. Hodna basin is regarded amongst the most important large watersheds in Algeria. Four future periods are chosed as near future (2021-2040), mid-century (2041-2060 and 2061-2080) and lastly the far future period (2081-2100). Ongoing work analyzes in the project were made using the ArcGIS vs 10.4 and OriginPro vs 2021b softwares.

The adopted methodology and principal followed procedures in this study are showed in Figure 4 with details of discussion in the next sections. The World Meteorological Organization (WHO, 2019) recommends the last 30-year period in a year whose climatological standard normal ends with zero. For climate study, the

30-years period is considered the basic for characterizing the weather statistics in a specific location and thus determining the climate in that location. At some point, the climate can be considered stationary (Görgen et al., 2010). For this reason, the years between 1901 and 2014 were chosen as the reference period. Finally, monthly total precipitation and maximum surface air temperature future projections are calculated over the Hodna basin region in Algeria. The Hodna basin is regarded among the most important large watersheds in Algeria. Four future periods are chosen as near future (2021-2040), mid-century (2041-2060 and 2061-2080) and finally the far future period (2081-2100). Ongoing work analyzes in the project were made using the ArcGIS vs 10.4 and OriginPro vs 2021b software.

The methodology adopted and the basic procedures followed in this study are showed in Figure 3.21 with details of discussion in the next sections.

a) Dataset

The variables related to the purpose of this study are precipitation and maximum surface air temperature obtained from 6 Atmosphere-Oceans General Circulation Models (AOGCMs) from CMIP6 archive of the earth system grid federation online system (*https://esgf-node.llnl.gov/search/cmip6/*). The ESGF data portal serves as GCMs downloading portal available for three phases of CMIP 3, 5 and 6 correspond to SRES, RCP and SSP scenarios, respectively. It is designed to provide access to CMIP model outputs hosted by several institutions worldwide (Ajibola et al., 2021).

The CMIP6 multi-model ensemble used here consists of monthly outputs from past and future scenario simulations from 6 models (see Table 1, presents climate models names, institutions, countries and horizontal resolution). Two SSPs are selected to simulate future projections, namely SSP1-2.6 and SSP3-7.0 as mentioned by the IPCC (2014). The r1i1p1f1 ensemble members are chosen for each model representing the realization, initialization and physics of model (Shiru and Chung, 2021). The selected scenarios explore and put the light on the lowest and highest challenges to both mitigation and adaptation, which they basically focus on environmental, regional, and local issues (Su et al., 2020).

Despite a more accurate understanding of climate change in the study region and occasional bias corrected CMIP6 data, monthly Hodna-mean precipitation and maximum surface air temperature AOGCMs simulations and observations from

global gridded datasets are compared. This can avoid unreliable climate change assessment (Ajjur and Al-Ghamdi, 2021). However, predictions cannot be made with complete safety, but to reach the least hazardous consequences (Şen, 2018).

Studies based on a single GCM can give misleading information. Therefore, the application of multiple GCMs helps to give different projections for the climate variables for the same future GHG emission scenario (Reshmidevi et al., 2017). In this study, the six (06) used models have been selected to show the effect of climate change in Hodna basin. For further comparative studies, other models can be sued without any particular difficulties. Additionally, the main variables adopted in our study (precipitation and maximum air surface temperature) need to be both included in the chosen model. Moreover, after a first selection of climate models based on available variables (pr and tmax), variant label (r1i1p1f1), and monthly scale, another final selection has to be made on the basis of WorldClim available models' outputs.

WorldClim is a dataset of CMIP6 future downscaled projections (Hijmans et al., 2005) (https://www.worldclim.org), and a baseline climate model that can calculate current climate conditions at a 1km² highest resolution (Molyneux et al., 2015). Only a specific number of models' outputs can be found within WorldClim; and this is the other reason why the authors have chosen only six models. Four periods are concerned; 2021-2040, 2041-2060, 2061-2080 and 2081-2100 for both scenarios SSP1-2.6 and SSP3-7.0.

Globally interpolated gridded datasets have been generated and developed by leading scientific research centers around the world to predict air, water, and climate change, the most common are: Global Precipitation Climatology Center (GPCC) (Lim Kam Sian et al., 2021), Tropical Rainfall Measurement Mission (TRMM), CICS High-resolution Optimally interpolated Microwave Precipitation from Satellite (CHOMPS), National Center for Environmental Protection (NCEP) and Climatic Research Unit (CRU) dataset (Mahmood et al., 2019).

For this, we referred to the University of East Anglia's, Climatic Research Unit – Time Series version 4.04 (CRU-TS vs 4.04, January 1901-2019) datasets. The datasets are available at 0.5° x 0.5° grid resolution (*https://crudata.uea.ac.uk/cru/data/hrg/)* (Harris et al., 2020). To accurately perform

the evaluation of CMIP6 models' historical simulations and observations, CMIP6 GCMs historical datasets and observations of precipitation and maximum surface air temperature variables are regridded to a common grid (Panagos et al., 2017; Kalmakar et al., 2019; Almazroui et al., 2020) so comparisons can be made at the same spatial resolution. As this study has been conducted at a basin scale, a finer resolution has to be used. The Geographically Weighted Regression (GWR) downscaling model has been used, to regrid all historical simulations from CMIP6 GCMs to 2.5 arc minutes (approximately equals to 0.0416°, which means 4.5 km²). The GWR model is one the statistical downscaling techniques, more specifically it corresponds to transfer function models (Sun et al., 2022; Wang et al., 2022). The GWR method provides significant outcomes when it is used to downscale climate change impacts to a small-scale catchment (Kara et al., 2016).

CRU data is widely used by the scientific community to access the performance of global models over different regions of the world (Almazroui et al., 2020; Rivera & Arnould, 2020). CRU data were evaluated with in-situ observed data with different statistical indicators in Mahmood and Jia (2018), which showed that CRU data can be used with high confidence. The dataset is derived from archives of meteorological stations from the national meteorological services and other agents subject to comprehensive quality measures (Rivera & Arnould, 2020).

b) NetCDF format of GCMs files

As a first step towards climate change impact study, monthly total precipitation and maximum surface air temperature are analyzed through ESGF CMIP6 climate models. They are only available in the Network Common Data Form (NetCDF) format. NetCDF is a data abstraction for storing and retrieving multidimensional data. It is distributed as a software library that provides a concrete implementation of this abstraction for representing scientific data (Rew and Davis, 1990). In summary, the implemented process went through the following steps for each variable:

1-Obtain the NetCDF data for each variable by specifying the historical scenario,

2-Select the baseline (reference period),

3-Regrid all GCMs to one common spatial resolution (2.5 arc minutes equals to 0.04167° x 0.04167° latitude-longitude) using GWR technique,

4-For each model and each variable, extract the estimated values for the baseline selected period over Hodna basin region using 1480 grid points,

5-Generate monthly means for each variable and each model,

6-After selecting the best performing models (discussed in section below), download the corresponding projections for each of the two variables in the two SSP scenarios,

7-Generate annual means for each time series and each SSP scenarios.

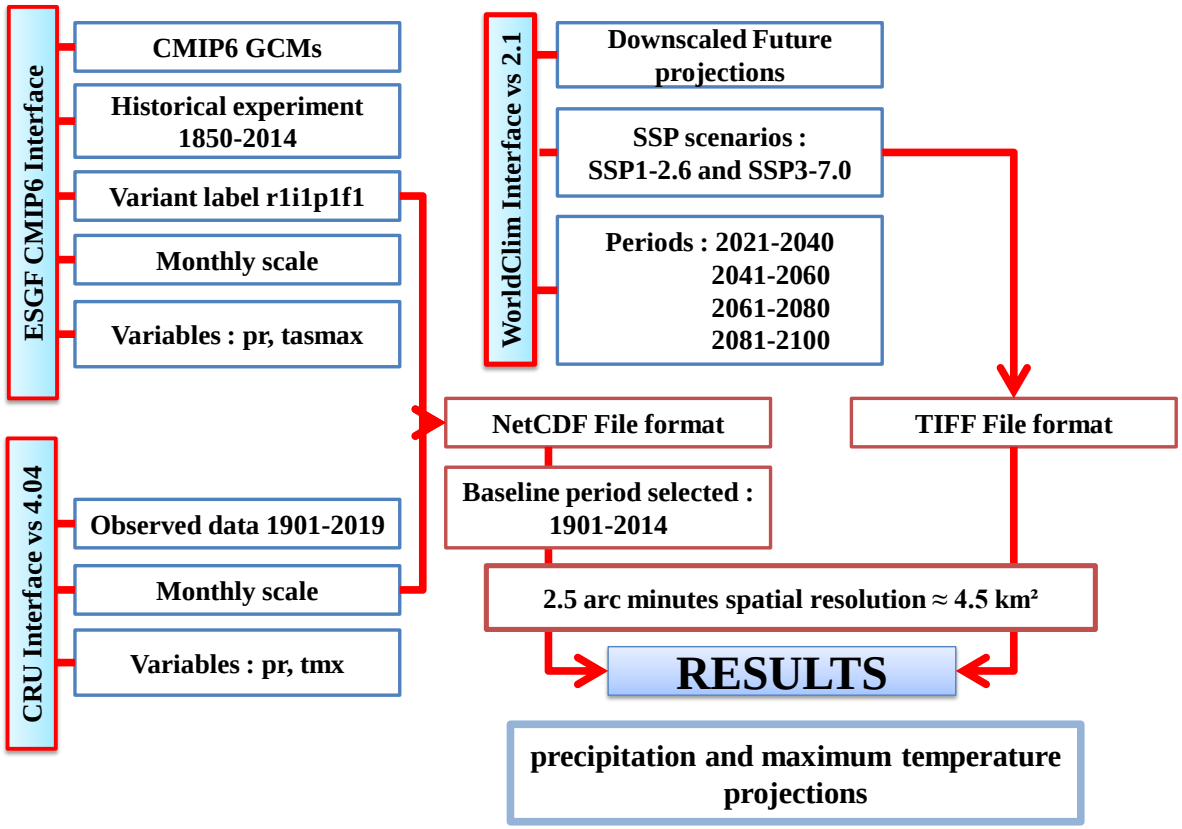

Fig. 3.21 Flowchart of the adopted methodology

c) Evaluation metrics of CMIP6 GCMs : ranking of climate models

Three statistics indices are used to evaluate the CRU dataset and CMIP6 simulations, namely coefficient of determination (R^2), mean absolute bias (MB) and root mean square error (RMSE). R^2 is used to evaluate the correlation between the observed and simulated values, while MB and RMSE are used to assess the bias between the previously mentioned values. There are publications on statistical metrics evaluation in the literature (Peng et al., 2019; Ajibola et al., 2020;

Babaousmail et al., 2021; Usta et al., 2022; Usta et al., 2022), that have mentioned the usefulness in assessing the accuracy of monthly precipitation and maximum surface air temperature in replicating the mean, variability and distribution of observed precipitation and surface air temperature.

$$MB = \frac{\sum_{i=1}^{n} D}{n} - \frac{\sum_{i=1}^{n} S}{n} \qquad \text{(Eq. 3.25)}$$

$$R^2 = \left(\frac{\sum_{i=1}^{n} \left(D - \overline{D}\right)\left(S - \overline{S}\right)}{\sqrt{\sum_{n=1}^{n} \left(D - \overline{D}\right)^2} \sqrt{\sum_{n=1}^{n} \left(S - \overline{S}\right)^2}} \right)^2 \qquad \text{(Eq. 3.26)}$$

$$RMSE = \sqrt{\frac{\sum_{i=1}^{n} (D - S)^2}{n}} \qquad \text{(Eq. 3.27)}$$

Where: S is the precipitation/surface air temperature value acquired from the observation dataset CRU; D is the precipitation/surface air temperature value from CMIP6 simulation; $\overline{S}$ is the mean value of precipitation/surface air temperature observations; $\overline{D}$ is the mean value of precipitation/surface air temperature simulations; n is the number of data pairs.

In this study, the Compromise Programming (CP) method (Zeleny and Cochrane, 1973) has been used for ranking of GCMs. It is a technique used for measuring the combined effect of several statistical performance measures (Ahmed et al., 2019). CP method is widely used in numerous climatic researches (Srinivasa Raju et al., 2017; Selman et al., 2019) mainly to determine the closest ideal and optimal solution compared to other methods of multi-criteria decision-making. Statistical indices are used for the estimation of the distance measure Lp metric of CP. The ideal value of a statistical performance measure refers to its value corresponding to a perfect match between the simulations produced by a model and observations The lowest value of Lp indicates the best-performence (best-ranking) GCM (Romero and Rehman, 2003; Srinivasa Raju et al., 2016; Ahmed et al., 2019; Sreelatha and Anand Raj, 2019; Shiru and Chung, 2021; Zafar et al., 2021). Lp metric is given by the following equation.

$$L_p = \left[\sum_{j=1}^{j} | f_j^* - f_j |^p \right]^{1/P} \quad \text{(Eq. 3.28)}$$

Where: f_j is the value of the statistical performance measure j; f_j^* s the ideal value of the statistical performance measure j; p is a parameter which equals to 1 (all weighted deviations are assumed to compensate each other perfectly).

Table 3.6 The six CMIP6 used models

N°	CMIP6 climate model	Country	Institution	Horizontal resolution (lon. by lat. in degrees)
1	ACCESS-ESM1-5	Australia	Australian Community Climate and Earth System Simulator	1.25° x 1.88°
2	BCC-CSM2-MR	China	Beijing Climate Center Climate System Model	1.13° x 1.13°
3	CanESM5	Canada	Canadian Centre for Climate Modelling and Analysis, Environment and Climate Change	2.81° x 2.81°
4	GFDL-ESM4	USA	Geophysical Fluid Dynamics Laboratory Earth System Model	1.25° x 1.00°
5	IPSL-CM6A-LR	France	Institut Pierre-Simon Laplace Climate Modeling Center	2.50° x 1.26°
6	MIROC6	Japan	Model for Interdisciplinary Research on Climate	1.4° x 1.4°

3.6. Conclusion

In this chapter, the tools and software required for the purpose of the thesis are described. In addition, detailed methodologies for peak flood assessment, flood hazard and risk assessment for different return periods are discussed. The chapter concludes with a description of necessary procedures required for climate change assessment in the Hodna basin, including the impact of changing climate on monthly precipitation and maximum surface air temperature until the 2100.

CHAPTER 4

Peak flow assessment and flood mapping: Interpretation of results

Chapter 4 Peak flow assessment and flood mapping: interpretation of results

4.1. Introduction

In this chapter, the assessment of peak discharges and zones exposed to flood risk is performed. In addition, historical evaluation and future projections continues in the Hodna basin. Hence, the results of the presented study are discussed in details here.

4.2. Peak discharge assessment for different return periods

The concentration time is estimated after application of Basso, Giandotti and ANRH-Sogreah formulas. The selected formulas find wide application in the technical literature due to the limited amount of information they need to estimate the concentration time at the basin scale (Grimaldi et al., 2012). The average concentration time evaluated for the El-Ham wadi sub-basin is 21.5 hours, which is used to estimate the above-mentioned methods.

Along the correction plots with the Gumbel's distribution law (Figures 4.1, 4.2 and 4.3) for the three stations, it is noticed that the Gumbel model is clearly adequate, and the tuning plots made via of the Gumbel PDF law are sufficient for this purpose. The main results of the maximum daily precipitation for the different return periods for three stations are presented in Table 4.1.

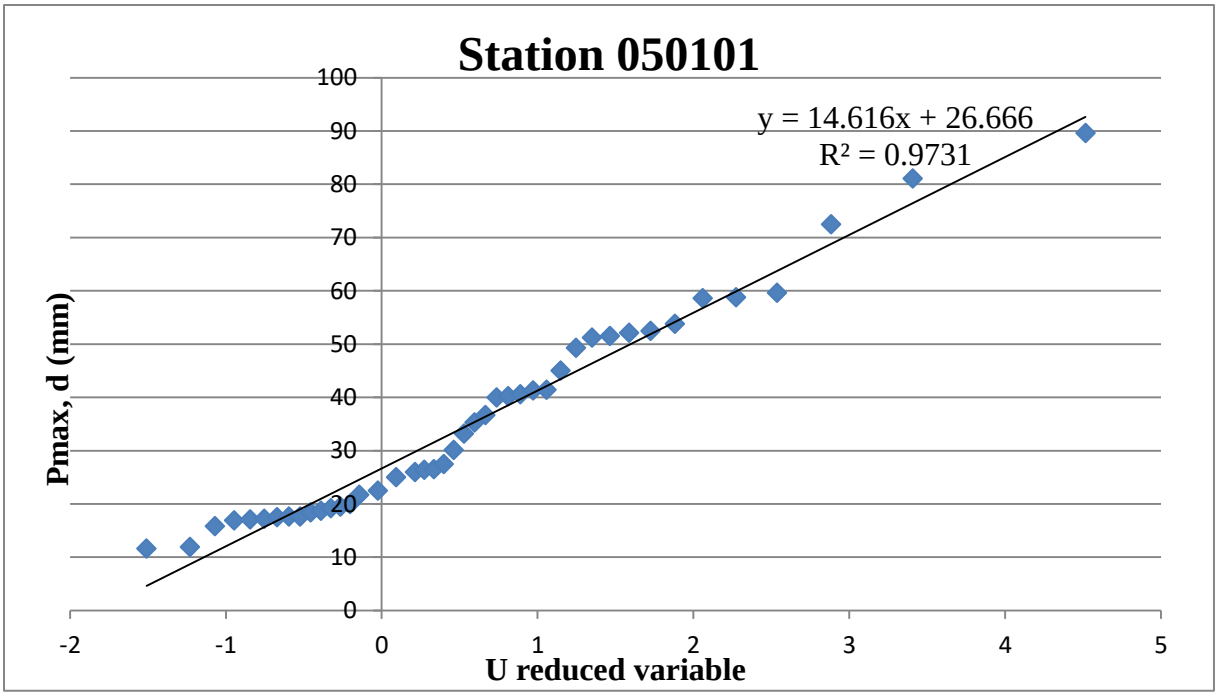

Fig. 4.1 Adjustment of maximum daily precipitation through Gumbel's law of Ain Nessissa (050101) station

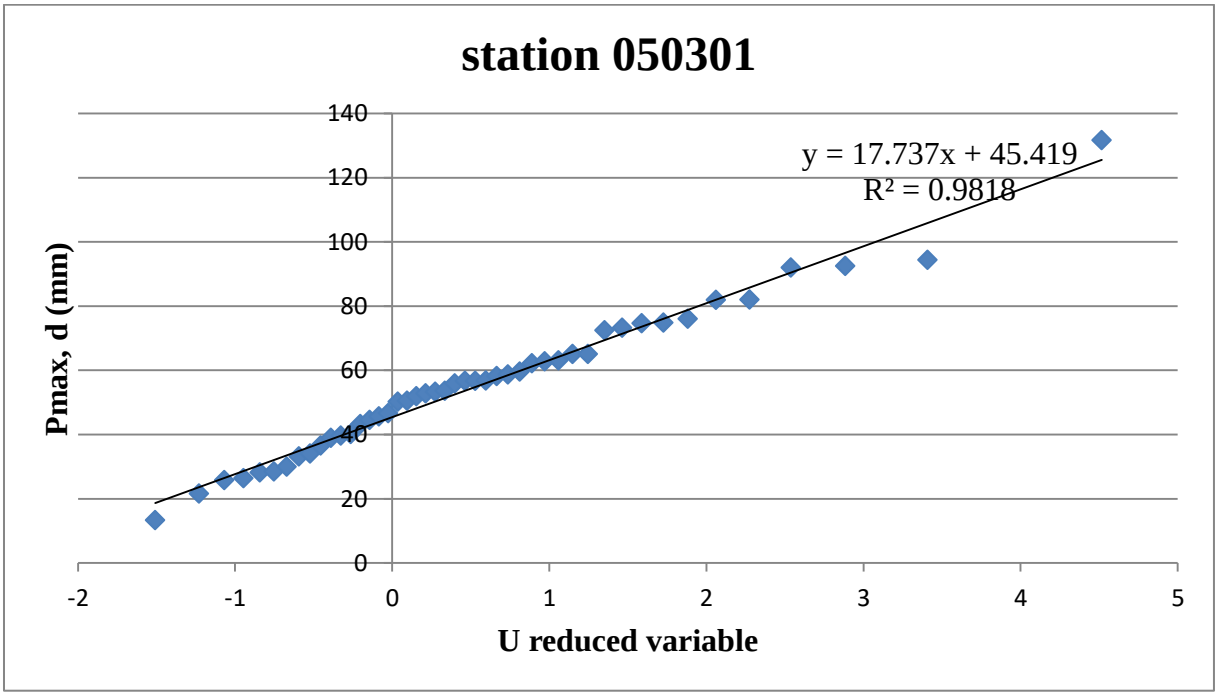

Fig. 4.2 Adjustment of maximum daily precipitation through Gumbel's law of Ain El Hadjel (050301) station

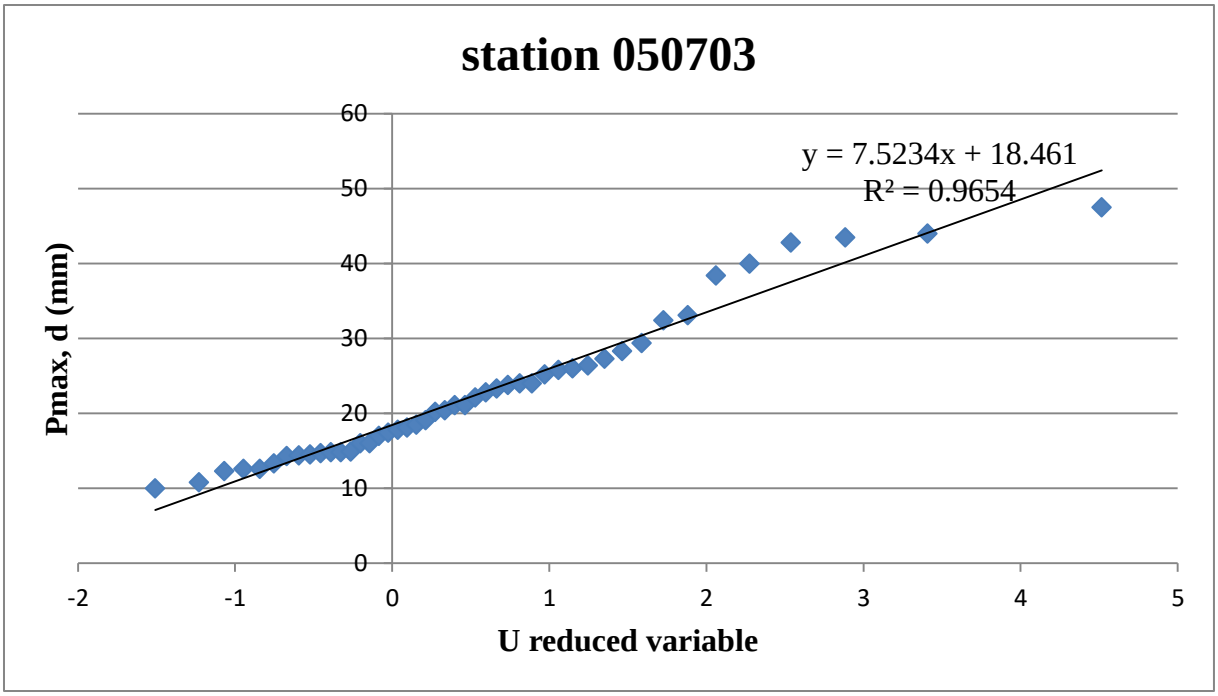

Fig. 4.3 Adjustment of maximum daily precipitation through Gumbel's law of Rocad Sud (050703) station

Table 4.1 Pmax, d (for period 1966 -2011) of El-Ham wadi sub- basin for different return periods at 3 gauging stations

		Return Period T					
		2 years	10 years	20 years	50 years	100 years	1000 years
	Frequency	0.5	0.9	0.95	0.98	0.99	0.999
	Reduced variable of Gumbel	0.37	2.3	2.9	3.9	4.6	6.9
Pmax, d (mm)	050101	32.0	59.6	70.1	83.7	93.9	127.6
	050301	51.9	85.3	98.1	114.6	127.0	167.9
	050703	21.2	35.4	40.8	47.8	53.1	70.4

Once the maximum daily precipitation Pmax,d(T) amounts are determined, it is then possible to proceed with the short-term rainfall Ptc (T) and the precipitation intensity Itc (T) calculations using the previously mentioned equations (see Tables 4.2, 4.3, 4.4 and 4.5). Ptc

and IDF curves are shown in Figures 4.4 and 4.5 for station 050101, in Figures 4.6 and 4.7 for station 050301, and finally in Figures 4.8 and 4.9 for station 050703.

Rainfall IDF curves are derived from statistical analysis of records of single storm rainfall over a period of time and they are used to capture important characteristics of point rainfall over short duration. In other word, it is defined as the calculation of average design rainfall intensity for a certain exceedance probability of exceedance over a range of duration (Subyani & Al-Amri, 2015).

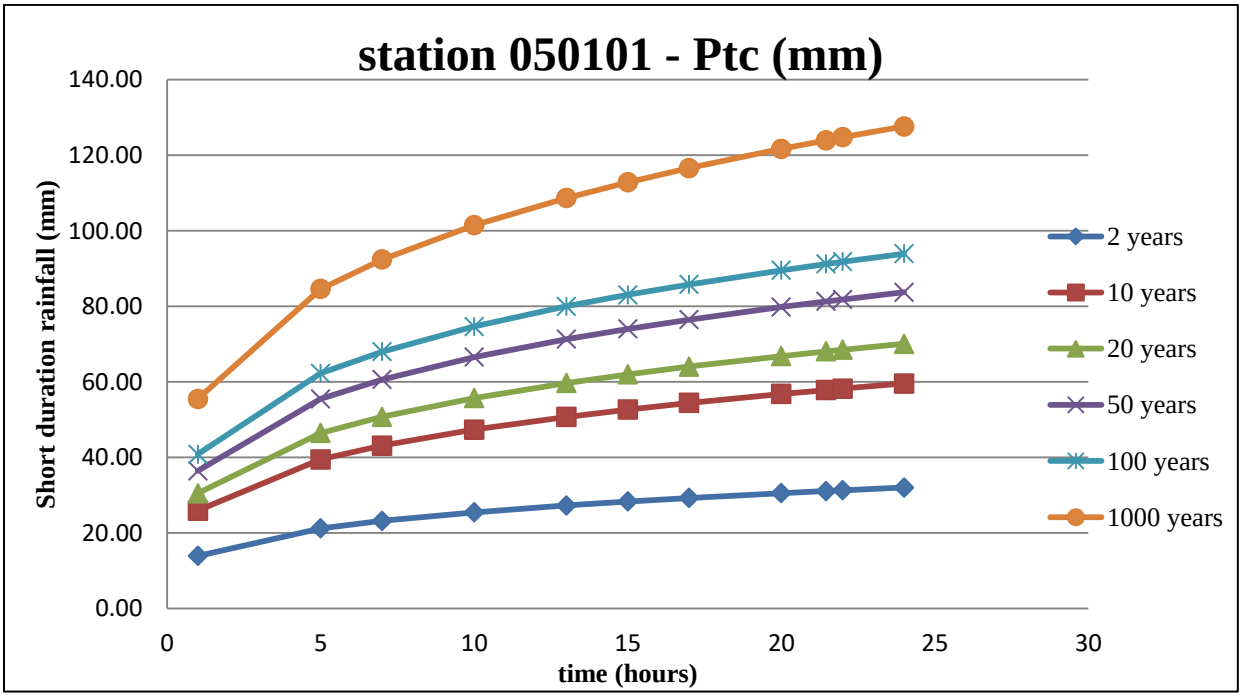

Fig. 4.4 Short-term rainfall Ptc (mm) curves for different return periods of station 050101

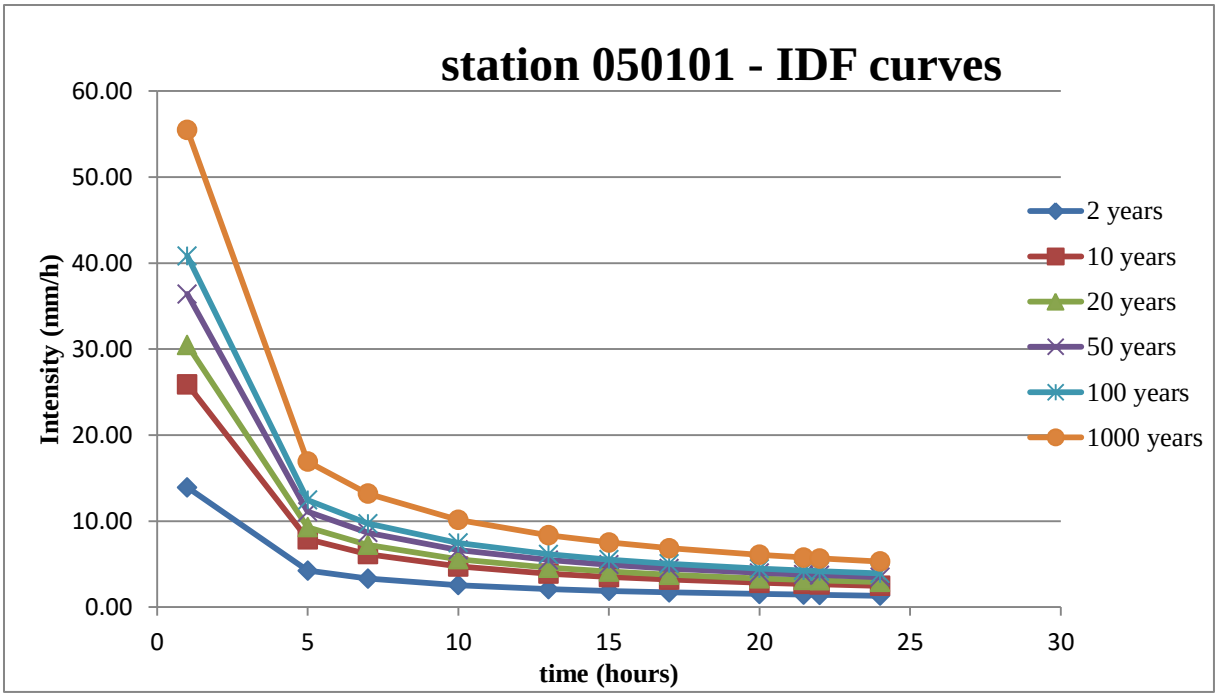

Fig. 4.5 IDF curves for different return periods of station 050101

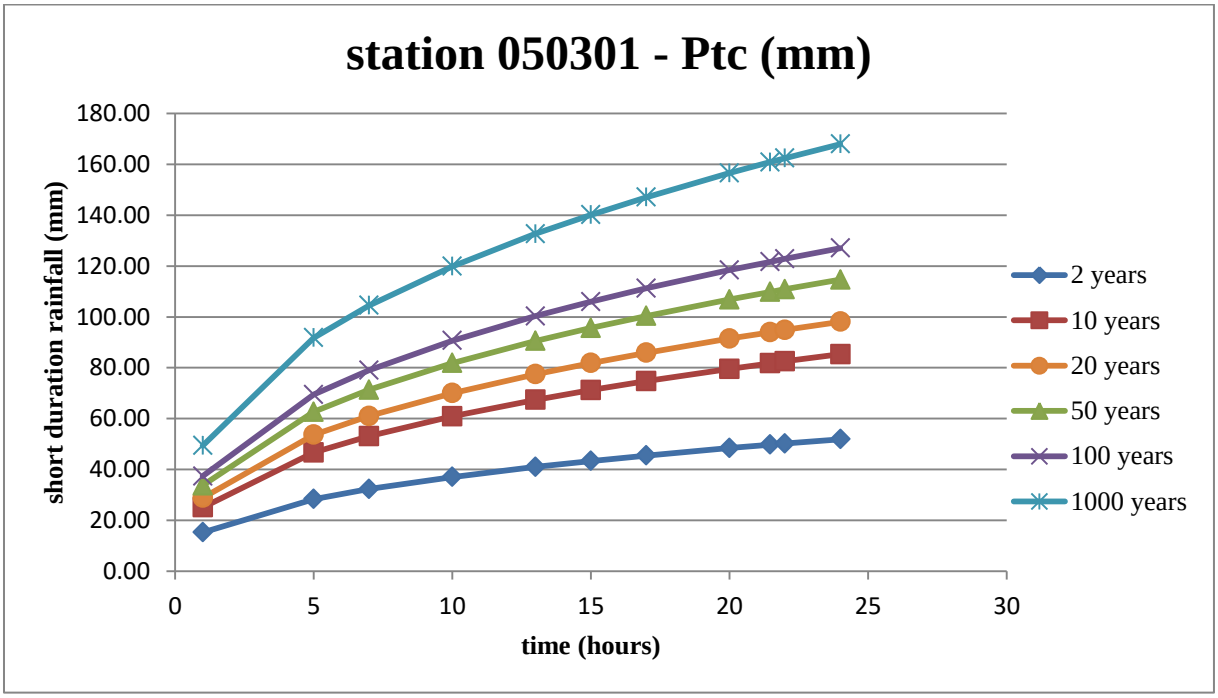

Fig. 4.6 Short-term rainfall Ptc (mm) curves for different return periods of station 050301

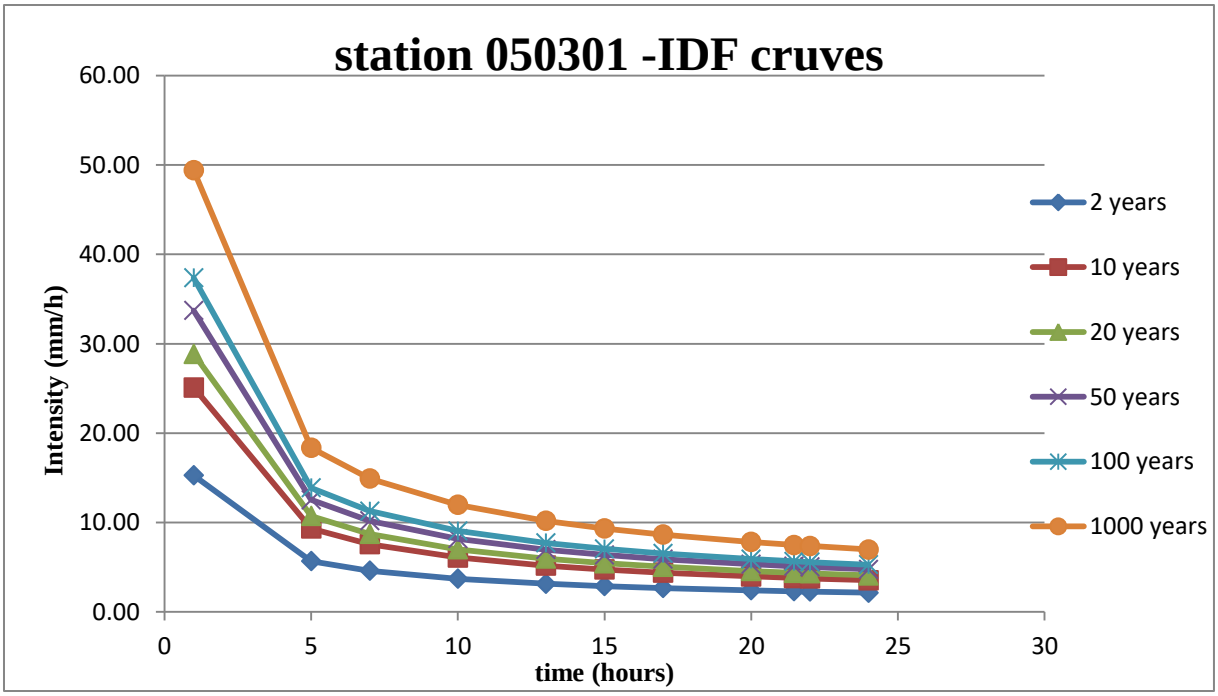

Fig. 4.7 IDF curves for different return periods of station 050301

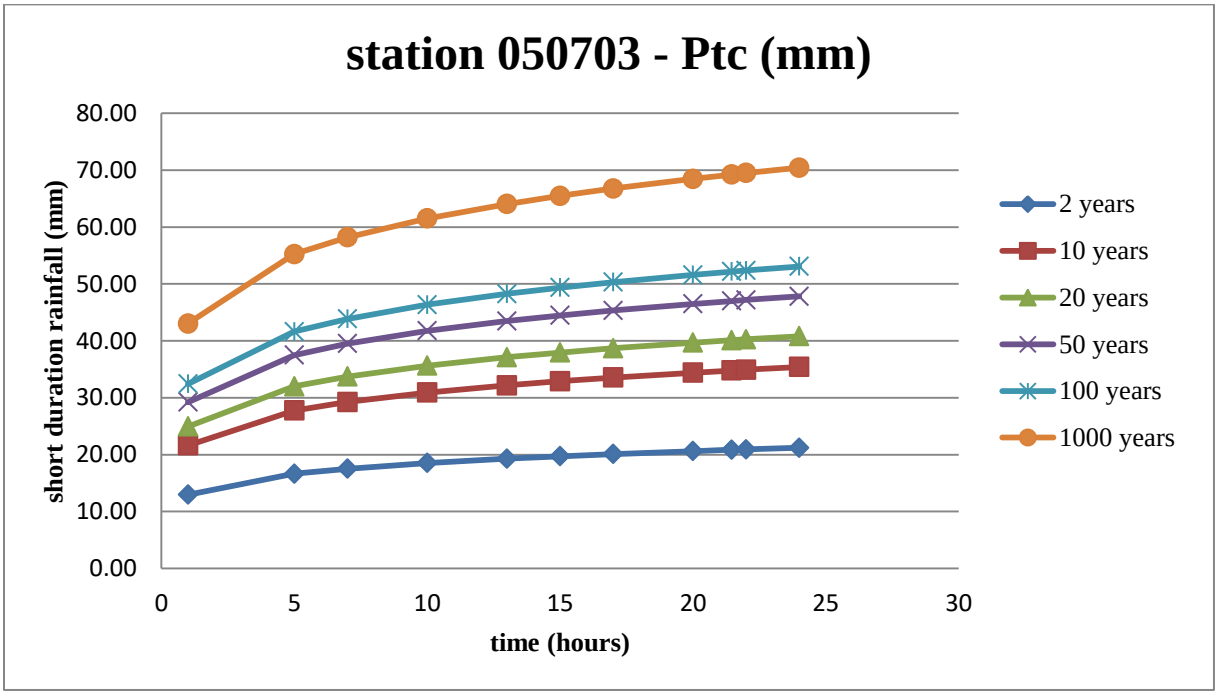

Fig. 4.8 Short-term rainfall Ptc (mm) curves for different return periods of station 050703

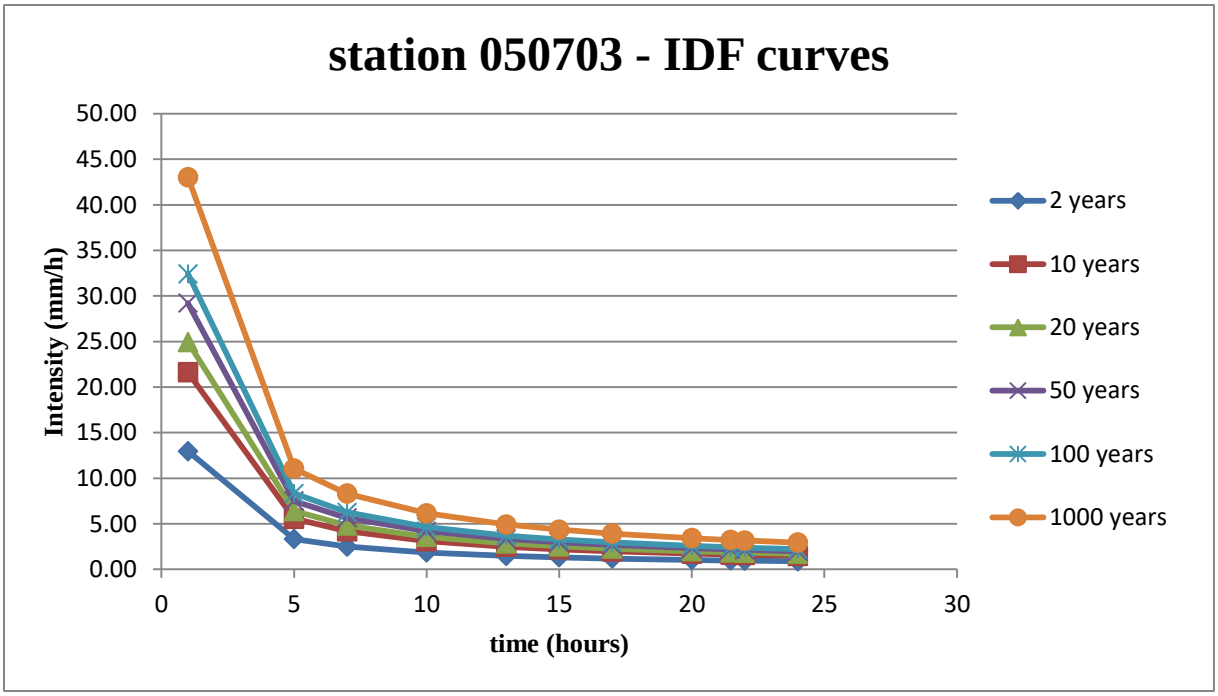

Fig. 4.9 IDF curves for different return periods of station 050703

Table 4.2 Pmax (d) and coefficient b values

Station code	Average Pmax, d (mm)	Coefficient b
050101	34.4	0.26
050301	55.6	0.39
050703	22.8	0.16

Table 4.3 Determination of Ptc and rainfall intensity for different return periods (station 050101)

Return period T	**2**		**10**		**20**		**50**		**100**		**1000**	
frequency	0.5		0.9		0.95		0.98		0.99		0.999	
time (hours)	**Ptc (mm)**	**I (mm/h)**	**Ptc (mm)**	**I (mm/h)**	**Ptc (mm)**	**I (mm/h)**	**Ptc (mm)**	**I (mm/h)**	**Ptc (mm)**	**I (mm/h)**	**Ptc (mm)**	**I (mm/h)**
1	13.9	13.9	25.9	25.9	30.5	30.5	36.4	36.4	40.8	40.8	55.5	55.5
5	21.2	4.3	39.5	7.9	46.5	9.3	55.5	11.1	62.3	12.5	84.6	16.9
7	23.2	3.3	43.1	6.2	50.8	7.3	60.6	8.7	68.0	9.7	92.4	13.2
10	25.5	2.6	47.4	4.7	55.7	5.6	66.5	6.7	74.7	7.5	101.5	10.2
13	27.3	2.1	50.7	3.9	59.7	4.6	71.3	5.5	80.0	6.2	108.7	8.4
15	28.3	1.9	52.7	3.5	62.0	4.1	74.0	4.9	83.0	5.5	112.8	7.5
17	29.3	1.7	54.4	3.2	64.0	3.8	76.5	4.5	85.8	5.1	116.6	6.9
20	30.5	1.5	56.8	2.8	66.8	3.3	79.8	4.0	89.5	4.5	121.7	6.1
21.5	31.1	1.5	57.8	2.7	68.1	3.2	81.3	3.8	91.2	4.3	123.9	5.8
22	31.3	1.4	58.2	2.7	68.5	3.1	81.8	3.7	91.8	4.2	124.7	5.7

24	32.0	1.3	59.6	2.5	70.1	2.9	83.7	3.5	93.9	3.9	127.6	5.3

Table 4.4 Determination of Ptc and rainfall intensity for different return periods (station 050301)

Return period T	**2**		**10**		**20**		**50**		**100**		**1000**	
frequency	0.5		0.9		0.95		0.98		0.99		0.999	
time (hours)	**Ptc (mm)**	**I (mm/h)**	**Ptc (mm)**	**I (mm/h)**	**Ptc (mm)**	**I (mm/h)**	**Ptc (mm)**	**I (mm/h)**	**Ptc (mm)**	**I (mm/h)**	**Ptc (mm)**	**I (mm/h)**
1	15.3	15.3	25.1	25.1	28.9	28.9	33.7	33.7	37.4	37.4	49.4	49.4
5	28.4	5.7	46.7	9.3	53.6	10.7	62.7	12.5	69.4	13.9	91.8	18.4
7	32.3	4.6	53.1	7.6	61.1	8.7	71.3	10.2	79.0	11.3	104.5	14.9
10	37.1	3.7	60.9	6.1	70.0	7.0	81.8	8.2	90.7	9.1	119.9	12.0
13	41.0	3.2	67.4	5.2	77.5	6.0	90.5	7.0	100.3	7.7	132.6	10.2
15	43.3	2.9	71.2	4.8	81.9	5.5	95.7	6.4	106.0	7.1	140.1	9.3
17	45.5	2.7	74.7	4.4	85.9	5.1	100.4	5.9	111.2	6.5	147.1	8.7
20	48.4	2.4	79.6	4.0	91.5	4.6	106.9	5.3	118.4	5.9	156.6	7.8
21.5	49.7	2.3	81.7	3.8	94.0	4.4	109.8	5.1	121.7	5.7	160.9	7.5
22	50.2	2.3	82.5	3.8	94.9	4.3	110.9	5.0	122.8	5.6	162.4	7.4
24	51.9	2.2	85.3	3.6	98.1	4.1	114.6	4.8	127.0	5.3	167.9	7.0

Table 4.5 Determination of Ptc and rainfall intensity for different return periods (station 050703)

Return period T	**2**		**10**		**20**		**50**		**100**		**1000**	
frequency	0.5		0.9		0.95		0.98		0.99		0.999	
time (hours)	**Ptc (mm)**	**I (mm/h)**	**Ptc (mm)**	**I (mm/h)**	**Ptc (mm)**	**I (mm/h)**	**Ptc (mm)**	**I (mm/h)**	**Ptc (mm)**	**I (mm/h)**	**Ptc (mm)**	**I (mm/h)**
1	13.0	13.0	21.6	21.6	24.9	24.9	29.2	29.2	32.4	32.4	43.0	43.0
5	16.6	3.3	27.8	5.6	32.0	6.4	37.5	7.5	41.6	8.3	55.2	11.1
7	17.5	2.5	29.2	4.2	33.7	4.8	39.5	5.6	43.8	6.3	58.2	8.3
10	18.5	1.9	30.9	3.1	35.6	3.6	41.8	4.2	46.3	4.6	61.5	6.2
13	19.3	1.5	32.2	2.5	37.1	2.9	43.5	3.3	48.3	3.7	64.1	4.9
15	19.7	1.3	32.9	2.2	37.9	2.5	44.5	3.0	49.3	3.3	65.5	4.4
17	20.1	1.2	33.6	2.0	38.7	2.3	45.3	2.7	50.3	3.0	66.8	3.9
20	20.6	1.0	34.4	1.7	39.7	2.0	46.5	2.3	51.6	2.6	68.5	3.4
21.5	20.9	1.0	34.8	1.6	40.1	1.9	47.0	2.2	52.2	2.4	69.2	3.2
22	20.9	1.0	34.9	1.6	40.3	1.8	47.2	2.1	52.4	2.4	69.5	3.2
24	21.2	0.9	35.4	1.5	40.8	1.7	47.8	2.0	53.1	2.2	70.4	2.9

For a 100-year return period and a concentration time equal to 21.5 hours, the Ptc (T) values in the stations 050101, 050301 and 050703 are 91.2 mm, 121.7 mm and 51.2 mm respectively. On the other hand, the 100-year return period intensity at these stations implies

high values at the station 050301 (5.67 mm/h) with 2.4 mm/h in the station 050703 and 4.3 mm/h in the station 050101.

Evaluation of flood discharges after statistical and hydro-meteorological technique (Gradex method) shows continuously increasing flows towards the return period in the El-Ham wadi sub-basin (see Table 4.6). The maximum flood discharge at Ain El Hadjel station is 5,868.1 m^3/s for 100-year. The empirical analysis of flood discharges in Table 4.7 repeats the same observations regarding return-periods with different discharges (also shown at Ain El Hadjel station at 5,581.9 m^3/s for 100-year).

Table 4.6 Results of flood discharges assessment using the Gradex method for stations 050101, 050301 and 050703

Return period T	station code	Precipitation amount (mm)	Pmax,d (mm)	reduced variable	discharge amount (m^3/s)	peak flow (m^3/s)
10 years RP	050101	14.6	59.6	2.3	1043.0	2373.9
	050301	17.7	85.3	2.3	1265.8	2893.8
	050703	7.5	35.4	2.3	536.9	1226.7
20 years RP	050101	14.6	70.1	3.0	1043.0	3124.8
	050301	17.7	98.1	3.0	1265.8	3804.9
	050703	7.5	40.8	3.0	536.9	1613.1
50 years RP	050101	14.6	83.7	3.9	1043.0	4096.5
	050301	17.7	114.6	3.9	1265.8	4984.3
	050703	7.5	47.8	3.9	536.9	2113.4
100 years RP	050101	14.6	93.9	4.6	1043.0	4824.8
	050301	17.7	127.0	4.6	1265.8	5868.1
	050703	7.5	53.1	4.6	536.9	2488.2
1000 years RP	050101	14.6	127.6	6.9	1043.0	7231.1
	050301	17.7	167.9	6.9	1265.8	8788.3
	050703	7.5	70.4	6.9	536.9	3726.9

Table 4.7 Results of flood discharge assessment through comparative empirical analysis for stations 050101, 050301 and 050703

	Peak flow (m3/s)					
	station code	**Giandotti**	**Possenti**	**Turazza**	**Temez**	**Average value**
10-year RP	050101	2073.2	2295.1	1901.3	2205.4	2118.7
	050301	2929.6	3288.4	2724.1	3131.1	3018.3
	050703	1246.8	1363.8	1129.8	1332.5	1268.2
20-year RP	050101	2439.4	2700.5	2516.8	2919.4	2644.0
	050301	3368.0	3780.4	3523.2	4049.5	3680.3

	050703	1437.6	1572.5	1465.5	1728.5	1551.0
50-year RP	050101	2913.4	3225.3	3673.8	4261.5	3518.5
	050301	3935.3	4417.2	5031.5	5783.2	4791.8
	050703	1684.5	1842.7	2098.9	2475.5	2025.4
100-year RP	050101	3268.7	3618.6	4496.5	5215.8	4149.9
	050301	4360.5	4894.5	6082.0	6990.5	5581.9
	050703	1869.6	2045.1	2541.3	2997.2	2363.3
1000-year RP	050101	4442.4	4918.0	6620.5	7679.6	5915.1
	050301	5765.4	6471.4	8711.6	10013.0	7740.3
	050703	2481.0	2714.0	3653.4	4308.9	3289.3

4.3. Flood hazard and risk assessment in Hodna basin

4.3.1. Flood assessment using AHP technique

4.3.1.1. AHP technique

Results on the application of the AHP techniques are obtained after the weights are determined using the pairwise comparison matrix presented in Table 4.8. Furthermore, the results regarding the calculation of the consistency index and consistency ration are presented in Table 4.9.

Table 4.8 Weights determination for each criteria using AHP method (R: rainfall distribution, S: slope, DD: drainage density, LULC: land use/ land cover; ST: soil type)

	Pairwise Comparison Matrix					Normalization					Weights
Criterion	**R**	**S**	**DD**	**LULC**	**ST**	**R**	**S**	**DD**	**LULC**	**ST**	
R	1	2	4	7	8	0.495	0.522	0.469	0.452	0.364	0.460
S	0.5	1	3	4	6	0.2475	0.267	0.352	0.258	0.273	0.279
DD	0.25	0.33	1	3	5	0.1238	0.088	0.117	0.194	0.227	0.149
LULC	0.14	0.25	0.33	1	2	0.0693	0.067	0.039	0.065	0.091	0.066
ST	0.13	0.17	0.2	0.5	1	0.0644	0.045	0.023	0.032	0.045	0.042
SUM	2.02	3.75	8.53	15.5	22	1	1	1	1	1	1

The importance of intensity starting with 1 (equal importance), 3 (medium importance), 5 (strong importance), 7 (very strong importance), 9 (extreme importance) can be used for 2, 4, 6 and 8 values to express intermediate values.

Table 4.9 Main results of CI and CR calculation

Parameter	Weighted sum vector	Consistency vector (CV)	λ	Consistency Index (CI)	Random Index (RI)	Consistency Ratio (CR)
R	2.301	5	5	0	1.12	0
S	1.396	5				
DD	0.749	5				
LC	0.330	5				
ST	0.210	5				

The weighting method is used to see importance of each factor relative to another factor. The larger the weight, the more important the parameter. The acceptable consistency ratio value should be less than 0.1. In our case, CR equals to 0 which means that the suggested weights are acceptable. Pairwise comparison indicates a higher weight for rainfall followed by slope, drainage density, land use and soil type. In addition, the calculated weight for each factor is combined with each map layer in ArcGIS in order to generate the final maps of flood hazard and flood risk.

4.3.1.2. Flood hazard mapping

All maps in the section below are determined using ArcGIS 10.4.1 Software. The resulting maps are then reclassified on scales from 1 (very low) to 5 (very high) using the Reclassify tool in Arc Toolbox (Sort method) (Rothman et al., 2013; Asare-Kyei et al., 2015; Rimba et al., 2017; Mokadem et al., 2018).

Rainfall distribution map

The highest maximum precipitation values are observed in the north and northeast regions of Hodna basin. In contrast, the lowest values are mainly observed in the Chott-El-Hodna saline lake and towards Barika city in the east, the city of Boussaada in the southwest and to the west near the lowest altitudes of El-Ham sub-basin (Figure 4.10).

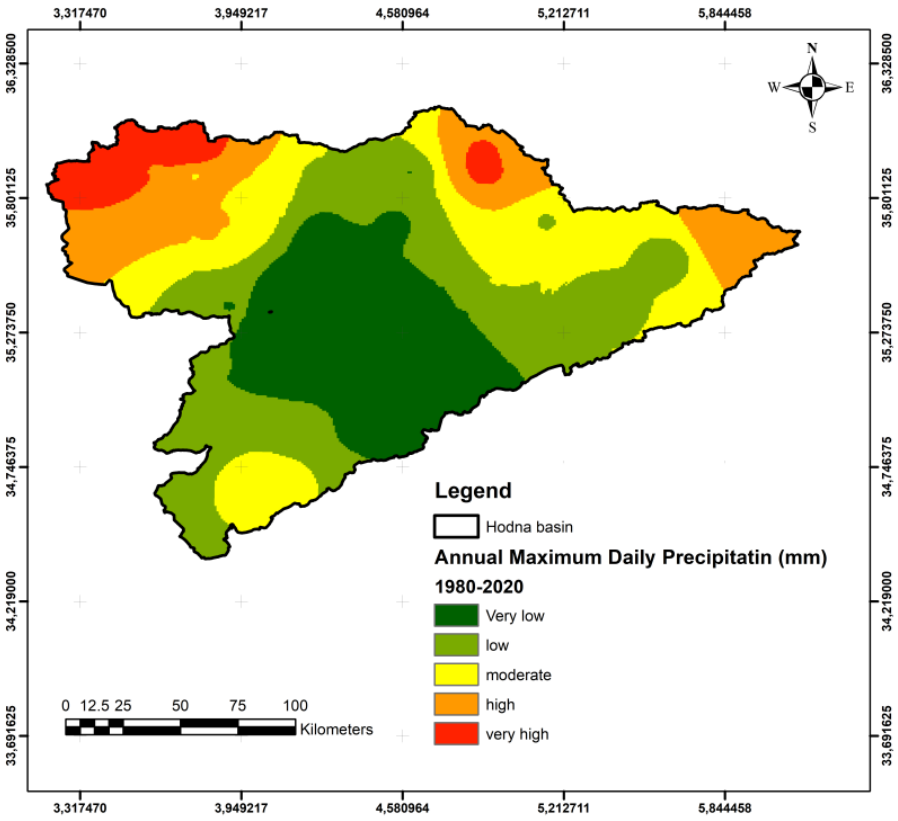

Fig. 4.10 Rating of rainfall distribution of Hodna basin

Slope map

Slope analysis shows that low slope values dominate the study area. Steep slopes are located in the northern and southern regions, and low slopes are in the center of the Hodna basin. From Figure 4.11, we can conclude that in gently sloping areas, the runoff is slow, allowing more time for rain water to accumulate on the surface. Areas with steep slopes promote fast runoff, which provides less residence time for rainwater to infiltrate (Abdalla, 2012).

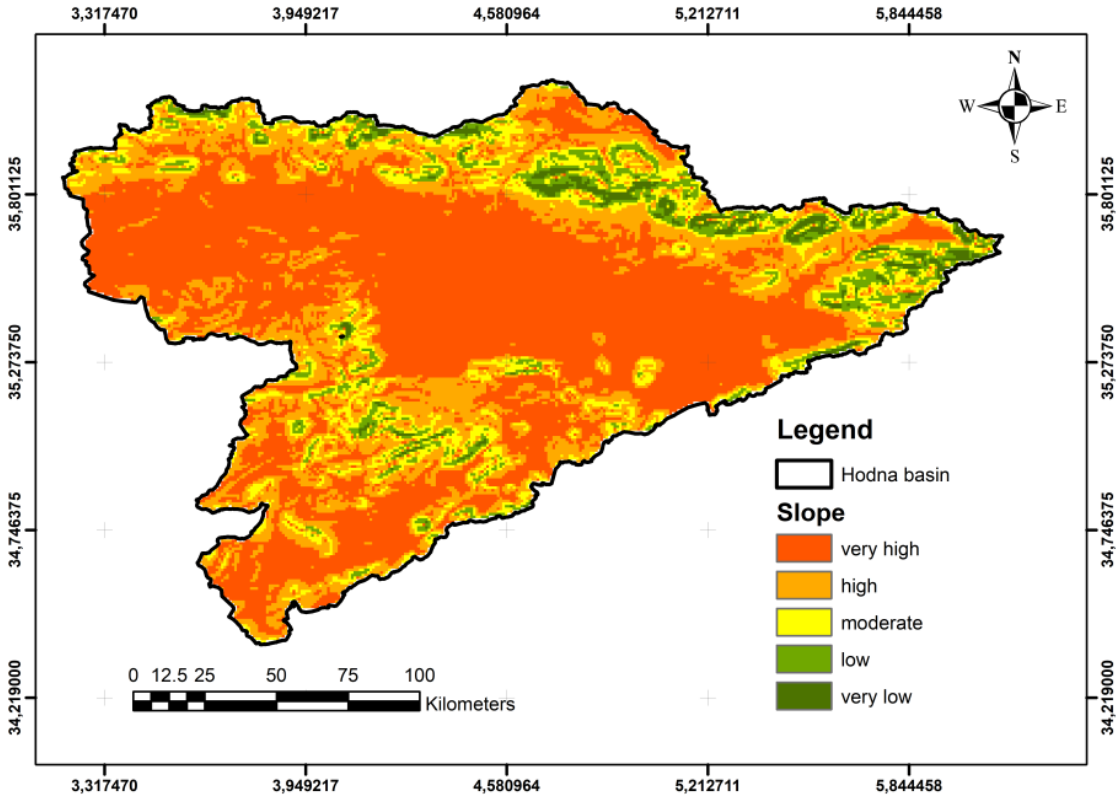

Fig. 4.11 Rating of slope in Hodna basin

Drainage density map

The wadi (valley) is characterized by high drainage density values in regions with many streams. Drainage density is low in regions, where the streams are not numerous (Figure 4.12). For instance, it is more concentrated in El-Ham, K'sob, Boussaada, and Soubella wadis.

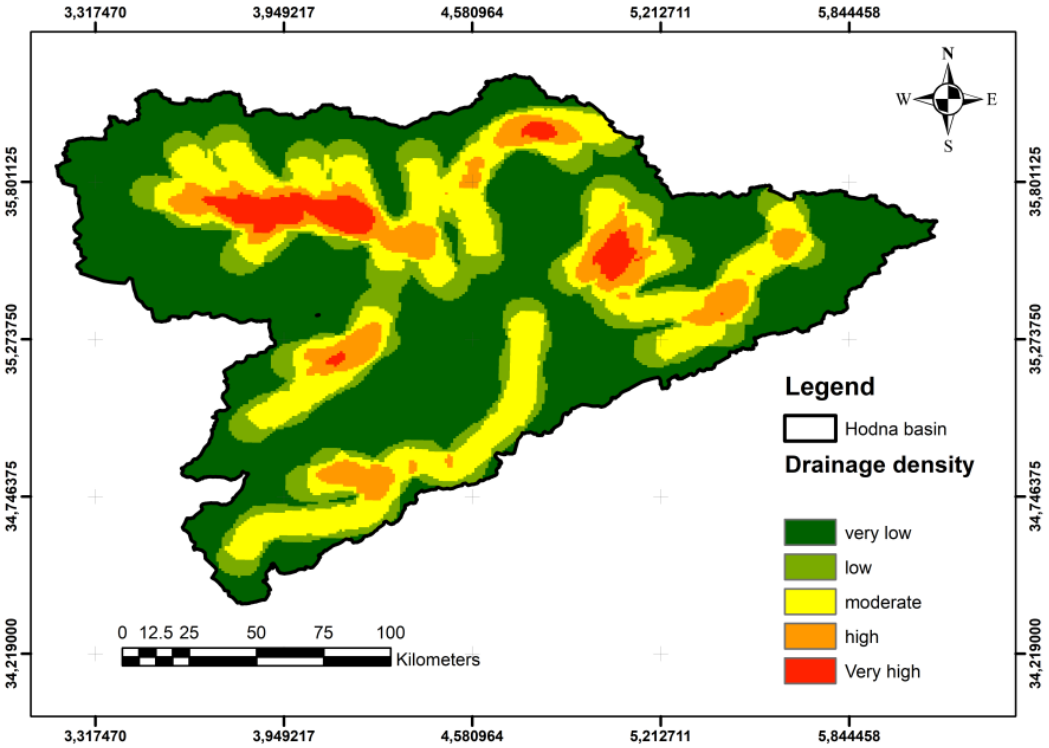

Fig. 4.12 Rating of drainage density in Hodna basin

Land use/ land cover map

The Hodna basin is characterized by several types of land use/cover. Therefore, surface runoff is very high in the center of the basin and is more concentrated in cities such as Sidi Aïssa in the northeast, Bordj Bou Arreridj and M'sila in the north, Barika and N'gaous towards the east and Boussaada and Maiter in the southern regions (Figure 4.13). Hence, the higher the runoff coefficient, the more important the surface runoff in these locations.

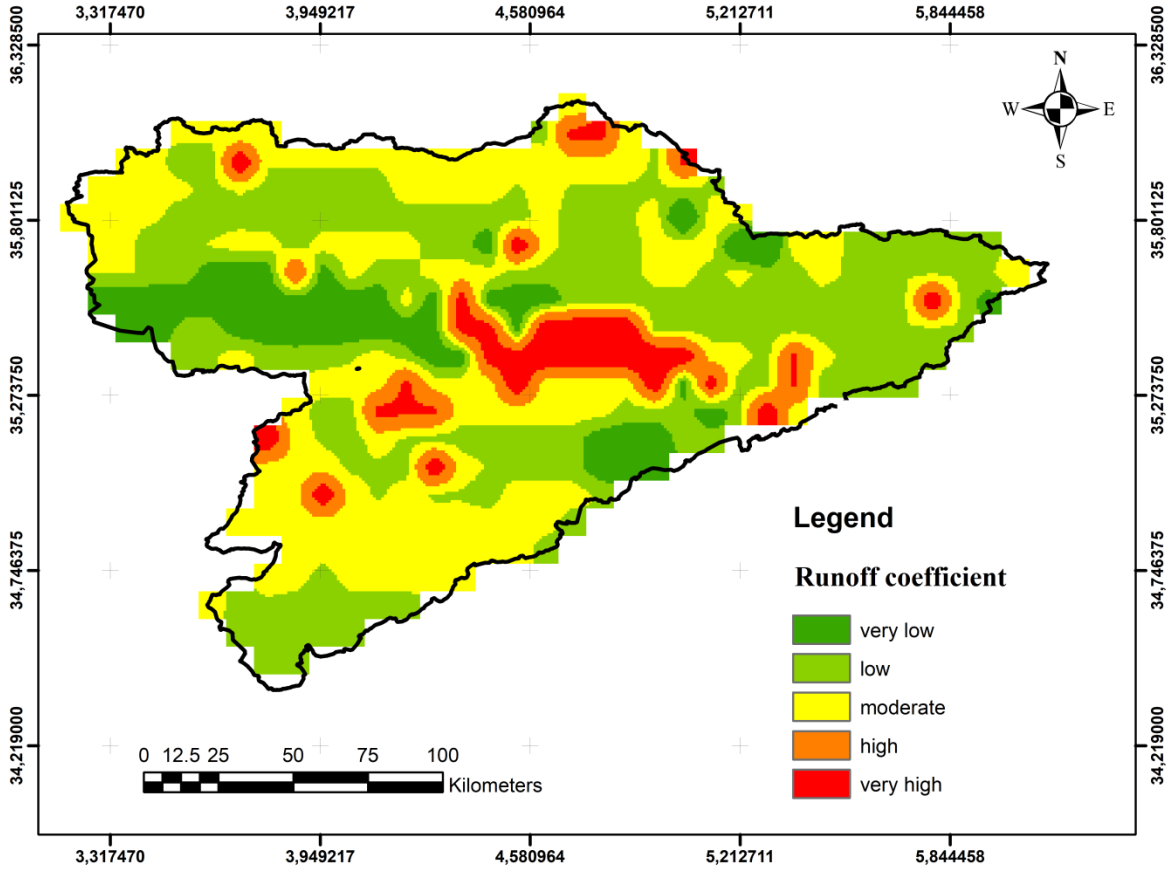

Fig. 4.13 Rating of runoff in Hodna basin

Soil type map

The runoff depends on the rocks that make up the soil. In the Hodna basin case, the soil type can be divided into five classes starting from the very low to very high (Figure 4.14). Therefore, regions forming Haplic, calcic, gypsic Yermosols (Yh, Yk, Yy) as well as takyric Solonchaks and calcic Xersols (Zt, Xk) pose a high flood hazard, particularly in Chott-El-Hodna, south and east parts of the basin. In addition to drought and high evaporation conditions, high salinity concentrations are found in lowland regions, characterized by medium permeability conditions as a result to the presence of loam, in addition to drought and high evaporation conditions. Otherwise, low and very low flood hazards are seen in the north and some parts of the basin in the south. The soil in these regions, is characterized by Lithosols (l) and calcic Cambisols (Bk). They are found in well drained areas of calcareous structures and soil conditions with high permeability and low erosivity.

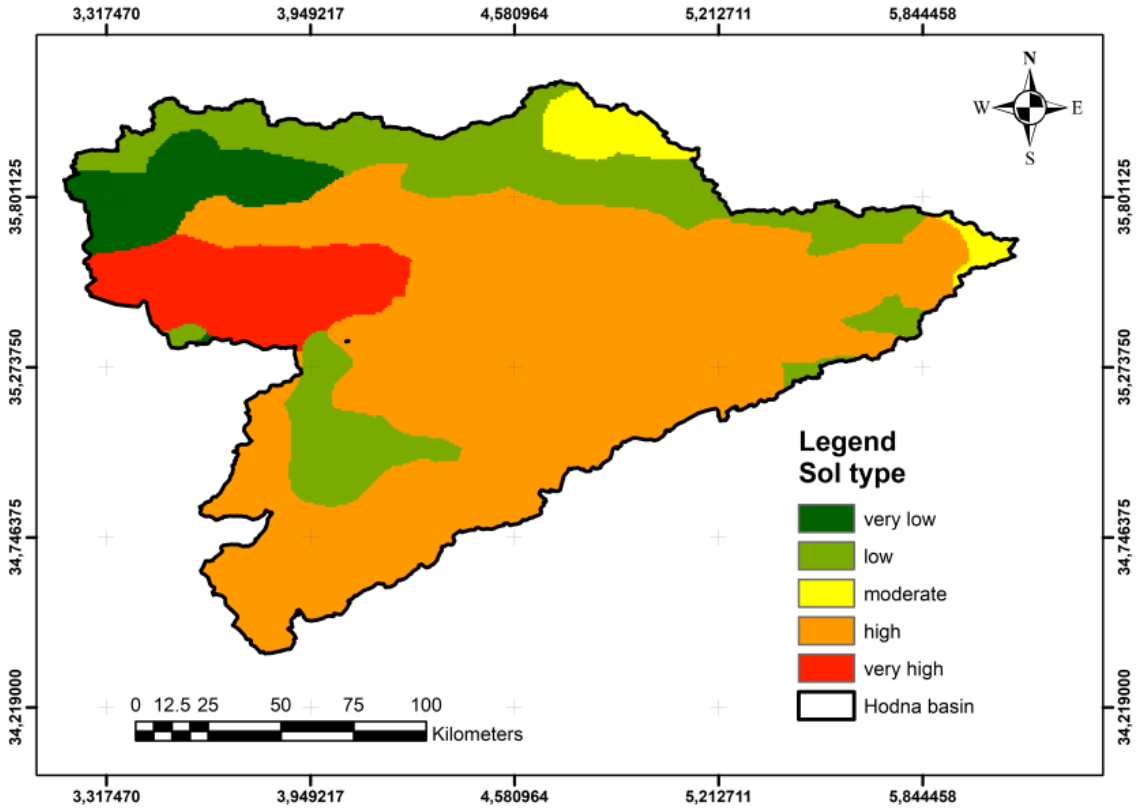

Fig. 4.14 Rating of soil type in Hodna basin

Flood hazard map

The flood hazard layer is determined for precipitation (R), slope (S), drainage density (DD), land use/cover (LULC), and soil type (ST) layers. Pre-calculated weights (Table X) are used to generate the flood hazard map, where:

- R (W1) = 46 %
- S (W2) = 27.9 %
- DD (W3) = 15 %
- LULC (W4) = 6.6 %
- ST (W5) = 4.2 %

The hazard map is shown is Figure 4.15. Actually, high and very high hazards are observed in all areas of the Hodna basin except Chott-El-Hodna and nearby areas.

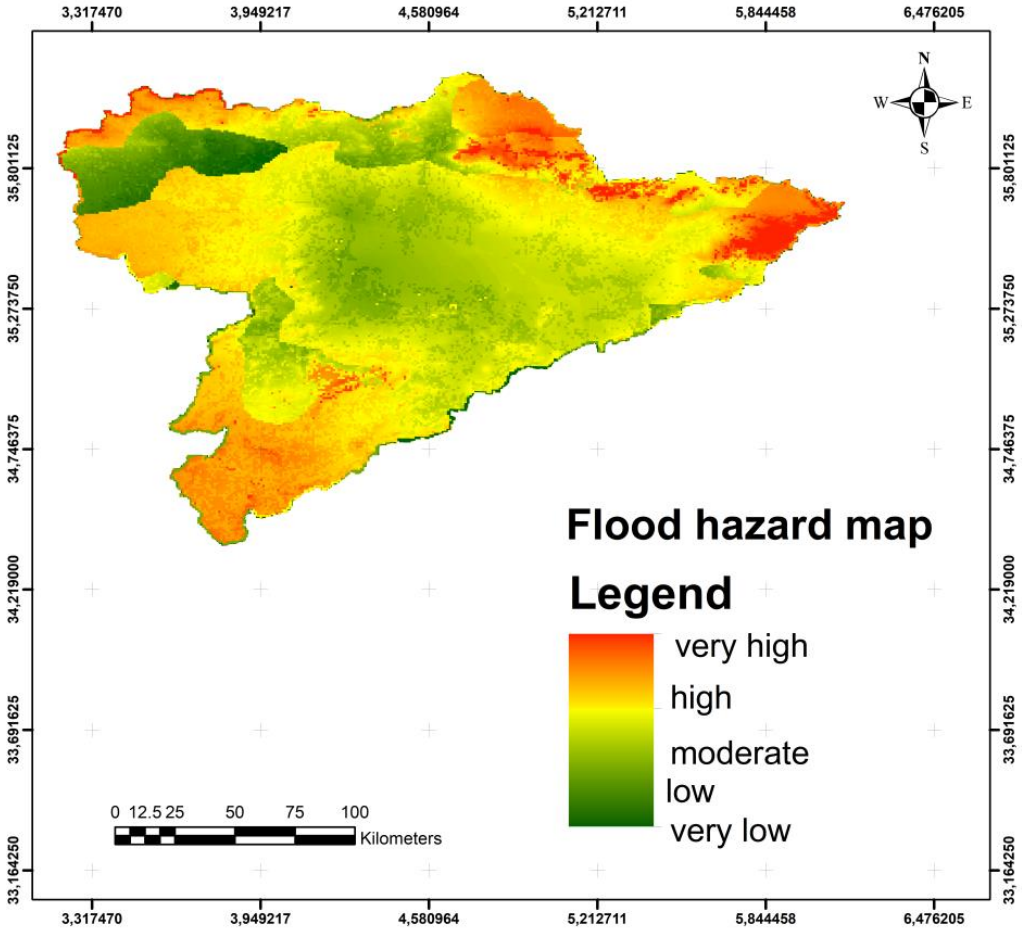

Fig. 4.15 Flood hazard map of the Hodna basin

4.3.1.3. Flood risk mapping

Flood hazard carries a risk is places with high population density. For instance, Sidi Aïssa, Bordj Bou Arreridj, M'sila, Boussaada and Barika cities are the most exposed built-up and residential areas to flooding (Figure 4.16).

Figure 4.17 shows the flood risk map based on GIS and multi-criteria method. The flood risk layer can be made following the same procedures as for flood hazard layer. It is composed of flood hazard (W6 = 70%) and social vulnerability (W7 = 30%).

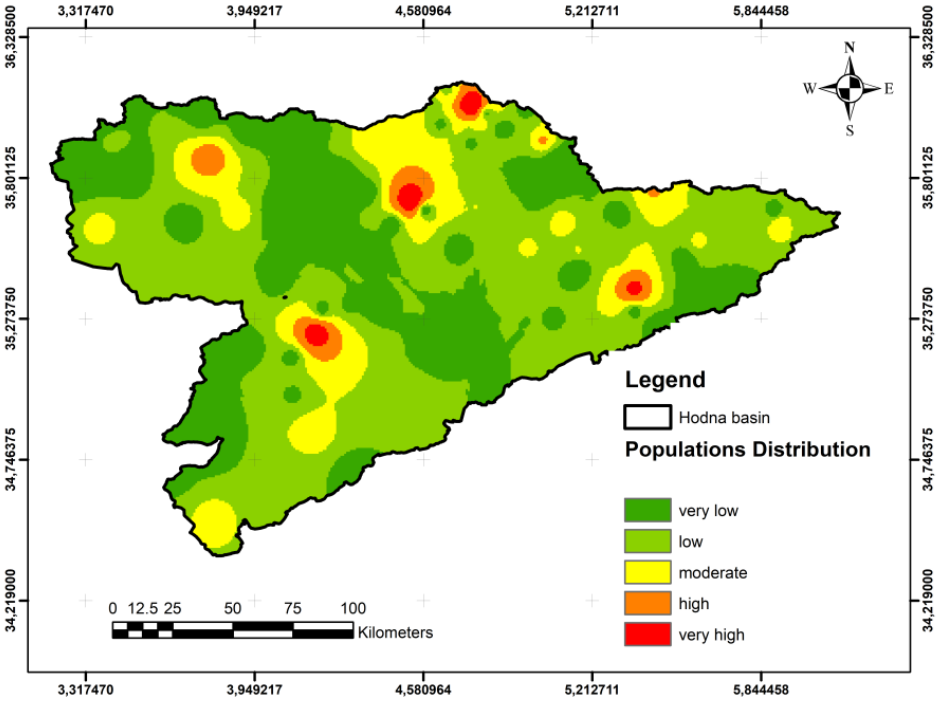

Fig. 4.16 Rating of population density in Hodna basin

The flood risk map provides us with insights about areas that are highly exposed areas to flooding risk. Therefore, it reveals that integrated risk is high where the spatial density of hazard and the population density overlap.

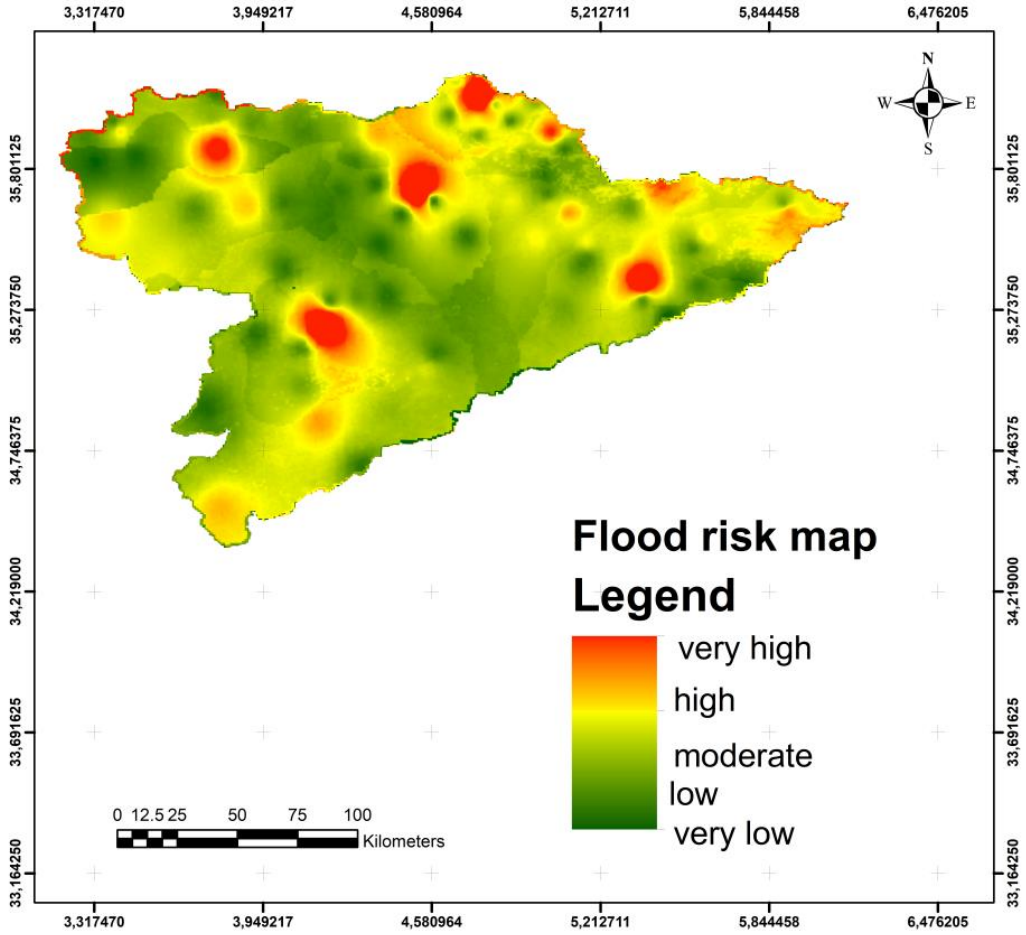

Fig. 4.17 Flood risk map of the Hodna basin

4.3.2. Flood assessment using HEC-RAS 1D model

The combined use of GIS and HEC-RAS can provide accurate flood hazard mapping. Therefore, based on the final flood risk map generated using ArcGIS, a 1D modeling is performed using HEC-RAS in order to give a detailed view of the areas most exposed zones to flood risk. For this purpose, Open Street Map and Google Earth imagery are used.

4.3.2.1. Sidi Aïssa city

High-density residential areas in the city of Sidi Aïssa are areas most at risk of flooding compared to other zones in El-Ham sub-basin (Figure 4.19). The flood wave propagation along the Djenene wadi is shown is Figure 4.18 for return periods of 10-year, 50-year, 100-year and 1000-year. The water height reaches the maximum values of 5.48 m, 6.41 m, 7.15 m and 7.75 m corresponding to 10-year, 50-year, 100-year and 1000-year return periods respectively.

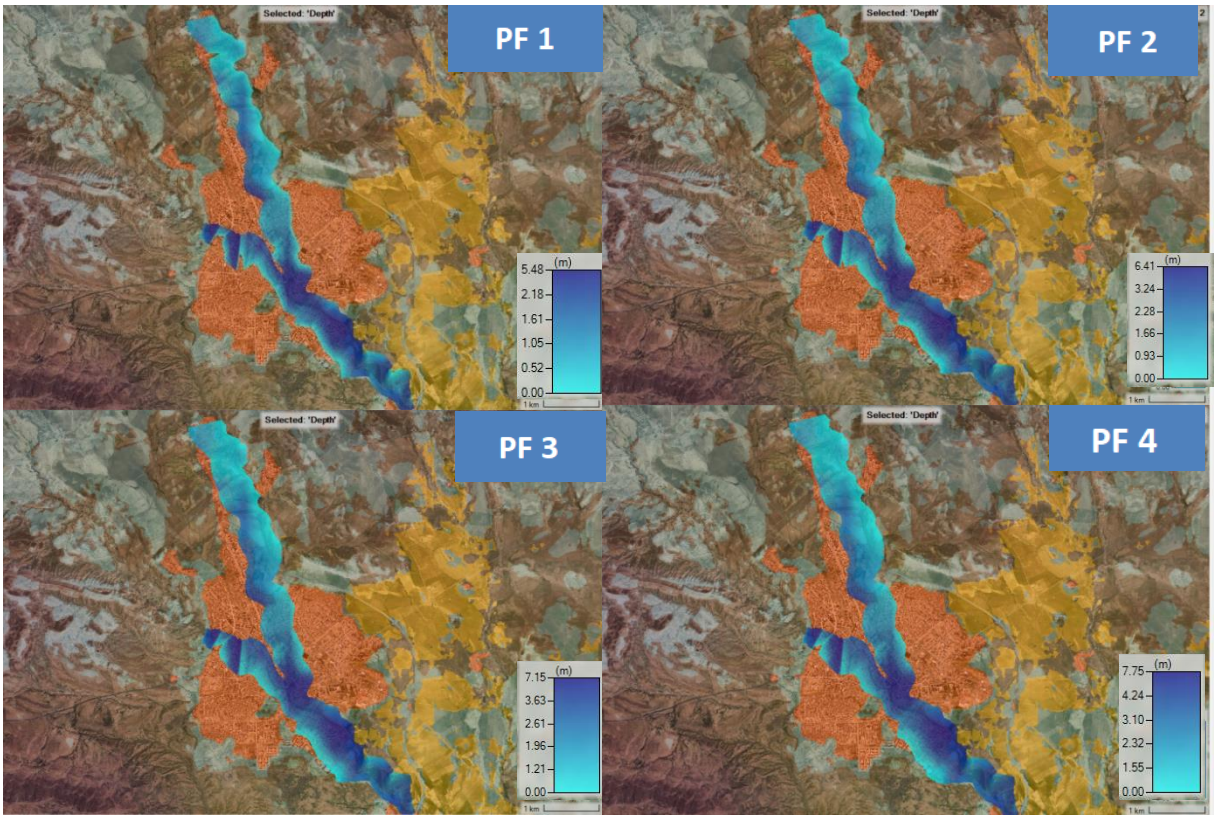

Fig. 4.18 Flooded areas for the 10-year, 50-year, 100-year and 1000-year return periods in Sidi Aïssa city (El-Ham watershed)

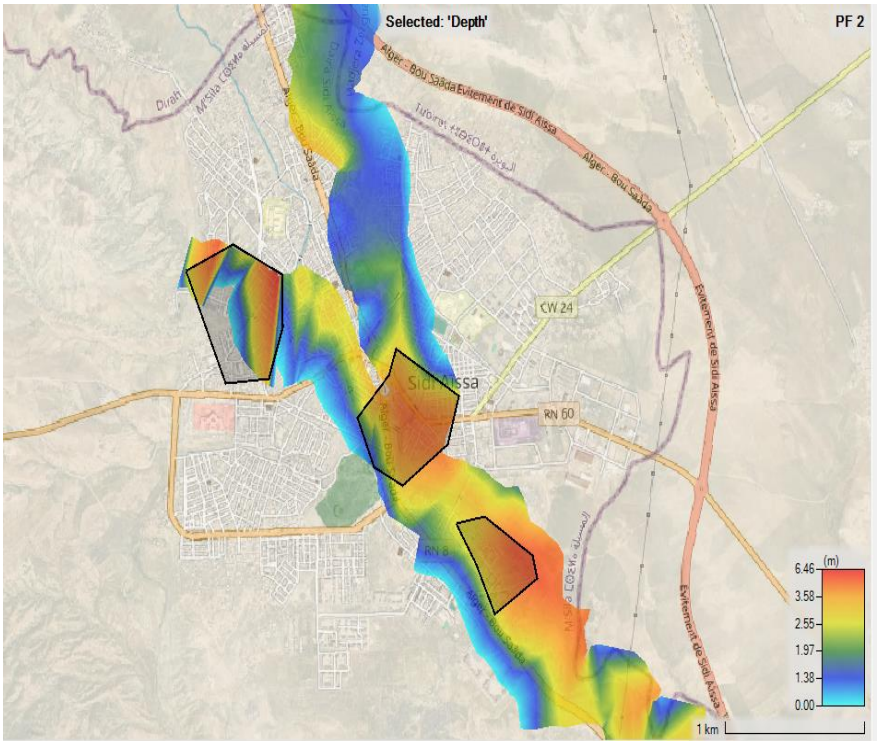

Fig. 4.19 Flood prone areas (polygons) near Djenene wadi for 50-year return period

4.3.2.2. Boussaada city

Flood wave propagation along the Boussaada wadi is shown is Figure 4.20 for return periods of 10-year, 50-year, 100-year and 1000-year. In addition to residential areas on the national highway N°46, middle school Tarek Ibn Ziad, middle school Moussa Ibn Noussair and High school Mohamed Cherif Benchabira. The rest is cropland with very little population density in the downstream of the river (Figure 4.21).

The water height reaches the maximum values of 4.65 m, 5.77 m, 6.07 m and 6.80 m corresponding to the return periods of 10-year, 50-year, 100-year and 1000-year respectively.

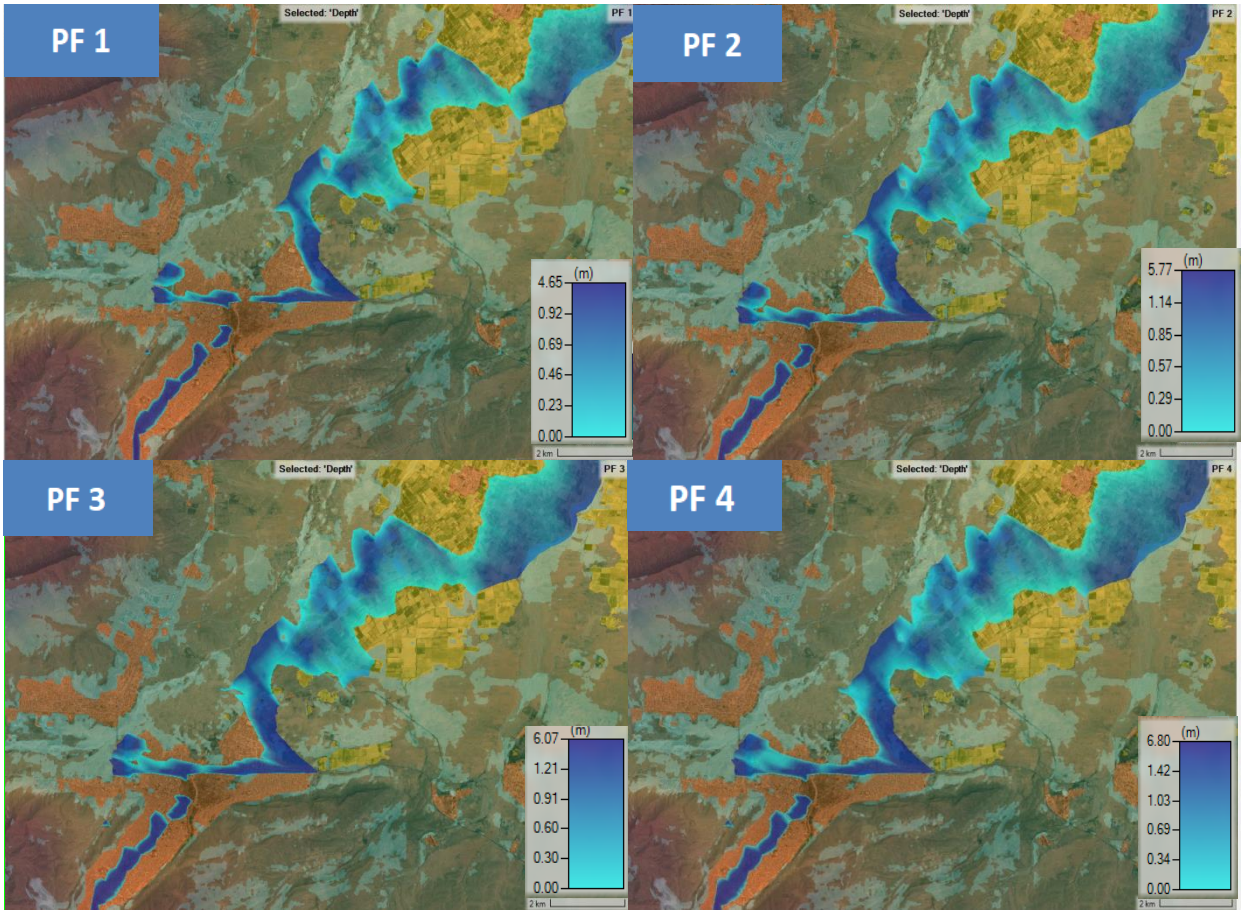

Fig. 4.20 Flooded area for the 10-year, 50-year, 100-year and 1000-year return periods in Boussaada city (Boussaada watershed)

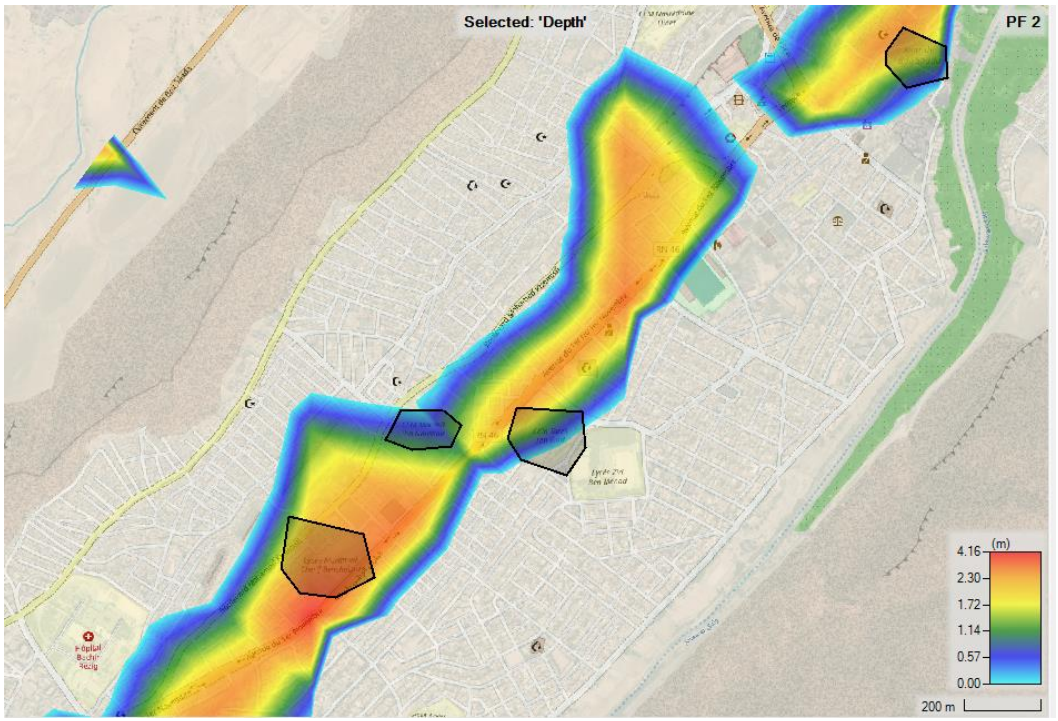

Fig. 4.21 Flood prone areas (polygons) near Boussaada wadi for 50-year return period

4.3.2.3. Barika city

Flood wave propagation along the Barika wadi is shown is Figure 4.22 for return periods of 10-year, 50-year, 100-year and 1000-year. High-density residential areas of high density as well as hospital and green spaces and weekly market near to high school Chahid Ouzil Abderrahman are the most exposed to flooding risk (Figure 4.23).

The water height reaches the maximum values of 2.92 m, 3.39 m, 3.50 m and 3.78 m corresponding to 10-year, 50-year, 100-year and 1000-year return periods, respectively.

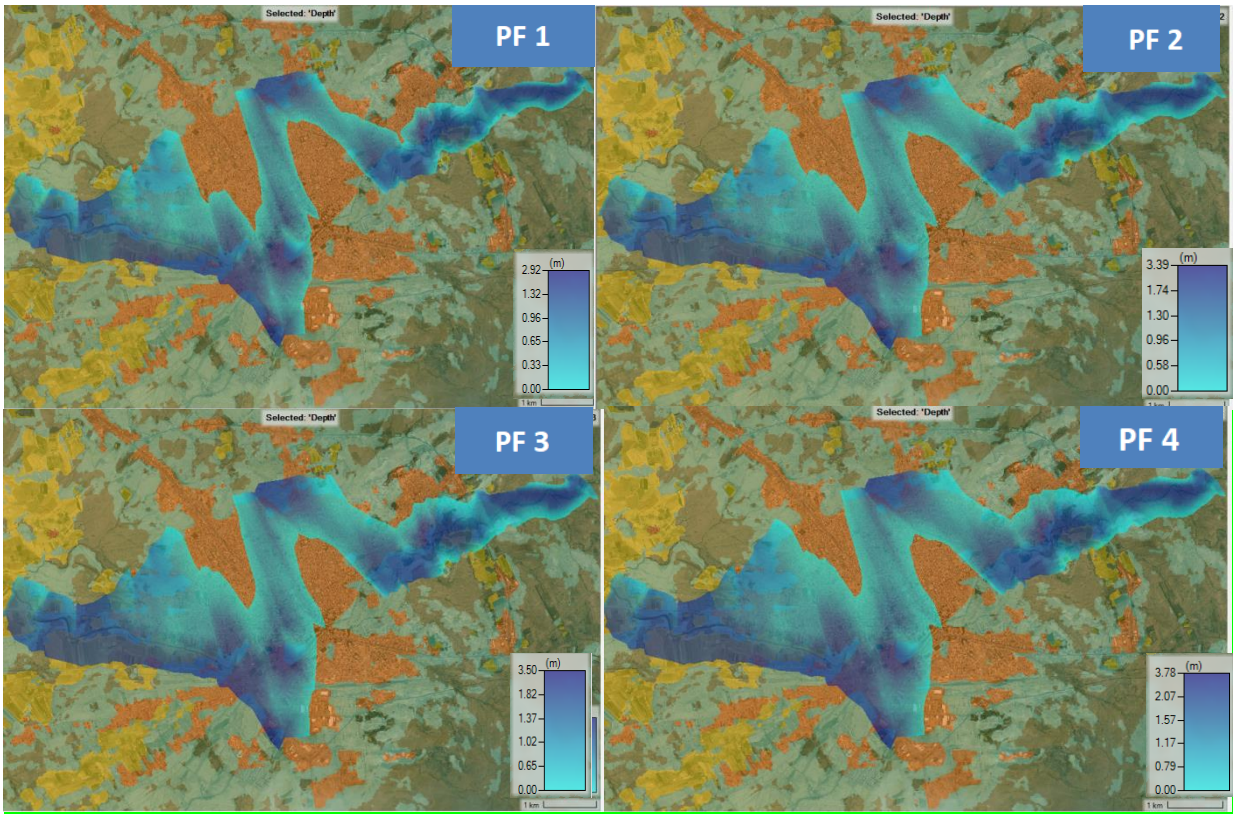

Fig. 4.22 Flooded area for the 10-year, 50-year, 100-year and 1000-year return periods in Barika city (Barika watershed)

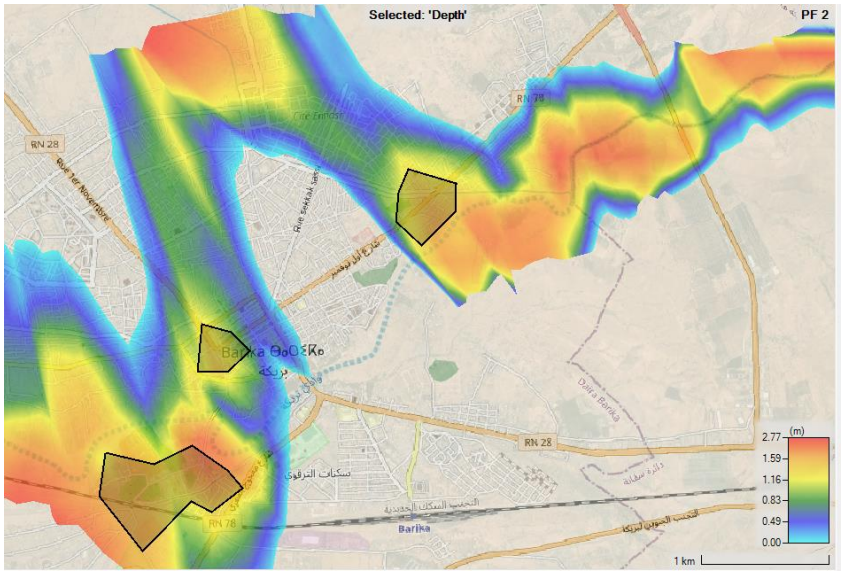

Fig. 4.23 Flood prone areas (polygons) near Barika wadi for 50-year return period

4.3.2.4. Bordj Bou Arreridj city

Flood wave propagation along the upstream of K'sob wadi is shown is Figure 4.24 for return periods of 10-year, 50-year, 100-year and 1000-year. Several western areas of the industrial

zone in Bordj Bou Arreridj and many other high-density residential areas are at risk of flooding (Figure 4.25).

The water height reaches the maximum values of 6.88 m, 7.36 m, 7.75 m and 8.03 m corresponding to 10-year, 50-year, 100-year and 1000-year return periods respectively.

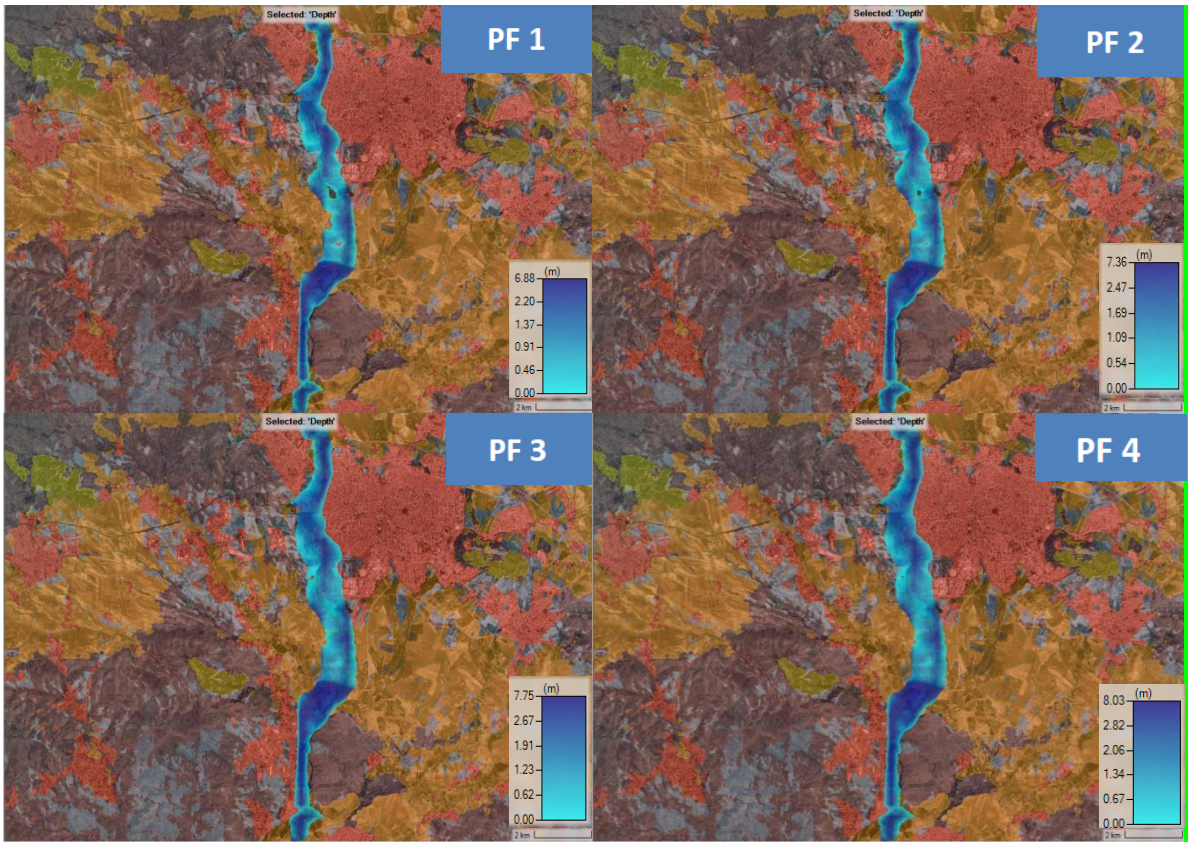

Fig. 4.24 Flooded areas for the 10-year, 50-year, 100-year and 1000-year return periods in Bordj Bou Arreridj city (K'sob upstream)

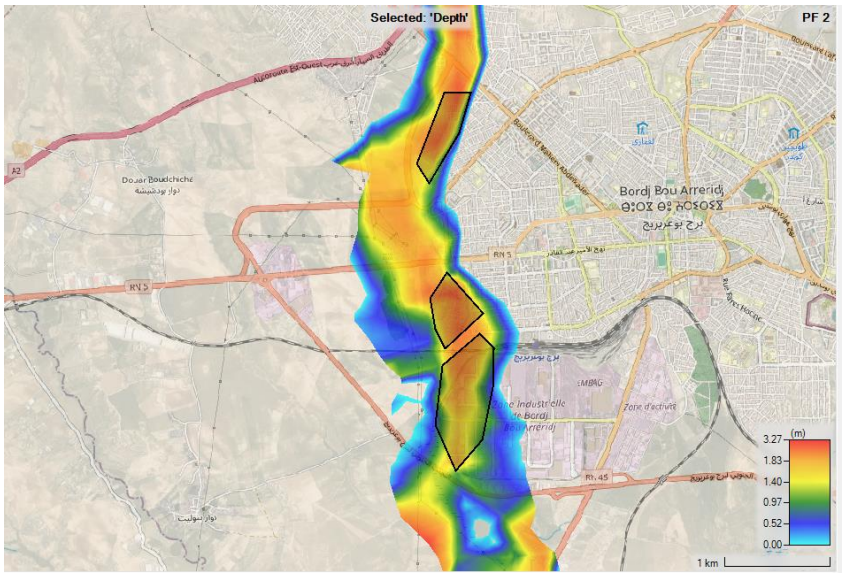

Fig. 4.25 Flood prone areas (polygons) near K'sob wadi (upstream) for 50-year return period

4.3.2.5. M'sila city

Flood wave propagation along the downstream of K'sob wadi is shown is Figure 4.26 for return periods of 10-year, 50-year, 100-year and 1000-year. Areas at risk of flooding are Ouled Bedira, as well as the eastern zones with 270 logs, 108 logs, 98 logs, and other settlements near Sidi Amara. The industrial area of M'sila city is also exposed to the risk of flooding, located in the west of M'sila city (Figure 4.27).

The water height reaches the maximum values of 2.75 m, 3.43 m, 3.66 m and 3.87 m corresponding to 10-year, 50-year, 100-year and 1000-year return periods respectively.

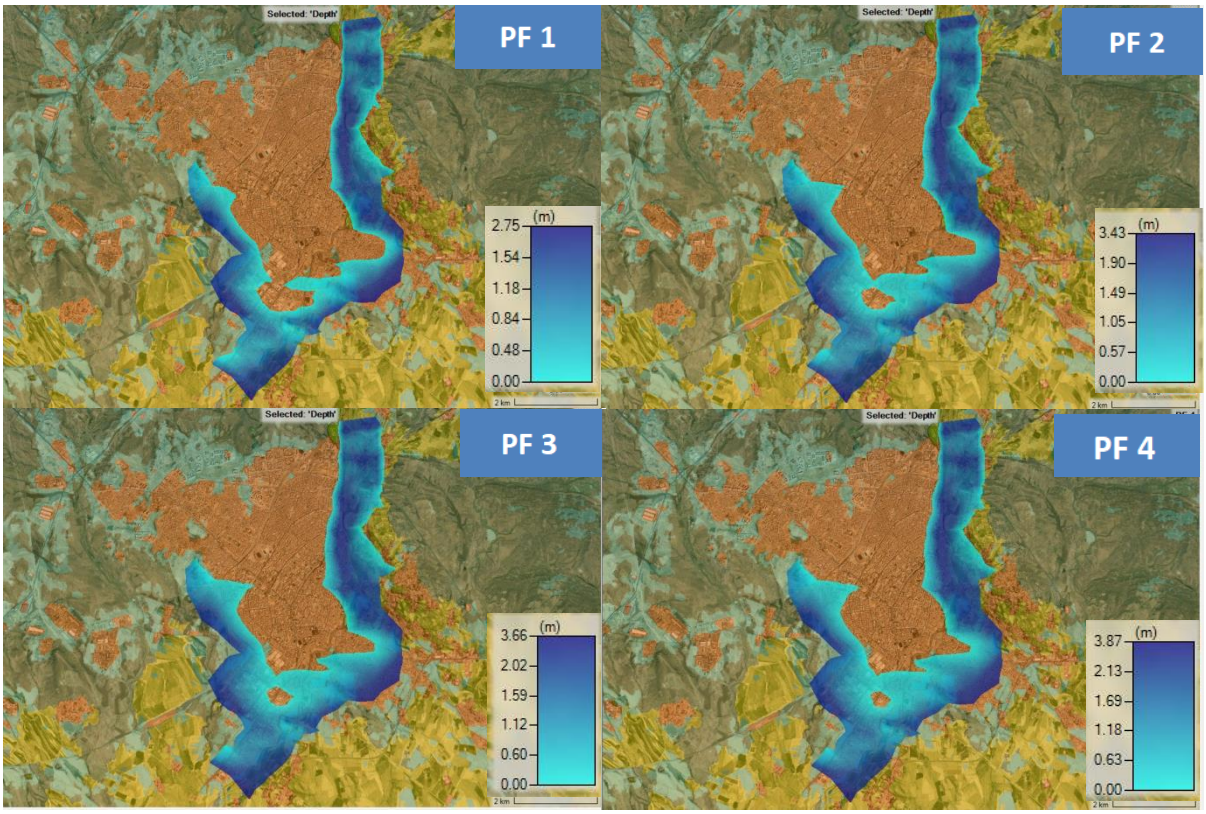

Fig. 4.26 Flooded areas for the 10-year, 50-year, 100-year and 1000-year return periods in M'sila city (K'sob downstream)

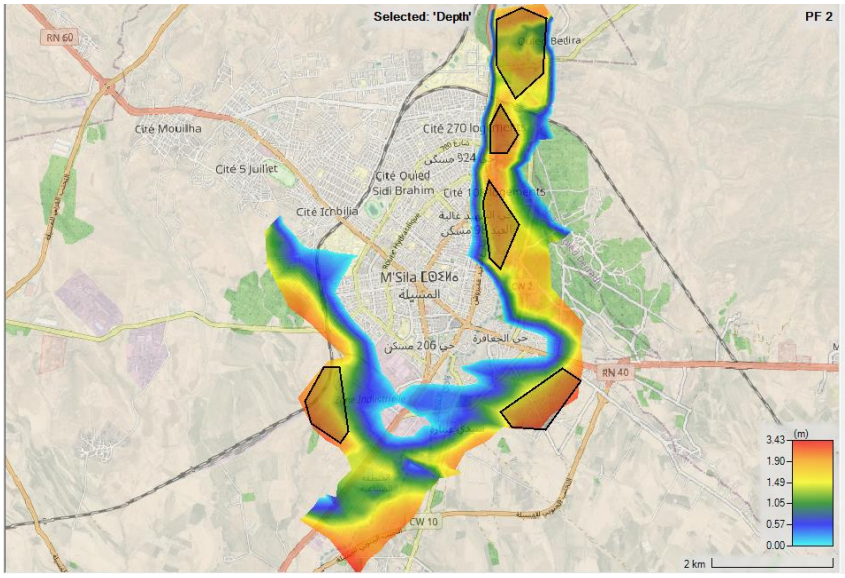

Fig. 4.27 Flood prone areas (polygons) near K'sob wadi (downstream) for 50-year return period

4.4. Conclusion

Flooding in arid regions is an anomalous and rarely recurring phenomenon, which is more important not because of the extreme and highly variable hydrological regime, but because of human settlement in flood-prone areas. Modeling that can provide a basic holistic understanding of technology is a major requirement (Oulad Naoui et al., 2018). Precipitation-runoff models are standard tools for hydrological analysis. These models are used for applications such as water resource studies and flood forecasting.

This chapter presents results for the assessment of peak flow, flood hazard and flood prone areas. The aim was to evaluate the design discharge in the El-Ham wadi sub-basin by applying empirical formulas (Giandotti, Possenti, Turazza and Temez) and statistical techniques (Gradex method). These methods are most suitable for the study area due to the availability and accessibility of precipitation data. In this case, the maximum daily records are adapted to the application. Concentration time is also determined using ANRH-Sogreah, Basso and Giandotti formulas. We should also note that it gives a clear picture of flood wave propagation over the Hodna basin on the integration of multi-criteria data such as rainfall distribution, slope, drainage density, land use and cover and soil type.

In this chapter, the usefulness of HEC-RAS in hydraulic simulations is also highlighted in many cities that make up the Hodna basin, such as Sidi Aïssa, Boussaada, Bordj Bou Arreridj, M’sila and Barika.

CHAPTER 5

Climate change effect in Hodna basin:

Interpretation of results

Chapter 5 Climate change effect in Hodna basin: interpretation of results

5.1. Introduction

The final chapter of this thesis presents main results for historical evaluation and future projections of precipitation and maximum temperature under CMIP6 GCMs.

5.2. Assessment and downscaling CMIP6 GCMs simulations and CRU observations

In Figure 5.1, monthly Hodna mean precipitations simulated by GCMs are compared with observations from the CRU dataset during the reference period 1901-2014. Here, the performance of CMIP6 models is examined according to ability to reproduce the mean monthly variability. The performances of GCMs vary in their abilities to reproduce the CRU precipitation. On one hand, the ACCESS-ESM4, BCC-CSM2-MR, GFDL-ESM4, MIROC6, and IPSL-CM6A-LR models show precipitation peaks (27.81 mm, 25.55 mm, 30.36 mm, 47.61 mm and 43.47 mm respectively). Furthermore, CanESM5 tended to overestimate the observed values during the reference period (120 mm at the Northwestern Mountains), while ACCESS-ESM4 and BCC-CSM2-MR models underestimated precipitation in the Southeastern part of Hodna basin.

Figure 5.2 shows a comparison between observations from CRU dataset for the reference period 1901-2014 and simulations of monthly Hodna mean maximum surface air temperature by GCMs. MIROC6 indicates a significant overestimation of maximum surface air in many parts of the study region. However, the IPSL-EM6A-LR model tends to underestimate the maximum surface air temperature in the Southern and Northwestern part of Hodna. The ACCESS-ESM4, BCC-CSM2-MR, CanESM5 and GFDL-ESM1-5 models show much better performance compared to observations with the values of 22.78 °C, 25.55 °C, 23.71 °C and 22.11 °C respectively.

The simulations presented in Figures 5.1 and 5.2 have been downscaled based on Geographically Weighted Regression (GWR) technique in ArcGIS software.

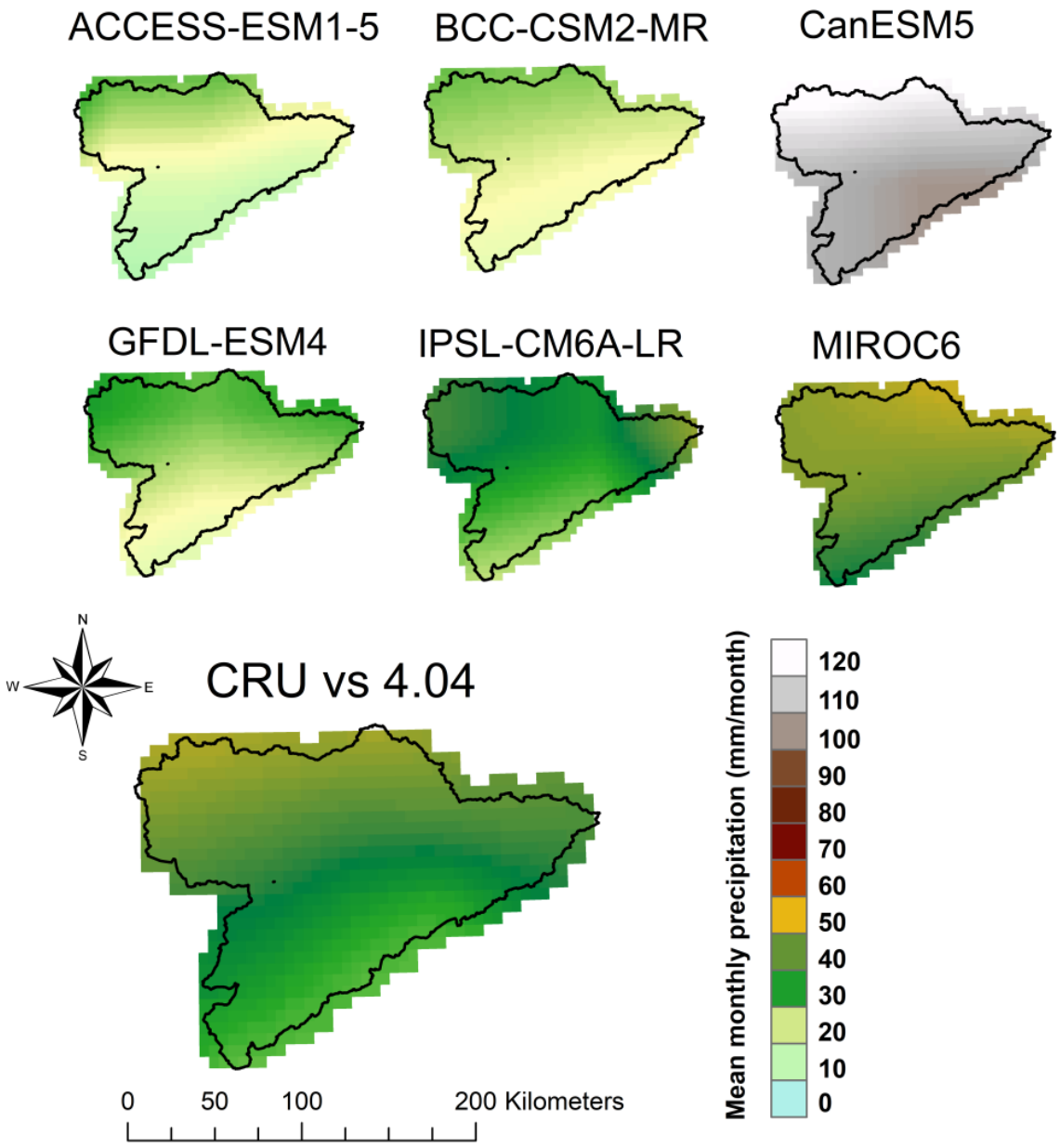

Fig. 5.1 Spatial distribution of mean monthly precipitation based on CRU and CMIP6 data of Hodna basin for the period 1901-2014

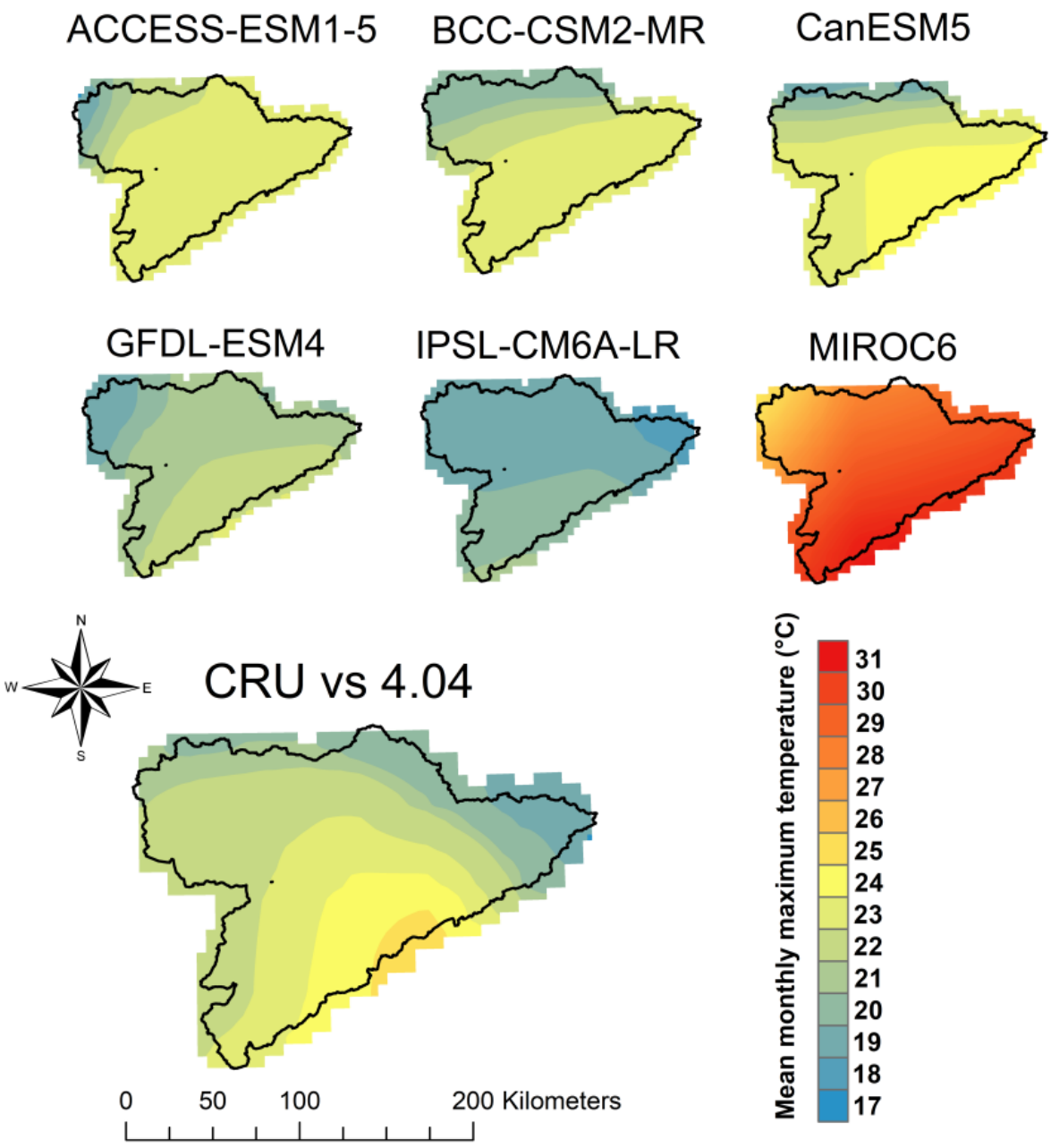

Fig. 5.2 Spatial distribution of mean monthly maximum temperature based on CRU and CMIP6 data of Hodna basin for the period 1901-2014.

In the next section, Tables 5.1 and 5.2 help validate the models' ability to spatially reproduce historical precipitation and maximum surface air temperature in the studied basin, using the CP method.

5.3. Ranking of GCMs using CP technique

5.3.1. Ranking of GCMs for precipitation

For the precipitation, the results of performance metrics calculated for all GCMs and the final ranking derived on the basis of CP method are presented in Table 5.1.

The main results show that the IPSL-EM6A-LR model is the top-rank model, followed by MIROC6 and GFDL-ESM4 models. The CanESM5 climate model is classified as the newest among all GCMs. These results mean that an ideal climate model is not required as with the IPSL-EM6A-LR model, so it may be in the best order. For example, ACCESS-ESM1-5 the fifth model in the list, although it has two ideal values as mean bias and coefficient of determination, . Finally, the spatial patterns of precipitation presented in Figure 5 are in excellent agreement with the CP results.

Table 5.1 Statistical performance metrics and ranking of CMIP6 climate models using CP method (case of total precipitation)

CMIP6 GCMs	Performance metrics			Differences in metrics and ideal values			Sum	Rank
	MB	RMSE	R^2	MB	RMSE	R^2		
ACCESS-ESM1-5	-22.35	34.57	0.71	17.13	0.63	0	17.76	5
BCC-CSM2-MR	-20.25	34.10	0.69	15.03	0.16	0.02	15.21	4
CanESM5	78.17	93.52	0.66	72.95	59.58	0.05	132.58	6
GFDL-ESM4	-18.05	34.11	0.70	12.83	0.17	0.01	13.01	3
IPSL-CM6A-LR	5.22	36.73	0.66	0	2.79	0.05	2.84	1
MIROC6	11.91	33.94	0.70	6.69	0	0.01	6.7	2
Ideal values	**5.22**	**33.94**	**0.71**					

5.3.2. Ranking of GCMs for maximum temperature

Table 5.2 below shows the main results for applying the CP method at the maximum surface air temperature of the six GCMs. Three statistical metrics are calculated to rank these GCMs.

It is clear from the results in this table that the highest coefficient of determination, if not first order, corresponds to the IPSL-CM6A-LR model. The GFDL-ESM4 model is identified as the best-performing model corresponding to the mean absolute bias ideal value. Additionally, ACCESS-ESM1-5, BCC-CSM2-MR and CanESM5 models are also classified as the 3 top-ranking models after the GFDL-ESM4 model. ACCESS-ESM1-5 model has the lowest RMSE, and the lowest coefficient of determination values. Not surprisingly, the CP method results are validated by

spatial models of maximum surface air temperature, confirming the best and worst ranks (Figures 5.1 and 5.2).

Table 5.2. statistical performance metrics and ranking of CMIP6 climate models using CP method (case of maximum temperature)

CMIP6 GCMs	Performance metrics			Differences in metrics and ideal values			Sum	Rank
	MB	RMSE	R^2	MB	RMSE	R^2		
ACCESS-ESM1-5	2.81	2.04	0.87	1.72	0	0.11	1.83	2
BCC-CSM2-MR	2.59	2.49	0.91	1.50	0.45	0.07	2.02	3
CanESM5	3.70	2.28	0.91	2.61	0.24	0.07	2.92	4
GFDL-ESM4	1.09	2.63	0.96	0	0.59	0.02	0.61	1
IPSL-CM6A-LR	-4.91	3.84	0.98	3.82	1.80	0	5.62	5
MIROC6	10.28	7.78	0.92	9.19	5.74	0.06	14.99	6
Ideal values	**1.09**	**2.04**	**0.98**					

5.4. Projected precipitation and maximum air temperature changes

In the projection analysis, the first two models showing the best performance on the study area are used for precipitation (IPSL-CM6A-LR) and maximum surface air temperature (GFDL-ESM4). Two different scenarios, SSP1-2.6 and SSP3-7.0, are chosen for four different future periods, namely, the near future (2021-2040), mid-century (2041-2060 and 2061-2080) and far future (2081-2100).

Under the most optimist forcing scenario SSP1-2.6, Figures 5.3 and 5.5 show the projected monthly mean changes in precipitation and maximum surface air temperature for the 2021 – 2100 timeline. Hodna's future precipitation projections show no signs of area-averaged variation and are likely to decline slightly towards the end of the century. In conjunction with precipitation changes, this study suggests that maximum surface air temperature will change at a slow rate of averaged-monthly (not more than 48.75 mm/month). The maximum surface air temperature may increase by 2°C in the next decades compared to observed and simulated values, but then almost stabilizes and reaches a monthly mean increase of 28.53 °C. Finally, the SSP1-2.6 scenario does not show any current signs of change in the current Hodna basin climate on global scale.

Under the strong forcing scenario SSP3-7.0, Figures 5.4 and 5.6 show the projected monthly mean changes in precipitation and maximum surface air temperature for the 2021 – 2100 timeline. Hodna's future precipitation projections could decrease very remarkably under this scenario with an averaged value of 10 mm on a monthly scale.

This decrease is mostly in the center and southeastern parts. Its counterparts, the maximum surface air temperature can rise steadily from 28°C to 31°C, reaching a maximum in the center and southeastern parts (almost 4.5 °C by 2100) and moving towards northwestern part of Hodna.

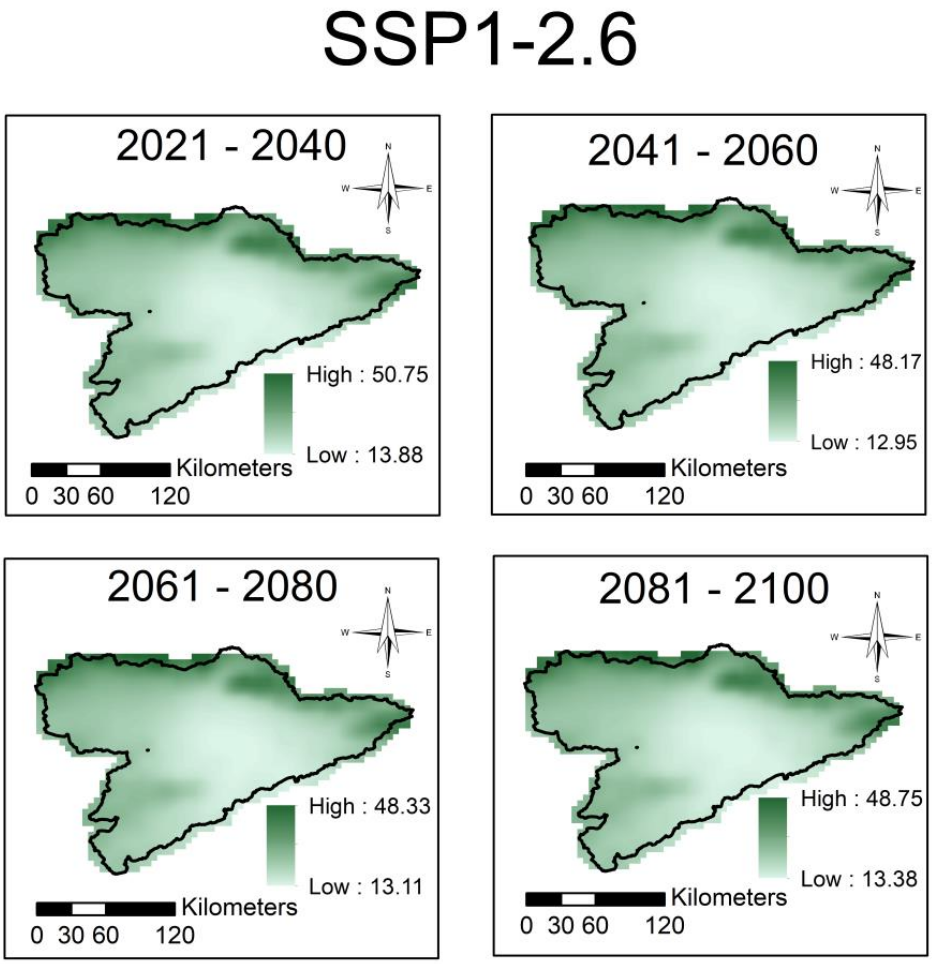

Fig. 5.3 Projected average monthly precipitation for SSP1-2.6 (IPSL-CM6A-LR) until 2100

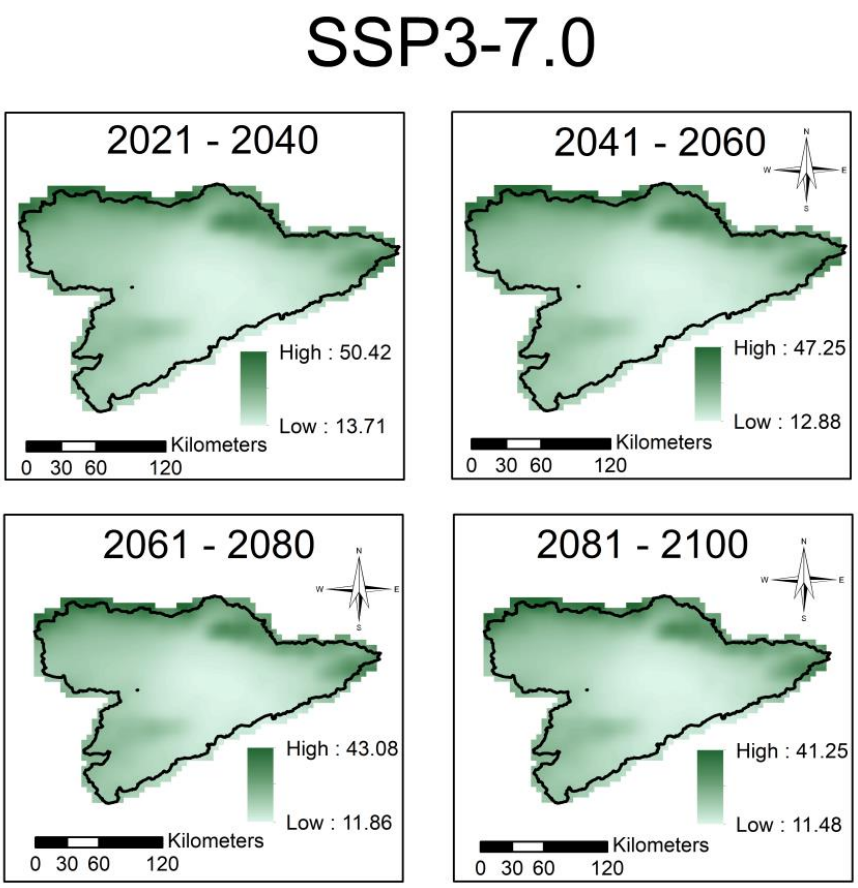

Fig. 5.4 Projected average monthly precipitation for SSP3-7.0 (IPSL-CM6A-LR) until 2100

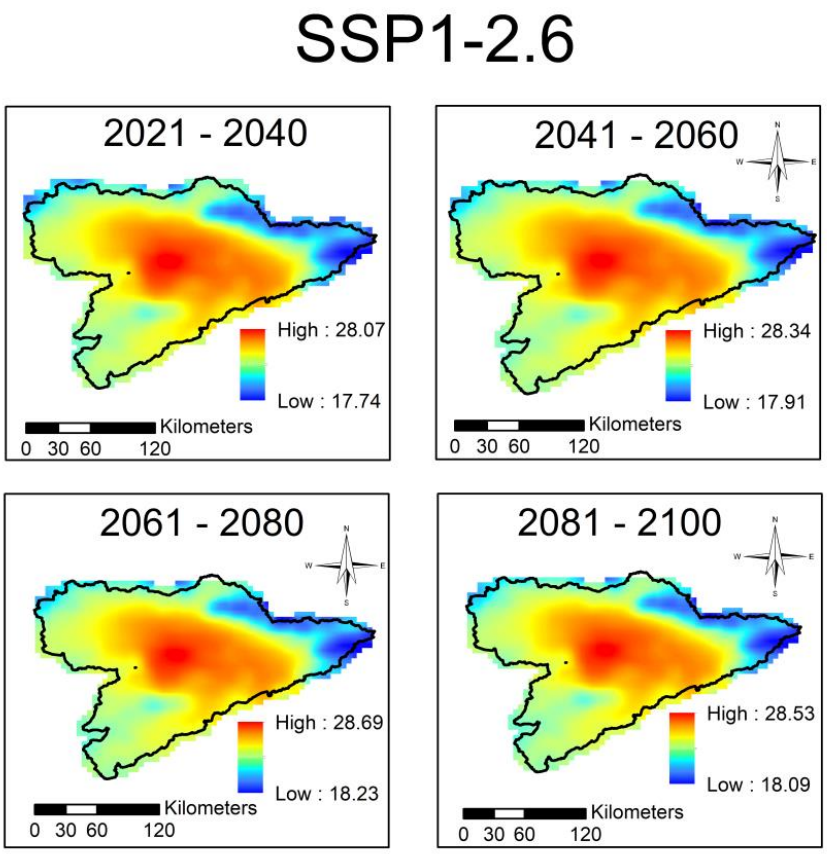

Fig. 5.5 Projected average monthly maximum temperature for SSP1-2.6 (GFDL-ESM4) until 2100

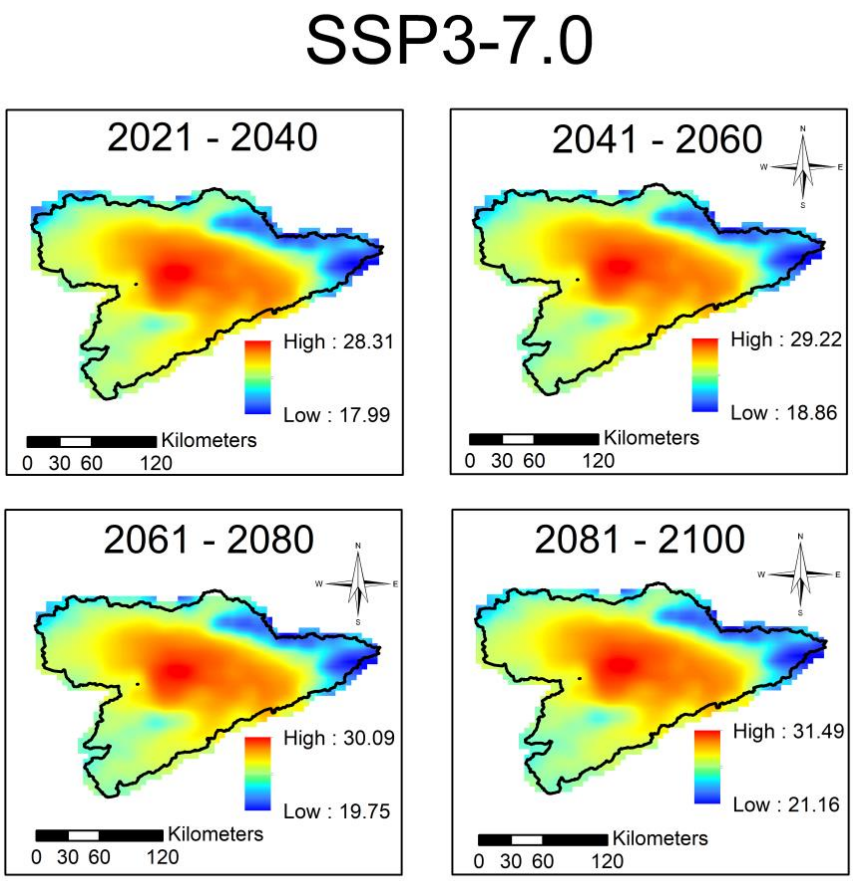

Fig. 5.6 Projected average monthly maximum temperature for SSP3-7.0 (GFDL-ESM4) until 2100

5.5. Conclusion

Regional and local research on climate change worldwide is of great importance and interest to scientists, policy makers and general public. In fact, a better understanding of the changes in our climate behavior can help appropriate mitigation procedures across all sectors.

This article evaluates the multi-model capability of 6 models from CMIP6 historical precipitation and maximum surface air temperature datasets in the Hodna basin in central Algeria with an area of 26 000 km² and their projected changes into the future.

All 6 GCMs simulate Hodna's monthly mean maximum surface air temperature, with a coefficient of determination ranging from 0.87 to 0.98, with minor biases. The GFDL-ESM4 model ranks first for maximum surface air temperature, while the IPSL-CM6A-LR model is the best-ranked GCM for precipitation, with coefficient of

determination ranges from 0.66 and 0.71. CMIP6 historical simulations reproduce precipitation and maximum surface air temperature with varying success intervals. Some had difficulties replicating the apparent spatial variability shown in the Compromise Programming method results. CanESM5 and MIROC6 overestimated monthly mean precipitations and maximum surface air temperature, respectively, while IPSL-EM6A-LR underestimated maximum surface air temperature.

In the projection analysis, the two first two models whowing the best performance on the study area were used for precipitation (IPSL-EM6A-LR) and maximum surface air temperature (GFDL-ESM4). Two different scenarios, SSP1-2.6 and SSP3-7.0, were chosen for four different future periods, namely, the near future (2021-2040), mid-century (2041-2060 and 2061-2080) and far future period (2081-2100).

Hodna's future precipitation projections under SSP1-2.6 show no signs of area-averaged variation (with 48.75 mm/month by 2100) and will likely decline slightly towards the end of the century. In conjunction with precipitation changes, this study suggests that maximum surface air temperature will change at a slow rate per month, on average. The maximum surface air temperature may increase by 2 °C in the next decades compared to observed and simulated values, but then almost stabilizes and reaches an average monthly increase of 28.53 °C. In conclusion, the SSP1-2.6 scenario does not show any current signs of change in the current Hodna basin climate on a global scale.

Future precipitation projections under Hodna's SSP3-7.0 can fall very dramatically, with an average value of 10 mm on a monthly scale. This decrease is mostly in the center and southeastern parts. Its counterparts, the maximum surface air temperature can rise steadily from 28 °C to 31°C, reaching a maximum in the center and southeastern parts (almost 4.5 °C by 2100) and moving towards the northwestern part of Hodna.

The results of this study can contribute to making the right climate decisions, such as using more solar and wind energy, more water resources management adaptive to drought and flood events, construction of additional dams for water and electricity availability for warmer future periods, the benefit of electric cars in reducing carbon emissions.

GENERAL CONCLUSION

General conclusion

1. A retrospective look at research objectives

Algeria has witnessed many flooding events that caused considerable damages. Nowadays, flood risk management is considered as a necessity to protect people and decrease damages to infrastructures. The Hodna basin, like many other semi-arid and arid climate basins is characterized by an irregular precipitation regime often leading to flash and disastrous floods.

This thesis aims to propose a methodological approach to determine the influence of peak flow estimation on flood intensity and to examine the effect of climate change on the hydrological behavior of Hodna basin, in particular precipitation and maximum temperature.

In this thesis, the methods used to conduct this study consist of:

- Evaluation and future projection of monthly maximum air temperature and precipitation in the Hodna basin. The Geographical Weighted Regression (GWR) technique was used to statistically downscale six of the CMIP6 GCMs outputs. The six climate models selected are: ACCESS-ESM4, BCC-CSM2-MR, CanESM5, GFDL-ESM1-5, IPSL-EM6A-LR and MIROC6. Before implementing the future projection using multiple models, it is necessary to evaluate their performance in the study area and apply bias correction. Two climate scenarios were applied, SSP1-2.6 and SSP3-7.0. In particular, these scenarios aim to show precipitation and temperature variabilities over the period 1901-2014 for both high and low mitigation and adaptation strategies respectively.
- Evaluation of flood discharge rates for different return periods (10-year, 50-year, 100-year and 1000-year) using different empirical and statistical formulas (Giandotti, Possenti, Turazza, Temez, Gradex),
- Assessment and modeling of flood hazard and risk in the Hodna basin using both GIS and HEC-RAS tools,
- Assessment of future climate using GCMs for effective planning and management of water resources using CMIP6 outputs for precipitation and temperature variables.

The first chapter of this thesis aims to provide a literature view on the behavior of basins, flood hazard and risk assessment and modeling, as well as climate system, greenhouse gas (GHG) emission effect and climate change modeling. The second chapter focuses on the

Hodna basin as a studied region. Different features are included (i.e. geographical location, climate, geomorphological features). Then, a third chapter has been dedicated to give the details of all the methodologies and tools to achieve the aim of the study. The last two chapters include the conclusion and discussion parts.

2. Summary of the findings

Specific conclusions regarding the results of the different parts of this study are summarized below.

The results of the peak flow assessment in the El-Ham sub-basin show that:

- Flood discharge rates increase with the increasing return period (10-year, 50-year, 100-year and 1000-year),
- Short-term precipitation values at stations of Ain Nessissa, Ain El Hadjel and Rocad Sud are 91.2 mm, 121.7 mm and 51.2 mm are for a 100-year return period,
- Centennial return period density shows high values at stations 050301 (5.67 mm/h), 2.43 mm/h, at station 050703 and 4.25 mm/h at station 050101,
- Empirical analysis of flood discharges repeats the same observations regarding return periods with different flow rates (5581.86 m^3/s for a 100-year, also shown at Ain El Hadjel station).

The flood assessment and mapping results in the Hodna basin indicate that:

- The latest flood risk map using AHP technique gives us with many insights into areas with high flood risk, including the cities of Sidi Aïssa, Boussaada, Barika, M'sila and Bordj Bou Arreridj. It is due to overlap of the spatial density of the hazard and the population density corresponding to 70% and 30% of the weights, respectively,
- 46%, 27.9%, 15%, 6.6% and 4.2% corresponding to the pre-calculated weights, rainfall distribution, slope, drainage density, land use/land cover and soil type used to generate the flood hazard map based on the AHP technique,
- The runoff depends on the rocks that make up the soil, the land slope, the rainfall distribution, the drainage density for each wadi and the land cover of the Hodna basin. Areas with low slope values, low drainage density and preferred soil type,
- Flood height levels were determined by using HEC-RAS one dimensional model for areas that are highly exposed to flood risk, and a flood risk map using the AHP method, including the same cities . The maximum water heights for the 10-year return period were equal to 5.55 m, 4.65 m, 2.92 m, 6.88 m and 2.75 m. The maximum water

heights for the 50-year return period were equal to 6.41 m, 5.77m, 3.39 m, 7.36 m and 3.43 m. For the 100-year return period, maximum water heights were equal to 7.15 m, 6.07 m, 3.50 m, 7.75 m and 3.66 m. On the lother hand, the maximum water heights for the 1000-year return period were equaled 7.75 m, 6.80 m, 3.78 m, 8.03 m and 3.87 m. These water heights correspond to the cities of Sidi Aïssa, Boussaada, Barika, Bordj Bou Arreridj and M'sila respectively.

The results of applying climate change models in the Hodna basin show that:

- Statistical downscaling allowed more reliable representation of monthly precipitation and maximum temperature in the Hodna region,
- The application of two climate scenarios (SSP1-2.6 and SSP3-7.0) was useful in reproducing precipitation and future maximum temperature variabilities,
- This study explored the potential of the compromise programming (CP) selection method in ranking GCMs to identify better performing GCMs suitable for projection of multiple climate variables for different seasons. The best-performing models are used for precipitation (IPSL-EM6A-LR) and maximum surface air temperature (GFDL-ESM4), after a comparison between CRU-TS observations and historical data,
- Model precipitation and temperature differences and were quantified using three statistical parameters, including bias error (BE), root mean square error (RMSE) and coefficient of determination (R^2),
- For the most optimist scenario, the maximum surface air temperature may increase by 2 °C compared to observed and simulated values in the next decades, but then almost stabilizes and reaches an average monthly increase of 28.53 °C. The same is shown in precipitation projection of 48.75 mm/month by 2100,
- In conclusion, the SSP1-2.6 scenario does not show any current signs in the current Hodna basin climate on a global scale. Future precipitation projections under Hodna's SSP3-7.0 may decrease by an average of 10 mm io a monthly scale. This decrease becomes mostly in the center and southeastern parts. The maximum surface air temperature can rise steadily from 28 °C to 31°C, reaching a maximum of 4.5 °C by 2100.

3. Direction of future research

The outcomes of this thesis have revealed important insights into the flood risk patterns under the climate change effects in Algeria's greater Hodna basin . Yet, it has some limitations that could be addressed in future research. In fact, the findings of this thesis may help explore

other ways of assessing inundation risk on the actual changing climate in Algerian watersheds.

More importantly, based on the results and findings presented in this thesis, the following issues could be implemented in further studies:

- The results of climate change assessment provide input for climate change impact assessment, adaptation and mitigation research. Future researches may consider the findings from this study to test and verify their reliability and accuracy in the Hodna basin. The study of extreme events, in particular precipitation, in the context of climate change is also of definite scientific interest.
- Comparative research is required between CMIP3, CMIP5 and current CMIP6 GCMs outputs ,
- An understanding of the mechanisms of future precipitation and temperature changes should be considered,
- Use one of the many distributed hydrological models based on future precipitations projections to assess changes in runoff and then determine future flood expanse and risk over the provinces studied,
- It is recommended to examine changes in maximum daily precipitation in the near and far future,
- It is important to have enough samples (climate models) to get good results in predicting future total precipitations and maximum temperature. In addition, the lack of some previous studies limited the possibility to discussing the implications for climate change.

.

LIST OF REFERENCES

List of references

Abdalla, F. (2012). Mapping of groundwater prospective zones using remote sensing and GIS techniques : A case study from the Central Eastern Desert, Egypt. Journal of African Earth Sciences. 70 (2012), 8-17. http://dx.doi.org/10.1016/j.jafrearsci.2012.05.003

Abdeddaim, H. (2018). Contribution à l'étude de l'influence de la structure du réseau hydrographique sur le risque hydrologique : cas des bassins de l'Est de l'Algérie. Thèse de Doctorat. Université de Biskra. 276 p.

Abdesselam, S., Halitim, A., Jan, A., Trolard, F. and Bourrié, G. (2013). Anthropogenic contamination of groundwater with nitrate in arid region: case study of southern Hodna (Algeria). Environ Earth Sci Journal. 70: 2129-2141. DOI 10.1007/s12665-012-1834-5

Adjinacou, A.M. (2016). Flood modeling and flood plain mapping based on Geographic Information System (GIS) and HEC-RAS in Oued Fez watershed (Morocco). Master thesis. Pan African university, institute of water and energy sciences. 115 p.

Ahmed K, Shahid S, Sachindra DA, Nawaz N, and Chung ES. (2019). Fidelity assessment of general circulation model simulated precipitation and temperature over Pakistan using a feature selection method. J. Hydrol. doi: 10.1016/j.jhydrol.2019.03.092

Ajibola FO, Zhou B, Gnitou GT, and Onyejuruwa A. (2020). Evaluation of the performance of CMIP6 HighResMIP on West African Precipitation. Atmosphere Journal. 11, 1053. doi:10.3390/atmos11101053

Ajjur SB. and Al-Ghamdi SG. (2021). Evapotranspiration and water availability response to climate change in the Middle East and North Africa. Climatic change 166: 28. http://doi.org/10.1007/s10584-021-03122-z

Albertson, M.L. and Simons, D.B. (1964). Fluid mechanics, flow in open channels. Handbook of Applied Hydrology, McGraw-Hill, New York, USA.

Almazroui M, Saeed S, Saeed F, Islam MN. and Ismail M. (2020). Projections of precipitation and temperature over the South Asian countries in CMIP6. Earth Systems and Environment 4:297-320. https://doi.org/10.1007/s41748-020-00157-7

Amroune, A., Mihoub, R., Guastaldi, E. and Urena-Nieto, C. (2020). Groundwater flow dynamics and distribution of hydrochemical facies using GIS in Hodna plain, M'sila, Southeastern Algeria. International Journal of sustainable development and planning. Vol, 15, No, 6, pp:789-800.

Arrhenius, S. (1896). On the influence of carbonic acid in the air upon the temperature of the ground. Philosophical magazine Series 5, 41(251), 237-276. doi:10.1080/14786449608620846

Asare-Kyei D., Forkuor, G., Venus, V. (2015). Modeling flood hazard zones at the Sub-District level with sensing approaches. *Water*, 7(7), 3531 3564. https://doi.org/10.3390/w7073531

Ayalew DW. (2019). Evaluating the potential impact of climate change on the hydrology of Ribb catchment, Blue Nile Basin, Ethiopia. Master dissertation. Pan African university, Institute of water and energy sciences, in collaboration with Tlemcen University. 132 p.

Ayugi B, Ngoma H, Babaousmail H, Karim R, Iyakaremye V, Lim Kam Sian KTC. and Ongoma V. (2021). Evaluation and projection of mean surface temperature using CMIP6 models over East Africa. Journal of African Earth Sciences. https://doi.org/10.1016/j.jafrearsci.2021.104226

Babaousmail H, Hou R, Ayugi B, Ojara M, Ngoma H, Karim, R., Rajaseker, A. and Ongoma, V. (2021). Evaluation of the performance of CMIP6 models in reproducing rainfall patterns over North Africa. Atmosphere Journal. https://doi.org/10.3390/atmos12040475

Banjoko, B. (2014). Chapter 4 of book: Handbook of engineering hydrology: environmental hydrology and water management. Pp:66 – 81

Barech, G., Khaldi, M., Ziane, S., Zedam, A., Doumandji, S., Sharaf, M. and Espadaler, X. (2016). A first checklist and diversity of ants (Hymenoptera: Formicidae) of the saline dry lake Chott El Hodna in Algeria, a Ramsar Conservation Wetland. African Entomology Journal. Vol. 24, NO. 1, 143:152. DOI: http://dx.doi.org/10.4001/003.024.0143

Barnes, H.H. (1967). Roughness characteristics of natural channels (No. 1849). US Government Printing Office.

Beck, C., Grieser, J., Kottek, M., Rubel, F. and Rudolf, B. (2005). Characterizing global climate change by means of Köppen climate classification. Technical report.

Bekhira, A., Habi, M. and Morsli, B. (2019). La gestion des risques d'inondations et aménagement des cours d'eaux dans les zones urbaines : cas de la ville de Béchar. Larhyss Journal, NO 37, pp :75-92

Belagoune, F. (2012). Etude et modélisation des crues des cours d'eaux en milieu semi aride (cas des grands bassins versants 05, 06 et 07), Thèse de magister en hydraulique, Université Kasdi Merbah, Ouargla, 157 p.

Belazreg, N.E.H. (2019). Fonctionnement hydrologique des bassins versants à réseaux hydrographiques différents. Mémoire de Master. Université de Biskra. 132 p.

Belazreg, N.E.H., Hasbaia, M., Şen, Z. and Ferhati, A. (2022). Peak flow assessment of El-Ham wadi in Hodna basin case study. Arabian Journal of Geosciences, 15:22. https://doi.org/10.1007/s12517-021-09295-2

Belazreg, N.E.H., Hasbaia, M., Şen, Z. and Ferhati, A. (2023). Historical evaluation of future projections of monthly precipitation and temperature under CMIP6 GCMs, case of Hodna basin (central Algeria). Arabian Journal of Geosciences, 16:39. https://doi.org/10.1007/s12517-022-11124-z

Bendine, S.E.I. (2019). Etude de la faisabilité de la recharge de la nappe d'El Maader (Boussaada) par les eaux de crues. Mémoire de Master. Université de Biskra. 100 p.

Bendjeddou, F. (2013). Analyse et cartographie de l'érosion hydrique dans le bassin versant de Hodna. Mémoire de Master, Université de M'sila. 101 p.

Boudjemline, F. and Semar, A. (2018). Assessment and mapping of desertification sensitivity with MEDALUS model and GIS : case study basin of Hodna, Algeria. Journal of water and land development, No.36, 17-26. DOI: 10.2478/jwld-2018-0002

Boultif, M. and Benmessaoud, H. (2017). Using climate-soil-socioeconomic parameters for a drought vulnerability assessment in a semi-arid region: application at the region of El Hodna (M'sila, Algeria). Geographica Pannonica, Vol. 21, Issue 3, pp:142-150. DOI: 10.5937/GeoPan1703142B

Bouslihim, Y. (2020). Hydrological and soil erosion modeling using SWAT model and Pedotransfert functions: a case study of Settat-Ben Ahmed watersheds, Morocco. Hassan First University, Settat. tel-03178705v2ff .Doctoral thesis.

Boutaghane, H., Boulmaiz, T., Lameche, E.K., Lefkir, A., Hasbaia, M., Abdelbaki, C., Moulahoum, A.W., Keblouti, M. and Bermad, A. (2022). Flood analysis and mitigation strategies in Algeria. Sumi, T et al. (eds). Wadi flash floods, Natural disaster science and mitigation engineering. https://doi.org/10.1007/978-981-16-2904-4_3

Brooks, K.N., Ffolliott, P.F. and Magner, J.A. (2013). Hydrology and the management of watersheds. Fourth edition. A Jogn Wiley & Sons, Inc., Publication. 545 p.

Burton, I., Smith, J.B. and Lenhart, S. (1998). Adaptation to climate change: theory and assessment. In Handbook on methods for climate change impact assessment and adaptation strategies. Eds. Feenstra, J.F., Burton, I., Smith, J.B. and Tol, R.S.J. United Nations programme and Institute for environmental studies, free university of Amesterdam, Amesterdam, Netherlands.

Bustos Usta, D.F. and Torres Parra, R.R. (2021). Ocean and atmosphere changes in the Caribbean Sea during the twenty-first century using CMIP5 models. Ocean Dynamics, 71(6), 757-777.

Carlson, D., Eyring, V., Well, N.V.D and Langendijk, G. (2017). WCRP's Coupled Model Intercomparison Project: a remarkable contribution to climate science. The European Geosciences Union (EGU).

Chang, H.K., Tan, Y.C., Lai, J.S., Pan, T.Y., Liu, T.M. and Tung, C.P. (2013). Improvement of a drainage system for flood management with assessment of the potential effects of climate change. Hydrological Sciences Journal, 58(8), 1581-1597. DOI: 10.1080/02626667.2013.836276

Chow, V.T. (1964). Handbook of applied hydrology: a compendium of water resources technology. 1525 p. New York; Mcgraw_Hill Book company.

Chowdhury, R.K. and Eslamian, S. (2014). Climate change and hydrologic modeling. In Handbook of engineering hydrology: modeling, climate change, and variability. Eds. Eslamian, S. CRC press. Pp: 72-81

Chu, J., Xia, J., Xu, C. Y. and Singh, V. (2010). Statistical downscaling of daily mean temperature, pan evaporation and precipitation for climate change scenarios in Haihe River, China. Theor Appl Climatol 99, 149–161, https://doi.org/10.1007/s00704-009-0129-6.

Cihlar, J. and Jansen, L. J. (2001). From land cover to land use: a methodology for efficient land use mapping over large areas. *The Professional Geographer*, *53*(2), 275-289.

D.R.E. (2018). Direction des Ressources en Eau - M'sila / Water Resources Directorates (W.R.D)

Dall'Osso, F., Cavalletti, A. and Polo, P. (2006) Risk assessment and evaluation ArcGIS toolbox. User's manual. Coastal Risk Analysis of Tsunamis and Environmental Remediation (CRATER). Italy Ministry for the Environment and Territory & Asian Disaster Preparedness Center.

Dang, N.M.; Babel, M.S. and Luong, H.T. (2010). Evaluation of food risk parameters in the Day River Flood Diversion Area, Red River Delta, Vietnam. *Nat. Hazards*, 56, 169–194. DOI 10.1007/s11069-010-9558-x

Demir, V. and Kisi, O. (2016). Flood hazard mapping by using geographic information system and hydraulic model: Mert River, Samsun, Turkey. *Advances in Meteorology*.

DHA, U. (1992). Internationally agreed glossary of basic terms related to disaster Management. DNA/93/36, United Nations, Department of Humanitarian Affairs, Geneva, Switzerland.

Djoukbala, O., Hasbaia, M., Benselama, O., Boutaghane, H., Djerbouai, S. and Ferhati, A. (2022). Water erosion and sediment transport in an ungauged semiarid area: the case of Hodna basin in Algeria. Sumi, T. (eds). Wadi flash floods, natural disaster science and mitigation engineering. https://doi.org/10.1007/978-981-16-2904-4_17

Djoukbala, O., Mazour, M., Hasbaia, M. and Benselama, O. (2018). Estimation of water erosion in semiarid regions using RUSLE equation under GIS environment. Case of El-Ham watershed in Hodna region, , Algeria. *Environmental Earth Sciences Journal. Springer*. 77(9), article number 345. 1-13. DOI: 10.1007/s12665-018-7532-1

Edwards, P.J., Williard, K.W.J. and Schoonover, J.E. (2015). Fundamentals of watershed hydrology. Journal of Contemporary Water Research & Education. Issue 154, pages 3-20,Universities Council on Water Resources.

Elsheikh, R.F.A., Ouerghi, S. and Elhag, A.R. (2015). Flood risk map based on GIS, multi-criteria techniques (case study Terengganu Malaysia). Journal of Geographic Information System, 7, 348-357. http://dx.doi.org/10.4236/jgis.2015.74027.

Eslamian, S. (2014). Handbook of engineering hydrology. Environmental hydrology and water management. CRC press, Taylor & Francis. 594 p.

Eslamian, S. (2014). Handbook of engineering hydrology: modeling, climate change, and variability. CRC press, Taylor & Francis. 634 p.

EU Floods Directive. (2007). ES of the European Parliament and of the Council on the assessment and management of flood risks.

Eyring, V., Bony, S., Meehl, G. A., Senior, C. A., Stevens, B., Stouffer, R. J. and Taylor, K. E. (2016). Overview of the Coupled Model Intercomparison Project Phase 6 (CMIP6) experimental design and organization. Geoscientific Model Development, 9(5), 1937–1958. https://doi.org/10.5194/gmd-9-1937-2016

Fagan, B. (2009). The Great warming: climate change and the rise and fall and civilizations. 304 p.

FAO (1970). Key to soil units for the soil map of the world. FAO/UNESCO project. Soil resources, development and conservation service land and water development division, FAO, Rome. 18 p.

FAO-UNESCO. (1974). Food and Agriculture Organization- UNESCO: Soil map of the World. Appendix V: major tropical soils and their susceptibility to land degradation.

Farzaneh, M.R., Eslamian, S. and Mirnezami, S.J.E. (2014). Climate change: uncertainty, impact, and adaptation. In Handbook of engineering hydrology: modeling, climate change, and variability. Eds. Eslamian, S. CRC press, Pp: 128-145

Ferahtia, A., Halilat, M.T., Mimeche, F. and Bensaci, A. (2021). Surface water quality assessment in semi-arid region (El-Hodna watershed, Algeria) based on water quality index (WQI). Studia UBB Chemia, LXVI, 1, 2021 (p. 127-142).

Ferhati, A., Belazreg, N.E.H., Dougha, M., Selmane, T., Oumlabat, M.A. and Hemdane, A. (2022). Spatio-temporel assessment of groundwater quality: a case study of M'sila province (Algeria). Arabian Journal of Geosciences. 15, 1775.

Ferhati, A., Mitiche-Kettab, R., Belazreg, N.H., Djafer Khodja, H., Djerbouai, S. and Hasbaia, M. (2021). Hydrochemincal analysis of groundwater quality in central Hodna basin, Algeria: a case study. *International Journal of Hydrology, Science and Technology*. DOI: 10.1504/IJHST.2021.10040507

Few, R., Ahren, M., Matthies, F. and Kovats, S. (2004). Floods, health and climate change: a strategic review. Tyndall Centre Working paper No. 63. 138 p.

Gan, T.Y., Ito, M., Huelsmann, S., Qin, X., Lu, X., Liong, S.Y., Rutschman, P., Disse, M. and Koivosalo H. (2015). Possible climate change/ variability and human impacts, vulnerability of African drought prone regions, its water resources and capacity building. Hydrological sciences Journal, Taylor & Francis. DOI: 10.1080/02626667.2015.1057143

Gehrels, R. (2010). Sea-level changes since the Last Glacial Maximum: an appraisal of the IPCC Fourth Assessment Report. Journal of Quaternary Science, 25(1), 26-38.

Gidden, M.J., Riahi, K., Smith, S.J., Fujimori, S., Luderer, G., Kriegler, E., ..and Takahashi, K. (2019). Global emissions pathways under different socioeconomic scenarios for use in CMIP6: a dataset of harmonized emissions trajectories through the end of the century. Geoscientific model development, 12(4), 1443-1475.

Glantz, M.H. and Krenz, J.H. (1992). Chapter 2: Human components of the climate system. Trenberth, K.E. 1992, in Climate system modeling.

Goncalves, J.A.V. (2017). Caracterização do coeficiente de rugosidade e seu efeito no escoamento em canais naturais: simulação e modelação (à escala) no laboratório de hidráulica: aplicação às ribeiras do Funchal (Doctoral dissertation).

Goodell, C. and Warren, C. (2006). Flood inundation mapping using HEC-RAS. Obras y Proyectos, N°2.

Goosse, H., Barriat, P.Y., Lefebvre, W., Loutre, M.F. and Zunz, V. (2010). Introduction to climate dynamics and climate modelling. Université catholique de Louvain (Belgium).

Görgen, K., Beersma, J., Brahmer, G., Buiteveld, H., Carambia, M., de Keizer, O., Krahe, P., Nilson, E., Lammersen, R., Perrin, C. and Volken, D. (2010). Assessment of climate change impacts on discharge in the Rhine River Bassin: Results of the RheinBlick2050 project. [Research Report] irstea. 2010, pp.211. ffhal-02594596f

Gravelius, H. (1914) Grundrifi der gesamten Gewcisserkunde. Band I: Flufikunde (Compendium of Hydrology, Vol. I. Rivers, in German). Goschen, Berlin.

Grimaldi, S., Petroselli, A., Tauro, F. and Porfiri, M. (2012). Time of concentration: a paradox in modern hydrology. *HSJ* , 57(2), 217-228. DOI: 10.1080/02626667.2011.644244

Guellouh, S., Dridi , H. and Kalla, M. (2016). Flood hazard mapping in the city of Batna (Algeria) by hydraulic modeling approach. Analele Universităţii din Oradea, Seria Geografie. Pp: 86-93

Hachemi, A. and Benkhaled, A. (2016). Flood-duration-frequency modeling application to wadi abiodh, biskra (algeria*). LARHYSS Journal* P-ISSN 1112-3680/E-ISSN 2521-9782, (27), 277-297.

Hailin, Z.Yi.J., Xuesong, Z., Gaoliao, J.Yi.Y. and Baoyin, H. (2009). GIS-based risk assessment for regional flood disaster. International Conference on Environmental Science and Information Application Technology; July 4–5; Wuhan, China: p. 564–567.

Hamblyn, R. (2009). The whistleblower and the canary: rhetorical constructions of climate change. Journal of historical geography, 35(2), 223-236. doi:10.1016/j.jhg.2008.09.006

Hansen, G. (2015). Assessing the observed impact of anthropogenic climate change. Wageningen University, NL. Ph. D thesis, 196 p.

Harkat, N., Chaouche S. and Bencherif, M. (2020). Flood hazard spatialization applied to the city of Batna. A methodological approach. Engineering, technology & applied science research. Vol. 10, No, 3, 5748-5758

Harris, I., Osborn, T.J., Jones, P. and Lister, D. (2020). Version 4 of the CRU TS monthly high-resolution gridded multivariate climate dataset. Scientific data Journal. 7. 109. doi:10.1038/s41597-020-0453-3

Harris, I., Osborn, T.J., Jones, P. and Lister, D. (2020). Version 4 of the CRU TS monthly high-resolution gridded multivariate climate dataset. Scientific data Journal. 7. 109. doi:10.1038/s41597-020-0453-3

Hasbaia, M. and Adoui, H. (2015). Contribution à l'étude du régime des crues dans les bassins semi-arides algériens. Cas du bassin versant du Hodna. International conference on african large river basins hydrology, Hammamet, Tunisia.

Hasbaia, M. and Benayada, L. (2010). Simulation numérique des crues par un modèle 1D (étude du cas d'un oued algérien et de trois autres rivières). Sécheresse, 21 (3) : 225-31.

Hasbaia, M., Adoui, H. and Paquier, A. (2015). Simulation of semiarid stream flow using 1D model (Rubarbe) case of Ksob wadi in Algeria. 7th Groundwater Symposium of the International Association for Hydro-Enviornment Engineering and Research. doi: 10.1016/j.proenv.2015.04.017

Hasbaia, M., Dougha, M. and Bendjeddou, F. (2017). Erosion sensitivity mapping using a multi-criteria approach under GIS environment : the case of the semiarid Hodna basin central Algeria. International Journal of water resources and arid environments 6(1): 13-19.

Hasbaia, M., Hedjazi, A. and Benayada, L. (2012). Variabilité de l'érosion hydrique dans le bassin de Hodna : cas du sous-bassin de l'oued elham. *Revue marocaine des sciences agronomiques et vétérinaires*. 1(1), 28-32.

Hasbaia, M., Hedjazi, A. and Benayada, L. (2012). Variabilité de l'érosion hydrique dans le bassin de Hodna : cas du sous-bassin versant de l'oued EL-Ham. Rev. Mar. Sci. Agron. Vet. 1:28-32.

Hasbaia, M., Paquier, A. and Herizi, T. (2017). Hydrological modeling of sediment transport in the semi-arid region, case of Soubella watershed in Algeria. Abdella et al. (eds). Water resources in Arid Areas: the way forward, Springer Water. DOI 10.1007/978-3-319-51856-5_14

Hasbaia, M., Seddi, A., Bournane, A., Hedjazi, A. and Paquier, A. (2012). Study of the water and sediment yields of Hodna basin in the centre of Algeria, examination of their impacts. ICSE6 Paris.

Hasbaia, M., Zeroual, S., Dougha, M., Paquier, A. and Poulard, C. (2018). Prediction of dams silting in semi-arid region using erosion map under GIS environment, case of K'sob watershed in Hodna region (Algeria). Kallel, A. (eds). Recent advances in environmental science from the euro-mediterranean and surrounding regions. Advances in science, technology, & innovation. https://doi.org/10.1007/978-3-319-70548-4_229

Hijmans, R. J., Cameron, S. E., Parra, J. L., Jones, P. G. and Jarvis, A. (2005). Very high resolution interpolated climate surfaces for global land areas. International Journal of Climatology: A Journal of the Royal Meteorological Society, 25(15), 1965-1978.

Hong, Y., Liu, L., Qiao, L. and Adhikari, P. (2014). Climate change and hydrological hazards. In Handbook of engineering hydrology: modeling, climate change, and variability. Eds. Eslamian, S. CRC press .Pp: 53-68

Horton, R. (1945) Erosional Development of Streams and Their Drainage Basins; Hydrophysical Approach to Quantitative Morphology. Geological Society of America Bulletin, 56, 275-370. http://dx.doi.org/10.1130/0016-7606(1945)56

Huntington, T.G. (2006). Evidence of intensification of global water cycle: review and synthesis. Journal of Hydrology 319:1-4.

IPCC (2014) Climate Change 2014: Africa. Impacts, Adaptation, and Vulnerability. Part B: Regional Aspects. Contribution of Working Group II to the Fifth Assessment Report of the Intergovernmental Panel on Climate Change . Cambridge University Press, Cambridge, United Kingdom and New York, NY, USA, pp. 1199-1265

IPCC (2018) Summary for Policymakers. In: Global warming of 1.5°C. An IPCC Special Report on the impacts of global warming of 1.5°C above pre-industrial levels and related global greenhouse gas emission pathways, in the context of strengthening the global response to the threat of climate change, sustainable development, and efforts to eradicate poverty. World Meteorological Organization, Geneva, Switzerland

IPCC (Intergovernmental Panel on Climate Change). (2007). Climate change 2007: synthesis report; contribution of Working Groups I, II, and III to the Fourth Assessment Report of the IPCC. Geneva.

IPCC Fifth assessment report (AR5). (2013). Climate change 2013: the physical science basis. Contribution of working group I to the fifth assessment report of the Intergovernmental Panel on Climate Change. Cambridge University Press, New York, USA.

IPCC First assessment report (FAR). (1990). Climate change: the IPCC scientific assessment. Cambridge University Press, Cambridge.

IPCC Fourth assessment report (AR4). (2007). Climate change 2007: climate change impacts, adaptation and vulnerability. Working Group II contribution to the Intergovernmental Panel on Climate Change Fourth Assessment Report. Summary for policymakers, 23.

IPCC Second assessment report (SAR). (1996). Climate change 1995: the science of climate change. Contribution of working group I to the second assessment report of the Intergovernmental Panel on Climate Change. Cambridge University Press, Cambridge, UK.

IPCC Third assessment report (TAR). (2001). Climate change 2001: the scientific basis. Contribution of working group I to the third assessment report of the Intergovernmental Panel on Climate Change.

IPCC. (2001). Climate change 2001: The science of climate change, Report of working group 1 to the third assessment report of IPCC, Cambridge university press, Cambridge, UK.

IPCC. (2014). Summary for policymakers. In: Climate change 2014: Impacts, adaptation, and vulnerability. Part A: Global and sectoral aspects. Contribution of Working Group II to the Fifth Assessment Report of the Intergovermental Panel on Climate Change 1–32 (Cambridge, UK and New York).

IUSS Working group WRB (2014). World reference base for soil resources 2014. International soil classification system for naming soils and creating legends for soil maps. World soil resources reports No. 106, Rome: FAO.

Jutla, A.S. (2006). Hydrologic modeling of reconstructed watersheds using a system dynamics approach. Master thesis, University of Saskatchewan, Canada. 199 p

Kang, M.S., Goo, J.H., Song, I., Chun, J.A., Her, Y.G., Hwang, S.W. and Park, S.W. (2013). Estimating design floods based on the critical storm duration for small watersheds. *jher* 7(3), 209-218. DOI: 10.1016/j.jher.2013.01.003

Kara, F., Yucel, I. and Akyurek, Z. (2016). Climate change impacts on extreme precipitation of water supply area in Istanbul : use of ensemble climate modeling and geo-statistical downscaling. Hydrological science Journal. Volume 61, Issue 14. DOI: 10.1080/02626667.2015.1133911

Karmalkar, A.V., Thibeault, J.M., Bryan, A.M. and Seth, A. (2019). Identifying credible and diverse GCMs for regional climate change studies –case study :Northeastern United States. Climatic Change Journal. 154:367–386. https://doi.org/10.1007/s10584-019-02411-y

Kebiche, M. (1994). Le bassin versant du Hodna (Algérie): Ressources en eau et possibilités d'aménagement. Travaux : Institue de Geographie de Reims. 85(1) : 25-34. DOI: 10.3406/tigr.1994.1298

Khoudour, D., Zedam, A. and Bensefia, S. (2021). Using cartographic documents and GIS for creation a hydrodatabase. Application on Hodna basin, Algeria. African Journal on Land Policy and Geospatial Sciences, Vol. 4, Issue, 4.

Konrad, C.P. (2003). Effects of Urban Development on Floods. USGS Numbered Series - Report 076-03, 4 p.. DOI: 10.3133/fs07603.

Köppen, W. (1923). Die klimate der erde. Walter de Gruyter, Berlin. Erde-Gundriss der Klimakunde. Walter de Gruyter & Co., Berlin, Leipzig, 369 p.https://doi.org/10.1515/9783111491530

Kottek, M., Grieser, J., Beck, K., Rudolf, B. and Rubel, F. (2006). World map of the Köppen-Geiger climate classification updated. Meteorologische Zeitschrift, Vol. 15, No. 3, 259-263. DOI: 10.1127/0941-2948/2006/0130

Kundzewicz, Z.W., Kanae, S., Seneviratne, S.I., Handmer, J., Nicholls, N., Peduzzi, P., Mechler, R., Bouwer, L.M., Arnel, N., Mach, K., Muir-Wood, R., Brakenridge, G.R., Kron, W., Benito, G., Honda, Y., Takahashi, K. and Sherstyukov, B. (2014). Flood risk and climate change: global and regional perspectives. Hydrological science Journal, 59:1, 1-28, DOI: 10.1080/02626667.2013.857411

Ladgham-Chicouche, A. and Zerguine, D. (2001). Fiche descriptive sur les zones humides. Rapport Ramsar, 13-23

Lencastre, A. and Franco, F.M. (2006). Lições de Hidrologia 3ª edição revista. Lisboa: Fundação da Faculdade de Ciências e Tecnologia da Universidade Nova de Lisboa.

Leon, J.G. (2003). GIS for water resources and watershed management. Taylor & Francis. 299 p.

Lim Kam Sian, K.T.C.; Wang, J.; Ayugi, B.O.; Nooni, I.K. and Ongoma, V. (2021) Multi-Decadal Variability and Future Changes in Precipitation over Southern Africa. Atmosphere Journal, 12, 742. https://doi.org/10.3390/atmos 12060742

Lohmann, U., Sausen, R., Bengtsson, L., Cubasch, U., Perlwitz, J. and Roechner, E. (1993). The Köppen climate classification as a diagnostic tool for general circulation models. Cliamte Research Journal. Vol. 3: 177-193

Lousada, S. and Loures, L. (2020). Modelling Torrential Rain Flows in Urban Territories: Floods-Natural Channels (The Case Study of Madeira Island). *American Journal of Water Science and Engineering*, 6(1), 17. DOI: 10.11648/j.ajwse.20200601.13

Lovino, M.A., Pierrestigui, M.J., Müller, O.V., Berbery, E.H., Müller, G.V. and Pasten, M. (2021). Evaluation of historical CMIP6 model simulations and future projections of temperature and precipitation in Paraguay. Climatic Change Journal. 164:46. https://doi.org/10.1007/s10584-021-03012-4

Mahmood, R. and Babel, M.S. (2013). Evaluation of SDSM developed by annual and monthly sub-models for downscaling temperature and precipitation in the Jhelum basin, Pakistan and India. Theor Appl Climatol 113, 27–44, https://doi.org/10.1007/s00704-012-0765-0.

Mahmood, R., Jia, S. and Zhu, W. (2019). Analysis of climate variability, trends, and prediction in the most active parts of the Lake Chad basin, Africa. Scientific reports. 9:6317. https://doi.org/10.1038/s41598-019-42811-9

Maidement, D. and Tate, E. (1999). Floodplain mapping using HEC-RAS and ArcVIEW GIS. Center for research in water resources(CRWR) online report 99-1

Malczewski, J. (1996). A GIS-based approach to multiple criteria group decision making. International Journal of Geographical Information Systems 10(8), 955-971.

Marolla, C. (2013). Climate change impacts on health: the urban poor in the world's megacities. Master's thesis, Harvard division of continuing education.

Maslin, M. (2009). Global warming: a very short introduction. Second edition. Oxford University Press, 162 pages.

Mathews, J. (2007). Seven steps to curb global warming. Energy policy 35:4247-4259

Mathez, E.A. and Smerdon, J.E. (2018). Climate change : the science of global warming and our energy future. Second edition. Columbia University press. 520 p.

McGuffie, K. and Henderson-Sellers, A. (2001). Forty years of numerical climate modelling. Int J Climatol 21:1067–1109

Meddi, M. and Humbert, J. (2000) Variabilité pluviométrique dans l'ouest Algérien durant les cinq dernières décennies. 13ème Colloque de l'Association Internationale de Climatologie. 6 au 8 Septembre (2000) Nice, France.

Meddi, M., Boucefiane, A. and Sadeuk belabbes, A. (2010). Impact des changements climatiques sur les débits dans le bassin du Chéllif (Algérie). In: Global Change: Facing Risks and Threats to Water Resources (ed. By E. Servat et al.) (Proc. Sixth World FRIEND Conference, Fez, Morocco). IAHS Publ. 340, 95- 102.

Meinshausen,M., Smith, S. J., Calvin, K., Daniel, J. S., Kainuma, M. L. T., Lamarque, J. F.,Matsumoto,K.,Montzka, S. A., Raper, S. C. B., Riahi, K., Thomson, A., Velders, G. J. M. and Vuuren, D. P. P. (2011). The RCP greenhouse gas concentrations and their extensions from1765 to 2300. Clim.Change 109 (1–2), 213–241.

Mendes, D. and Marengo, J.A. (2010). Temporal downscaling: a comparison between artificial neural network and autocorrelation techniques over the Amazon basin in present and future climate change scenarios. Theor Appl Climatol 100:413–421

Mendoza, G., Macoun, P., Prabhu, R., Sukadr, D., Purnomo, H. and Hartanto, H. (1999). Guidelines for applying multi-criteria analysis to the assessment of criteria and indicators. Center for International Forestry Research

Messad, A. and Moussai, B. (2015). Effect of water salinity on Atterberg limits of El-Hodna Sabkha soil. Bull Eng Geol Environ Journal. DOI 10.1007/s10064-015-0733-x

Miranda, D.G., Camacho, R. F., Lousada, S. and Castanho, R. A. (2018). Hydraulic studies and their influence for regional urban planning: A pratical approach to Fynchal's rivers. *Revista Brasileira de Planejamento e Desenvolvimento*, 7(1), 145-164. DOI: 10.3895/rbpd.v7n1.7179

Młyński, D. (2020). Analysis of Problems Related to the Calculation of Flood Frequency Using Rainfall-Runoff Models: A Case Study in Poland. *Sustainability*, 12(17), 7187. DOI: 10.3390/su12177187

Mokadem, N., Boughariou, E., Mudarra, M., Ben Brahim, F., Andreo, B., Hamed, Y. and Bouri, S. (2018). Mapping potential zones for groundwater recharge and its evaluation in arid environments using a GIS approach: Case study of North Gafsa Basin (Central Tunisia). Journal of African Earth Sciences. 10.1016/j.jafrearsci.2018.02.007.

Molyneux, N., Soares, I. and Neto, F. (2015). Modeling current and future climates using WorldClim and DIVA software: case studies from Timor Leste and India. Journal of crop improvement. Taylor & Francis. 28:5, 619-640. DOI: 10.1080/15427528.2014.924369

Morell, M., Bernard, T. and L'Hote, Y. (1999). Acquisition et constitution d'une information hydrologique de base, Ecole Polytechnique Fédérale de Lausanne. ISBN 973-98954-I–7.

Moser, S.C. (2010). Communicating climate change : history, challenges, process and future directions. Wiley Interdisciplinary reviews: Climate Change, 1(1), 31-53.

Moss, R. H., Edmonds, J. A., Hibbard, K. A., Manning, M. R., Rose, S. K., Van Vuuren, D. P., Carter, T. R., Emori, S., Kainuma, M., Kram, T., Meehl, G. A., Mitchell, J. F. B., Nakicenovic, N., Riahi, K., Smith, S. J., Stouffer, R. J., Thomson, A. M., Weyant, J. P. and Wilbanks, T. J. (2010). The next generation of scenarios for climate change research and assessment. Nature 463, 747–756.

Mujere, N. and Eslamian, S. (2014). Climate change impacts on hydrology and water resources. In Handbook of engineering hydrology: modeling, climate change, and variability. Eds. Eslamian, S. CRC press. Pp: 114-125

Musungu, K., Motala, S. and Smit, J. (2012). Using Multi criteria evalution and GIS for flood risk analysis in informal settlements of Cape Town: the case of Graveyard Pond. *South African journal of Geomatics.* Vol , No 1, 92-108.

Musy, A. and Higy, C. (1998). Hydrologie appliquée. Ecole polytechnique fédérale de Lausanne. 368 p.

National hydraulic resources agency ANRH. (2020). Monthly and maximum daily precipitation records.

Neelin, J.D. (2011). Climate change and climate modeling. Cambridge University press. 300 p.

Ogato, G.S., Bantider. A., Abebe, K. and Geneletti, D. (2020). Geographic Information System (GIS)-Based multicriteria analysis of flooding hazard and risk in Ambo Town and its watershed, West shoa zone, Oromia regional state, Ethiopia. *Journal of Hydrology: Regional studies*. Volume 27, http://doi.org/10.1016/j.ejrh.2019.100659.

Oki, T. and Kanae, S. (2006). Global hydrological cycle and world water resources. Science, 313(5790): 1068-1072

Olson, S. (2022). Engineering responses to climate change. Proceedings of a forum. National academy of engineering (USA). https://doi.org/10.17226/26458.

Ouarda, T.B.M.J., Gingras, H., Bobée, B. and Lemonier, M. (2001). Synthèse des méthodes simples de régionalisation. *INRS-Eau, Québec.* V 65, rapport de recherche. 71 pages.

Oulad Naoui N., Cherif A. and Djehiche A. (2018). Hydrological modeling of watersheds using the only corresponding competitor method: the case of M'Zab basin, South East Algeria. World academy of Science, Engineering and Technology. *International journal of environmental and ecological engineering*. Vol 12, No 1, 6 pages. DOI: 10.1999/1307-6892/10008345

Panagos, P., Ballabio, C., Meusburger, K., Spinoni, J., Alewell, C. and Borelli, P. (2017). Towards estimates of future rainfall erosivity in Europe based on REDES and WorldClim datasets. Journal of hydrology, jhydrol 548: 251-262. 0022-1694. http://dx.doi.org/10.1016/j.jhydrol.2017.03.006

Papaioannou, G., Vasiliades, L., Loukas, A. and Aronica, G.T. (2017). Probabilistic flood inundation mapping at ungauged streams due to roughness coefficient uncertainty in hydraulic modeling. Adv. Geosci., 44, 23-24. doi:10.5194/adgeo-44-23-2017

Peng, S., Ding, Y., Liu, W., and Li, Z. (2019). 1 km monthly temperature and precipitation dataset for China from 1901 to 2017, Earth Syst. Sci. Data, 11, 1931–1946, https://doi.org/10.5194/essd-11-1931-2019.

Phillips, N.A. (1956). The general circulation of the atmosphere: a numerical experiment. Q J R Meteorol Soc 82:123–164

Phongsapan, K., Chishtie, F., Poortinga, A., Bhandari, B., Meechaiya, C., Kunlamai, T., Aung, K.S., Saah, D., Anderson, E., Markert, K., Market, A. and Towashiraporn, P. (2019). Operational flood risk index mapping for disaster risk reduction using earth observations and cloud computing technologies: a case study on Myanmar. Front. Environ. Sci. 7:191. Doi: 10.3389/fenvs.2019.00191

Pittok, A.B. and Jones, R.N. (2000).adaptation to what and why? Environmental Monitoring and Assessment journal 61:9-35

Portier, C.J., Thigpen, T.K., Carter, S.R., Dilworth, C.H., … and Whung, P. (2010c). A human perspective on climate change: a report outlining the research needs on the human health effects of climate change. Research Triangle Park (NC): Environmental Health Perspectives/ National Institute of Environmental Health Sciences (1), 51-63

Praskievicz, S. (2009). Impacts of climate change and urban development on water resources in the Tualatin river basin. Master dissertation. Portland State University.

Raaijimakers, R., Krywkow, J. and Veen, A. (2008). Flood risk perspections and spatial multi-criteria analysis : an exploratory research for hazard mitigation. *Naturals Hazards*, 46 (3), 307-322. Springer.

Redjem, A., Nouibat, B. and Naghel, M. (2020). Pour des villes résilentes aux inondations. Cas de la ville de M'sila, Algérie. Sciences & Technologie, N°51. 33-42.

Reilly, J., Stone, P.H., Forest, C.E., Webster, M.D., Jacoby, H.D. and Prinn, R.G. (2001). Uncertainty and climate change assessments. MIT joint Program on the science and policy of global change. 293 (5529):430-33.

Reshmidevi, T.V., Nagesh Kumar, D., Mehrotra, R. and Sharma, A. (2017). Estimation of the climate change impact on a catchment water balance using an ensemble of GCMs. Journal of Hydrology. http://dx.doi.org/10.1016/j.jhydrol.2017.02.016

Rew, R. and Davis, G. (1990). NetCDF : an interface for scientific data access. IEEE Computer Graphics & Applications. Vol 10, issue 4. Pp, 76-82. DOI: 10.1109/38.56302

Rimba, A.B., Setiawati, M.D., Sambah, A.B. and Miura, F., 2017. Physical Flood Vulnerability Mapping Applying Geospatial Techniques in Okazaki City, Aichi Prefecture, Japan. *Urban Science* 1 (7), 1–22. https://doi.org/10.3390/urbansci1010007.

Rincón, D., Khan, U.T. and Armenakis, C. (2018). Flood risk mapping using GIS and multi-criteria analysis: a greater Toronto area case study. Canada. *Geosciences 8(8), 275.* https://doi.org/10.3390/geosciences8080275. Special issue : Hydrology of Urban catchments.

Rivera, J.A. and Arnould, G. (2020). Evaluation of the ability of CMIP6 models to simulate precipitation over Southwestern South America : climatic features and long-term trends (1901-2014). Atmospheric Research Journal. 241, 104953, doi:10.1016/j.atmosres.2020.104953

Robinson, W.A. (2001). Modeling dynamic climate systems. Springer.

Roche, M. (1963). Hydrologie de surface. Gauthier-Villars, Paris (France).

Romero, C. and Rehman, T. (2003). Chapter five Compromise programming. Developmentsin agricultural economics Journal. Vol 11, pp: 63-78. https://doi.org/10.1016/S0926-5589(03)80007-9

Rothman, D.S., Romero-Lankao, P., Schweizer, V.J. and Bee, B.A. (2013). Challenges to adaptation: a fundamental concept for the shared socio-economic pathways and beyond. *Climatic Change*, 122, 495-507. https://doi.org/10.1007/s10584-013-0907-0.

Saaty, T. L. (1980). The Analytic Hierarchy Process. NewYork: McGraw Hill.

Saaty, T.L. (1977). A scaling method for priorities in hierarchical structures. Journal of mathematical psychology, 15(3), 234-281. https://doi.org/10.1016/0022-2496(77)90033-5.

Saidi, S., Ghattassi, A., Anselme, B. and Bouri, S. (2019). GIS based Multi-criteria Analysis for flood risk assessment : case of Manouba Essijoumi Basin, NE Tunisia. *Springer Nature Switzerland. Advances in Science, Technology & Innovation*. Pp 273-279. https://doi.org/10.1007/978-3-030-01440-7_64

Salhi, A., Okacha, A., Benabdelouahab, S., Himi, M., Benabdelouahab, T. and Ponsati, A.C. (2019) Modelling flood risk in rural areas: the case of the Arbaa Taourirt centre (Morocco). 2nd Springer Euro-Mediterranean Conference for environmental integration (EMCEI), Tunisia. Springer Nature. Poster.

Salimi, E.T., Nohegar, A., Malekian, A., Hoseini, M. and Holisaz, A. (2017). Estimating time of concentration in large watersheds. *Paddy and Water Environment,* 15(1), 123-132. DOI: 10.1007/s10333-016-0534-2

Sassolas-Serrayet, T., Cattin, R. and Ferry, M. (2018). The shape of watersheds. Nature communications 9, 3791. https://doi.org/10.1038/s41467-018-06210-4

Savornin, J. (1908). L'hydrologie du Hodna. Bulletin du service de la carte géologique de l'Algérie. 3ème série :géologie appliquée, études régionales. 150 p.

Scheuer, S., Haase, D. and Meyer, V. (2011). Exploring multi-criteria flood vulnerability by integrating economic, social and ecological dimensions of flood risk and coping capacity: from a starting point view towards an end point view of vulnerability. *Natural hazards*, 58, 731-751. DOI: 10.1007/s11069-010-9666-7.

Schneider, S.H. (1992). Chapter 1: Introduction to climate modeling. Eds.Trenberth, K.E. 1992, in Climate system modeling. 141 pages

Şen, Z. (2018). Flood modeling, prediction, and mitigation. Springer International Publishing AG. Pp: 337-379. https://doi.org/10.1007/978-3-319-52356-9_8

Şen, Z. and Öztopal, A. (2013). Turkish water foundation climate change downscaling model principals. Causes, impacts and solutions to global warming, chapter 5. Pp 87-101.

Shameem, M. (2016). Public perception and communication of climate change risks in the coastal region of Bangladesh: a grounded theory study. University of Hamburg, Germany. Doctoral thesis.

Shiru, M.S. and Chung, E.S. (2021). Performance evaluation of CMIP6 global climate models for selecting models for climate projection over Nigeria. Theoretical and Applied Climatology Journal. https://doi.org/10.1007/s00704-021-03746-2

Shivaprasad Sharma, S.V., Roy, P.S., Chakravarthi, V. and Srinivasa Rao, G. (2017). Flood risk assessment using multi criteria analysis : a case study from Kopili River basin, Assam, India. Geomatics, Naturals hazards and risk, Vol 9, Issue 1. http:// doi.org/10.1080/19475705.2017.1408705.

Shivaprasad Sharma, S.V., Srinivasa Rao, G. and Bhanumurthy, V. (2012). Development of village-wise flood risk index map using multi-temporal satellite data: a study of Nagaon district, Assam, India. Curr Sci J. 103(6):705–712.

Sillmann, J., Kharin, V.V., Zwiers, F.W., Zhang, X. and Bronaugh, D. (2013). Climate extreme indices in the CMIP5 multimodel ensemble: Part 2, Future climate projections. Journal of Geophysical Research : Atmospheres. Vol. 118, Pp: 2475 -2493. https://doi.org/10.1002/jgrd.50188

Sime, C.H. and Abebe, W.T. (2022). Sediment yield modeling and mapping of the spatial distribution of soil erosion-prone areas. Applied and Environmental Soil Science Journal. https://doi.org/10.1155/2022/4291699

Sreelatha, K and Anand Raj, P. (2019). Ranking of CMIP5-based global climate models using standard performance metrics for Telangana region in the southern part of India. ISH Journal of Hydraulic Engineering. Taylor & Francis.

Srinivasa Raju, K.; Sonali, P. and Nagesh Kumar, D. (2016). Ranking of CMIP5-based global climate models for India using compromise programming. Theoretical Applied Climatology Journal. DOI 10.1007/s00704-015-1721-6

Stakhiv, E.Z. (1996). Managing water resources for climate change adaptation. In Adaptation to climate change : An International Perspective. Eds. Smith, J., Bhatti, N., Menzhulin, G., Benioff, R., Budyko, M.I., Campos, M., Jallow, B. and Rijsberman, F. Springer, New York, pp: 243-264.

Stocker, T.F., Qin, D., Plattner, G.K. et al. (2013). Technical summary. In Climate change 2013: the physical science basis. Contribution of Working Group I to the Fifth Assessment Report of the Intergovernmental Panel on Climate Change (pp. 33-115). Cambridge University Press.

Strahler, A. (1964) Quantitative Geomorphology of Drainage Basins and Channel Networks. In: Chow, V., Ed., Handbook of Applied Hydrology, McGraw Hill, New York, 439-476.

Su, B., Huang, J., Mondal, S.K., Zhai, J., Wang, Y., Wen S., .. and Li, A. (2021). Insight from CMIP6 SSP-RCP scenarios for future drought characteristics in China. Atmospheric Research, 250, 105375. doi:10.1016/j.atmosres.2020.10537

Subyani, A.M. and Al-Amri, N.S. (2015). IDF curves and daily rainfall generation for the Al-Madinah city,western Saudi Arabia. Arabian Journal of Geosciences. 8(50) ,11107-11119. DOI: 10.1007/s12517-015-1999-9

Sun, X., Wang, J.C., Zhang, L.W., Chenjia, J., Zhang, W. and Li, W. (2020). Spatial downscaling model combined with the Geographically Weighted Regression and multifractal models for monthly GPM/IMERG precipitation in Hubei Province, China. Atmosphere, 13(3), 476, https://doi.org/10.3390/atmos13030476

Tan, M.L., Ficklin, D.L., Ibrahim, A.L. and Yusop, Z. (2014). Impacts and uncertainties of climate change on streamflow of the Juhor River Basin , Malaysia using a CMIP5 general circulation models ensemble. Doi: 10.2166/wcc.2014.020

Tokarska, K.B., Stolpe, M.B., Sippel, S., Fischer, E.M., Smith, C.J., Lehner, F. and Knutti, R. (2020). Past warming trend constrains future warming in CMIP6 models. Science Advances, Vol.6, NO. 12, DOI: 10.1126/sciadv.aaz9549

Trenberth, K.E. (1992). Climate system modeling. National Center for Atmospheric Research.

Treut, L., Somerville, R., Cubasch, U., Ding, Y., Mauritzen, C., Mokssit, A., …Tignor, M. (2007). Historical overview of climate change science. In S. Solomon, D. Qin, M. Manning, Z. Chen, M. Marquis, K.B. Averyt, …H.L. Miller (Eds), Earth (Vol. Chapter 1, pp: 93-127). Cambridge university Press. Doi: 10.1016/j.soilbio.2010.04.001.

Trzaska, S. and Schnarr, E. (2014). A review for downscaling methods for climate change projections. African and Latin American resilience to climate change project (ARCC). 56 p.

UNFCCC. (2010). Climate change: impacts, vulnerabilities and adaptation in developing countries. 68 (Bonn, Germany).

UNISDR. (2011). Global assessment report on disaster risk reduction: revealing risk, redefining development.

United Nations Department of Humanitarian Affairs (UNDHA), 1992: GIossary - lnternationaly agreed glossary of basic terms related to disaster management, 83 PP.

US EPA. (2012). US Environmental Protection Agency. In climate change indicators in the United States, 2nd Edition. P.3. EPA 430-R-12-004

Usta, D. F. B., Teymouri, M. and Chatterjee, U. (2022). Assessment of temperature changes over Iran during the twenty-first century using CMIP6 models under SSP1-26, SSP2-4.5, and SSP5-8.5 scenarios. Arabian Journal of Geosciences, 15(5), 1-16.

Usta, D. F. B., Teymouri, M., Chatterjee, U. and Bandyopadhyay, N. (2022). Projections of atmospheric changes over Iran in 2014-2050 using the CMIP6-HighResMIP experiment. Arabian Journal of Geosciences, 15(15), 1-18.

Van Vuuren, D. P., Edmonds, J., Kainuma, M., Riahi, K., Thomson, A., Hibbard, K., ... and Rose, S. K. (2011). The representative concentration pathways: an overview. Climatic change, 109(1), 5-31

Vargas, R. (2016). Deterministic hydrological modeling for flood risk assessment in large urban environments: application to Mexico city (USA). Thesis, University of Nice-Sophia Antipolis, Stic doctoral school, information and communication sciences. 258 p.

Vojtek, M. and Vojtekova, J. (2016). Flood hazard and flood risk assessment at the local spatial scale: a case study. Geomatics, natural hazards, and risk, Vol. 7, NO. 6, 1973-1992. http://dx.doi.org/10.1080/19475705.2016.1166874

Wang, H., Zang, F., Zhao, C. and Liu, C.L. (2022). A GWR Downscaling method to reconstruct high-resolution precipitation dataset based on GSMaP-Gauge data: a case study in the Qilian Mountains, Northwest China. Science of total environment. DOI: 10.1016/j.scitotenv.2021.152066

Weart, S.R. (2010). The idea of anthropogenic global climate change in the 20th century. Wiley Interdisciplinary reviews: Climate Change, 1(1), 67-81.

Whitmarsh, L.E. (2005). A study of public understanding and response to climate change in the south of England. University of Bath, Department of Psycology. Ph. D. thesis, 427 p.

Wilson, K.M. (2000). Communicating climate change through the media. In C.C.Stuart Allan, Barbara Adam (Eds.), Environmental risks and the media (pp. 201-217). UK: Routledge.

Winsemius, H., Van Beek, L., Jongman, B., Ward, P. and Bouwman, A. (2013). A framework for global river flood risk assessments, Hydrol. Earth Syst. 17, 1871-1892. https://doi.org/10.5194/hess-17-1871-2013

Wisner, B., Gaillard, J.C. and Kelman, I. (2012). Framing disaster: theories and stories seeking to understand hazards, vulnerability and risk. Taylor and Francis.

WMO (2019). World Meterological Organization statement on the state of the global climate in 2018. WMO-No. 1233. ISBN 978-92-63-11233-0. Accessed at : https://library.wmo.int/doc_num.php?explnum_id=5789

WMO. (2017). World Meteorological Organization Guidelines on the calculation of climate normal vol 2019.

WMO. (2021). World Meteorological Organization, United Nations :Weather, climate, water.

Xu, C. (1999). From GCMs to river flow : a review of downscaling methods and hydrologic modelling approaches. Progress in Physical Geography 23:229-249

Yalcin, G. and Akyurek, Z. (2004). Analyzing flood vulnerable areas with multicriteria evaluation. The West of Black Sea, north of Turkey. In 20th ISPRS Congress. Pp: 359-364.

Yazdandoost, F., Moradian, S., Izadi, A. and Aghakouchak, A. (2021). Evaluation of CMIP6 precipitation simulations across different climatic zones; uncertainty and model Intercomparison. Atmospheric Research Journal. https://doi.org/10.1016/j.atmosres.2020.105369

Yeganeh, N. and Sabri, S. (2014). Flood Vulnerability Assessment in Iskandar Malaysia Using Multi-criteria Evaluation and Fuzzy Logic. *Res. J. Appl. Sci. Eng. Technol.* 2014, 8, 1794–1806. Maxwell scientific organization.

Zafar, I., Shamsuddin, S., Kamal, A., Tarmizi, I., Ghaith Falah, Z., Chung, E.S. and Wang, X. (2021). Evaluation of CMIP6 GCM rainfall in mainland Southeast Asia. Atmospheric research Journal. https://doi.org/10.1016/j.atmosres.2021.105525

Zeleny, M. and Cochrane, J.L. (1973). Compromise Programming. Multiple criteria decision making. University of South Carolina. Press.

Zeroual A., Assani A.A., Meddi M et al. (2019) Assessment of climate change in Algeria from 1951 to 2098 using the Köppen–Geiger climate classification scheme. Clim Dyn 52: 227–243. https://doi.org/10.1007/s00382-018-4128-0

Zeroual, A., Assani, A.A., Meddi, H., Bouabdelli, S., Zeroual, S. and Alkama, R. (2020). Assessment of projected precipitations and temperatures changes signals over Algeria based on Regional Climate Model: RCA4 simulations. In: the Handbook of Environmental Chemistry. Springer. . https://doi.org/10.1007/698_2020_526

Zeroual, A., Meddi, M. and Bensaad, S. (2013). The impact of climate change on river flow in arid and semi-arid rivers in Algeria. Proceedings of H01, IAHS-IAPSO-IASPEI Assembly, Gothenburg, Sweden. Climate and Land-surfaces Changes in Hydrology.

Zeroual, S. (2016). Etude de la sensibilité du sous bassin de K'sob à l'érosion hydrique par une approche quantitative. Mémoire de Master, Université de M'sila. 150 p

Zeroual, S. (2022). Etude des precipitations extremes dans le context de changement climatique : Cas du bassin versant Hodna. Université de M'sila.

Zeroual, S., Şen, Z., Boutaghane, H. and Hasbaia, M. (2021). Monthly extreme rainfall risk envelope graph method development and application in Algeria. Journal of Water and Climate Change, 12(5), 1838-1853. DOI: 10.2166/wcc.2020.176

Zeroual, S., Sen, Z., Boutaghane, H., Hasbaia, M. and Zeroual, A. (2022). Probable maximum precipitation (PMP) and flood (PMF) risk chartes in Hodna basin, Algeria. Meteorology and Atmospheric Physics Journal. https://doi.org/10.1007/s00703-022-00879-5